D 2021

U.PORTO
FEUP FACULDADE DE ENGENHARIA
UNIVERSIDADE DO PORTO

ASSESSMENT AND IMPROVEMENT OF MICROALGAE BIOMASS PRODUCTIVITY IN DIFFERENT PHOTOBIOREACTORS

MARIANA RIBEIRO CARNEIRO

THESIS SUBMITTED TO THE FACULTY OF ENGINEERING OF THE UNIVERSITY OF PORTO
TO OBTAIN THE DEGREE OF DOCTOR IN CHEMICAL AND BIOLOGICAL ENGINEERING

Assessment and improvement of microalgae biomass productivity in different photobioreactors

Mariana Ribeiro Carneiro

Supervision:

Prof. F. Xavier Malcata, Prof. João Carlos Serafim Varela
and Prof. Ana Maria Otero Casal

Porto, September 2021

«“O frati”, dissi, “che per cento milia	*«“Ó irmãos”, disse, “que por tanta milha*
perigli siete giunti a l’occidente,	*de perigos vistes a ocidente,*
a questa tanto picciola vigilia	*a tão breve vigília que nos brilha*
d’i nostri sensi ch’è del rimanente	*nos sentidos, e que é remanescente,*
non vogliate negar l’esperïenza,	*não negueis experiência e sem detença*
di retro al sol, del mondo sanza gente.	*siga-se o sol, no mundo sem ter gente!*
Considerate la vostra semenza;	*E que a vossa semente agora vença:*
fatti non foste a viver come bruti,	*não fostes feitos a viver quais brutos,*
ma per seguir virtute e canoscenza."»	*mas a seguir virtude e conhecença.”»*

Canto XXVI, Inferno
A Divina Comédia de Dante Alighieri
Tradução de Vasco Graça Moura

Acknowledgments

During the last years, I have been fortunate enough to have crossed paths with extraordinary people in many different places who have helped me grow scientifically and personally, without which this thesis could not have been completed. Although there are not enough pages in this thesis to express my gratitude to everyone involved, I would briefly – and insufficiently – like to say thank you.

Starting from the beginning, I would like to express my gratitude to my supervisor Prof. F.X. Malcata for the opportunity to engage in this doctoral program and the valuable lessons and institutional and scientific support. A thank you is also due to LEPABE's Biotechnology group, where I first met Vânia and Joana A., friends that brought their color to my greyer days during the thesis.

I was lucky enough to have Prof. João Varela as a supervisor, who welcomed me in his laboratory and opened a myriad of opportunities for me to grow and discover the microalgae world. I am deeply grateful for his unwavering support and his kind words. I would also like to thank the MarBiotech group, particularly Paulo, Vera, Katkam, Lisa, Peter, Zé, Etiele, Tamara, and Prof. Luísa, for all the help and support during the trials performed in Algarve. I am deeply grateful for the opportunity of having met Luísa Gouveia in Greece, who has shown nothing but support and friendship. A special thank you is necessary to Inês M. not only for her valuable help but also for her warm friendship.

To Prof. Ana Otero, I will be forever grateful for teaching me to be better, think harder, and push further. More than a supervisor, she was a support and a friend, and I can also say an aspiration. Thank you to all in the Acuicultura y Biotecnologia group I met during my stay, specifically Andrea M., for her friendship.

Not all supervisors have an official title. Such is the case of Prof. Giuseppe Torzillo, a spectacular and inspiring mentor and a work machine with whom I had the pleasure to work with. I am also grateful to all the people I met in CNR for their friendship during my stay and beyond, particularly Left (sorry about the plant), Graziella, Cecilia, Edoardo, Sili, Niccolai, Pietro, Margarita, and Sílvia. Thank you as well as to Adele, Andrea, and Eva for all their support and fun. And also, a special thank you to Bernardo for all the help and big fat jokes.

Further North, in Algatech, I could not forget another great un-official supervisor, Prof. Jiří Masojídek, with whom I had the absolute pleasure to work with as well as with people from the Laboratory of algal biotechnology specifically Karolína, Tomáš, Gergely, João, and Soňa and their contaminating good mood. Also, a special thank you to all the people I met in Algatech, with a highlight to Avik for his friendship and stubbornness to get me out in the wild.

I would like to extend my sincere thanks to Necton S.A., where they allowed me to perform several experiments and moreover in the company of incredible people. So a big thank you to everyone and in particular to João Navalho, Vitória, Alexandre, Yago, Ana C., Jorge, Fernando, Pedro, Dário, Hugo, Oleh, Inês P., Cristina, Paula, Sandra, Hélia, Teresa and Lídia for all the smiles, sweat and laugh shared, and to Tânia for her energy and friendship.

Another significant milestone was accomplished in Allmicroalgae S.A., where I would like to offer a special thank you to Joana L., Maria, Joana T., Nuno, Bernardo, Quelhas, Mafalda, Ana B., Adriana, Nádia, Manel e Rui. A special thanks to Pedro and Inês for all their willingness to help and learn and to Margarida, with whom I hope to never stop crossing paths.

A special thank you to Tiago for his patience and heart that walked me through the first steps of this adventure.

To all of my dear friends that have continuously plagued me with encouragement and support, Aldo, Bruno, Raquel, Sara, João, Pedro, Mafalda, Mariana R., Sofs, Sandra, Joaninha, Graziano, Ana S., Pedro, Di, Andreia, André, Francisco, Hugo P., Pedro, Ana R., Sosse, Alves, Chiqui, Sérgio, Xana, Sandra P., Mariana, Cassapo, Elsa, Ricky e Bárbara. I blame all of you for my success and partial sanity. A special thank you to my soulmate, Daniela, without whom I could not be where I am, and if I was, I am sure I would be half as happy.

Although it was a late entrance in this period, it was no less critical; thank you to Hugo for his saint-like patience, for making me laugh, and for all the happiness you bring to my life.

Finally, I would like to thank my whole family for their support, particularly my parents, to Né, Ju, David, Joana M., and Pedro for always having the patience and love to give and encourage me to keep improving.

I apologize to anyone who was not mentioned by name but rest assured that it does not diminish my gratitude in any way.

Thank you to you all

Funding

This work was financially supported by:

- The doctoral research fellowship by the Portuguese Foundation for Science and Technology (FCT) [SFRH/BD/129952/2017].
- The European Cooperation in Science and Technology (COST) Action ES1408: European network for algal-bioproducts (EUALGAE).
- The base and programmatic funding for Laboratory for Process Engineering, Environment, Biotechnology, and Energy (LEPABE), by national funds through FCT/MCTES (PIDDAC) [UIDB/00511/2020 and UIDP/00511/2020].
- The "LEPABE-2-ECO-INNOVATION", by the North Portugal Regional Operational Program (NORTE 2020), under the Portugal 2020 Partnership Agreement, through the European Regional Development Fund (ERDF) [NORTE-01-0145-FEDER-000005].
- The project DINOSSAUR, by ERDF through COMPETE2020 – Programa Operacional Competitividade e Internacionalização (POCI), and by FCT [PTDC/BBB-EBB/ 1374/2014-POCI-01-0145-FEDER-016640].
- The pluriannual budget awarded to the Centre of Marine Sciences of Algarve (CCMAR) [UID/Multi/04326/2019] and [UID/Multi/04326/2020].
- The ALGAVALOR project "MicroALGAe: integrated production and VALORization of biomass and their diverse applications", by ERDF, POCI and CRESC-Algarve [ALG-01-0247-FEDER-035234].
- The SABANA project, by the European Union's Horizon 2020 Research and Innovation program [Grant Agreement No. 727874].
- INTERREG V-A España-Portugal through 0055 ALGARED+5E project

And supported by the following institutions:

- Laboratory for Process Engineering, Environment, Biotechnology and Energy (LEPABE), Faculty of Engineering of the University of Porto, Rua Dr. Roberto Frias, 4200-465 Porto, Portugal.
- Instituto de Acuicultura and Departamento de Microbiología y Parasitología, Facultad de Biología, Universidade de Santiago de Compostela, 15782 Santiago de Compostela, Spain.
- Consiglio Nazionale delle Ricerche - Istituto per la BioEconomia (CNR-IBE), Via Madonna del Piano 10, Sesto Fiorentino, 50019 Florence, Italy.
- MarBiotech group from the Centre of Marine Sciences (CCMAR), University of Algarve, Gambelas, 8005-139 Faro, Portugal.
- Necton S.A., Belamandil, 8700-152 Olhão – Algarve, Portugal.
- Allmicroalgae Natural Products S.A., R&D Department, Rua 25 de Abril 19, 2445-287 Pataias, Portugal.
- Institute of Microbiology of the Czech Academy of Sciences, Centre Algatech, Laboratory of Algal Biotechnology, Novohradská 237, Třeboň, Czech Republic.

Thesis outputs

Papers in international scientific periodicals with referees:

Carneiro, M., Pôjo, V., Malcata, F. X. and Otero, A., 2019. Lipid accumulation in selected *Tetraselmis* strains. Journal of Applied Phycology 31, 2845-2853. DOI: 10.1007/s10811-019-01807-8.

Carneiro, M., Cicchi, B., Maia, I.B., Pereira, H., Zittelli, G. C., Varela, J., Malcata, F.X. and Torzillo, G., 2020. Effect of temperature on growth, photosynthesis and biochemical composition of *Nannochloropsis oceanica*, grown outdoors in tubular photobioreactors. Algal Research 49, 101923. DOI: 10.1016/j.algal.2020.101923.

Carneiro, M., Ranglová, K., Lakatos, G.E., Câmara Manoel, J.A., Grivalský, T., Kozhan, D.M., Toribio, A., Moreno, J., Otero, A., Varela, J., Malcata, F. X., Suárez Estrella, F., Acién-Fernández, F.G., Molnár, Z., Ördög, V., Masojídek, J., 2021. Growth and bioactivity of two chlorophyte (*Chlorella* and *Scenedesmus*) strains co-cultured outdoors in two different thin-layer units using municipal wastewater as a nutrient source. Algal Research 56, 102299. DOI: 10.1016/j.algal.2021.102299.

Carneiro, M., Chini-Zittelli, G., Cicchi, B., Touloupakis, E., Faraloni, C., Maia, I.B., Pereira, H., Santos, T., Malcata, F.X., Otero, A., Varela, J., Torzillo, G., 2021. *In-situ* monitoring of chlorophyll a fluorescence in *Nannochloropsis oceanica* cultures to assess photochemical changes and the onset of lipid accumulation during nitrogen deprivation. Biotechnology and Bioengineering 118, 4375-4388. DOI: 10.1002/bit.27906.

Maia, I.B.*, Carneiro, M.*, Magina, T., Malcata, F.X., Otero, A., Navalho, J., Varela, J., Pereira, H., 2021. *Skeletonema costatum* and *Phaeodactylum tricornutum* grown in outdoor pilot-scale flat panel photobioreactors. Journal of Biotechnology 343, 110-119. DOI: 10.1016/j.jbiotec.2021.11.008.

Carneiro, M., Maia, I., Cunha, P., Guerra, I., Magina, T., Santos, T., Schulze, P.S.C., Pereira, H., Malcata, F.X., Navalho, J., Silva, J., Otero, A., Varela, J., 2021. Effects of LED lighting on *Nannochloropsis oceanica* grown in outdoor raceway ponds. Submitted to Algal Research.

Abstracts in conference proceedings (oral):

Carneiro, M., Cicchi, B., Touloupakis, E., Zittelli, G.C., Malcata, F.X., Sili, C., Torzillo, G. "Acclimation process of high lipid-producing microalgae subjected to nutrient stress under different lighting". 2nd Eualgae Workshop of Algae Bioproducts for Early Career Investigators. Thessaloniki, Greece – March 6th, 2018.

Carneiro, M., Cicchi, B., Maia, I., Pereira, H., Faraloni, C., Zittelli, G.C., Varela, J., Malcata, F.X., Torzillo, G. "Temperature effects on *Nannochloropsis oceanica* night biomass loss". EUALGAE Final Conference - European Recent Advances in the Microalgae Field. Madrid, Spain – February 26-27th, 2019.

Carneiro, M., Cicchi, B., Maia, I., Pereira, H., Faraloni, C., Zittelli, G.C., Varela, J., Malcata, F.X., Torzillo, G. "Temperature effects on *Nannochloropsis oceanica* night biomass loss". Symposium on Chemical and Biological Engineering. Porto, Portugal – June 27-28th, 2019.

Carneiro, M., Maia, I., Pereira, H., Santos, T., Magina, T., Schulze, P., Navalho J., Malcata, F.X., Varela, J. "The effect of led lighting on night biomass losses of *Nannochloropsis oceanica* grown in outdoor pilot scale raceways". 7th European Phycological Congress. Zagreb, Croatia – August 25-30th, 2019

Carneiro, M., Maia, I., Cunha, P., Guerra, I., Pereira, H., Magina, T., Schulze, P., Santos, T., Navalho, J., Silva, J., Malcata, F.X. and Varela, J. "Effects of LED lighting on *Nannochloropsis oceanica* grown in pilot-scale raceways". Webinars on Algal Biotechnology: Light in Algal Biotechnology. Online – November 12th, 2020.

Carneiro, M., Maia, I.B., Magina, T., Malcata, F.X., Rodrigues, A., Pereira, H., Varela, J., Navalho, J. "Growth and PSII performance of *Nannochloropsis oceanica* grown in three different pilot-scale cultivation systems outdoors". The 7th Conference of the International

Society for Applied Phycology (ISAP2020-2021-virtual). Online – May 14th to August 13th, 2021. Granted “Best Student Oral Presentation Award from the ISAP”.

Carneiro, M., Maia, I., Cunha, P., Guerra, I., Magina, T., Santos, T., Schulze, P., Pereira, H., Navalho, J., Silva, J., Malcata, F.X. and Varela, J. “Effects of LED lighting on outdoor raceway ponds”. Microbiotec Web Conference. Online – November 25th, 2021.

Abstracts in conference proceedings (poster):

Carneiro, M., Maia, I., Pereira, H., Santos, T., Magina, T., Schulze, P., Navalho, N., Malcata, F.X., Varela J. "Light it up: effects of LED lighting upon *Nannochloropsis oceanica* grown in pilot raceways". Algaeurope. Paris, France – December 3-5th, 2019.

Maia, I.B., Carneiro, M., Navalho, J., Pereira, H., Varela, J. "Let there be light: fluorescence response of three diatoms grown in pilot-scale flat panels". Algaeurope. Paris, France – December 3-5th, 2019.

Carneiro, M., Touloupakis, E., Zittelli, G.C., Faraloni, C., Cicchi, B., Pereira, H., Varela, J., Malcata, F. X., Torzillo, G. "Fluorescence analysis to assess the effects of different cultivation modes on a high lipid-producing microalgae under nutrient stress". 3rd EUALGAE Training school: Microalgal bioeconomy in modern society. Florence, Italy – September 24-25th, 2018.

Ethics statement

I declare to have contributed to the manuscripts referred in "Thesis outputs" as stated in the author contributions within each respective chapter of this thesis. Others works are duly cited in the text, and listed in the global "References" at the end of the thesis.

Student:

(Mariana Ribeiro Carneiro)

Abstract

Despite their small size, the role of microalgae in biotechnology is quite greater, and it is undergoing a current boom. These photosynthetic organisms can provide biomass for a wide array of applications, thus alleviating the pressure upon less sustainable feedstocks. However, production costs have become a significant bottleneck in microalgae commercialization, thus limiting their application to high-value commodities. To truly unveil the potential of these microorganisms, a deeper understanding of their physiology, coupled with the development of efficient cultivation systems, is a must. Notwithstanding these challenges, microalgae production must be both cost-effective and sustainable; otherwise, they will not constitute a viable feedstock option for medium- and low-value products. The first goal of this thesis was to improve microalgal productivity in terms of biomass and intended end-bioproducts by focusing on strain selection and the effect of abiotic factors upon growth. Afterward, work was developed toward assessing the photosynthetic status of microalgae by unfolding the applicability of monitorization through chlorophyll *a* fluorescence regarding nutrient and weather conditions in laboratory and outdoor environments, respectively. Focusing on cultivation systems, revamping of an open cultivation system – specifically raceway ponds – was assessed via integration of artificial light in the most light-limited zone thereof. Finally, integration of microalgae production in wastewater treatment was performed using thin-layer cultivation systems. Cultivation was followed by biomass fractionation into growth-promoting (biostimulants), protective (biopesticides) and nutritional (biofertilizers) products, for agricultural application in an effort to stimulate circular economy. Therefore, this thesis provides a multi-task approach using different cultivation systems and species, from lab to pilot-scale, and from indoor to outdoor conditions. This work aims, in particular, at elucidating the impacts of several biological, operational, and engineering parameters to improve microalgae productivity, and accordingly develop a more cost-effective and sustainable production.

Keywords: microalgae; productivity; photobioreactors, bioproduct synthesis; photosynthetic fitness.

Resumo

Apesar do seu tamanho pequeno, o papel das microalgas na biotecnologia é bem maior, e está actualmente em crescimento. Estes organismos fotossintéticos podem fornecer biomassa para diversificas aplicações, liberando a pressão de outras matérias-primas menos sustentáveis. No entanto, os custos de produção tornaram-se num dos principais obstáculos na comercialização de microalgas, limitando sua aplicação em mercados de alto valor. Para explorar o verdadeiro potencial destes microrganismos, é necessário um conhecimento mais profundo da sua fisiologia, em conjunto com o desenvolvimento de sistemas de cultivo mais eficientes. A produção de microalgas também necessita de ser mais económica e sustentável; ou poderão não constituir uma opção de matéria-prima viável para produtos de médio e baixo valor. Deste modo, o primeiro objectivo desta tese foi melhorar a produtividade em termos de biomassa e dos metabolitos finais pretendidos, focando na importância da seleção das estirpes e no efeito de factores abióticos no crescimento de microalgas. Posteriormente, o estado fotossintético das microalgas foi avaliado e revelada a aplicabilidade da monitoração pela fluorescência da clorofila *a* em relação às condições nutricionais e climáticas em laboratório e no exterior, respectivamente. Focando nos sistemas de cultivo, foi avaliada a optimização de um sistema de cultivo aberto – especificamente em *raceways* – integrando luz artificial na zona com maior limitação de luz. Finalmente, o tratamento de efluentes integrado com produção de biomassa algal usando sistemas de camada fina foi realizado à escala piloto. Posteriormente seguiu-se o fracionamento da biomassa em produtos com ação estimulante (bioestimulantes), protectora (biopesticidas) e nutricional (biofertilizantes) para aplicação agrícola de modo a estimular a economia circular. Desta forma, esta tese fornece múltiplas abordagens usando diferentes sistemas de cultivo e espécies, de escalas laboratorial a piloto, e de condições internas a externas. Este trabalho visa elucidar os impactos de diversos parâmetros biológicos, operacionais e de engenharia para melhorar a produtividade das microalgas e desenvolver uma produção mais económica e sustentável.

Palavras-chave: microalgas; produtividade; fotobiorreactores; síntese de bioprodutos; fitness fotossintético.

Table of contents

List of Figures

Chapter 2

Chapter 3

Chapter 4

Chapter 5

Chapter 6

Chapter 7

Chapter 8

Annex I

Annex II

Annex III

Annex IV

List of Tables

Chapter 2

Chapter 3

Chapter 4

Chapter 6

Chapter 7

Chapter 8

Annex I

Annex III

Annex IV

Nomenclature

Acronyms

Abbreviation	Meaning
A	Antheraxanthin
ADP	Adenosine diphosphate
ANOVA	Analysis of variance
ATP	Adenosine triphosphate
BOD	Biological oxygen demand
CAPEX	Capital expenditure
COD	Chemical oxygen demand
DHA	Docosahexaenoic acid
DW	Dry weight
EDTA	Ethylenediamine tetra-acetic acid
EPA	Eicosapentaenoic acid
EU	European Union
FAME	Fatty acid methyl esters
FP	Flat panel
GC	Gas chromatography
HPLC	High performance liquid chromatography
LC	Light curves
LED	Light emitting diodes
LHC	Light harvesting complex
ML	Measuring light
MUFA	Monounsaturated fatty acids
$NADP^+$/NADPH	Nicotinamide adenine dinucleotide phosphate (oxidized/reduced)
NH_4-N	Ammonium-nitrogen
NO_2-N	Nitrite-nitrogen

NO_3-N	Nitrate-nitrogen
NPQ	Non-photochemical quenching
OD	Optical density
OPEX	Operational expenditure
PAM	Pulse-amplitude modulation
PAR	Photosynthetically active radiation
PBR	Photobioreactor
PC	Plastocyanin
PE	Photosynthesis versus irradiance
PO_4-P	Orthophosphate-phosphorus
PQ	Plastoquinone (free)
PSI	Photosystem I
PSII	Photosystem II
PUFA	Polyunsaturated fatty acids
PVC	Polyvinylchloride
Q_A	Primary quinone acceptor of PSII
RC	Reaction centers
RLC	Rapid light curves
ROS	Reactive oxygen species
RWP	Raceway pond
SFA	Saturated fatty acids
STCC	Spanish type culture collection
TAG	Triacylglycerols
TFA	Total fatty acids
TL	Thin-layer
TLC	Thin-layer cascade
TN	Total nitrogen
TOC	Total organic carbon
TP	Total phosphorus
V	Violaxanthin
VAZ	Xanthophyll cycle, involving violaxanthin, antheraxanthin, and zeaxanthin
WW	Wastewater
WWTP	Wastewater treatment plant
Z	Zeaxanthin

Notation

Symbol	Unit	Description
A	m^2	Area
ABS		Photon flux absorbed by the antenna of PSII units
A_n		Absorbance at wavelength *n*
*a**		Chlorophyll-specific absorption cross-section
C	mm	Diameter of the zone of the pathogen patches in the absence of microalgal extract
DI		Part of ABS dissipated in PSII antenna in processes other than trapping
E	W m^{-2}	Irradiance
ET		Energy flux associated with the electron transport from Q_A^- to the intersystem electron acceptors
ETR		Electron transport rate
ET_0/TR_0		Efficiency with which a PSII trapped electron is transferred from Q_A^- to PQ at time zero (at onset of excitation)
F’		Fluorescence of a light-adapted sample
F_i		Fluorescence intensity at the I-step (at 30 ms)
F_j		Fluorescence intensity at the J-step (at 2 ms)
F_m		Maximum fluorescence
F_m’		Maximum fluorescence
F_v		Maximum variable fluorescence
F_v/F_m (φ_{Po})		Maximum quantum yield of PSII
F_x		Fluorescence intensity at time x
F_0		Minimum fluorescence
F_0’		Minimum fluorescence in the light
f_{PSII}		Fraction of absorbed quanta by PSII
GI	%	Germination index
G_S	%	Germinated seeds in the presence of the microalgal extract
G_W	%	Germinated seeds in the presence of distilled water
H_e	J m^{-2}	Radiant exposure
I	%	Inhibition index
L_S	mm	Mean of radicle elongation in the presence of the microalgal extract
L_W	mm	Mean of radicle elongation in the presence of distilled water
max		Maximum

NPQ		Non-photochemical quenching
qN		Non-photochemical quenching coefficient
RE		Energy flux associated with the electron transport from Q_A^- to the final electron acceptors of PSI
R^2		Coefficient of determination
rETR		Relative electron transport rate through PSII
t		Time
T	mm	Diameter of the zone of the pathogen patches in the presence of microalgal extract
T	ºC	Temperature
TR		Part of ABS trapped by the active PSII units that leads to Q_A reduction
V_i		Fluorescence yield at I-step
V_j		Fluorescence yield at J-step
$\Delta F'/F_m'$		Actual photochemical yield
μ	d^{-1}	Specific growth rate
ψ_0		Probability/efficiency (at time zero) that a trapped exciton moves an electron into the electron transport chain beyond Q_A

Chapter 1

Introduction

Nowadays, the photosynthetic microorganisms known as microalgae are considered as multipurpose feedstocks with a panoply of biotechnological applications, including for food, feed, cosmetics, agriculture, biofuel, bioplastic, and bioactive molecules, in addition to bioremediation of effluents and CO_2 mitigation. However, high production costs have hindered commercial microalgae-based systems, limiting their commercialization to high-value niche markets. In this context, it is critical to technologically improve productivity and develop robust and reliable processes, thus lowering production costs to achieve a more feasible industrial alternative to other, less sustainable feedstocks. As such, awareness of the photosynthetic status of microalgae that can improve these parameters is of the utmost importance. Accordingly, this thesis focuses on different approaches to optimize and monitor microalgae growth. The current chapter presents a brief background of the importance and challenges posed upon microalgae biomass production; followed by personal motivation and objectives and ending with the description of the thesis layout.

1.1. Background

As the human population grows exponentially, ecosystem degradation coupled with the pressing demand for food, fuel, and clean water has become a growing and urgent concern. In this context, the search for innovative and sustainable renewable sources is becoming increasingly important worldwide. This concern is evident in the European Union (EU) policy priorities, which include strategies such as the Blue Bioeconomy (EC, 2018) and the Circular Economy action plan (EC, 2020); that fall within the goals of the European Green Deal (EC,

2019), aimed at implementing a more sustainable circular bioeconomy. With this in view, algal biomass has been put forward as an efficient and blue alternative to land-based crops – with significant potential to increase worldwide biomass production for various biotechnological purposes (Gangl et al., 2015; Gerotto et al., 2020; Spolaore et al., 2006). Currently, the commercialization of microalgae biomass is mainly targeted at high-value nutritional supplements and feed for the aquaculture market (Garrido-Cardenas et al., 2018; Raja et al., 2008; Suleria et al., 2015). However, several companies (e.g., Corbion N.V., Qualitas Health Inc., and Veramaris V.O.F.) have started exploring the potential of microalgae for oil production, a commodity with a lower market value.

Despite the potential and the growing demand for microalgal biomass (and its derivatives) pushing production facilities to increase their supply, current processes still suffer from several constraints that hamper the economic use of microalgae for large-scale applications. From a bioeconomy point of view, the biomass production requirements should enhance process efficiency rather than merely increasing overall production to meet the market demand. Although microalgae productivities exceed that of agricultural crops (Wijffels and Barbosa, 2010), there is a margin for further development at biological, technological, and operational levels toward stimulation of using microalgae as feedstocks in markets as diverse as food, feed, cosmetic, biomedical and energy. The specific processes that need urgent optimization range from optimal strain selection to establishing an effective microalgae-based biorefinery.

1.2. Motivation

The global algal database reports 161,419 species and infraspecific names of algae reported to date (Guiry and Guiry, 2021) – of which more than half pertain to microalgae, with new species being discovered every year. These photosynthetic organisms have evolved from basal nodes of the prokaryotic and eukaryotic branches of the tree of life and have constituted an untapped resource for many years. Fortunately, microalgae are currently under the biotechnology spotlight, with an increasing number of applications, ranging from biodegradable sandals (Gunawan et al., 2020) to bioregenerative life support systems for space missions (Shepelev, 1975; Yang et al., 2019) or wastewater treatment and manufacture of biofuels (Acién Fernández et al., 2018). These microscopic treasures harbor an impressive array of biochemical compounds with different biotechnological applications. However, all applications rely on efficient biomass production, economic feasibility, and sustainability. This thesis examines different alternative paths leading to better control of biomass production in

different cultivation systems and resorting to different species. The results bring us one step closer to a more sustainable and controllable production of microalgal biomass.

1.3. Objectives

The current research on microalgae cultivation has unfolded many gaps that need to be filled to improve biomass production and the sustainability of the process. In this sense, a clearer understanding of the optimum growth conditions of microalgae cultures, the search for photosynthetic monitoring applications, the selection of adequate strains, the development of new cultivation technologies, and the integration of circular economy approaches are crucial efforts to optimize the productivity of the biomass and target metabolites, as well as to improve the stability and sustainability of microalgae production.

Toward this goal, this thesis tested the effects of several abiotic parameters in several species, particularly cultivation regime, temperature, and nutrient availability – namely, upon biomass growth, photosynthetic efficiency, and biochemical profile. Afterward, in an industrial setting, the growth, photosystem II (PSII) performance, and biochemical composition of two diatoms were monitored outdoors. Subsequently, the integration of artificial lighting in a typically light-limited cultivation system was considered again under outdoor conditions. Finally, the feasibility of employing microalgae in wastewater treatment with an end-product was evaluated to meet the circular economy requirements. Accordingly, this thesis aimed at addressing the following issues:

1) How do growth conditions affect biomass productivity, and are they applicable at industrial scale?
2) Is fluorometry a helpful tool to monitor and identify hindrances to cellular performance?
3) Is artificial lighting a promising solution to enhance microalgal production in raceway pond (RWP) cultivation systems?
4) Can microalgae treat municipal wastewater centrate using thin-layer (TL) cultivation systems, and can the resulting biomass be re-applicated in other activities?

1.4. Thesis layout

This thesis is divided into nine chapters. Beyond the current chapter, the second chapter provides a general introduction to microalgae biotechnology, followed by six chapters in the form of scientific papers describing the experimental work performed to respond to the objectives previously defined (see section 1.3. Objectives); and ending with a chapter composed by a general discussion and conclusions from the work undertaken.

Chapter 2 starts with a short presentation of general concepts regarding photosynthesis in microalgae, its applications, and their significance. A subsequent small introduction arises on cultivation systems, production strategies, and the importance of monitorization – with a focus on fluorometry – paves the way to clarify current bottlenecks in microalgae production. The attention lies on upstream-related processes, as this constituted the primary approach of the thesis work.

Chapter 3 addresses the effects of different renewal rates upon the biomass and neutral lipid content of five strains – classified as lipogenic or non-lipogenic, depending on their stationary-phase cell flotation features. This work emphasizes the importance of strain screening in the selection of suitable microalgae, in this case, for biodiesel production.

Chapter 4 tackles the effect of different temperatures on the relation between biomass growth and nighttime biomass loss through respiration, while assessing photochemical changes and biomass composition to determine the best conditions toward increased biomass valorization.

Chapter 5 assesses the use of online chlorophyll *a* fluorescence analysis to monitor changes in the photosynthetic apparatus between nitrate-replete and -deplete microalgae cultures. The evaluation of biochemical parameters such as growth, lipid, fatty acids, and pigment contents revealed the value of having timely information on the photosynthetic state of the cultures.

Chapter 6 focuses on the effect of light-emitting diode (LED) implementation in outdoor RWPs by monitoring culture areal productivity at small and pilot scales. This work analyzes the cost of preventing biomass losses related to cell respiration overnight.

Chapter 7 follows the growth of two commercially relevant diatoms grown in an industrial setting, targeting variations in biomass productivity and intracellular accumulation of macronutrients and fatty acids. Photosynthetic fitness is examined to address the adaptation ability of two species to environmental conditions and its effect on biomass growth.

In Chapter 8, municipal wastewater centrate is used to grow microalgae using two different TL cultivation systems. Culture growth, photosynthetic performance, and nutrient removal rate are monitored under both batch and semi-batch cultivation modes. The bioactivity

analysis of the resulting biomass determines the possibilities of biomass re-application, thus assessing the integration of circular economy in microalgae production.

Finally, Chapter 9 presents the general discussion and conclusions of the work performed in this thesis and presents prospects for further development towards microalgae production.

Chapter 2

Literature review

2.1. Microalgae

Oxygen-producing photosynthetic microorganisms – including prokaryotic cyanobacteria and eukaryotic microalgae – can use light energy to oxidize water and reduce carbon dioxide to organic carbon compounds using chlorophyll *a*, although some species can also grow hetero- and mixotrophically (Falkowski and Raven, 2013). This review will focus on autotrophic growth since all experiments were performed using this mode of cultivation. As prokaryotes, cyanobacteria are not, strictly speaking, algae since they lack a nucleus or membrane-bound organelles (i.e., chloroplasts). However, cyanobacteria will be included in the definition of microalgae in the current thesis for the sake of simplicity.

With sizes from 1 µm up to ca. 1 mm, microalgae are generally unicellular species, but can also form small colonies or filaments (Hallmann, 2016). They can be classified according to pigment content, energy storage components, and cell wall constituents. The most famous groups comprise green algae (*Chlorophyta*), red algae (*Rhodophyta*), diatoms (*Bacillariophyta*), and golden algae (*Chrysophyceae*). However, other evolutionary lines can also be mentioned, such as haptophytes (*Haptophyta*), cryptophytes (*Cryptophyta*), and euglenas (*Euglenozoa*), among others. Their separate evolution lineages affect their biochemistry and physiology, as is the case of chlorophyll *a* accessory pigments that vary according to phylogenetic group. For example, chlorophyll *b* is found in chlorophytes, chlorophyll *c* in diatoms, and phycobilins in cyanobacteria and red algae (Gerotto et al., 2020). As a consequence of their vast diversity, microalgae can be found ubiquitously on Earth in both aquatic (freshwater and seawater) and terrestrial environments, including extreme ones

(extremophiles). Their biodiversity also promotes an assorted range of biochemical features among species and strains, thus increasing the potential for many different biotechnological applications, all thanks to photosynthesis.

2.1.1. Microalgae as sources of natural products

The organic carbon obtained from the photosynthetic process is converted into proteins, lipids, carbohydrates, and nucleic acids, through a series of biosynthetic pathways. Microalgal metabolic diversity provides yet another advantage, resulting in a variety of products with high and low-value applications. Selected examples are given in Table 2.1 However, it is important to note that novel microalgae-based products keep emerging at a fast pace, especially those with biological (e.g., antioxidant, antibiotic, antifungal, antiviral, antidiabetic, antitumoral, anti-inflammatory, and neuroprotective) activity.

Table 2.1. Examples of products, and related market applications, from various feedstocks that can be found in microalgae. Adapted from Gerotto et al. (2020).

Feedstock	**Valuable products**	**Market**
Proteins, peptides, amino acids		Food, feed
Lipids	Triacylglycerols (TAG)	Biofuels
Fatty acids (mainly PUFA)	ARA (C20:4*n*-6), GLA (C18:3*n*-6), EPA (C20:5*n*-3), DHA (C22:6*n*-3)	Food, feed
Carbohydrates	Ethanol and alcohols, starch, glucose, *β*-glucans	Nutraceuticals, biofuels
Pigments	ß-Carotene, astaxanthin, lutein, zeaxanthin, canthaxanthin, chlorophyll, fucoxanthin, phycocyanin, phycoerythrin	Nutraceuticals, cosmetics, dyes
Vitamins	A, B1, B2, B3, B5, B6, B7, B9, B12, C, E, Folic acid	Food supplements
Enzymes	Catalases, superoxide dismutase	Nutraceuticals, cosmetics, pharmaceuticals
Antioxidants	Polyphenols	
Phytosterols	Cholesterol, brassicasterol, sitosterol, ergosterol, campesterol, stigmasterol	Pharmaceuticals, cosmetics
Terpenoids	Squalene	Cosmetics
Biotoxins	Tetrodotoxin, okadaic acid, brevetoxin	Pharmaceuticals, bioactive molecules

Frustules and silica shelves	Nanoparticles	Drug delivery, new materials
H_2 producing enzymes	H_2	Biofuels
Glycolate	Fermentable substrate for methane production	Biofuels
Polyhydroxyalkanoates	Poly-3-hydroxybutyrate	Bioplastics
Phytohormones	Cytokinins, auxins, gibberellins, betaines	Agriculture
Exopolymeric substances	Mostly polysaccharides, proteins, DNA, RNA, other macromolecules	Surfactants, lubricants, biomedical and cosmetic applications

Despite the wide range of possible applications, microalgal biomass is chiefly produced for human consumption (nutraceuticals and food) and aquaculture feed (Garrido-Cardenas et al., 2018; Raja et al., 2008; Suleria et al., 2015). This selectivity arises from an economic limitation, since microalgal biomass is produced at a cost above 5 € kg^{-1} (Garrido-Cardenas et al., 2018; Llamas et al., 2021). The vitamin market is a good example of tough competition between production costs of microalgae with other alternative sources (i.e., fungi, bacteria and higher plants) with lower production costs (Borowitzka, 2013). Furthermore, microalgae biomass commonly presents low yields of high-value products. Therefore, several induction strategies have been applied at the operational level. For example, control of temperature and light can increase the content of the desired high-value metabolite of the cell. Unfortunately, this is commonly accompanied by a decrease in biomass productivity since the approaches for high added-value compound induction are mostly based on the employment of stressful conditions. Therefore, in microalgae screening, it is crucial to evaluate the productivity of the end product, as opposed to its content in algal-biomass alone (Slocombe et al., 2015).

Looking at the algal biomass production in Europe, there are still challenges to be addressed. EU food regulations are heavily applied to novel foods (EC 178/2002), food additives (EC 1331/2008), and genetically modified organisms (EC 1830/2003). However, the lack of a clear definition for the different microorganisms and their classification in the legislation (i.e., algae, cyanobacteria, and non-photosynthetic microorganisms such as thraustochytrids classified as “algae”), together with the diverse requirements of origin, safety standards, and organic certification criteria for EU and non-EU countries (mainly Asia), coupled with the weak control of biomass importation that fails to follow European rules, constrains EU competitiveness, and leads to unfair market competition.

Nonetheless, there are several benefits of using microalgae biomass over other biological sources or synthetic production:

- First, microalgae photosynthetic efficiency is known to easily surpass that of terrestrial plants, besides lower needs of drinkable water and arable land (Vecchi et al., 2020);
- Numerous microalgae have higher protein content than land plants with a relevant essential amino acid profile (Koyande et al., 2019), and the protein and free aminoacid contents can be easily manipulated through cultivation conditions;
- Several algae-based products present better bioactive activities than their alternative synthetic counterparts. For example, phycobiliproteins provide a non-toxic and non-carcinogenic natural food pigment alternative (Sekar and Chandramohan, 2008) while microalgal astaxanthin bears a superior antioxidant activity compared to its synthetic alternative (Capelli et al., 2013);
- Some microalgal products are still not economically feasible for organic synthesis, as is the case of fucoxanthin (D'Orazio et al., 2012);
- Microalgae provide an alternative source for long-chain polyunsaturated fatty acids (PUFA) such as eicosapentaenoic (C20:5*n*-3; EPA) and docosahexaenoic (C22:6*n*-3; DHA) acids, thus alleviating the pressure upon non-sustainable feedstocks (e.g., fish/soybean meal and oils) and avoiding the contaminants often present in these oil sources (Pereira et al., 2012);
- Life cycle analysis and product environmental footprint of microalgae production, with integration of wastewater bioremediation support the claim that microalgae-based products can be a sustainable process, while contributing to waste valorization (Arashiro et al., 2018).

However, to extend microalgal applications, it remains crucial to reduce production costs and increase productivity.

2.2. Cultivation

In general, autotrophic microalgae growth depends on light, CO_2, inorganic nutrients, and water. There are several types of microalgal production systems that provide suitable microalgae growth. They are usually classified as open systems, such as raceway ponds (RWP) or TL cascades (TLC); and closed systems, such as tubular or flat panel (FP) photobioreactors (PBRs) (Karemore et al., 2015) (Figure 2.*1*). Light is one of the most limiting factors in these cultivation systems; additional efforts to increase light availability are still required to attain high productivity goals.

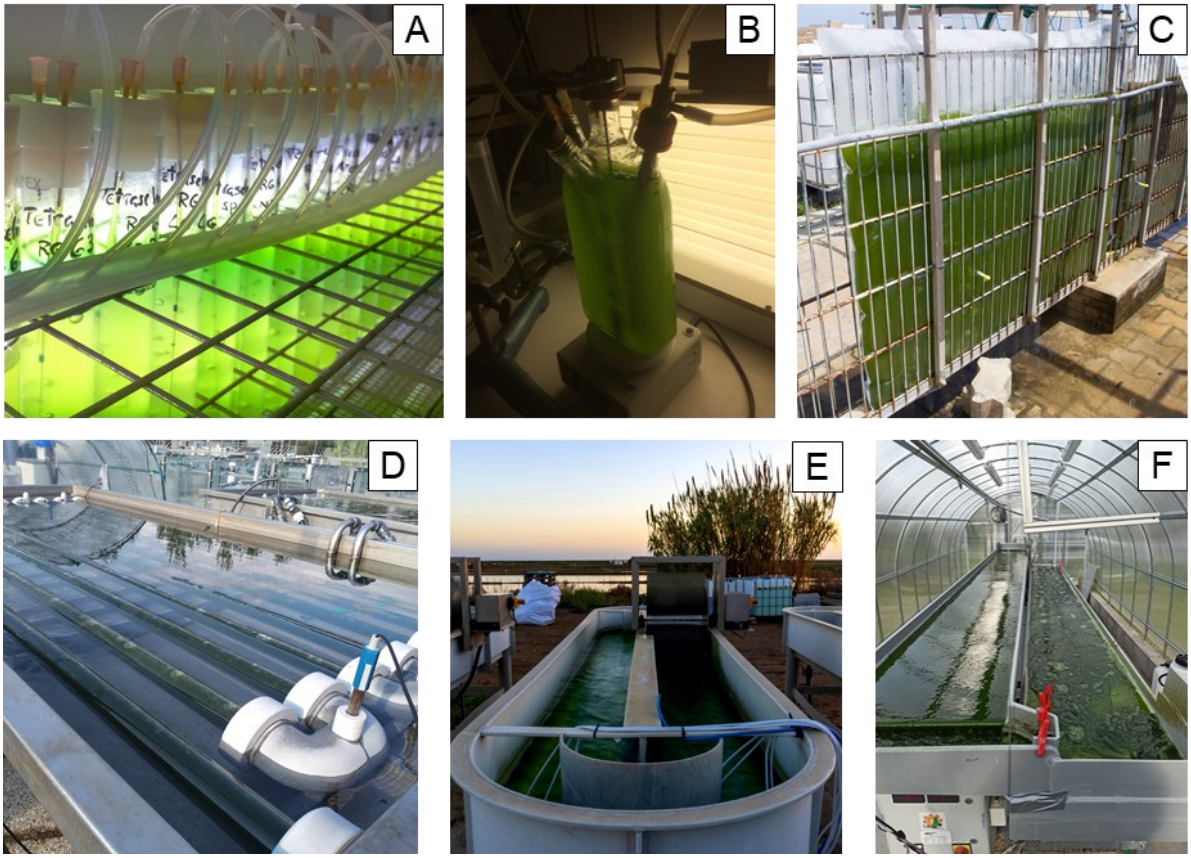

Figure 2.1. Photographs of different cultivation systems considered in this thesis. Closed systems at lab-scale: bubble columns (A) and flat-plate roux bottle (B); closed systems outdoors: flat plate (C) and horizontal tubular (D); open systems outdoors: raceway pond (E) and thin-layer cascade (F).

Cultivation systems differ significantly in biomass productivity, depending on their specific design and control of operational conditions. Open systems are conveniently cheaper, but have poor light penetration and CO_2 absorption, along with higher O_2 build-up and susceptibility to contamination by other microalgae, predators (e.g., rotifers and amoebae), and parasites (e.g., fungi and chytrids). Consequently, lower areal productivities range typically from 12 to 28 g m^{-2} day^{-1} (Davis et al., 2011; Llamas et al., 2021; Tredici, 2004). While closed systems exhibit a better performance in terms of light distribution, CO_2 absorption, and lower rates of contamination, with productivities between 10 and 45 g m^{-2} day^{-1}, they are more prone to overheating (Acién et al., 2012; Guerra et al., 2021; Llamas et al., 2021). Nonetheless, the high cost of closed systems makes them fit for high-value products only (Llamas et al., 2021).

Beyond the importance of the species and strains selected, the operation mode – batch, semi-continuous, and continuous – and metabolite induction strategies also greatly affect the success of cultivation. The quantity and quality of microalgal biomass and metabolites are influenced by several biotic and abiotic factors – including irradiance, temperature, nutrient availability, and renewal rate (Fábregas et al., 1984; Hu, 2013; Spoehr and Milner, 1949), even

among closely related strains. Even when all other culture parameters are optimized, cells in concentrated cultures are potentially exposed to high light and darkness on time scales much shorter than their acclimation responses. Regarding the cultivation system design and operation, attempts to improve photon distribution and minimize self-shading in the culture are focused on designing optically thin (shallow) cultures, e.g., TL systems (Grivalský et al., 2019), "fine-tuning" turbulence (Grobbelaar et al., 1996), and optimizing renewal rates to stimulate productivity.

Depending on its environment, the biochemical pathways in microalgal cells can undergo regulatory shifts to promote viability (e.g., towards protein, carbohydrate, or lipid biosynthesis) (Masojídek et al., 2013). Predictably, significant variations of biosynthesis rate of these compounds also occur during the circadian cycle. Understanding daily fluctuations of biomass and accumulation of biocompounds (lipid, protein, or carbohydrates) in microalgal cultures is of the utmost importance for the microalgal industry – and is one of the aspects that is greatly overlooked in most academic works. However, it is essential to note that the whole production process needs to be tailored to the final application, so one size does not fit all (Garrido-Cardenas et al., 2018). In this sense, using a multidisciplinary approach, the selected microalgae, and the most appropriate culture system and operational conditions are crucial steps to take into account to enhance productivity and satisfy marine-based bioproduct market (Haefner, 2003). These choices should be accompanied by an understanding of photosystem adaptation in the algal cell to prevent lower productivities or even culture crashes.

2.2.1. Photosynthesis

Green microalgae (*Chlamydomonas reinhardtii*, *Chlorella* spp.) and cyanobacteria (*Synechocystis* spp.) have been largely used as models for the study of photosynthesis (Jensen and Leister, 2014; Zallen, 1993). In these organisms, carbon dioxide and water are converted to carbohydrate and oxygen in thylakoid membranes, in the chloroplast for eukaryotes, and in the cytosol for prokaryotes (Walker, 1992). This process is divided into "light reactions", that occur in the thylakoid membrane of the chloroplast (Figure 2.2), and "dark reactions" (which may also occur in the light), that take place in the stroma (Falkowski and Raven, 2013; Whitmarsh and Govindjee, 1995).

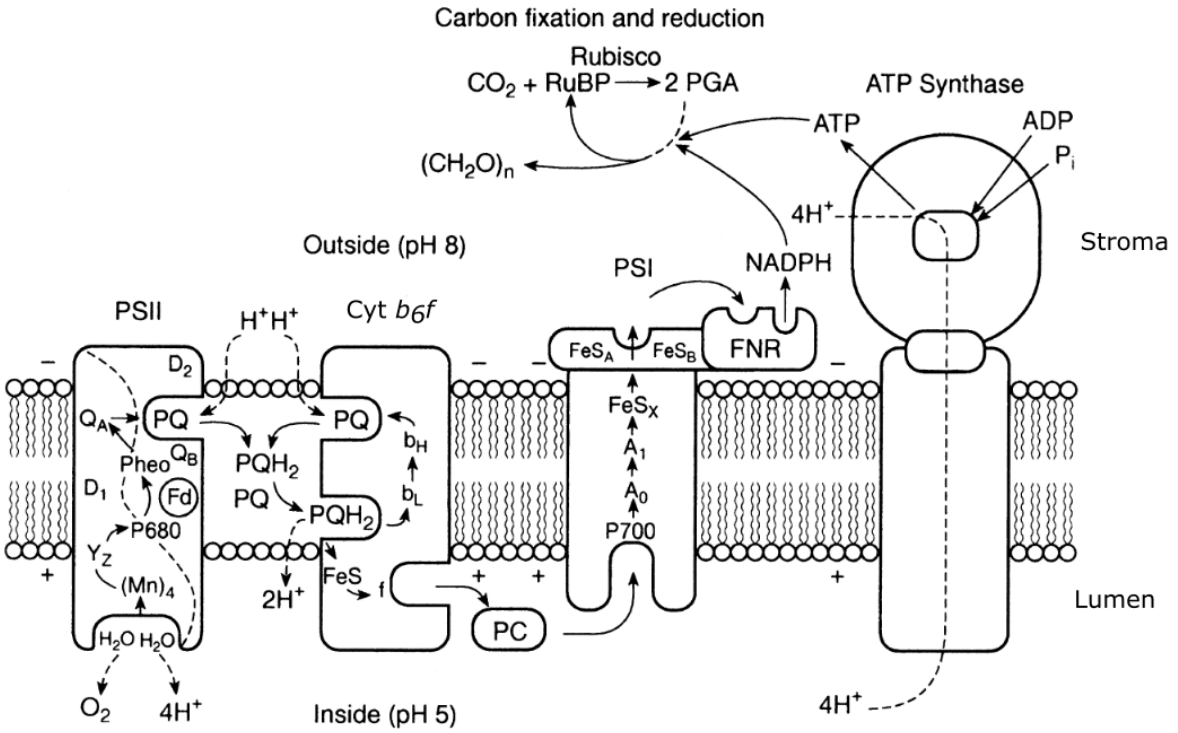

Figure 2.2. Schematic cross-section through a thylakoid membrane, showing the major components of the photosynthetic apparatus. Solid arrows indicate the electron-transport chain, and proton transport is indicated with dashed lines. Details are given in the text. *Abbreviations*: ADP, adenosine diphosphate; ATP, adenosine triphosphate; A_0, chlorophyll; A_1, phylloquinone; b_L and b_H, low and high forms of *b*-type cytochromes; *Cyt* b_6f, cytochrome b_6f complex; *f*, cytochrome *f*; Fd, ferredoxin; FeS, iron-sulfur centers; FNR, ferredoxin/$NADP^+$ oxidoreductase; H^+, *protons;* NADPH, nicotinamide adenine dinucleotide phosphate (reduced); PC, plastocyanin; PGA, 3-phosphoglycerate; Pheo, pheophytin *a* molecule; PQ, free (oxidized) plastoquinone; PQH_2, free (reduced) plastoquinol; PSI/PSII, photosystem I/II; P_{680} and P_{700}, the reaction center chlorophyll *a* molecules of PSII and PSI, respectively; P_i, inorganic phosphate; Q_A, bound plastoquinone; Rubisco, ribulose-1,5-bisphosphate carboxylase/oxygenase; RuBP, ribulose-1,5-bisphosphate; Y_z, tyrosine residue; +/−, polarity of electrical potential difference across the membrane established in the light; $(CH_2O)_n$, generalized carbohydrate. Light-harvesting complexes are not shown. The stoichiometry of protons, electrons, O_2, ATP, NADPH, and CO_2 is not indicated. Original from Whitmarsh and Govindjee (1995), and modified from Falkowski and Raven (2013).

Photosystems are composed of light-harvesting complex (LHC) antennas and reaction centers (RC). In LHC, antenna pigments are responsible for photon absorption and energy transfer to the photosynthetic RC. The photons captured by LHC are converted to an excited state of the antenna pigment molecule (Whitmarsh and Govindjee, 2003), and this energy is transferred until it reaches a particular chlorophyll *a* molecule in the RC known as the primary electron donor of photosystem II (PSII), and labeled as P680 (Cardona et al., 2012). The energy which is not used for photochemistry (photochemical processes) is dissipated thermally (via non-photochemical processes), and in the form of fluorescence or transferred to molecular oxygen forming excited singlet state oxygen species (Cessna et al., 2010; Logan, 2014). Microalgae have two types of RCs where charge separation occurs, and proton and electron transfer ensues (Gerotto et al., 2020; Guidi et al., 2017; Nugent et al., 2003). A type I RC is represented by photosystem I (PSI), since it uses iron-sulfur clusters as terminal electron acceptors; and a type II RC uses quinones as terminal electron acceptors, and is

represented by PSII (Antonkine and Golbeck, 2004). The photosystems operate in series, being connected by a chain of electron carriers, commonly termed the "Z scheme", as proposed by Hill & Bendall (1960). Starting with PSII and followed by PSI, the electron transport results in formation of adenosine triphosphate (ATP) molecules from ADP and inorganic phosphorus, and in production of nicotinamide-adenine dinucleotide phosphate (reduced; NADPH). This electron transport depends on metal ion complexes and aromatic molecules (including quinones, pheophytin, NADPH, tyrosine residues and flavoprotein) that function as electron carriers (Whitmarsh and Govindjee, 2003). In PSII, the manganese-containing enzyme from the oxygen-evolving complex starts by donating an electron to the tyrosine residue, which in turn donates an electron to P680. This results in the release of oxygen and protons to the thylakoid lumen, and in the formation of a strong reducing agent (P680*) (Leegood, 2004). Hence, P680* transfers the electron to a permanently RC-matrix bound plastoquinone (PQ) molecule, Q_A, via a pheophytin molecule (de Wijn and van Gorkom, 2001). In turn, Q_A^- reduces the loosely bound PQ, Q_b, until it forms plastoquinol (PQH_2) with two protons, which binds to, and reduces the cytochrome *b_6f* complex, releasing protons to the thylakoid lumen (de Wijn and van Gorkom, 2001; Leegood, 2004). Simultaneous to electron transport, a pH gradient is formed by higher accumulation of protons in the lumen and use of protons in the stroma for the reduction of nicotinamide adenine dinucleotide phosphate (oxidized; $NADP^+$) to NADPH. This gradient is then used to drive ATP synthesis (photophosphorylation) from ADP and inorganic phosphorus, catalyzed by the protein complex ATP synthase (Leegood, 2004; Masojídek et al., 2013).

A similar electron-excitation process occurs in PSI. A Cu-containing protein, plastocyanin (PC), mediates the continuity of electron transfer from the cytochrome *b_6f* complex to the RC of PSI (P700) (Leegood, 2004; Whitmarsh and Govindjee, 2003). P700* then reduces the small iron-sulfur protein, ferredoxin (F_d), via several electron carriers, specifically a chlorophyll monomer (A_0), a phylloquinone (A_1), and iron-sulfur clusters (F_x, F_A, F_B). This transport culminates in the reduction of $NADP^+$ to NADPH, with the help of ferredoxin-NADP reductase (Masojídek et al., 2013; Whitmarsh and Govindjee, 2003).

The NADPH and ATP formed provide the necessary reducing equivalents and energy for the dark reactions of photosynthesis – known as the Calvin-Benson cycle. These reactions promote reduction of carbon dioxide to carbohydrates or other compounds (Masojídek et al., 2013). This process develops in distinct phases, starting with carboxylation, where carbon dioxide and ribulose bisphosphate (RuBP) form phosphoglycerate, catalyzed by ribulose 1,5-bisphosphate carboxylase-oxygenase (Rubisco). The carboxylation product is converted to 3-carbon products (Triose-P) using NADPH and ATP in the reduction phase. Finally, RuBP is regenerated for further CO_2 fixation (Leegood, 2004; Masojídek et al., 2013). Although

carbohydrates are the primary end-product of photosynthesis, the actual resulting product can vary with growth conditions of the microalgal culture (Masojídek et al., 2013).

Microalgal photosystems are susceptible to multiple stressors, and therefore, they must display some plasticity to help in situations of potential damage. Although polypeptide D1 – part of the heterodimeric RC core of PSII, is the most frequent target of photodamage, it is also efficiently repaired (Rochaix, 2020; Whitmarsh and Govindjee, 2003). Photodamage can originate from the strongly oxidizing, water-splitting reaction in PSII, or when the energy of the absorbed light exceeds the photosynthetic apparatus capacity, thus resulting in the generation of reactive oxygen species (ROS) (Rochaix, 2020). Photodamage can be avoided by photoacclimation, or by releasing the excess exciton energy via dissipation as heat (Raven et al., 2020; Rochaix, 2020). However, if the rate of repair is lower than the rate of photodamage, this results in decreased photochemical activity of PSII, designated as photoinhibition (Raven et al., 2020).

In addition, it should be taken into account that photon capture events (~10^{-6} s) have much shorter timescales than CO_2 fixation (~1 s), and even shorter than acclimation to different light intensities (~10^3 s) (Beardall and Raven, 2013). Therefore, high photon fluxes often lead to "congestion" in electron transport and wasted photon energy. Hence, high light-adapted algae reduce the size of the light-harvesting antenna to decrease the collection rate of photons and prevent photoinhibition. This allows more light to penetrate into the culture and be utilized more efficiently (Beardall and Raven, 2013). While increasing pigment content improves light harvesting at low light levels, it also increases the chance of photodamage as well as of intracellular self-shading (package-effect), therefore, photon acquisition can actually become less efficient (Malerba et al., 2018).

Photoacclimation is achieved by different strategies including by changes in photosynthetic unit (PSU) number (RCs per cell; Pniewski and Piasecka-Jędrzejak, 2020) and size (Chl *a* per RC; Pierangelini et al., 2015; Six et al., 2008) as well by changing the light absorption efficiency per RC or the effective absorption cross-section (σ; Six et al., 2008). For example, at low irradiances, PSU size is decreased (less pigment per cell) which lowers photosynthetic rates, since less light is absorbed; however, this provides higher protection at excess irradiances (Six et al., 2008). In turn, there is a reduced need for investment in photoprotection mechanisms such as the water-water cycle and non-photochemical quenching (NPQ) (including the xanthophyll cycle) (Asada, 1999). Even though decreasing photosynthetic unit size can limit photoinhibition around midday, such a strategy would also decrease photosynthetic capacity near dawn and dusk – when photon flux is lower. Nonetheless the strategy employed is group (Falkowski and Owens, 1980), species (Six et al., 2008) and even strain-specific (Suggett et al., 2007). Therefore, ideally, the species chosen should be capable of good photosynthetic efficiencies at low light levels, have a high

tolerance for high light, and good stress management such as that from ROS in attempts to improve algal performance.

2.3. Chlorophyll *a* fluorescence

Successful cultivation depends on constant monitoring to ascertain the conditions that favor microalgae growth. This is typically accomplished by measuring cell concentration, culture nutrients, temperature, pH, and microscopic observation to analyze cell morphology and occurrence of contaminants. Additionally, monitorization of O_2 production or CO_2 uptake can provide information on the photosynthetic performance of the culture. However, the analysis of chlorophyll *a* fluorescence has the benefit of offering sensitive data on energy distribution between photochemical and non-photochemical processes (i.e., pathways that lead or not to production of reduced compounds, respectively) (Logan, 2014; Masojídek et al., 2021). When an excited chlorophyll singlet state returns to the ground state after transferring excitation energy for photochemistry, it can re-emit a photon – fluorescence – while another fraction is converted to heat – NPQ (Whitmarsh and Govindjee, 2003). Fortunately, this energy (which is not used for photochemistry) can be measured by a fluorimeter. Chlorophyll *a* fluorescence is thus a powerful, non-invasive, and fast tool to provide an array of information including, but not limited to, primary photochemistry and rates of electron transfer reactions in PSII (Govindjee, 2004; Masojídek et al., 2021). Fluorescence analysis can be divided into two types of measurements, fast fluorescence induction kinetics and saturating pulse analysis of fluorescence quenching, using pulse-amplitude modulation (PAM) techniques. Fast changes in chlorophyll *a* fluorescence, also termed the Kautsky effect (Kautsky and Hirsch, 1931), fluorescence transients or OJIP curves, can be used to understand the efficiency of electron transport through PSII by revealing the redox status of the photosynthetic electron transport chain (Stirbet et al., 2018). Conversely, the distribution of the absorbed energy between photochemical and non-photochemical processes is given by modulated fluorescence techniques, namely the measurement of NPQ and Photosynthesis-Irradiance curves, also known as light curves (LC; Masojídek et al., 2021). Chlorophyll *a* fluorescence was primarily used to provide a sensitive signature of photosynthesis status in plants and phytoplankton in natural environments and is currently acknowledged as a valuable tool in mass cultures of microalgae (Masojídek et al., 2021). A brief explanation of the three most frequently used protocols is detailed below.

2.3.1. Fluorescence transients – OJIP

The measurement of fluorescence transients, also known as OJIP curves are characterized by a fast (1 s) polyphasic rise from the origin (O = F_0) to the highest peak (P = F_m) via two curve inflections, J and I, even though more inflections can occur (Figure 2.3A).

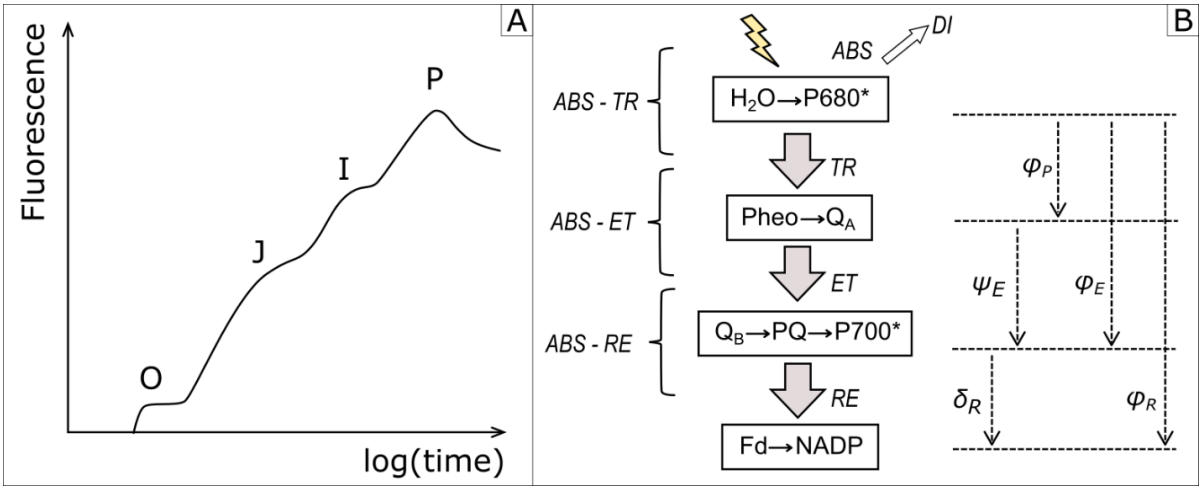

Figure 2.3. **A:** Schematic representation of the chlorophyll *a* fluorescence induction curve, known as the OJIP curve. **B:** Sequential energy fluxes from absorbance (ABS) of photons by PSII antenna and dissipation (DI), intermediate trapping flux (TR), electron transport (ET), and reduction of end-electron acceptors at the PSI electron acceptor side (RE) driven by PSI; φ_P (= TR/ABS), φ_E (= ET/ABS), φ_R (= RE/ABS), ψ_E (= ET/TR), and δ_R (= RE/ET) are proposed proxies for the ratios of the respective energy fluxes; the lighting symbol represents light, P680* is the primary electron donor of PSII; Pheo is pheophytin, the primary electron acceptor of PSII; Q_A, is the primary plastoquinone associated to PSII, Q_B is the secondary (electron acceptor) plastoquinone associated to PSII; PQ is plastoquinone in the PQ pool, P700* is the excited RC of PSI, Fd is ferredoxin, and NADP is nicotinamide adenine dinucleotide phosphate. **A** modified from Malapascua et al. (2014), and **B** from Gururani et al. (2015) and Stirbet et al. (2018).

To measure OJIP curves, the culture is dark-adapted to oxidize (open) all RC and is afterward exposed to a weak modulated measuring light (ML), which gives the fluorescence at the origin. A strong saturating actinic light is then turned on, promoting the rapid O-J rise (~2 ms) that reflects the reduction of Q_A. The dip after the J inflection suggests electron transport from one quencher to the next (e.g., $Q_A^- \rightarrow Q_B$). The second inflection I (~30 ms) reflects a temporary maximum of $Q_A^- Q_B^{2-}$ (Govindjee, 2004). The peak P is reached when the PQ pool becomes fully reduced (fully closed RC). Based on the dogma by Duysens and Sweers (1963), where the state of PSII RC is defined only by the redox state of Q_A when the primary acceptor is reduced (Q_A^-) and the RC closes, there is an increase in antenna chlorophyll *a* fluorescence. Conversely, this fluorescence is quenched when Q_A is in the oxidized state (Strasser et al., 2004).

This fast transient has been widely used to produce a proxy for the maximum quantum yield of PSII photochemistry, F_v/F_m, using the maximum (F_m) and minimum (F_0) fluorescence (Butler and Kitajima, 1975; Govindjee, 2004), calculated as shown in equation (2.1):

$$\frac{F_v}{F_m} = \frac{F_m - F_0}{F_m} \quad (2.1)$$

The popularity of this parameter is due to its sensitivity, with typical values of unstressed cultures ranging from 0.7 to 0.8 in microalgae. However, these values are dependent on irradiance regime and physiological treatment (Masojídek et al., 2013). Although these fluorescence parameters also exhibit circadian fluctuations, F_v/F_m values decrease considerably under stressful conditions. This decrease has been correlated with reduced O_2 evolution or CO_2 uptake (Genty et al., 1989).

Five energy fluxes are considered in the OJIP curves (Figure 2.3B): the absorbance flux (ABS) by the antenna of PSII RC, the trapping flux (TR) of open PSII RC that lead to the reduction of Q_A, the dissipation flux (DI) of untrapped excitation energy, and the energy flux associated with the electron transport from Q_A^- to intersystem electron acceptors (ET) and to the final electron acceptors of PSI (RE) (Stirbet et al., 2018). From the ratios of the corresponding energy fluxes, we can obtain several important parameters (equations 2.2-2.6; Strasser and Strasser, 1995):

$$\varphi_{P0} = \frac{TR_0}{ABS} = 1 - \frac{F_0}{F_m} = \frac{F_v}{F_m} \quad (2.2)$$

$$\varphi_{E0} = \frac{ET_0}{ABS} = 1 - \frac{F_j}{F_m} \quad (2.3)$$

$$\varphi_{R0} = \frac{RE_0}{ABS} = 1 - \frac{F_i}{F_m} \quad (2.4)$$

$$\Psi_{E0} = \frac{ET_0}{TR_0} = \frac{F_m - F_j}{F_v} = 1 - V_j \quad (2.5)$$

$$\delta_{R0} = \frac{RE_0}{ET_0} = \frac{F_m - F_i}{F_m - F_j} \quad (2.6)$$

The subscript "$_0$" refers to the fluxes at the onset of the fluorescence induction, while fluorescence levels are determined based on specific times of the transient (F_0, F_K, F_j, and F_i at ≈0.05, ≈0.3, ≈2, and ≈30 ms, respectively) and maximum fluorescence (F_m at ≈1 s). These examples are just a small sample of all the information provided by a one-second measurement (plus the time for dark adaptation) (Stirbet et al., 2018). The φ_{P0} parameter gives information on Q_A reduction, while ψ_{E0} gives the efficiency (ψ) with which a trapped exciton by PSII RC leads to electron transfer (ET_0) from Q_A^- to PQ, in the PQ pool, and δ_{R0} the efficiency (δ) of the electron transport (RE_0) from plastoquinol (PQH_2), in the PQ pool, to the final electron acceptors of PSI (e.g., Fd, $NADP^+$, O_2, thioredoxin) (Stirbet et al., 2018; Strasser et al., 1999).

Under stress, the electron transport chain can be compromised and thus is reflected in the OJIP curve and its parameters. Because of the extent of the topic, the reader is referred to the excellent review by Stirbet et al. (2018) for further details.

2.3.2. Modulated fluorescence

2.3.2.1. NPQ

Absorbed photons that cannot be used for photochemistry represent excess energy that needs to be dissipated to prevent damage to the photosynthetic apparatus. Because of the long period of photoacclimation – that can have a time scale of days –, this process can be insufficient for photoprotection which needs activation within minutes of excess light exposure to prevent photoinhibition (Nikolaou et al., 2016). NPQ is a fast regulatory response (within minutes) of PSII that can prevent damage to the photosynthetic machinery (Lavaud and Lepetit, 2013; Muller et al., 2001). NPQ introduces an alternative pathway to shorten the lifetime of the singlet chlorophyll excited states and hence competes with the production of chlorophyll triplet states (Schiphorst and Bassi, 2020). Therefore, NPQ can be activated by shifts in the redox potential of intramembranous electron transport intermediates, by shifts of the electrostatic potential at membrane surfaces, or by a high proton concentration in the lumen (Papageorgiou and Govindjee, 2014). Excess light can lead to inhibition of ATP synthase activity, which favors thylakoid lumen acidity, forming a trans-thylakoid pH gradient (ΔpH) and activating NPQ and violaxanthin de-epoxidase activity (Schiphorst and Bassi, 2020). De-epoxidation promotes conversion from the xanthophyll violaxanthin, primarily involved in light harvesting, to the photoprotective zeaxanthin (Z) via antheraxanthin (A). The xanthophyll cycles serve to dissipate excess electronic excitation and present a big diversity among microalgae which is dependent on their phylogeny (Papageorgiou and Govindjee, 2014; Tamaki et al., 2021). Found in many microalgae, zeaxanthin is a strong antioxidant and promoter of NPQ (Schiphorst and Bassi, 2020). NPQ can be further decomposed in its energy-dependent quenching (qE), inhibitory quenching (qI), state transitional quenching (qT), and zeaxanthin-dependent pH-independent quenching (qZ). A higher capacity to adapt to high irradiances relies on an effective quenching mechanism. However, a high qI can indicate photoinhibitory damage to PSII that can take from hours to days to be reversed, and can negatively impact the rate of photosynthetic production (Masojídek et al., 1999; Papageorgiou et al., 2007).

To analyze quenching components, it is necessary to start by dissipating the thylakoid pH gradient by dark adaptation. A low intensity ML, too low to induce electron transport but enough to elicit a minimum fluorescence value (F_0), is turned on (Figure 2.4).

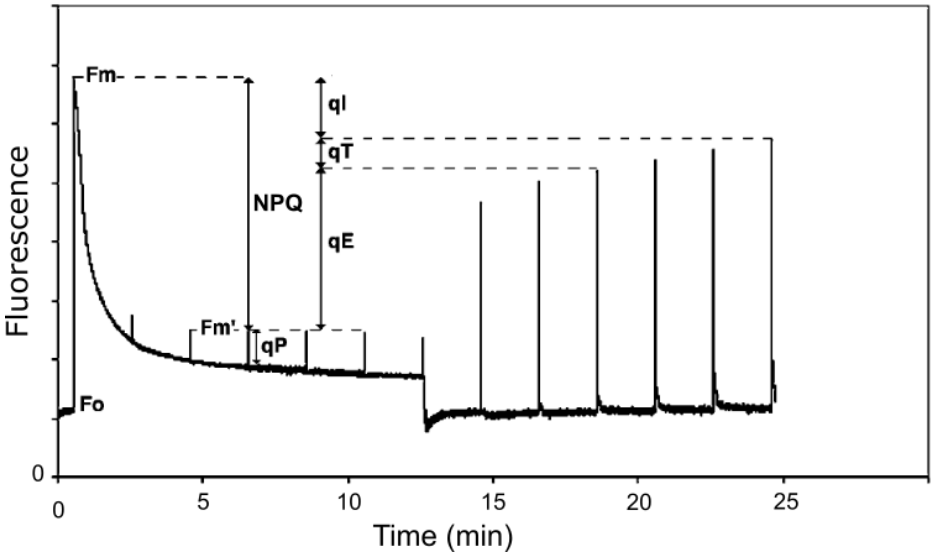

Figure 2.4. Example of a chlorophyll *a* fluorescence measurement, showing photochemical (qP) and non-photochemical quenching (NPQ). See text for details. Modified from Muller et al. (2001).

A saturating pulse is then emitted to close all RC, keep NPQ negligible and achieve maximum fluorescence (F_m). An actinic light is turned on to enable photosynthesis. Saturating pulses are applied until a steady state of maximum fluorescence in the light (F_m') is reached, which enables measurement of NPQ. NPQ can thus be determined by the Stern-Volmer relation, as shown in equation (2.6):

$$\mathrm{NPQ} = \frac{\mathrm{F_m} - \mathrm{F_m}'}{\mathrm{F_m}'} \tag{2.7}$$

A relaxation analysis can be performed by extending the protocol with the actinic light turned off. This allows observation of the dark recovery of cells and decomposition of NPQ to several of its components. A photochemical quenching parameter (qP) can also be found by using equation (2.7):

$$\mathrm{qP} = \frac{\mathrm{F'_m} - \mathrm{F}'}{\mathrm{F_m}' - \mathrm{F_0}'} \tag{2.8}$$

where, F' and F_0' represent the steady-state and minimum chlorophyll fluorescence in the light. Together, qP and NPQ allow the attribution of changes in PSII operating efficiencies to NPQ processes or the ability of an excited PSII RC to drive electron transport (Baker, 2008).

A more detailed description of non-photochemical quenching can be found by Demmig-Adams et al., (2014) and Muller et al. (2001).

2.3.2.2. Light curves

LC can reveal information about the photoacclimation status, and help explain the involvement of alternate oxygen-consuming electron transfer pathways (Masojídek et al., 2010). LC are derived from a culture exposed to several saturating pulses, under increasing light intensities. This allows the determination of the effective quantum efficiency of charge separation in actinic irradiance – effective quantum yield ($\Delta F'/F_m'$) according to Genty et al. (1989) as shown in equation 2.9:

$$\frac{\Delta F_v{}'}{F_m{}'} = \frac{F_m' - F'}{F_m{}'} \tag{2.9}$$

To estimate the photosynthetic rate from each data point, the relative electron transport rate (rETR) through PSII can be obtained by the product of $\Delta F'/F_m'$ by the irradiance intensity (E_{PAR}) as shown in equation (2.10) (Maxwell and Johnson, 2000):

$$\mathrm{rETR} = \frac{\Delta F'}{F_m{}'} \times E_{PAR} \tag{2.10}$$

while the linear electron transport rate (ETR) needs estimation of the light absorption specific cross-section of PSII (a^*) as equation 2.11:

$$\mathrm{ETR} = \frac{\Delta F'}{F_m{}'} \times E_{PAR} \times a^* \times \frac{\mathrm{PSII}}{\mathrm{PSI} + \mathrm{PSII}} \tag{2.11}$$

which is often not available; as well as the partition of electrons attributed to each PS, commonly assumed as 0.5 (i.e., agreeing with equal electron distribution among photosystem, although this is not always the case). Even though rETR is more susceptible to deviations caused by possible cyclic electron transport (Prášil et al., 1996), rETR is more frequently used than absolute ETR owing to its simplicity.

In view of the established relationship between quantum yield of CO_2 fixation and O_2 evolution to the effective quantum yield measured by chlorophyll *a* fluorescence (Genty et al., 1989; Masojidek, 2001), ETR is often assumed as a proxy for photosynthetic rate. In this sense, plotting ETR versus irradiance, yields a LC or rapid light curve (RLC; if steady-state is

not achieved) comparable to a photosynthesis versus irradiance (PE) curve. A schematic of a PE curve is shown in Figure 2.5.

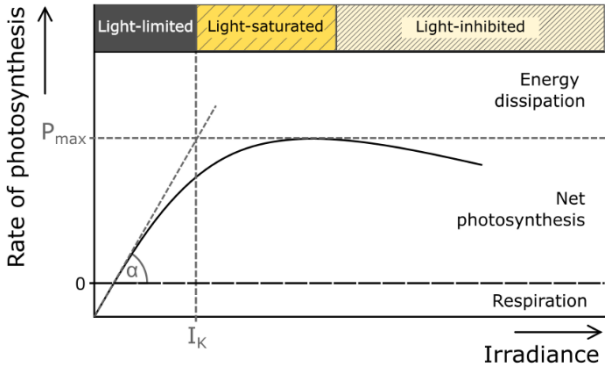

Figure 2.5. Schematic representation of the photosynthetic light-response curve (solid line), i.e., the dependency of photosynthesis on irradiance. The initial slope of the curve (α, dashed line) shows the maximum quantum efficiency of photosynthetic electron transport. The intersection between the maximum rate of photosynthesis (P_{max}) and α defines the end of the light-limiting region and the beginning of the light saturation irradiance (I_k). Light inhibition begins when the rate of photosynthesis starts to decline, commonly called down-regulation or photoinhibition. The rate of photosynthesis below zero is attributed to dark respiration. When the curve crosses 0 (light compensation point), it begins net photosynthesis (oxygen production), and over above P_{max} is excess energy dissipated. Modified from Malapascua et al. (2014) and Masojídek et al. (2013).

These curves unfold the irradiance where maximum ETR is attained (P_{max} or ETR_{max}) and the transition of light-limiting irradiance to light-saturating irradiance (I_k) from the intersection of the initial slope of the curve (α) with P_{max}. The eventual decrease in the photosynthesis rate at greater irradiances may indicate the onset of apparent photoinhibition. In this way, information on the saturation characteristics of electron transport has been found to directly reflect photosynthetic performance and growth of microalgal cultures (Malapascua et al., 2014; Masojídek et al., 2021). Excellent reviews of light-response curves have been published by Ralph and Gademann (2005) and Serôdio et al. (2006).

All these fluorescence analyses have proven useful to ascertain the physiological conditions of microalgae for different applications, including nutrient availability (Lakatos et al., 2021), monitoring of metabolite accumulation (White et al., 2011), estimation of growth (Figueroa et al., 2013; Gorbunov and Falkowski, 2021; Torzillo et al., 2012), monitoring photoinhibition (Serôdio et al., 2017; Torzillo et al., 1996), and determination of temperature

optima (Ranglová et al., 2019); and have been recently proposed as a possible indicator of the presence of predators in microalgae cultures (Deore et al., 2020).

2.4. Current challenges

Current challenges in the production of these photosynthetic micro-factories include selecting strains capable of withstanding potentially stressful conditions – light and temperature extremes and shifts, and tolerance to oxidative stress –, improved early detection of physiological stress and potential predators that can lead to culture crashes, and design of efficient cultivation systems. Although there are many applications and even advantages of using microalgae biomass, only a few species have been "domesticated" so far (Araújo et al., 2021).

Other approaches have focused on optimizing culture conditions and on advanced strain engineering designs, both of which greatly increased prediction accuracy and improve metabolite productivity. However, many metabolic pathways are complex, as their metabolites might be the substrates for more than one pathway, undergo bypasses (shunts) between alternative pathways, or even be under opposing, multifactorial regulatory loops due to one or multiple biotic or abiotic factors, all of which increase the difficulty of predictive modelling. Therefore, efforts should focus on a deeper understanding of carbon metabolism, nutrient dependence, and distribution of reactions on physiological and environmental factors controlling microalgal resource allocation to the multiple metabolic pathways (Gerotto et al., 2020). Hence, it is not surprising that strategies to prevent photodamage, that lead to a lower photosynthetic efficiency, are currently the subject of intensive research efforts toward increasing productivity (Vecchi et al., 2020). To attain the latter goal, biological (e.g., the selection of adequate strains), operational (e.g., optimization of cultivation conditions), and engineering (e.g., improvement of cultivation system designs) approaches should be proposed and implemented.

In microalgae cultivation systems, light is attenuated exponentially with culture depth and cell concentration, thus leading to growth-limiting conditions. Hence, optically dense cultures receive supra-optimal incident irradiances close to the surface of the cultivation system, using photons very inefficiently and possibly suffering from severe photoinhibition. Conversely, the remaining culture is severely light-limited and thus exists in virtual darkness (Ritchie and Larkum, 2012). Thus, one of the major challenges in mass culture of algae is still the maximization of light utilization efficiency.

Other constraints worth mentioning are production costs. Much effort has been put forward to diminish production costs by increasing productivity, while lowering capital (CAPEX) and operational (OPEX) expenditures and implementing low-cost biomass harvesting. Up until recently, cultivation costs only justified the extraction of high-value niche components. However, the integration of wastewater treatment in microalgae production permitted the valorization of the process by providing a service that results in clean water and cheaper biomass.

In summary, microalgae biotechnology should focus on screening and characterization of new robust algae strains (preferably not genetically modified); monitoring and understanding metabolic pathways that lead to increased productivity; and integration of cost-effective approaches that make the biological production system economically and sustainably viable.

Chapter 3

Lipid accumulation in selected *Tetraselmis* strains

This Chapter is based on the published article: Carneiro, M., Pôjo, V., Malcata, F. X. and Otero, A., 2019. Lipid accumulation in selected *Tetraselmis* strains. Journal of Applied Phycology 31, 2845-2853. DOI: 10.1007/s10811-019-01807-8.

Marine microalgae constitute a natural source of compounds (e.g., alkanes, TAG) useful for biodiesel production – yet improvement of lipid productivity by microalgae is a *sine qua non* for the economic feasibility of such a microalga-based process. Toward this goal, five *Tetraselmis* strains, *Tetraselmis suecica* UW605, *T. suecica* AROSA, and three *Tetraselmis* sp. strains, coded as lipogenic (63LG and 75LG) or non-lipogenic (46NLG) on the basis of stationary-phase cell flotation features, were cultured semi-continuously, and subjected to 10 and 30% renewal rates; the effects upon growth rate and lipidic profile were accordingly assessed. As expected, cell productivity by all strains was higher under a renewal rate of 30%. Chlorophyll, protein, and total lipid content per cell also increased with the highest renewal rate. Conversely, cell content of neutral lipids, measured with Nile red staining, decreased with increasing renewal rate. The non-lipogenic strain 46NLG revealed a much lower total lipid content, at the 10% renewal rate, than all other strains, but a higher neutral lipid content. This result supports the use of the flotation method for the selection of lipogenic strains. The diverse profiles of the various *Tetraselmis* strains, and the effect of renewal rate upon their neutral lipid content emphasize the importance of strain screening to promote a suitable microalgae selection for eventual biodiesel production purposes.

3.1. Introduction

Optimization of microalgae biomass production systems and selection of suitable strains are key factors for successful development of microalga-based cell factories. The intended profile of such biomass depends on the final product desired – be it for pharmaceutical, cosmetic, food, aquaculture, or biofuel purposes. Specifically for the latter, the rate of synthesis and accumulation of substrates, such as neutral lipids, mainly in TAG form that are susceptible to esterification to fatty acid methyl esters (FAMEs), is critical (Hu et al., 2008; Montero et al., 2011). The genus *Tetraselmis* comprises well-known, easy to cultivate species, bearing an interesting lipid profile that has been already explored for biofuel production suitability (Custódio et al., 2014; Montero et al., 2011; Pereira et al., 2016; Sansone et al., 2017; Tulli et al., 2012). Previous reports have shown that, under stress conditions, such as nitrogen deprivation (but not exclusively), *Tetraselmis* spp. contents in total lipids and (intracellular) neutral lipids and TAGs can increase significantly (Fon-Sing and Borowitzka, 2016; Pereira et al., 2016; Sharma et al., 2014; Tsai et al., 2016; Xu et al., 2013). However, other reports (Bondioli et al., 2012; Otero and Fábregas, 1997; Rodolfi et al., 2009) could not find substantially altered lipid contents when *T. suecica* was cultured under nitrogen-deficient conditions. This emphasizes that distinct mechanisms of stress response exist within the same genus of microalgae, which may lead to species-specific divergence.

Regarding abiotic parameters, the importance of operation mode has been overlooked in many studies. Several operational modes (e.g., batch, continuous, semi-continuous cultures) can be employed for microalgae production, depending on species and bioreactor configuration selected. Nonetheless, the elected regime will likely affect productivity and biochemical profile of the culture (Brown et al., 1993; He et al., 2016; Martínez-Macías et al., 2018; Otero and Fábregas, 1997). Continuous and semi-continuous cultivation modes can provide a stable biochemical profile – essential when assessing differences in biochemical profile and productivity of different strains (Otero and Fábregas, 1997). The semi-continuous cultivation mode is based on removal of part of the culture volume, and immediate replacement by fresh medium (at a given renewal rate); when this renewal process is repeated every 24 h under circadian light/dark cycles, the results obtained are similar to chemostat operation (Brown et al., 1993; Otero and Fábregas, 1997). The renewal rate by itself also affects growth parameters, as well as biochemical profile of the microalga at stake (Chini Zittelli et al., 2006; Fábregas et al., 1998, 1996; Otero and Fábregas, 1997; San Pedro et al., 2014). Renewal rate logically affects nutrient availability, as well as the amount of light received per cell, and consequently influences the stress level of cells; this leads to metabolic changes, and allows fine-tuning of the biochemical profile of the resulting biomass.

By resorting to the *Tetraselmis* genus, an economically appealing and biodiesel candidate, the present study aimed at evaluating differences in lipid productivity between different strains of said genus—including strains originally isolated by Prof. Ralph A. Lewin and categorized as lipidogenic (LG) and non-lipidogenic (NLG). This study compares growth and total lipid productivity of five *Tetraselmis* strains and includes use of the MUSE Cell Analyzer cytometer to rapidly and easily assess this effect upon neutral lipids. Flow cytometry, in combination with Nile Red staining (Satpati and Pal, 2015), can provide a rapid detection of neutral lipids. Strains were cultivated in semi-continuous mode, and subjected to two different daily renewal rates that generated nitrogen-limited and nitrogen-sufficient conditions.

3.2. Methods

3.2.1. Strains

Five different strains of *Tetraselmis* sp. were supplied by the laboratory of the Microbiology Department of the Centre for Biological Research of the University of Santiago de Compostela (CIBUS). These included two *T. suecica* strains tagged as AROSA (Otero and Fábregas, 1997) and UW605 (Provasoli-Guillard National Center for Marine Algae and Microbiota), and three strains of *Tetraselmis* sp. isolated by Prof. Ralph A. Lewin, and previously classified as lipogenic (63LG, 75LG) or non-lipogenic (46NLG) as per the flotation characteristics of stationary phase cells (R.A. Lewin, personal communication). This classification was based on the floating capabilities of cells under nitrogen starvation – when cells tend to synthesize more lipids or carbohydrates (Lewin and Cheng, 1989). The experiments were performed using three biological replicates for each strain.

3.2.2. Culture system

Cultures were maintained in tubular glass units, with 80 mL of culture medium, at 21 ºC. They were subjected to 12 h light/12 h dark cycles; two fluorescent tubes provided lighting equivalent to 160 µmol photons m^{-2} s^{-1}. The culture medium was composed of sterilized seawater (salinity 35‰), enriched with $NaNO_3$, 8 mM; NaH_2PO_4, 0.4 mM; $ZnCl_2$, 4 µM; $MnCl_2$, 4 µM; Na_2MoO_4, 4 µM; $CoCl_3$, 0.4 µM; $CuSO_4$, 0.4 µM; ferric citrate, 80 µM; thiamine, 0.528 µM; biotin, 0.082 µM; B_{12}, 0.009 µM; and Ethylenediamine tetra-acetic acid (EDTA) 106 µM (Fábregas et al., 1984). Cultures were aerated with filtered air, and supplemented with CO_2

every 10 min to keep pH between 7 and 8; the pH was monitored via two additional replicates of the cultures, placed on both ends of the air flow.

Cultures were inoculated at a cell density of 5 × 10^5 cells mL^{-1}, and maintained in batch mode; they were allowed to reach the early stationary phase (14th day) before the semi-continuous regime was started. This was accomplished by a daily harvest of 10% (from the 14th to the 18th day), and 30% (from the 18th to the 22nd day) of the volume of the cultures, with concomitant replacement with fresh medium enriched with nutrients at the same concentration. Renewal of cultures was carried out during the first hour of the light period.

Cell density was measured daily in the harvested cultures using Lugol to immobilize cells and counting with a Neubauer haemocytometer.

3.2.3. Chlorophyll

Samples were collected at the steady state, under the two renewal rates mentioned. For chlorophyll analysis, 3 mL of culture were centrifuged at 3,000 rpm for 10 min at 4 ºC. The supernatant was discarded and the pellets were stored at −20 ºC, and protected from light for later analysis. Then, 6 mL of methanol were added and vortexing took place for 30 s (or until the pellet was dissolved). The solution was sonicated on ice for 30 s × 3 (except 30 s × 6 for *Tetraselmis* sp. 46NLG replicates, as they proved more difficult to extract), in an ultrasonic homogenizer (4710 series). Afterwards, the samples were centrifuged, the supernatant collected, and absorbance measured in a spectrophotometer at 665 and 652 nm. Methanol was used as blank. Chlorophyll *a* and *b* concentration was determined using extinction coefficient calculations as mentioned in Porra et al. (1989) according to the following equations:

$$\text{Chl } a\ (\mu\text{g mL}^{-1}) = (16.29 \times \text{A}_{665.2}) - (8.54 \times \text{A}_{652.0}) \quad (3.1)$$

$$\text{Chl } b\ (\mu\text{g mL}^{-1}) = (30.66 \times \text{A}_{652.0}) - (13.58 \times \text{A}_{665.2}) \quad (3.2)$$

Total chlorophyll content was calculated as the sum of Chl *a* and Chl *b*.

3.2.4. Protein

Samples were collected at the end of the steady state, for the two renewal rates (10% on the 18th day, and 30% on the 22nd day). For protein analysis, 5 mL of culture were centrifuged at 5,000 rpm, for 5 min at 4 ºC. The supernatant was discarded, and the pellets

stored at −20 ºC for later analysis that was accomplished according to the Lowry method (Lowry et al., 1951) as modified by Herbert et al. (1971).

3.2.5. Lipid quantification

Samples were collected at early stationary phase, before the onset of the semi-continuous regime (14th day), and at steady state for each renewal rate (10% on the 18th day, and 30% on the 22nd day). For lipid analysis, 7 mL of culture were centrifuged at 3,000 rpm for 10 min at 4 ºC. Lipids were extracted according to Bligh & Dyer, (1959). The lipid extracts were dried, resuspended in chloroform and distributed in three replicates for quantification by the sulfuric acid charring method – using tripalmitine (Sigma-Aldrich, USA) as standard (Marsh and Weinstein, 1966).

3.2.6. Neutral lipid analysis

The stock solution of Nile Red reagent was prepared in acetone (100 µg mL^{-1}) in a flask protected from light. A working solution was prepared by diluting the stock solution in phosphate buffer solution (PBS; dilution factor 1:2.5).

Cell suspensions (100 µL) were diluted to ca. 3.0 × 10^5 cells mL^{-1} in PBS. From this dilution, 195 µL of each single-cell suspension was transferred, upon vigorous mixing, to Muse Cell Analyzer tubes, to which 5 µL of the previously prepared solution of Nile Red in PBS were added (Nile Red final concentration of 1 µg mL^{-1}). A blank was prepared by adding 5 µL of PBS to the cell suspension, instead of Nile Red solution. The samples were incubated for 5 min in the dark, resuspended, and read in the Muse Cell Analyzer, starting with the unstained sample to adjust parameters. Data were acquired using the Algae Nile-Red software module of the Muse Cell Analyzer (Millipore, Germany). Results were screened according to size to remove contaminants and debris, and specific populations were selected according to relative values of neutral lipid content (i.e., low, middle, and high).

3.2.7. Statistic treatment

The results were expressed as mean ± standard deviation (SD). Parametric tests were used to seek significant differences between means – in terms of chlorophyll, protein, lipid, and neutral lipid contents. These tests included one-way analysis of variance (ANOVA) and

Tukey test. Outliers, when found, were removed according to Bonferroni outlier test. Only results with $p < 0.05$ were considered as statistically different.

3.3. Results and discussion

3.3.1. Growth and chlorophyll concentration

All strains achieved similar cell densities within each renewal rate of 10 and 30%, but *Tetraselmis* sp. 46NLG that showed significantly lower cell density at both renewal rates (Table 3.1). Under the 10% renewal rate, *T. suecica* AROSA reached a cell density of 1.27 × 10^7 cells mL^{-1}, i.e., only slightly higher than *T. suecica* UW605 that achieved 1.21 × 10^7 cells mL^{-1} under the same conditions. Cell density predictably decreased in all strains upon application of the 30% renewal rate; the highest steady-state cell density, 1.17 × 10^7 cells mL^{-1}, was achieved by *T. suecica* UW605. Cell densities obtained were higher than those reported by (Otero et al., 1997) for *T. suecica* AROSA who found ca. 9 × 10^6 cells mL^{-1} and 6.5 × 10^6 cells mL^{-1}, under renewal rates of 10 and 30%, respectively, in an identical culture system. These results are, in any case, much higher than 1.5 × 10^6 cells mL^{-1}, reached by (Lim et al., 2012) in the stationary phase using batch cultures. Our higher values could be due to the higher concentration of $NaNO_3$ used in our cultures, coupled with a better control of pH; and also because strains *T. suecica* AROSA and UW605 were characterized by a smaller cell size (data not shown) when compared to the other strains and were thus able to reach higher densities (Agusti et al., 1987).

Table 3.1. Cell density of *T. suecica* AROSA, UW605, *Tetraselmis* sp. 63LG, 75LG and 46NLG at stationary phase and after 4 days under under renewal rates of 10 and 30%. Values are depicted as mean of four days during which they were subjected to each renewal rate ± standard deviation. Strains that do not share a letter, within each renewal rate, represent statistically significant differences ($p < 0.05$).

Strain	**Stationary phase** (10^6 cells mL^{-1})	**Renewal rate 10%** (10^6 cells mL^{-1})	**Renewal rate 30%** (10^6 cells mL^{-1})
T. suecica AROSA	12.7 ± 0.58	12.7 ± 0.59 (a)	11.0 ± 1.8 (a)
T. suecica UW605	13.8 ± 1.2	12.1 ± 0.92 (a,b)	11.7 ± 2.2 (a)
Tetraselmis sp. 63LG	8.54 ± 0.14	10.5 ± 0.91 (a,b,c)	9.66 ± 1.2 (a,b)
Tetraselmis sp. 75LG	8.65 ± 0.070	10.0 ± 2.0 (b,c)	8.84 ± 1.3 (a,b)
Tetraselmis sp. 46NLG	7.05 ± 0.15	7.85 ± 1.2 (c)	7.22 ± 1.1 (b)

Steady-state chlorophyll concentration did not reflect the differences between strains observed in steady-state cell density. Total chlorophyll content (chlorophyll *a* + *b*), in mg mL^{-1}, was higher for *Tetraselmis* sp. 75LG at both renewal rates, 10 and 30%, i.e., 0.046 and 0.047 mg mL^{-1}, respectively (Figure 3.1).

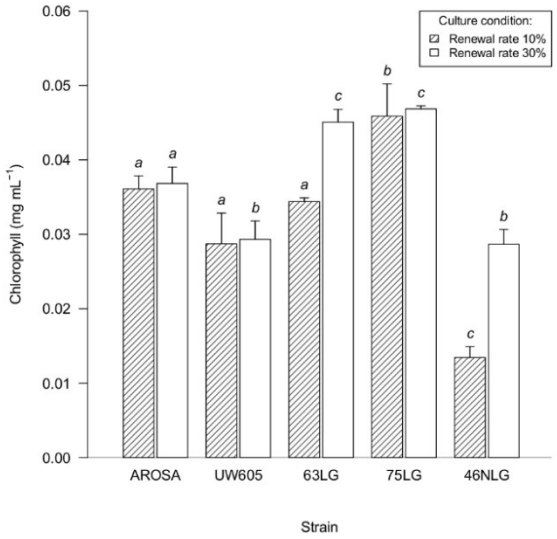

Figure 3.1. Average chlorophyll concentration, in mg mL^{-1}, in steady-state of semi-continuous cultures of *T. suecica* AROSA, UW605, *Tetraselmis* sp. 63LG, 75LG, and 46NLG for 10% renewal rate (dashed bars) and 30% renewal rate (open bars). Error bars represent the associated standard deviations. Strains that do not share a letter, within each renewal rate, represent statistically significant differences ($p < 0.05$).

Strain 46NLG showed a great increase in chlorophyll concentration between 10 and 30% renewal rates, thus indicating that this strain reduces drastically its photosynthetic machinery under nitrogen-limited conditions. Despite cell densities being lower under 30% renewal rates, chlorophyll concentration was in all cases higher than or equal to those under a renewal rate of 10%, as the result of an increase in cell chlorophyll content at higher renewal rates (Figure 3.2).

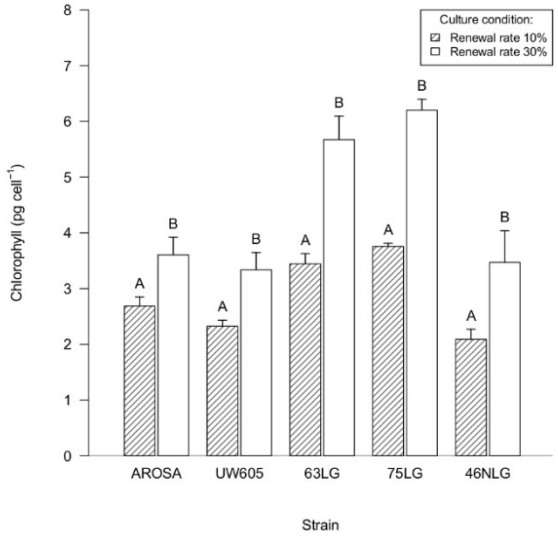

Figure 3.2. Average chlorophyll content, in pg cell^{-1}, in steady-state of semi-continuous cultures of *T. suecica* AROSA, UW605, *Tetraselmis* sp. 63LG, 75LG, and 46NLG for 10% renewal rate (dashed bars) and 30% renewal rate (open bars). Error bars represent the associated standard deviations. Renewal rates that do not share a letter, within each strain, represent statistically significant differences ($p < 0.05$).

The increase in chlorophyll cell content at higher renewal rate indicates that cultures maintained under renewal rates of 10% were nutrient-limited for all strains (Fábregas et al., 1995; Otero and Fábregas, 1997).

3.3.2. Protein concentration

In general, protein concentration increased when 30% renewal rates were applied, despite the lower steady-date cell density attained (Figure 3.3).

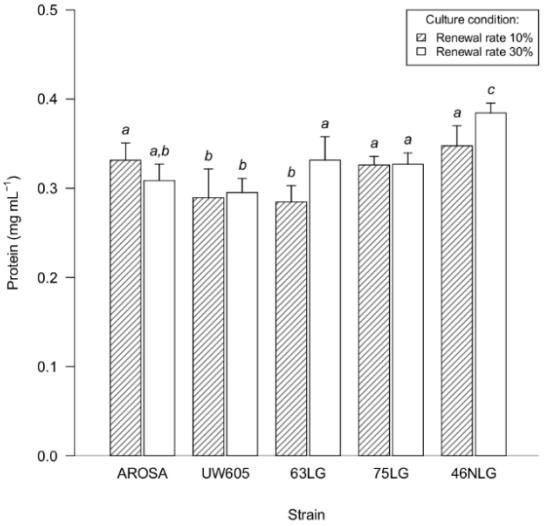

Figure 3.3. Average protein concentration (mg mL^{-1}) in the steady-state of semi-continuous cultures of *T. suecica* AROSA, UW605, *Tetraselmis* sp. 63LG, 75LG, and 46NLG, for 10% renewal rate (dashed bars) and 30% renewal rate (open bars). Error bars represent the associated standard deviations. Strains that do not share a letter, within each renewal rate, represent statistically significant differences ($p < 0.05$).

This is due to the increase in cell protein content, derived from the higher nitrogen availability at higher renewal rates, and again indicates that cultures were nitrogen-limited, at a renewal rate of 10% under the culture conditions applied (Dammak et al., 2017; Otero and Fábregas, 1997). Despite exhibiting the lowest steady-state cell densities, *Tetraselmis* sp. 46NLG achieved the highest protein content per cell of 44.3 pg $cell^{-1}$ and 53.2 pg $cell^{-1}$, for renewal rates of 10 and 30%, respectively, compared to the lowest protein contents per cell of 24.0 and 25.3 pg $cell^{-1}$, respectively, obtained with the strain UW605.

Protein synthesis mechanisms appeared more active under the 30% renewal rate. Increasing protein cellular content with increasing renewal rates has been previously reported, even under nitrogen sufficient conditions (Fábregas et al., 1996; Otero et al., 1997).

3.3.3. Lipid productivity

Looking at the results encompassing total lipid content per cell, an overall increase in lipid synthesis rate at higher renewal rates is apparent (Figure 3.4A).

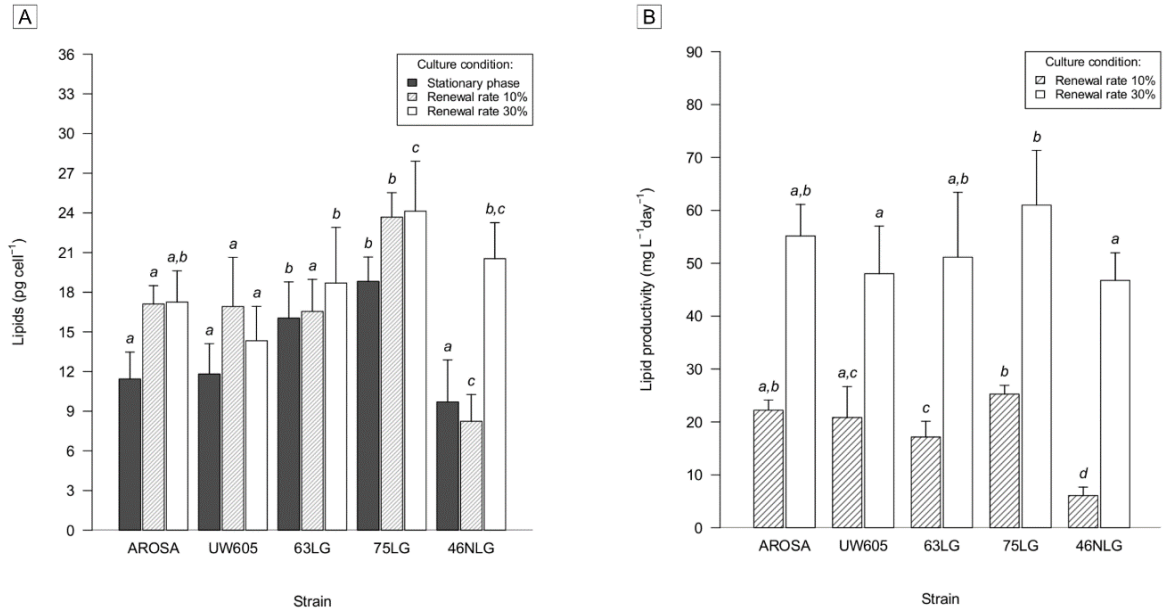

Figure 3.4. **A** Average total lipid content (pg cell^{-1}) of *T. suecica* AROSA, UW605, *Tetraselmis* sp. 63LG, 75LG, and 46NLG at the beginning of stationary phase, and after 4 days under 10% renewal rate (dashed bars) and 30% renewal rate (open bars). **B** Average lipid productivity, in mg mL^{-1} day^{-1}, of five different *Tetraselmis* strains (*T. suecica* AROSA, UW605, *Tetraselmis* sp. 63LG, 75LG, and 46NLG), under renewal rates of 10 and 30%. For both A and B, error bars represent the associated standard deviations (n = 3). Strains that do not share a letter, within each renewal rate, represent statistically significant differences ($p < 0.05$).

Such an increase in total lipids per cell is attributable to a gain of membrane lipids, derived from the photosynthetic machinery being activated by the increase in nutrient availability from the increased renewal rates, as previously reported for *T. suecica* AROSA in the same system (Otero and Fábregas, 1997). In fact, lipid cell content in cultures maintained at a renewal rate of 10% is clearly higher than that observed at stationary phase cells (Figure 3.4A); this holds for all strains but 46NLG. *Tetraselmis* sp. 75LG was again the strain with the highest lipid content under all conditions, with 23.7 and 24.1 pg of lipids cell^{-1}, under 10 and 30% renewal rates, respectively. Values of total lipid content per cell are similar to those found by Guzmán et al. (2010). The "non-lipogenic" strain *Tetraselmis* sp. 46NLG showed the lowest values of lipid content per cell after a 10% renewal rate, which correlates with the low chlorophyll values found; hence, the flotation method used to select cells with higher lipid content can be efficiently used for strain selection at large. It seems that strain 46NLG lost most of the photosynthetic membranes in response to nutrient limitation. Nonetheless, the same strain revealed the largest increment of lipid content under the 30% renewal rate, compared to the stationary phase (Figure 3.4). The low total lipid content in the stationary phase of strain 46NLG supports its classification of non-lipogenic – as assigned by the flotation method; and confirms suitability of this method for selection of strains and mutants with higher lipid content.

The *Tetraselmis* genus, when subjected to nitrogen deficiency, has revealed species-specific responses regarding lipid production (Bondioli et al., 2012; Dahmen-Ben Moussa et

al., 2017; Fon-Sing and Borowitzka, 2016; Otero et al., 1997; Pereira et al., 2016; Rodolfi et al., 2009; Sharma et al., 2014; Tsai et al., 2016; Xu et al., 2013). The lipid synthesis response to higher nutrient availability, at 30% renewal rate, by all strains reveals both absence of significant synthesis of reserve lipid under nutrient deficiency, and induction of membrane structural lipid synthesis under nutrient-sufficient conditions – which agrees with the increment of chlorophyll content.

As a consequence of higher lipid cell content, lipid productivity was higher under the 30% renewal rate for all strains (Figure 3.4B). The increase of renewal rate from 10 to 30% caused a 2–3-fold increase in lipid productivity, except for strain 46NLG that increased almost 8-fold, thus indicating once again a different metabolic control in this strain. Total lipid productivity was not that different among strains, except for the 46NLG strain, with a much lower lipid content under a renewal rate of 10%, resulting in much lower productivity (Figure 3.4B). The highest productivity, 61.0 mg L^{-1} day^{-1}, was achieved by *Tetraselmis* sp. 75LG, under a 30% renewal rate.

Nonetheless, protein content per cell (ranging from 24.0 to 53.2 pg protein $cell^{-1}$) was always higher than lipid content (ranging from 8.2 to 24.4 pg of lipids $cell^{-1}$), for all strains under every renewal rate. This was expected, considering that *Tetraselmis* is a well-known genus of protein-producing microalgae, although other strains have been reported to be high lipid producers as well (Pereira et al., 2016).

The presence of neutral lipids was quantified using Nile red staining and measured with the Algae Nile Red software of the Muse Cell Analyzer. Cell analysis clearly showed a downshift in the average cell neutral lipid content when increasing renewal rates. This shift in neutral lipid content of the population with higher renewal rates could be observed in all strains, but was much steeper in the case of strain 46NLG (Figure 3.5B).

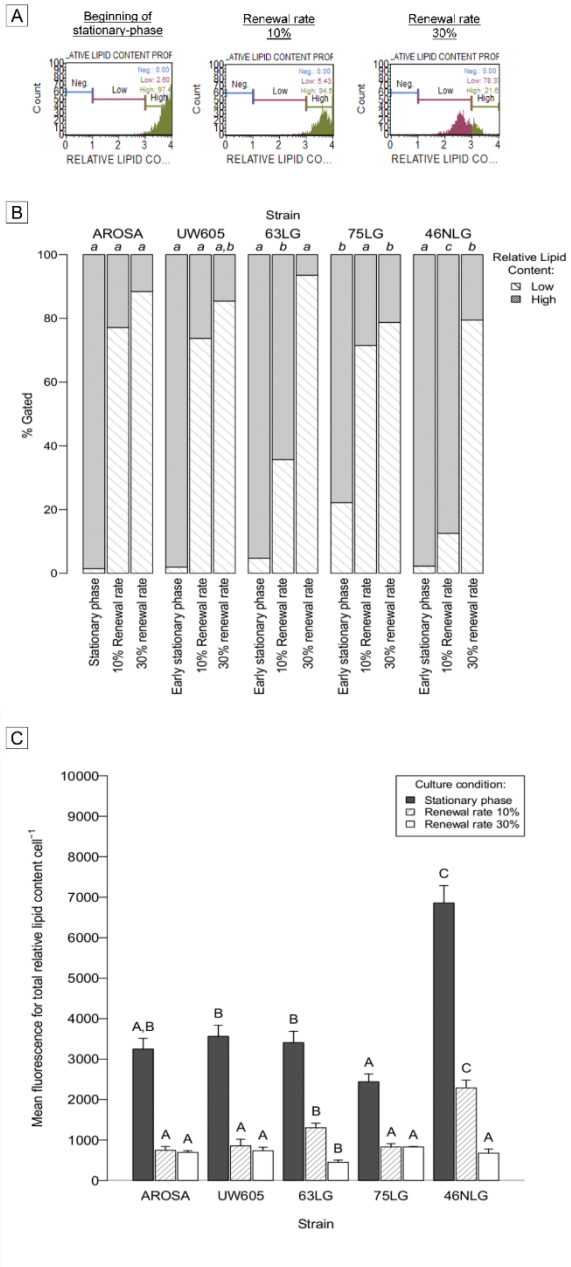

Figure 3.5. **A:** Example of flow cytometric histogram of a replicate of strain 46NLG using Algae Nile Red software module of Muse Cell Analyzer, showing the percent gated of the defined negative, low, and high lipid content populations at the beginning of the stationary phase, renewal rate 10% and renewal rate 30%. **B:** Percentage of gated cells, according to relative neutral lipid content profile, obtained using Algae Nile Red software module of Muse Cell Analyzer. Populations were separated by high and low (which includes low and negative) lipid content, as shown in A. Strains that do not share a letter, within each renewal rate, represent statistically significant differences ($p < 0.05$). **C:** Mean fluorescence of total neutral lipid content of the same five *Tetraselmis* strains under the same conditions, obtained with Algae Nile Red software module of Muse Cell Analyzer. Error bars represent the associated standard deviations. Strains that do not share a letter, within each renewal rate, represent statistically significant differences ($p < 0.05$).

In stationary phase, the strains had more than 95% of their population with relatively high lipid content, with the exception of *Tetraselmis* sp. 75LG. Under the 10% renewal rate, *T. suecica* AROSA and UW605, as well as *Tetraselmis* sp. 75LG underwent an abrupt change within the population – with more than 72% of cells categorized under low relative lipid content.

After the 30% renewal rate, cells with high relative lipid content represented no more than 21% of the population; strains *Tetraselmis* sp. 75LG and 46NLG exhibited the highest percentages of lipid content. Despite the low total lipid content of strain 46NLG (Figure 3.4A), this strain entails the highest percentage of cells with high neutral lipid content under a renewal rate of 10% (Figure 3.5B).

The average neutral lipid cell content, measured via Nile red fluorescence, revealed an opposite response to that pertaining to total lipid content per cell (Figure 3.5C). Neutral lipid content for all strains was negatively affected when renewal rates were applied. Furthermore, strain *Tetraselmis* sp. 46NLG showed the highest neutral lipid content in both early stationary phase and under the 10% renewal rate. Highest neutral lipid content after the 30% renewal rate was achieved by *Tetraselmis* sp. 75LG strain. However, values do not differ much among species for this renewal rate, with the exception of *Tetraselmis* sp. 63LG that exhibits a significantly lower value (Figure 3.5C).

Results of synthesis of neutral lipid content followed a pattern distinct from that of total lipid content. In fact, the former indicates that total lipid content data alone can lead to an incomplete interpretation of the cell profile. A great change in neutral lipid content, from the early stationary phase, is unfolded when compared to the 10% renewal rate. This suggests that neutral lipids are accumulated by *Tetraselmis*, but only during the late stationary phase. This was also observed by (Guzmán et al., 2010) who reported higher cell content of neutral lipids in *T. suecica* in the stationary growth phase than in the exponential phase.

Absence of lipid accumulation, found in most of our strains under nitrogen limitation, has also been reported elsewhere (Bondioli et al., 2012; Otero et al., 1997; Rodolfi et al., 2009). Nevertheless, preceding work using nitrogen deprivation produced improvements in lipid accumulation using this genus. With regard to *Tetraselmis* sp. cultures, Tsai et al. (2016) observed a lipid content maximum of 24.5% of the biomass in 7-day, nitrogen-starved cultures, as opposed to 15.3% of nitrogen-sufficient cultures grown in 3.3% NaCl. An increase in lipid content from 10% to ca. 33% of DW was also observed in *Tetraselmis* sp. lipid bodies, after the aforementioned nitrogen starvation (Tsai et al., 2016). A 1.6-fold increase of the maximum volume of intracellular neutral lipid to 9.78 μm^3 $cell^{-1}$ was observed using *Tetraselmis subcordiformis*, when compared to nitrogen sufficient conditions (Xu et al., 2013). In addition, *Tetraselmis* sp. that received an additional treatment of UV-C radiation increased TAG content to about 60 μg mL^{-1} (Sharma et al., 2014). Nile red staining of these cells also indicated an increase in cell size and additional accumulation of lipid bodies after the said treatment.

Our results unfold important variations in total and neutral lipid accumulation profiles within the *Tetraselmis* genus. For the microalga-based biodiesel industry, robust species as the ones found within this genus are relevant, since they can have an appropriate fatty acid profile for biodiesel production in addition to other advantages (Pereira et al., 2016).

Nonetheless, understanding the mechanisms that lead to accumulation of lipids and other storage metabolites are important in order to increase our knowledge of these biological systems, and also to achieve the high productivities required by commercial processes. For this reason, fast screening techniques able to identify higher total lipid or neutral lipid contents (like the ones used in this study) appear important to rapidly select high-lipid producers.

3.4. Conclusion

The results generated indicate that different strains within the same genus may entail different cellular biochemical profiles, despite their common behavior upon application of renewal rates. Although application of 30% renewal rates increased lipid productivity, it had a negative effect upon neutral lipid production. The non-lipogenic strain 46NLG exhibited the most disparate behavior among all *Tetraselmis* strains – with a much lower total lipid content, but a much higher neutral lipid fraction under 10% renewal rates than all remaining strains. This supports that the flotation method, originally used by R. A. Lewin, is a useful tool to select lipogenic strains using total cell lipid content as criterion.

After acquaintance with a given microalga behavior and profile, rapid assessment of neutral lipids, through flow cytometry, can aid in the determination of the harvesting time (Guzmán et al., 2010). On the other hand, the correlation between fatty acid profiles and renewal rates could reveal interesting information on strain specific behavior.

Chapter 4

Effect of temperature on growth, photosynthesis and biochemical composition of *Nannochloropsis oceanica*, grown outdoors in tubular photobioreactors

This Chapter is based on the published article: Carneiro, M., Cicchi, B., Maia, I.B., Pereira, H., Zittelli, G. C., Varela, J., Malcata, F.X. and Torzillo, G., 2020. Effect of temperature on growth, photosynthesis and biochemical composition of *Nannochloropsis oceanica*, grown outdoors in tubular photobioreactors. Algal Research 49, 101923. DOI: 10.1016/j.algal.2020.101923.

Since temperature is an important factor affecting microalgal growth, photosynthetic rate and biomass composition, this study has accordingly focused on its effects on biomass yield and nighttime biomass loss, as well as photochemical changes, using *Nannochloropsis oceanica* as model species, grown in two outdoor 50-L tubular photobioreactor (PBR). In two independent trials, cultures were subjected to a diurnal light:dark cycle, under a constant temperature of 28 ºC and, on the second trial, at 18 ºC. Changes in culture performance were assessed by measuring growth, lipid and fatty acid composition of the biomass in both morning and evening. Our results revealed that *N. oceanica* shows a wide temperature tolerance with relevant nighttime biomass loss, that decreased at lower temperatures, at the expense of lower daily productivity. Fluorescence measurements revealed reversible damage to photosystem II in cells growing in the PBR under optimal thermal conditions, whereas

microalgae grown at suboptimal ones exhibited an overall lower photosynthetic activity. Lipids were partially consumed overnight to support cell division and provide maintenance energy. eicosapentaenoic acid (EPA) catabolism reached a maximum after the dark period, as opposed to their saturated counterparts; whereas lower temperatures led to higher EPA content, which reached the maximum in the morning. These findings are relevant for the production of *Nannochloropsis* at industrial scale.

4.1. Introduction

Microalgae entail a multitude of applications that make them attractive as commercial commodities (Spolaore et al., 2006). However, the industrial production of microalgal biomass is hindered by many biotic and abiotic factors that reduce productivity, thus compromising attempts to reduce production costs. Suboptimal temperature is one of the environmental factors known to significantly decrease biomass productivity (Grobbelaar and Soeder, 1985; G Torzillo et al., 1991). Unfavorable thermal conditions can bring about a decrease in biomass productivity throughout the day, as well as an increased nighttime biomass loss (Grobbelaar and Soeder, 1985; G. Torzillo et al., 1991). In fact, cells metabolize a wide array of reserve biomolecules at night, in order to produce maintenance energy, support cell division, and provide carbon skeletons for the synthesis of compounds, resulting in biomass loss (Ogbonna and Tanaka, 1996). Previous reports have described nighttime biomass losses reaching up to 30% of the daily yield, and the highest value reported was 42% of the daily yield by *Arthrospira platensis* (Edmundson and Huesemann, 2015; Geider et al., 1989; Torzillo et al., 1993). In addition, microalgae are exposed to high radiation levels when grown outdoors which, combined with suboptimal temperatures, can unbalance biochemical composition and promote nighttime biomass losses (Ogbonna and Tanaka, 1996). Since both temperature and irradiance have a great influence on photosynthesis, and concomitant biomass growth, it is important that these parameters are monitored for putative commercial applications – and, if possible, adjusted to their optimal values, making it possible to direct synthesis towards specific target molecules.

The Eustigmatophyte *Nannochloropsis oceanica* is a unicellular, fast growing, resilient microalga, able to accumulate large quantities of lipids and eicosapentaenoic acid (EPA), which constitutes a key factor for its commercial development (Sukenik, 1991). The aim of this study was to study the influence of suboptimal temperature on the growth physiology, biochemical composition and nighttime biomass loss of *N. oceanica*, grown outdoors in thermoregulated tubular photobioreactors (PBRs).

4.2. Methods

4.2.1. Outdoor pilot PBR

The study was carried out in Florence, Italy (N 43.8º, E 11.3º). Each PBR consisted of ten parallel Pyrex tubes (length 2 m, i.d. 4.85 cm) connected by PVC (polyvinylchloride) U-bends with watertight flanges, providing a working volume of 50 L. Each reactor was placed in a stainless-steel basin containing thermostatted demineralized water. The culture was recycled by a PVC pump with three flat PVC blades at 120º from each other on the propeller shaft; the distance between blades and casing was 1.3 cm. The PBR included a 2.2-L transparent PVC cylindrical degasser, where air and CO_2 were supplied. The cultures were operated at a constant pH of 8, by CO_2 injection on demand. A circadian cycle was set by covering the cultures with a dark plastic sheet in the evening at 6:00 pm and removing it at 8:00 am of the following morning, thus providing a 10:14 light:dark (L:D) period. Two identical tubular PBRs were used for the experiments.

4.2.2. Experimental set-up

One PBR (i.e., the control) was kept at 28 ± 1 ºC during the light periods, from 8:00 am to 6:00 pm; in the evening, the temperature was decreased to 18 ± 1 ºC and kept constant overnight (from 6:00 pm to 8:00 am). Two sequential experiments were carried out, in which two different temperature regimes were applied to the second PBR (Table 4.1).

Table 4.1. Experimental plan reporting the temperatures during daytime (starting at 8:00 am) and nighttime (starting at 6:00 pm), for each condition within each trial. Because only two photobioreactors (PBR) were available, the trials were carried out in sequence with a control PBR for each experiment.

Trial	Condition	Daylight temperature (8 am-6 pm)	Nighttime temperature (6 pm-8 am)	Experimental period	Mean daily irradiance
1	28:18 ºC L:D	28 ± 1 ºC	18 ± 1 ºC	July 26th to August 3rd	20.3 ± 3.21 MJ m^{-2} day^{-1}
	28:28 ºC L:D	28 ± 1 ºC	28 ± 1 ºC		
2	28:18 ºC L:D	28 ± 1 ºC	18 ± 1 ºC	August 27th to September 4th	16.4 ± 4.03 MJ m^{-2} day^{-1}
	18:18 ºC L:D	18 ± 1 ºC	18 ± 1 ºC		

In the first trial, the PBR was kept at the constant temperature of 28 ± 1 ºC by day and by night. While in the second trial, the PBR was maintained at 18 ± 1 ºC by day and by night.

4.2.3. Microorganism and culture conditions

The microalga *N. oceanica*, kindly provided by Dr. Avigad Vonshak (Institute for Desert Research, Ben-Gurion University, Israel), was selected for its fast growth, high lipid content and commercial interest. Cultivation was scaled up to two outdoor 50-L tubular PBRs using F medium enriched with $NaHCO_3$ (6 mM), and 10-fold the values of $NaNO_3$ (17.7 mM) and NaH_2PO_4 (0.84 mM) of the original recipe (Guillard and Ryther, 1962). Once the culture reached a biomass concentration of ca. 0.8 g L^{-1} of dry weight (DW), a semi-continuous regime was initiated. For this purpose, a part of the culture was removed every day and replaced with fresh medium to achieve ca. 0.45 g L^{-1} of DW at the beginning of the light period, which avoided any nutrient depletion. Solar irradiance data were supplied by the Laboratory for Meteorology and Environmental Modelling (LAMMA; CNR, Florence, Italy), located close to the area where experiments took place. Sampling was performed every morning at 8:00 am (i.e., before removing the culture covers), and at 6:00 pm at the end of light period (i.e., before covering the PBRs).

4.2.4. Measurements

4.2.4.1. Growth

Growth was assessed through both biomass DW and cellular concentration. DW measurements were performed in duplicate by filtering 10 mL of culture through pre-weighed 47-mm diameter glass microfiber filter membranes (Whatman GF/F, Maidstone, England). The pellets on the filters were washed twice with deionized water and oven-dried afterwards at 105 ºC until constant weight. Cell counts were carried out in duplicate, using a Bürker counting chamber. Nighttime biomass loss was calculated as the difference between DW measured in the evening and that measured in the following morning, just before removing the covers.

4.2.4.2. Fluorescence measurements

Chlorophyll fluorescence measurements were carried out with a pulse-amplitude-modulation fluorimeter (PAM-2100, H. Walz, Effeltrich, Germany), operated with PamWin

(version 2.00f) PC software. Triplicate samples were incubated for 15 min in the dark, to oxidize all plastoquinone (Q_A) and ensure membrane relaxation. A weak light (0.5 µmol m^{-2} s^{-1}) was applied to measure the minimum fluorescence in the dark-adapted state (F_0). A strong saturating pulse (6,000 µmol m^{-2} s^{-1}) was then supplied to close all RC (i.e., to fully reduce all Q_A) and reach the maximum fluorescence yield (F_m). The maximum photochemical quantum yield of PSII (F_v/F_m) was then calculated as the ratio between variable ($F_v = F_m - F_0$) and maximum fluorescence (F_m) (Butler, 1978; Genty et al., 1989). Kautsky's curves (OJIP fluorescence induction kinetics) were recorded daily, in the morning and evening, using the Handy Plant Efficiency Analyser (PEA; Hansatech Instruments). Samples were dark adapted for 15 min, and then illuminated with continuous saturating light. The fluorescence transients were analyzed with the Biolyzer HP3 software package. Since the light intensities were high enough to reach the maximum value F_m, the transients were normalized both on F_0 and F_m basis, so as to permit comparison of the shapes of the curves. Measurements were conducted in triplicate. OJIP-determined parameters for each condition were normalized to their corresponding controls, in order to clarify the impacts of temperature upon the photosynthetic machinery. OJIP curves are shown for the second and seventh day (which is the last complete day) of each trial.

4.2.4.3. Oxygen evolution and respiration measurements

For photosynthetic oxygen evolution measurements, 2 mL samples were loaded in a Liquid-Phase Oxygen Electrode Chamber (Hansatech, DW3) thermostated at 28 ºC, and equipped with an oxygen control electrode unit (Hansatech, Oxy-lab) and a magnetic stirrer. Light was supplied via a red light emitting diode (LED) source (Hansatech LH36/ 2R), with nominal wavelength of 660 nm, providing 600 µmol photons m^{-2} s^{-1}. Before oxygen measurements, samples were purged with N_2 to reduce dissolved O_2 below saturation. Afterwards, the light was turned on, and the O_2 concentration monitored at an acquisition frequency of 1 reading s^{-1}. Measurements of respiration were carried out in triplicate, at the end of the photosynthesis measurements. Results are shown in µmol of O_2 μg^{-1} chl *a* h^{-1}.

4.2.4.4. Pigments

For pigment extraction, duplicate samples of 2 mL were collected, and centrifuged at 2,650 *g* for 10 min. The supernatant was discarded, and glass beads were added to the pellet – which was then resuspended in 3 mL of acetone (90% v/v). The samples were vortexed for 5 min, and centrifuged again afterward. The supernatant was transferred to a clean tube, and the pellet subjected to two additional extractions with 2 mL of acetone, and a final centrifugation. Absorbance measurements were taken at 663 (A_{663}) and 750 nm (A_{750}; to

correct for turbidity). The total chlorophyll *a* was determined based on the equation by SCOR-UNESCO (1966):

$$\text{Chlorophyll } a \ (\mu\text{g mL}^{-1}) = 11.64(\text{A}_{663} - \text{A}_{750}) \quad (4.1)$$

the equation was duly truncated, since this microalga is known to possess only chlorophyll *a* (Brown, 1987).

4.2.4.5. Lipid content

The lipid content was determined by collecting 5 mL of culture, in triplicate, which was centrifuged at 2,650 *g* for 10 min. Lipids were extracted according to Bligh and Dyer (1959), and quantified according to Marsh and Weinstein (1966). The pellets were previously washed with a solution of sodium chloride (9 g L^{-1}). For extraction, a mixture of chloroform:methanol (1:2 v/v) was used, along with bead beating for 5 min, and sample heating in a thermoblock at 60 ºC for 3 min. Following extraction, the organic phase was collected and dried. Extracts were resuspended in a known volume of chloroform and distributed in duplicate. The samples were heated in sulphuric acid at 200 ºC for 15 min, along with the prepared standard of tripalmitine (Sigma-Aldrich, USA). After the samples were cooled and distilled water added, the absorbance was read at 375 nm. Measurements are expressed in pg of lipids $cell^{-1}$.

4.2.4.6. Fatty acid analysis

Extraction and conversion of samples to fatty acid methyl esters (FAME) were done following a protocol by Folch et al. (1957) and Lepage and Roy (1984), with modifications as described by Pereira et al. (2012). Briefly, freeze-dried biomass samples were mixed, in a reaction vessel, with a solution of methanol:acetyl chloride (20:1 v/v), and then homogenized with an Ultra-Turrax disperser (1.5 min at 23,000 rpm; T18 digital ULTRA-TURRAX, IKA-Werke GmbH & Co. KG, Staufen, Germany). After adding *n*-hexane, the mixture was subjected to derivatization at 70 ºC for 1 h. The lipidic phase was separated via addition of distilled water and *n*-hexane, followed by vortexing and centrifuging (this step was repeated 3 times). The residual water of the organic phase was removed by adding anhydrous sodium sulphate. Extracts were filtered, dried under nitrogen gas flow, and resuspended in gas chromatography (GC) grade *n*-hexane. Analysis was performed in a Bruker gas chromatograph, coupled with an MS detector (Bruker SCION 456/GC, SCION TQ MS) equipped with a ZB-5MS capillary column (30 m × 0.25 mm internal diameter, 0.25 µm film thickness, Phenomenex), and using helium as carrier gas. The GC oven temperature profile was set to 60 ºC (1 min), 30 ºC min^{-1} to 120 ºC, 5 ºC min^{-1} to 250 ºC, and 20 ºC min^{-1} to 300 ºC (2 min). The commercial standard,

Supelco® 37 Component FAME Mix (Sigma-Aldrich, Sintra, Portugal), was used to prepare the different calibration curves. Results are expressed as percentage of the total fatty acid content.

4.2.5. Statistical analysis

In each day, differences in biomass growth and loss between each condition (28:28 ºC, L:D and 18:18 ºC, L:D), relative to the corresponding controls, were analyzed using repeated-measures analysis of variance (ANOVA) – followed by an assessment of linear relationships using Pearson's test ($p < 0.05$). A one-way ANOVA, followed by Tukey's post-hoc test, was performed to detect statistical differences between tested conditions (28:28 ºC, L:D and 18:18 ºC, L:D) and the corresponding controls. All tests were done using R software. The significance level was set as $\alpha = 0.05$.

4.3. Results and discussion

4.3.1. Growth

N. oceanica grown in a semi-continuous regime in tubular PBR outdoors (July to September of 2018), showed, in both trials, a clear biomass loss during the night period (see Figure 4.1). The night biomass loss pattern was mirrored by changes in cell number, which were maximal at the end of the dark period (data not shown). These findings are supported by previous reports that documented a timed cell division occurring during the dark periods in *Nannochloropsis* cells (Fábregas et al., 2002; Sukenik and Carmeli, 1990).

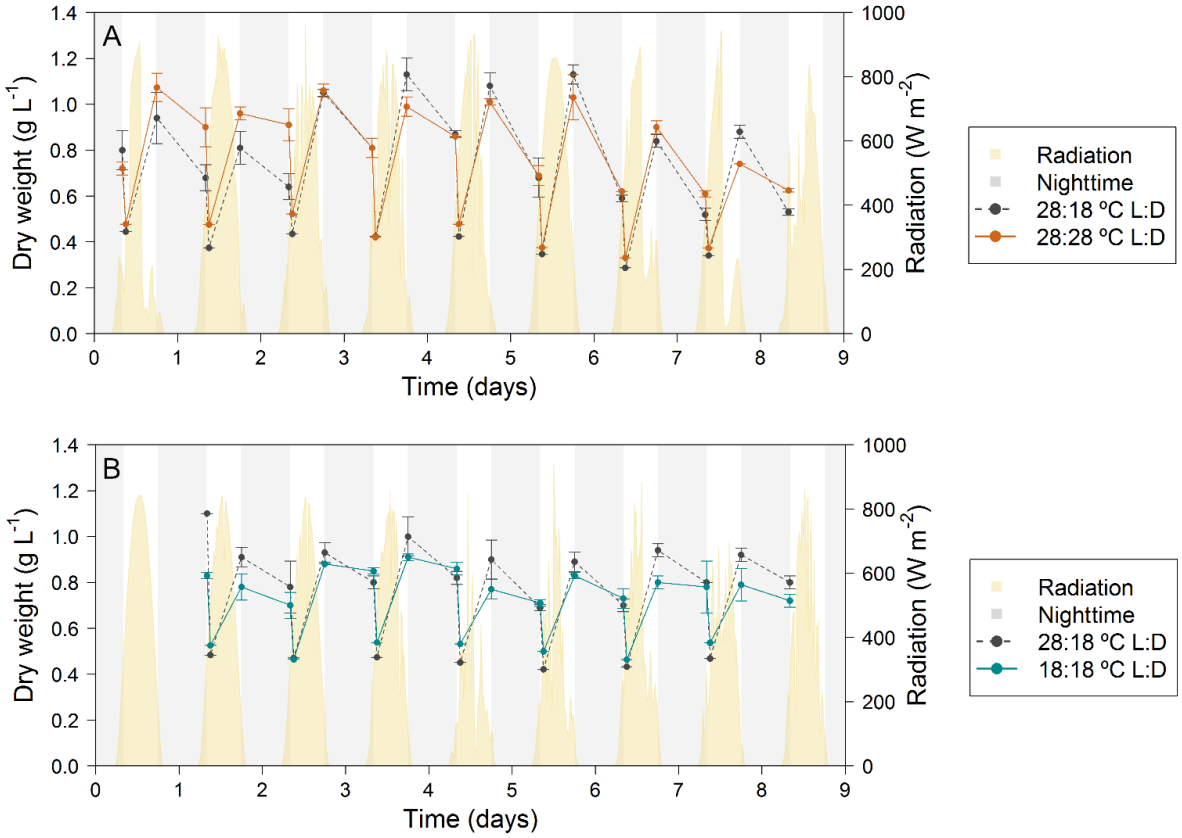

Figure 4.1. Changes in *Nannochloropsis oceanica* biomass dry weight (DW) grown outdoors in a semi-continuous mode under different temperature regimes (n = 1). After the morning sample, cultures were diluted to 0.45 g L^{-1} of DW, and allowed to grow until the following morning. Both the first (**A**) and second (**B**) trials show the corresponding 28:18 ºC L:D controls (dashed grey lines), the programmed night periods when the photobioreactors were covered (light grey bars), and the solar irradiance for each day (yellow). Each trial shows the tested condition (28:28 ºC L:D and 18:18 ºC L:D), represented as a solid line in orange for the first trial (A) and in blue for the second trial (B).

The maximum DW in the first trial was 1.13 ± 0.07 and 1.07 ± 0.06 g L^{-1}, for the control culture maintained at 28:18 ºC (L:D) and for the one kept at 28:28 ºC (L:D), respectively; while in the second trial, the culture maintained at 28:18 ºC (L:D) reached 1.00 ± 0.08, and the culture grown at 18:18 ºC (L:D) reached 0.91 ± 0.01 g L^{-1}. In order to better grasp the biomass variations due to temperature, each day was used as a replicate; and the daily yield and biomass loss were compared (Figure 4.2). In both trials, performed in July– August and August–September, the cultures kept at dual temperatures (28:18 ºC, L:D) revealed higher daylight productivities of 0.57 ± 0.09 and 0.47 ± 0.04 g L^{-1} day^{-1}; but also higher nighttime biomass losses, reaching up to 53% and 33% of the daily produced biomass in trial 1 and 2, respectively. Differences between controls are a result of a slightly higher solar irradiation in the first trial when compared to trial 2, which took place between August and September 2018, characterized by more unstable weather conditions. Detailed information on daily productivities and night losses can be found in Annex I Supplementary Table I.1.

Figure 4.2. Daily average (+SD) of biomass dry weight (DW) changes in *Nannochloropsis oceanica* grown outdoors in a semi-continuous mode, under different temperature regimes, in two sequential trials (trial 1 $n = 8$; trial 2 $n = 7$). Positive and negative values represent the daily biomass yield and loss, respectively. Dots represent individual data points for each condition. The first two bars (Trial 1) represent the cells kept at 28:18 ºC L:D (grey) and the ones kept at 28:18 ºC L:D (orange). The last two bars (Trial 2) represent the cells kept at 28:18 ºC L:D (grey) and the cells kept at 18:18 ºC L:D (blue). Significant differences ($p < 0.05$) to the corresponding control are marked with an asterisk (*).

The culture maintained at 28:28 ºC (L:D) produced a similar response to the control culture (28:18 ºC, L:D), although less pronounced for both productivity and nighttime loss. However, this difference was more notorious in other studies. Upon using *N. salina*, higher biomass losses at higher temperatures in the dark were found (Edmundson and Huesemann, 2015). A comparable outcome was also reported in previous experiments encompassing *Chlorella pyrenoidosa*, *Phaeodactylum tricornutum* and *A. platensis*, for which lower nighttime temperatures led to lower biomass loss (Molina Grima et al., 1995; Ogbonna and Tanaka, 1996; G. Torzillo et al., 1991).

The slowest growth was achieved in cultures maintained at 18:18 ºC (L:D), which can be considered as a suboptimal temperature for *Nannochloropsis* spp. growth. The optimum growth temperature for microalgae of this genus lies around 24-26 ºC, whereas values above 30 ºC or below 15-20 ºC are known to be supra- and suboptimal temperatures, respectively (Chini Zittelli et al., 1999; Crowe et al., 2012; de Vree et al., 2015; Hoffmann et al., 2010; M. H. A. Michels et al., 2014; San Pedro et al., 2014; Sandnes et al., 2005; Van Wagenen et al., 2012; Wei et al., 2015). In the culture grown at the 18:18 ºC (L:D) temperature regime, both a lower daylight productivity (0.31 g L^{-1} day^{-1}) and a lower night biomass loss (as much as 19%) were found. An opposite behavior was reported in a previous study using *C. pyrenoidosa*, where the night biomass loss increased as growth temperature decreased, although the lowest day temperature used was 25 ºC, which was significantly higher than the 18 ºC used in this study (Ogbonna and Tanaka, 1996). A slightly faster growth was previously found in *N. oculata*, kept under sinusoidally-varying temperatures, than at a fixed temperature (Tamburic et al., 2014). Although different conclusions were reached using *Tetraselmis suecica* and cooling overnight (M. H. A. Michels et al., 2014), our findings suggest that the dual temperature

regime allows the culture to recover faster after the high irradiances received during daytime, thus resulting in higher productivities, as seen in the cultures grown at 28:18 ºC (L:D). However, the higher growth was coupled to a higher nighttime biomass loss. In order to find out whether this correlation held a statistical meaning, the productivities versus the corresponding nighttime biomass loss are graphically reported, combining every data point of both trials (Figure 4.3).

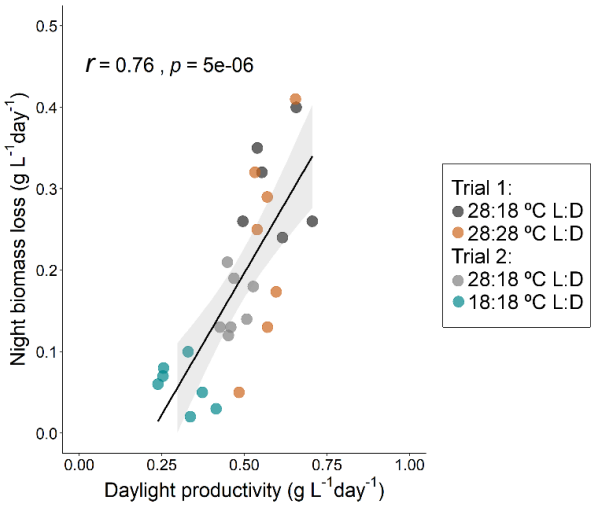

Figure 4.3. Correlation between daily yield and biomass loss, combining all data points from both trials using *Nannochloropsis oceanica* grown outdoors in tubular photobioreactors under different temperatures. Data points from the 28:18 ºC L:D (controls) cultures are depicted in dark (Trial 1) and light (Trial 2) grey; cells kept at 28:28 ºC L:D (Trial 1) and 18:18 ºC L:D (Trial 2) are depicted in orange and blue, respectively. The shaded grey area represents the confidence interval (95%) of Pearson's correlation. The correlation coefficient (r = 0.76) and the significance level ($p < 0.05$) are shown in the upper left corner of the plot (n = 27).

As can be grasped in Figure 4.3, the daily biomass yield (productivity) exhibited a positive correlation to the nighttime biomass loss (r (25) = 0.76, $p < 0.05$). Linear relationships between biomass loss and growth rates have been reported before in experiments encompassing nutrient-sufficient cultures kept in L:D cycles (Geider et al., 1989; M. H. A. A. Michels et al., 2014). The high dispersion of the cells kept at 28:28 ºC (L:D) reveals that at a constant temperature of 28 ºC, nighttime biomass loss was more affected by temperature than by daily yield. On the other hand, the low dispersion of the data points of the cells kept at low temperature, reveals that cells kept constantly at 18:18 ºC (L:D) had their yield and nighttime biomass loss inhibited. These observations suggest that temperature can influence nighttime biomass loss as well as productivity, even though these factors (nighttime biomass loss and daylight productivity) seem to correlate with each other.

A summary of the daily areal productivities and the corresponding nocturnal biomass loss is shown in Annex I Supplementary Table I.2 Although the light period in both trials was equally controlled (from 8 am to 6 pm), due to differences in the amount of light energy and intensities that occurred between the two trials, gross areal productivities (g m^{-2} day^{-1}) of both

cultures were normalized to their corresponding daily energy received (MJ m^{-2} day^{-1}). Cultures grown according to the temperature regime of 28:18 ºC (L:D; control) showed comparable biomass growth yields between the first (1.517 g MJ^{-1}) and second trial (1.475 g MJ^{-1}), indicating that the light utilization efficiency of the cultures was very similar (Annex I Supplementary Table I.2). However, the culture grown at 18:18 ºC (L:D) presented a much lower value (0.987 g MJ^{-1}) indicating a clear effect of the low temperature on daylight growth (Annex I Supplementary Table I.2). Daylight biomass productivity showed a good correlation to light irradiance. Indeed, higher daylight productivities were recorded with cultures grown under higher light irradiance that occurred during the first trial (July 26th - August 3rd, 2018), with a mean value of 30.8 g m^{-2} day^{-1} for the culture maintained at the dual temperature (28:18 ºC, L:D), and 27.8 g m^{-2} day^{-1} for the one maintained at the constant temperature of 28 ºC (28:28 ºC, L:D). However, due to the impact of night biomass loss, the net productivity was reduced to 14.5 and 16.6 g m^{-2} day^{-1} respectively (Annex I Supplementary Table I.2). In September, although the light irradiance declined significantly, the net productivity of the culture maintained at 28:18 ºC (L:D) was slightly better (16.1 g m^{-2} day^{-1} in September vs 14.5 g m^{-2} day^{-1} in August). This may indicate that the growth of *Nannochloropsis* gets saturated over about 16 MJ m^{-2} day^{-1}. The said finding is supported by previous research carried out by Chini Zittelli et al. (1999) who found, in a two year experiment, better yields in *Nannochloropsis* in September, when light irradiance declined to about 13 MJ m^{-2} day^{-1}. A close relationship between light intensity (to which cultures were exposed) and dark respiration was reported elsewhere (Falkowski and Owens, 1978; Kliphuis et al., 2011). Night biomass loss was mostly related to daylight temperature rather than to nocturnal temperature. Biomass loss in *N. oceanica* was always very impressive ranging between 19% and 53% of the biomass synthesized during the daylight period (Annex I Supplementary Table I.2).

4.3.2. Fluorescence parameters

The maximum quantum efficiency of PSII (F_v/F_m) showed a steady trend, with higher values in the morning and lower in the evening, for all experiments (see Table 4.2). This indicates that photosynthetic activity was probably downregulated in the middle of the day due to the prevailing high light (Torzillo et al., 1996). This trend for the maximum photochemical efficiency was previously observed in *Nannochloropsis* sp. grown in two different PBRs outdoors (Sukenik et al., 2009).

Table 4.2. Daily average (± SD) of maximum quantum efficiency of PSII (F_v/F_m) values of *Nannochloropsis oceanica* cells grown under different temperature regimes in outdoors tubular photobioreactors in semi-continuous cultivation mode. Statistical differences between the 28:28 ºC L:D and the control of Trial 1, and the 18:18 ºC L:D and the control of Trial 2 are depicted with "*" (n = 8). Values of F_v/F_m are significantly different (p < 0.05) from morning to the corresponding evening for all conditions.

Time of day	**Trial 1**		**Trial 2**	
	28:18 ºC L:D	28:28 ºC L:D	28:18 ºC L:D	18:18 ºC L:D
Morning	0.680 ± 0.024	0.672 ± 0.018	0.679 ± 0.021	0.630 ± 0.016 *
Evening	0.633 ± 0.031	0.621 ± 0.032	0.634 ± 0.045	0.570 ± 0.023 *

Cultures maintained at the constant temperature of 18 ºC (overnight and in the daytime) caused a negative impact upon the PSII performance, compared to the others. Lower daily temperature can promote sensitivity to light stress – and accordingly slow down the photosynthetic rate, thus inhibiting PSII repair mechanisms, and hampering the protective mechanisms underlying photoinhibition prevention (Torzillo et al., 1996). This higher susceptibility to photoinhibition when the culture was maintained at lower temperatures can explain the lower productivity of microalgal cells under this condition. Similar results of lower F_v/F_m were found for *A. platensis*, when kept at suboptimal temperatures (Torzillo et al., 1996).

Fast fluorescence curves, of the 2nd and 7th day of each trial, are depicted in Figure 4.4.

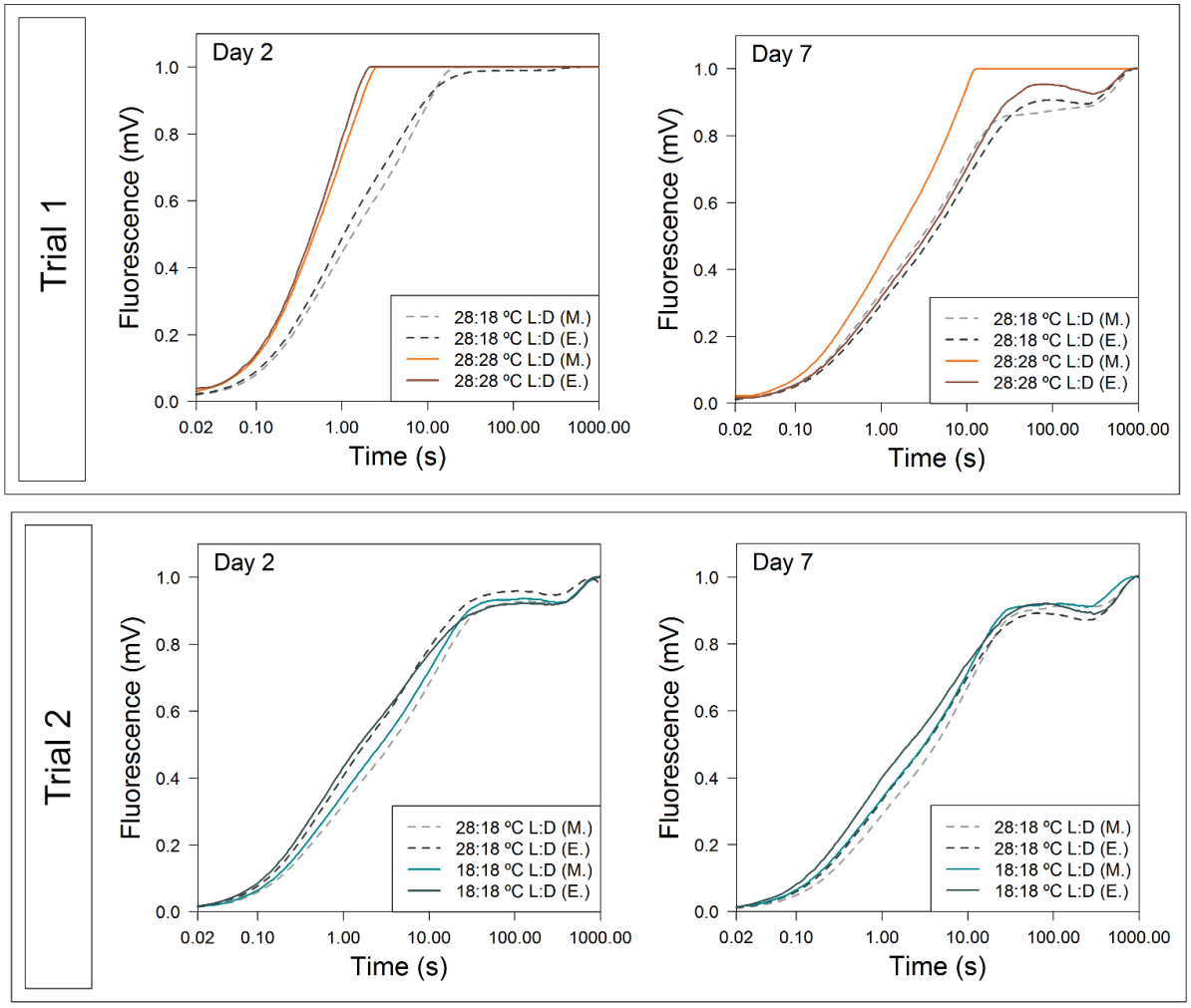

Figure 4.4. Kinetic representation of the OJIP transients from *Nannochloropsis oceanica* grown in tubular photobioreactors outdoors under semi-continuous regime and subjected to different temperatures (n = 1). The first row shows the OJIP curves for the morning (M.; orange) and evening (E.; brown) samples of the 2nd and 7th days of the cells kept at 28:28 ºC L:D (solid lines) in Trial 1. The second row shows the results of the second trial when cells were kept at 18:18 ºC L:D (solid lines) in the morning (M.; light blue) and evening (E.; dark blue). Control curves (28:18 ºC L:D) are represented as dashed lines for morning (M.; light grey) and evening (E.; dark grey) samples in both trials. Curves were double normalized to F_0 and F_m, when possible.

The culture maintained at 28:28 ºC (L:D) revealed a very high slope of the O-J fluorescence rise relative to the control, thus making it impossible to normalize fluorescence intensity of the P point in the OJIP transient for this culture (Figure 4.4, Trial 1). This effect can also be detected in Figure 4.5 (where the OJIP parameters are represented as ratios to the corresponding controls), with values of V_j and M_0 being 1.5-fold higher than those of the control. M_0 represents net rate of the closure of PSII RCs (Stirbet and Govindjee, 2011), which was fastest in the cells grown at 28:28 ºC (L:D), particularly after the dark period. Given that $1 - V_J = ET_0 / TR_0$ (also referred to as ψ_{E0}), one concludes that the transfer efficiency of a PSII trapped electron from Q_A^- − onward is lowest in the beginning of the run in the first trial. Nonetheless, microalgae kept at 28:28 ºC (L:D) overcame the damage caused by the high temperature stress during the dark period by day 7. A relation between high temperature

damage to PSII and V_j was previously reported in *Nannochloropsis* sp. (Sukenik et al., 2009). The F_v/F_0 values are proportional to the activity of the water-splitting complex on the donor side of PSII and were suppressed at the beginning of the first trial due to the warmer temperatures overnight (28:28 ºC, L:D) – but also approached the control values by the end of the experiment.

Concerning the energy fluxes per absorbed photon flux, the maximum quantum yield of primary photochemistry that leads to reduction of pheophytin and Q_A (Φ_{P0} = TR_0 / ABS = F_v / F_m) was suppressed in the beginning for the cells kept at 28:28 ºC (L:D) but came close to control values only in the end. The same pattern was found for the quantum yield of electron transport (Φ_{E0} = ET_0 / ABS), where the probability that an absorbed photon will move an electron into the electron transport chain was lowest in the beginning but eventually recovered, reaching values closer to the control. Reaction centre densities (RC/CS_m) were a bit lower than the control, yet they remained constant along the trial.

Phenomenological energy fluxes per excited cross section, at completely closed RC, were also affected by high temperatures in the beginning when the culture was kept at 28:28 ºC (L:D). Even though absorption by the PSII antenna pigments (ABS/CS_m) was unaltered, the trapped photon flux used for the primary charge separation and stabilization of the RCII for closing all PSII RCs (TR_0/CS_m) decreased in the beginning, when cells were kept at 28:28 ºC (L:D). However, the overall electron transport flux (ET_0/CS_m) was strongly affected right from the start, until the end of the experiment, in the case of cells kept at higher temperatures during the night for being unable to perform as well as microalgae grown under control conditions. As significant changes in electron transport flux are mirrored by the variation of the fraction of reduced Q_A (Stirbet and Govindjee, 2011), this would explain the fast rise of the transients at the beginning of the first trial. Excitation energy dissipation (DI_0/CS_m) was higher at the beginning of the trial. Apart from the morning samples after the culture was kept at 28 ºC overnight, the values for the dissipation flux reverted more closely to the control values.

Finally, the performance index on an absorption basis (PI_{ABS}; Srivastava et al., 1999; Strasser et al., 1999) reflects the functionality of both PSII and PSI, thus providing information on the current state of algae performance under stress conditions (Strasser et al., 2004). Compared to the control, the cells kept at 28:28 ºC (L:D) revealed high stress from the beginning yet recovering towards the end. Nonetheless, the cells kept under constant 28 ºC were apparently unable to deal with the high temperature of the dark periods; hence, PI_{ABS} was more sensitive than Φ_{P0} (F_v/F_m).

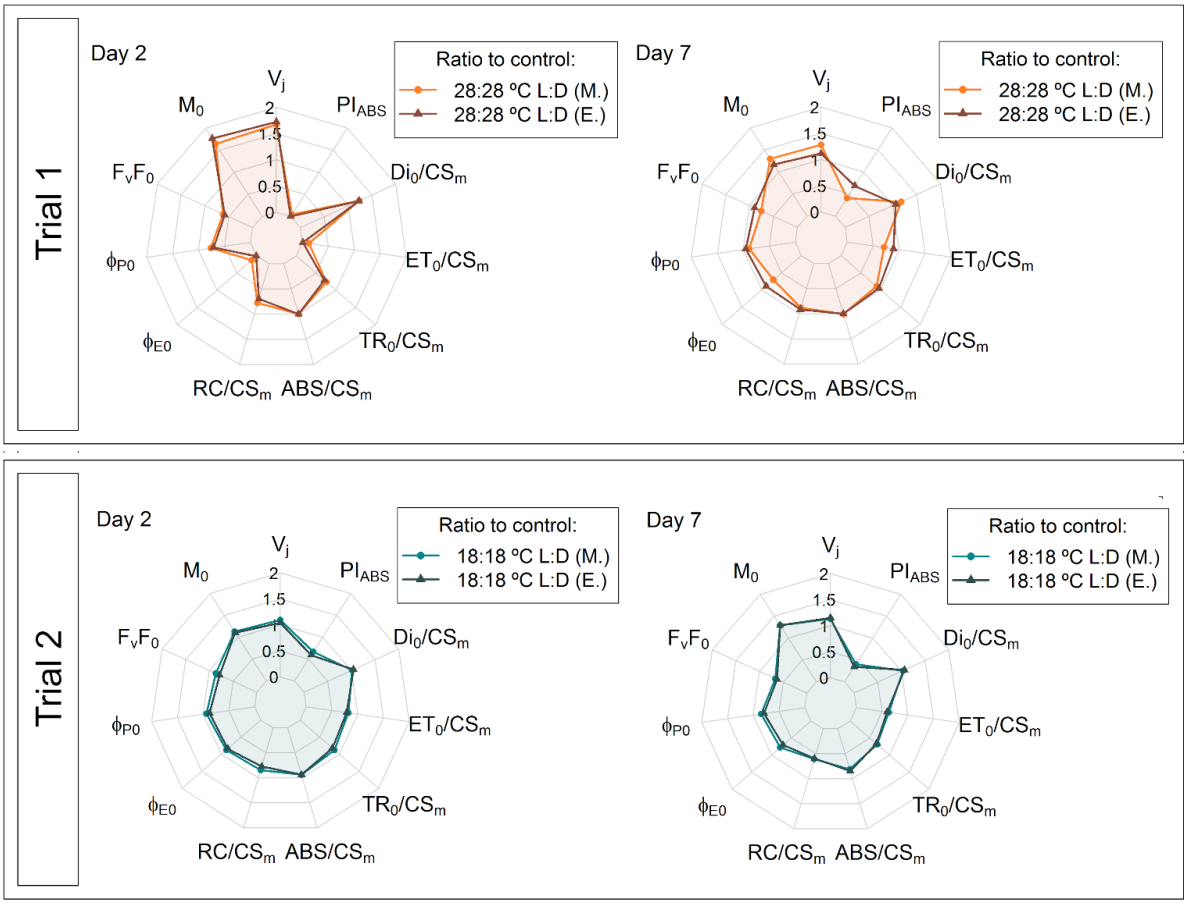

Figure 4.5. Temperature influence on OJIP determined parameters of *Nannochloropsis oceanica*, grown in tubular photobioreactors outdoors under semi-continuous regime and subjected to different temperatures (n = 1). Spider plots depict the ratio of the conditions (28:28 ºC L:D in the first trial, and 18:18 ºC L:D in the second trial) to their corresponding controls (28:18 ºC L:D). The first row shows the results of Trial 1 on the 2nd and 7th day, respectively, with morning (M.; orange) and evening (E.; brown) samples, and of Trial 2 on the second row, also with morning (M.; light blue) and evening (E.; dark blue) samples for each day.

Although slightly lower, ratios to the control in the beginning of the second trial were quite similar with the exception of F_v/F_0, RC/CS_m, ET_0/CS_m and PI_{ABS} (Figure 4.5, Trial 2). At the end of this trial, all ratios to the control dropped, except for M_0 and V_j that increased. This limitation within electron transport could be explained by a diminished RC density, caused by the cold temperature the cells were exposed to (18:18 ºC, L:D). This could reflect a self-defense mechanism to avoid low-temperature induced photoinhibition, already reported in PAM measurements of F_v/F_m (Davison, 1991).

4.3.3. Photosynthetic and respiration measurements

The relation found between respiration and net photosynthesis lies within the expected values (Geider et al., 1989), but the correlation between nighttime biomass loss and respiration values by the end of the dark period (morning samples) using all data points revealed a high dispersion (r (29) = 0.64); nevertheless, the underlying correlation was found

to be significant ($p < 0.05$; Annex I Supplementary Figure I.1). Overall, respiration values in the first trial started to increase with time for both cultures (Figure 4.6).

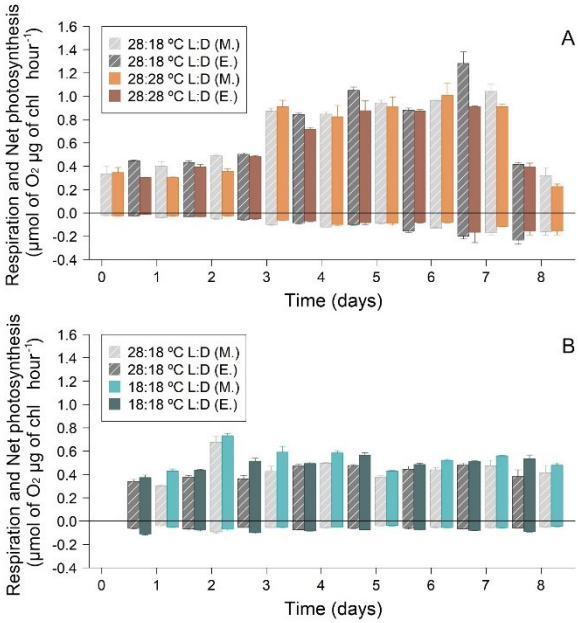

Figure 4.6. Net photosynthetic oxygen evolution (y > 0) and respiration (y < 0), normalized to chlorophyll of *Nannochloropsis oceanica* grown in semi-continuous mode in outdoor tubular photobioreactors at different temperatures, showing Trial 1 (A) and Trial 2 (B). Values for cells grown at 28:28 ºC L:D or at 18:18 ºC L:D are depicted as orange (lighter for morning [M.] and darker for evening [E.] samples) or blue (lighter for morning [M.] and darker for evening [E.] samples) bars, respectively. Grey stripped shaded bars correspond to the values of the corresponding controls, kept at 28:18 ºC L:D (n = 1).

However, oxygen production doubled after the evening of day 2, and remained stable until the morning of the 7th day. Gross O_2 production (net O_2 production plus respiration rate) was mostly higher for the culture kept at 28:18 ºC (L:D; control). On the other hand, the respiration values increased from the beginning to the end of the trial, under both conditions. In the second trial, oxygen production and consumption rates were more stable along the experiment. Net oxygen production was higher for cells cultivated at 18:18 ºC (L:D) when compared to the control (28:18 ºC, L:D). Respiration values in the morning were quite similar under both conditions; however, the cells kept at 18 ºC after the light period showed a slightly higher respiration rate. This apparent contradiction is explained by the fact that cells grown at 18 ºC, were characterized by a 20% higher spectral averaged optical cross-section of chlorophyll *a* compared to the 28:18 ºC (L:D; results not shown), and by a lower cellular chlorophyll content (see Section 4.3.4). Moreover, the oxygen measurements were carried out at 28 ºC which may have allowed the cell to recover its photosynthetic capacity. A previous study using *N. oculata* reported a different behavior at the beginning of the light period, with the increase of O_2 production levels being slower when the cells were kept at 25:15 ºC (L:D) than at 20:20 ºC (L:D), due to a reduced net photosynthesis (Tamburic et al., 2014). In our

study, the low temperature of 18 ºC maintained in the culture at 18:18 ºC (L:D) did not seem to limit electron transport or ability of light use by the microalga when transferred to 28 ºC, thus indicating that photosynthetic activity can recover quickly.

4.3.4. Chlorophyll content

The cell chlorophyll content was tendentially higher after the light period for both trials, as expected, owing to the high irradiation to which they were subjected to. This is consistent with previous reports on *Nannochloropsis* sp., subjected to a photoperiod containing L:D cycles (Figure 4.7; Fábregas et al., 2002; Sukenik and Carmeli, 1990). However, if chlorophyll content was expressed per biomass DW it would be highest by the end of the dark period, since biomass DW dropped during the night.

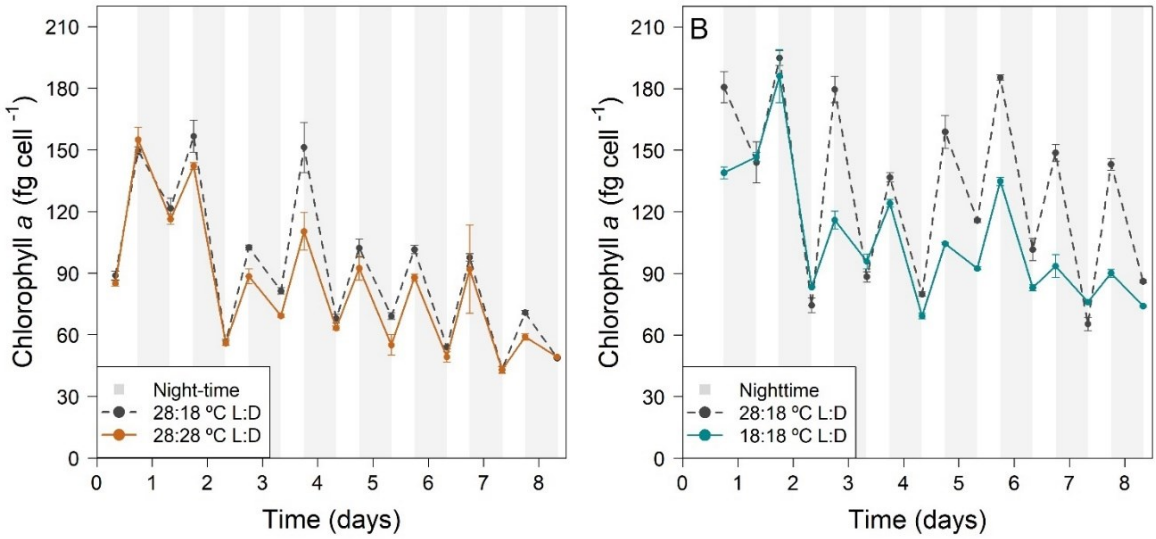

Figure 4.7. Chlorophyll *a* content per cell of *Nannochloropsis oceanica*, grown in outdoor tubular photobioreactors, under semi-continuous regime and subjected to different temperatures, showing Trial 1 (A) and Trial 2 (B). Grey lines represent the controls when cells were kept at 28:18 ºC L:D, and orange and blue lines represent the cells kept at 28:28 ºC L:D and 18:18 ºC L:D for each trial, respectively. Grey bars represent the dark period, when the cultures were covered (n = 1).

In the culture maintained at constant temperature of 28 ºC along the diel cycle, a slightly lower chlorophyll production per cell was observed compared to the control (28:18 ºC, L:D). Nonetheless, chlorophyll a production was noticeably more suppressed when cells were grown at 18:18 ºC (L:D) in the second trial. This finding was expected, as low temperature-acclimated algae tend to have lower contents of photosynthetic pigments; and higher temperature-grown cultures usually exhibit higher chlorophyll production (Carvalho et al., 2009; Chen et al., 2011; Davison, 1991). Lower temperatures can, in general, inhibit chlorophyll build-up by decreasing the light harvesting complex, thus affecting the values of

maximum photochemical efficiency of PSII in the cells kept at 18:18 ºC (L:D), see discussion above (Gill et al., 2018).

4.3.5. Lipids

The lipid content per cell of *N. oceanica* exhibited a trend similar to that of chlorophyll *a*, being highest by the end of the light period, in both runs and for both conditions (Figure 4.8).

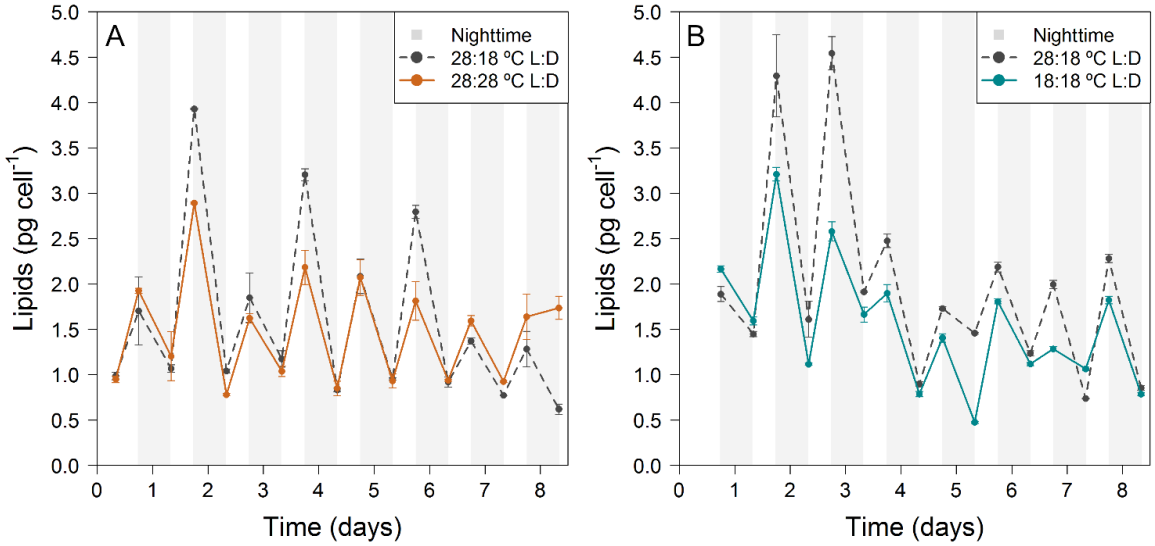

Figure 4.8. Temperature influence on the lipid content of *Nannochloropsis oceanica* cells, grown in tubular photobioreactors outdoors under semi-continuous regime and different temperature profiles (n = 1). In Trial 1 (A) the culture was kept at 28:28 ºC L:D (orange line), and in Trial 2 (B) the cells were kept at 18:18 ºC L:D (blue line). Grey lines represent the controls (28:18 ºC L:D) for each trial, and light grey bars represent the dark period.

This finding supports the idea that cells consume a part of their lipid reserves to support the energy demand associated to cell division during the night. This observation has been previously reported in *Nannochloropsis* sp. synchronized cultures, where lipids are the main energy reserve (Fábregas et al., 2002; Sukenik and Carmeli, 1990). A similar pattern was also found in outdoor cultures of *Phaeodactylum tricornutum* (Silva Benavides et al., 2013). The lipid content was higher in the cultures kept at dual temperatures (28:18 ºC, i.e., control), in both trials; while a slower lipid synthesis was observed for the cells kept at 18 ºC. Previous experiments showed a higher lipid production by *N. oculata* cultures, when temperature was increased from 20 to 25 ºC (Converti et al., 2009). In addition, a strong correlation was found between higher temperatures and lipid contents in *N. salina* (Fakhry and El Maghraby, 2015). The lipid content in *Nannochloropsis* sp. usually increases under stress conditions, mostly nutrient limitation, yet this does not hold for low temperature-stress (18 ºC).

4.3.6. Fatty acids

The FAME profile of *N. oceanica* was mainly composed of myristic (C14:0), palmitic (C16:0), palmitoleic (C16:1) and EPA (C20:5*n*-3) acids, while linoleic (C18:2*n*-6), oleic (C18:1), stearic (C18:0) and arachidonic (C20:4*n*-6; AA) acids were detected to a lower extent (Table 4.3). Because of the high myristic and palmitic acids contents, saturated fatty acids (SFA) represented around half of the total FAME detected under all growth conditions tested. The FAME profile of cultures, from the beginning until the end of each trial, was relatively stable under all conditions, due to the stable culture conditions (light, temperature, dilution rate). Overall, the FAME profile was similar to those previously reported for *Nannochloropsis* species (Hulatt et al., 2017; Sukenik, 1991).

Table 4.3. Daily average (± SD) of fatty acid composition, as percentage of total fatty acids of *Nannochloropsis oceanica*, grown in a semi-continuous cultivation mode in tubular photobioreactors outdoors under different temperature regimes. For each trial, statistical differences between the 28:18 ºC L:D or 18:18 ºC L:D regimes and their corresponding controls (28:18 ºC L:D) are marked with an "*" ($p < 0.05$; trial 1 $n = 8$; trial 2 $n = 7$).

Fatty Acid (%)	Trial 1				Trial 2			
	28:18 ºC L:D		28:28 ºC L:D		28:18 ºC L:D		18:18 ºC L:D	
	Morning	Evening	Morning	Evening	Morning	Evening	Morning	Evening
C14:0	7.49 ± 0.52	7.36 ± 1.05	7.48 ± 0.65	6.59 ± 0.60	7.47 ± 0.81	7.88 ± 0.98	5.97 ± 0.63 *	6.33 ± 0.89 *
C16:1	18.87 ± 0.97	16.53 ± 0.56	18.37 ± 0.65	16.28 ± 0.82	17.88 ± 1.48	17.02 ± 1.52	19.51 ± 0.86	20.49 ± 1.45 *
C16:0	43.67 ± 4.28	53.41 ± 4.19	45.12 ± 6.23	52.75 ± 5.02	46.22 ± 6.63	52.57 ± 2.31	37.75 ± 6.35	43.89 ± 4.61 *
C18:2*n*-6	2.75 ± 0.39	1.44 ± 0.41	2.43 ± 0.35	1.78 ± 0.36	2.06 ± 1.04	1.76 ± 0.55	2.26 ± 0.78	1.56 ± 0.47
C18:1	3.06 ± 0.44	2.35 ± 0.16	3.07 ± 0.16	2.37 ± 0.13	2.61 ± 0.58	2.40 ± 0.24	2.03 ± 0.28 *	1.97 ± 0.19 *
C18:0	1.00 ± 0.16	3.37 ± 0.59	1.21 ± 0.27	3.00 ± 0.51	1.11 ± 0.40	2.88 ± 0.71	0.85 ± 0.49	1.44 ± 0.58 *
C20:4*n*-6	3.74 ± 1.17	1.87 ± 1.06	3.62 ± 1.67	2.76 ± 1.69	2.52 ± 1.35	1.76 ± 0.68	3.80 ± 1.17	3.05 ± 1.23 *
C20:5*n*-3	19.42 ± 3.44	14.34 ± 2.26	18.7 ± 5.27	14.46 ± 3.45	18.33 ± 1.73	13.90 ± 2.07	26.99 ± 3.41 *	20.05 ± 2.77 *

Lower growth temperatures led to a significant decrease of myristic, palmitic, oleic and stearic acids, and a consequent increase of AA, EPA and palmitoleic acid content. The increase of PUFA, at the expense of SFA, under lower temperature conditions is in agrees with previous reports (Chini Zittelli et al., 1999; Gill et al., 2018; Sukenik, 1991; Sukenik et al., 1993). Interesting enough, the higher content of EPA was observed in the culture maintained at the suboptimal temperature of 18 ºC by day and by night, which reached 20% of the total fatty acids by the end of the light period and rose up to 27% in the following morning. This

difference can contribute greatly to increase the value of the biomass, particularly when harvested in the morning. Nonetheless, attention must be paid to the balance between biomass productivity and EPA content of the biomass, in order to obtain the highest EPA productivity possible.

Analysis of the daily-averaged fatty acid changes showed a sizeable decrease in EPA and total PUFA percentage in the evening, under all conditions; while palmitic acid and SFA were, in general, more represented in the evening (Figure 4.9). On the other hand, monounsaturated fatty acids (MUFA) did not show major changes between morning and evening samples. The decrease of EPA content with increasing radiation, and consequent accumulation in the dark phase have been also reported elsewhere for *Nannochloropsis* sp. (Fábregas et al., 2002; Sukenik, 1991).

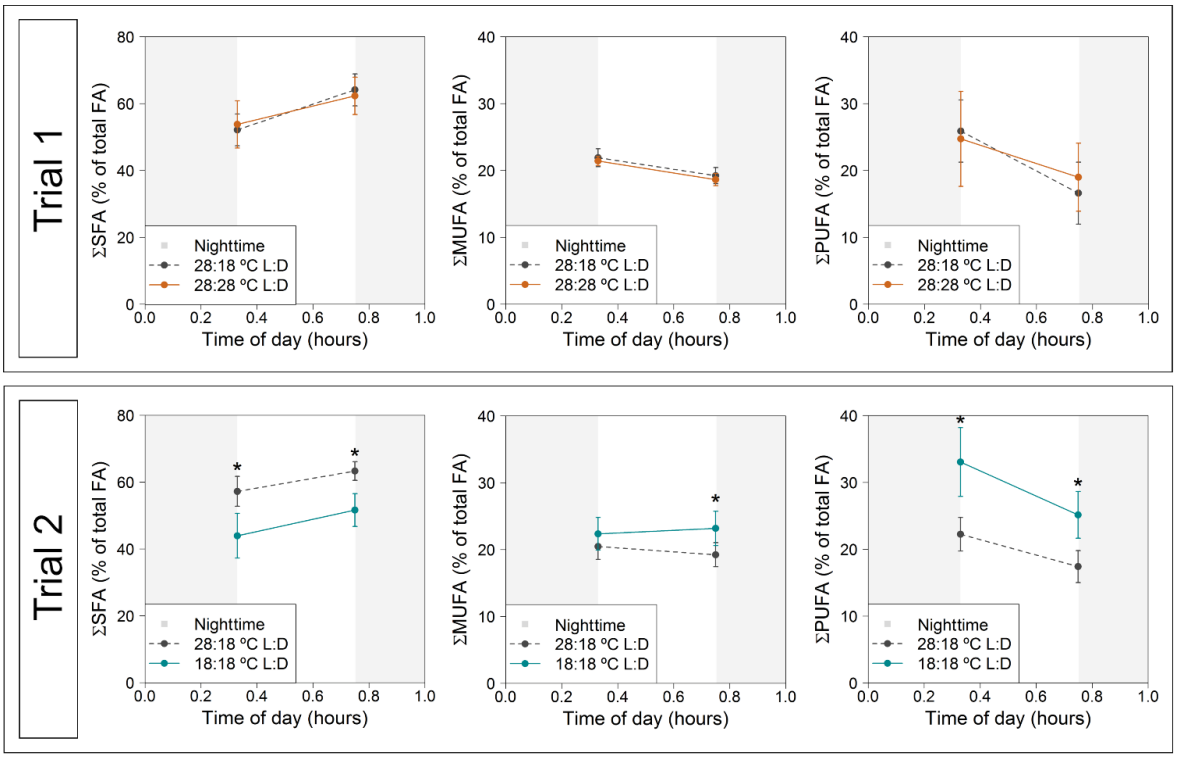

Figure 4.9. Daily average (± SD) of saturated fatty acids (SFA), monounsaturated fatty acids (MUFA) and polyunsaturated fatty acids (PUFA) for morning and afternoon samples of *Nannochloropsis oceanica*, grown in a semi-continuous cultivation mode in tubular photobioreactors outdoors under different temperature regimes. The first row shows Trial 1, with the orange solid lines representing the cells kept at 28:28 ºC L:D. The second row shows Trial 2, with the blue solid lines representing the cells kept at 18:18 ºC L:D. For both trials, dashed grey lines represent the corresponding controls (28:18 ºC L:D). Statistical differences between the tested condition and the respective control are marked with an "*" ($p < 0.05$; trial 1 $n = 8$; trial 2 $n = 7$).

The observed diel changes in FA levels can be explained by *Nannochloropsis* cells accumulating storage lipids (SFA) during daytime, which are later metabolized during nighttime to generate the necessary adenosine triphosphate (ATP) levels for cell survival during the dark period, as well as synthesize DNA and enter mitosis (Miyagishima et al., 2019).

Conversely, EPA increases during the dark period, when cell division occurs, since PUFA are important constituents of the thylakoid membranes (Fábregas et al., 2002; Sukenik, 1991). Regarding the effect of temperature over the diel cycle, no differences were found in the cells maintained at 28 ºC throughout the day and night periods, and those subjected to 28:18 ºC (L:D). However, cultures permanently kept at 18 ºC showed lower SFA, and increased contents of PUFA and MUFA in the evening, perhaps a metabolic response that counteracts the decrease in membrane fluidity in cells under this environmental condition. The ratio of unsaturated fatty acids to SFA was also highest when the culture was kept at 18 ºC constantly, but with low values of 1.24 and 0.94 in the morning and afternoon, respectively. A previous report also claimed a minor influence of temperature upon this ratio in *N. salina* (Hoffmann et al., 2010).

4.4. Conclusions

Unlike one might expect, higher night biomass losses were observed, especially for the cultures operated at dual temperatures of 28 ºC during daytime and 18 ºC during nighttime. Suboptimal temperature (18 ºC during all the diel cycle) led to lower biomass productivity, but also lower biomass loss overnight. The results gathered in this work support a strong correlation between daily yield and nighttime biomass loss, in cultures operated in a semi-continuous regime. However, this relation can be influenced by temperature. Relative EPA content was always higher in the morning cultures suggesting that, in agreement with productivity, harvesting should be performed preferably in the early morning hours. Although the cells kept constantly at 28 ºC experienced some stress, fluorescence measurements revealed that they fully recovered overnight. On the other hand, those kept at 18 ºC throughout the day and night periods underwent a decrease in F_v/F_m, coupled to a lower photosynthetic activity and biomass productivity. Nonetheless, *N. oceanica* tolerated a wide range of temperatures – which is a desirable trait for biomass production. Chlorophyll production was highest by the end of daily radiation exposure, and overall lowest in the culture grown at 18 ºC. Lipids synthesized during the day were partially consumed overnight to support cell division. PUFA production reached a maximum after the dark period, as opposed to SFA. This effect is most likely a consequence of plastidial biogenesis, which is tightly linked to cell division. Lower temperatures led to higher EPA accumulation, which represented most of the PUFA profile – a trait that increases the economic value to the biomass.

Chapter 5

In-situ monitoring of chlorophyll *a* fluorescence in *Nannochloropsis oceanica* cultures to assess photochemical changes and the onset of lipid accumulation during nitrogen deprivation

This Chapter is based on the published article: Carneiro, M., Chini Zittelli, G., Cicchi, B., Touloupakis, E., Faraloni, C., Maia, I.B., Pereira, H., Santos, T., Malcata, F.X., Otero, A., Varela, J., Torzillo, G., 2021. *In-situ* monitoring of chlorophyll *a* fluorescence in *Nannochloropsis oceanica* cultures to assess photochemical changes and the onset of lipid accumulation during nitrogen deprivation. Biotechnology and Bioengineering 118, 4375-4388. DOI: 10.1002/bit.27906.

In-situ chlorophyll *a* fluorescence measurements were applied to monitor changes in the photochemical variables of *Nannochloropsis oceanica* cultures, under nitrate-deplete and nitrate-replete (control) conditions. In addition, growth rate, and lipid, fatty acid, and pigment contents were also monitored. In the control culture, growth was promoted along with pigment content, electron transport rate, and polyunsaturated fatty acids, while total lipid content and fatty acid saturation level diminished. Under nitrate-deplete conditions, the culture showed a

higher de-epoxidation state of the xanthophyll cycle pigments. Fast transients revealed a poor processing efficiency for electron transfer beyond Q_A^-, which was in line with the low electron transport rate due to nitrate depletion. Lipid content and the de-epoxidation state were the first biochemical variables triggered by the change in nutrient status, which coincided with a 20% drop in the *in-situ* effective quantum yield of PSII ($\Delta F'/F_m'$), and a raise in the V_j measurements. A good correlation was found between the changes in $\Delta F'/F_m'$ and lipid content ($r = -0.96$, $p < 0.01$). The results confirm the reliability and applicability of *in-situ* fluorescence measurements to monitor lipid induction in *N. oceanica*.

5.1. Introduction

With the ongoing expansion of microalgae applications in a large variety of commercial sectors (e.g., food, feed, nutraceuticals, pharmaceuticals, biofuels, biomaterials, and bioremediation), biomass supply must be ensured to fulfill its continuously growing demand. Hence, microalgal mass cultivation should be carried out under optimum conditions to achieve a stable productivity. Microalgae have evolved diverse adaptation and protection strategies to manage critical conditions that can arise from several abiotic factors, affecting their productivity, such as nutrients, light, and temperature. The activation of these strategies can trigger induction and/or inhibition of particular metabolic pathways that alter cellular content (Carneiro et al., 2020; Hulatt et al., 2017; Ördög et al., 2012; Otero and Fábregas, 1997; Rodolfi et al., 2009). However, these shifts are preceded by changes in chlorophyll *a* fluorescence quenching (Murata et al., 2007). Previous studies have linked specific fluorescence changes to certain stressors in distinct photosynthetic organisms, such as plants and microalgae (Beardall et al., 2001; Kalaji et al., 2014, 2016; Lichtenthaler & Miehé, 1997; Torzillo et al., 1996; White et al., 2011).

A more specific application includes monitoring fluorescence signals to gain insight into the cell's nutritional status. Nutrient deficiency such as that associated to N, P, or Fe, can severely impact the light-harvesting system, energy transduction, and cellular metabolism, which in turn affects the photochemical efficiency of photosystem II (PSII) (Beardall et al., 2001). Several studies have focused on this topic in different algal strains, including *Dunaliella tertiolecta* (Berges et al., 1996; Geider et al., 1998; Greene et al., 1992; Kolber et al., 1988; Pereira & Otero, 2019; Sosik & Mitchell, 1991), *Phaeodactylum tricornutum* (Geider et al., 1993; Greene et al., 1992), *Scenedesmus acuminatus* (Zhang et al., 2019), *Chlorella* spp. (Malapascua et al., 2014; Plyusnina et al., 2019, 2020; Qiao et al., 2015; White et al., 2011), *Porphyridium cruentum* (Zhao et al., 2017), *Tetraselmis subcordiformis* (Yao et al., 2012),

Thalassiosira weissflogii (Berges et al., 1996; Kolber et al., 1988), and *Nannochloropsis* spp. (Li et al., 2020; Liang et al., 2019; Liu et al., 2018), among others (Beardall et al., 2001a). Moreover, several studies have attempted to correlate fluorescence signals with lipid accumulation induced by nutrient starvation, which could act as a proxy and thus fast-track determination of the harvesting time (Li et al., 2020; Qiao et al., 2015). Although fluorescence measurements are relatively fast, only *in-situ* measurements can provide timely information on changes of the photosynthetic apparatus in cultures exposed to stress. Just a few studies have employed *in-situ* fluorescence measurements in controlled microalgae cultivations (non-natural environments) (Antal et al., 2019; Cao et al., 2019; Červený et al., 2009; Faraloni et al., 2011; Jerez et al., 2016; Ma et al., 2018; Masojídek et al., 1999, 2009, 2011; Nedbal et al., 2008; Solovchenko et al., 2014; Torzillo et al., 1996, 1998; Touloupakis et al., 2015). Even fewer have dwelled on the monitoring of chlorophyll *a* fluorescence signals to ascertain the culture nutritional status resorting to fast fluorescence in *Chlorella vulgaris* (Plyusnina et al., 2020, 2019) and *Chlamydomonas reinhardtii* (Antal et al., 2019), and slow fluorescence in *C. reinhardtii* (Faraloni et al., 2011) and *Nannochloropsis oceanica* (Liu et al., 2018).

Under nitrogen deprivation, biosynthesis pathways of the light-harvesting complex and D1 subunit of PSII proteins are blocked, leading to a down-regulation of photosynthesis and carbon fixation. While metabolic fluxes lead to either lipid or carbohydrate accumulation (Beardall et al., 2001b; Tran et al., 2016). In the genus *Nannochloropsis,* nitrogen deprivation results in increased lipid content (Benvenuti et al., 2015; Ma et al., 2016; Simionato et al., 2013; Solovchenko et al., 2014; Tran et al., 2016). These metabolic changes should be synced with chlorophyll *a* fluorescence.

Our goal was to look for triggering fluorescence signals indicating shift of the cells from a basal physiological state to the stressed one, characterized by the start of lipid accumulation. Therefore, *N. oceanica* growth was monitored at the beginning of nitrate depletion and replenishment. Biochemical and fluorescence changes *in-situ* and *ex-situ* (for validation) were simultaneously measured.

5.2. Methods

5.2.1. Microorganism and culture conditions

N. oceanica was kindly provided by Prof. Avigad Vonshak (Institute for Desert Research, Ben-Gurion University, Israel). Cells were pre-cultured in a glass cultivation column (0.4 L

working volume; i.d. = 5 cm), placed in a thermostatted bath at 25 ºC, and bubbled with a mixture of air and CO_2 (97/3 v/v). Light intensity was increased gradually from 80 to 600 µmol photons m^{-2} s^{-1}. Cells were acclimated for 3 d before the experiments began. Saltwater was prepared with 33 g L^{-1} Tropic Marin Zoo Mix (Tropic Marin® SEA SALT), and supplemented with a modified F medium, with pH correction to 7.5 prior to sterilization (Guillard and Ryther, 1962). The medium was enriched with $NaHCO_3$ (6 mM) and 10-fold the values of $NaNO_3$ (17.7 mM) and NaH_2PO_4 (0.84 mM) of the original recipe. The culture was allowed to grow until the beginning of the stationary phase, thus reaching nutrient limitation before the experiment was initiated.

5.2.2. Experimental set-up

The inoculum of *N. oceanica*, previously grown in bubble columns up to a dry weight (DW) of 3-4 g L^{-1}, was centrifuged at low speed, washed with saline water, and resuspended in fresh medium. For the control (NO_3-replete), cells were resuspended in complete medium, while nitrate was omitted in the other condition (NO_3-deplete). The photobioreactor (PBR) used consisted of a 1-L Roux type bottle, with a flat cross-section (12 × 5 cm width) and flat bottom, with five ports at the top (Touloupakis et al., 2015) (Figure 5.1A).

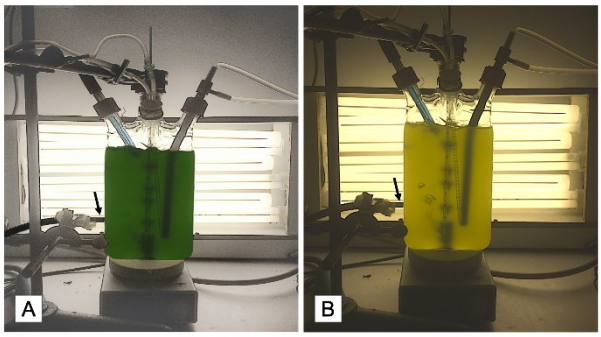

Figure 5.1. General view of the experimental set up used in this study, composed by a fully controlled 1-L photobioreactor illuminated from one side. *In-situ* chlorophyll fluorescence was monitored with a PAM-2100, with the optical fiber directly attached on to the lateral face of the flat photobioreactors. Nutrient replete culture (control) (**A**), and nutrient deplete culture (**B**), after 48 h of culture are represented. The arrows indicate the positioning of the optical fiber connected to the PAM-2100.

Mixing was achieved with a specially designed rotating impeller, driven magnetically by a stirrer at the bottom of the bottle (Giannelli et al., 2009). A cooling finger connected to an external thermostat (MPM Instruments, Italy) maintained the culture temperature at 25.0 ºC. A pH sensor connected to a controller (Chemitec, Scandicci, Italy) kept pH at the pre-set value of 7.5, by automatic addition of CO_2. The fourth port was used for the filtered air and CO_2 inlet, pumped through 0.2 µm filters (Whatman, UK). The culture was illuminated from one side,

with 600 µmol photons m^{-2} s^{-1} provided by cool white neon tubes (Dulux L, 55W/840, Osram, Italy).

Experiments started with a biomass concentration of ca. 0.37 g DW L^{-1}. The cultures grew for 4 d, under continuous illumination in batch cultivation mode. To follow the initial cell acclimation, sampling was carried out at 0, 1, 3, and 5 h after the experiments began. Afterward, sampling was done at 09:00, and again at 16:00.

5.2.3. Measurements

5.2.3.1. Growth

Culture samples (5 mL) were aseptically withdrawn from the photobioreactors, and filtered through pre-weighed 47-mm diameter glass microfiber filter membranes (Whatman GF/F, Maidstone, England). The pellets on the filters were rapidly washed twice with distilled water, and oven-dried afterward at 105 ºC until constant weight (Zittelli et al., 2000). Measurements were performed in triplicate, and results expressed in g DW L^{-1}

5.2.3.2. Fluorescence

For the *in-situ* chlorophyll *a* fluorescence measurements, the optical fiber of the pulse-amplitude modulation fluorometer (PAM-2100 with DA-2000 as the data acquisition software, Heinz Walz GmbH, Germany) was set perpendicularly to incoming light on the lateral wall of the PBR to avoid signal interference with aeration bubbles (Figure 5.1B). Monitored fluorescence parameters included the effective quantum yield of PSII ($\Delta F'/F_m'$), calculated as $\Delta F'/F_m' = [F_m' - F'] / F_m'$, where F_m' and F' are the maximum and basal fluorescence yield in the light, respectively, and the coefficient of non-photochemical fluorescence quenching (qN) calculated by $qN = [F_m-F_m']/[F_m-F_o']$, where F_m is the maximum fluorescence yield in the dark, and F_o' the minimum fluorescence yield in the light. A moving average was plotted on top of the individual data points collected by the fluorometer every 15 min to highlight culture trend.

Ex-situ chlorophyll *a* fluorescence measurements were carried out with a PAM fluorimeter (PAM-2100, H. Walz, Effeltrich, Germany), operated with PamWin (version 2.00f) PC software. Triplicate samples were incubated for 15 min in the dark prior to the F_v/F_m measurement. For this purpose, a weak light (0.5 µmol photons m^{-2} s^{-1}) was applied to measure the minimum fluorescence in the dark-adapted state (F_o). Afterward, a strong saturating pulse (6,000 µmol photons m^{-2} s^{-1}) was supplied to close all reaction centers (RC) and reach the maximum fluorescence yield (F_m). The maximum photochemical quantum yield

of PSII (F_v/F_m) was then calculated as the ratio of variable fluorescence ($F_v = [F_m - F_o]/ F_m$) to F_m (Butler, 1978).

The average chlorophyll specific optical absorption cross-section (a^*) of the cells (m^2 mg chl^{-1}) was determined from the *in vivo* absorption spectra (range 400–750 nm; Varian Cary50 UV–visible spectrophotometer; Kromkamp & Limbeek, 1993). The irradiance was measured outside the PBR, on the surface and behind the culture, with a flat quantum radio-photometer (LI-250A, LI-COR). The incident irradiance (E) measured was incorporated in the electron transport rate (ETR) equation. The ETR expressed in µmol e^- mg chl^{-1} s^{-1} was determined according to Kromkamp & Forster (2003), as the product of $\Delta F'/F_m'$ from *in-situ* measurements, a^*, E and 0.5 (assuming that the proportion of energy directed to PSII is 50% of the total); hence, one obtained ETR = $E \times \Delta F'/F_m' \times 0.5 \times a^*$.

OJIP fluorescence induction kinetics were recorded using the Handy Plant Efficiency Analyser (PEA; Hansatech Instruments, UK). Samples were also dark-adapted for 15 min, and then illuminated with continuous saturating light. The fluorescence transients were determined according to Strasser et al. (2000). All measurements were conducted in triplicate.

5.2.3.3. Pigment analysis

For pigment extraction, triplicate samples of 2 mL were centrifuged at 2650 *g* for 10 min. The supernatant was discarded, and the pellet was homogenized in 3 mL of acetone (90% v/v) using glass beads. The samples were vortexed for 5 min and centrifuged. The supernatant was then transferred into a clean tube, and the pellet was subjected to two additional extractions with 2 mL of acetone and a final centrifugation. Absorbance measurements were taken at 663 (A_{663}) and 750 nm (A_{750}; to correct for turbidity). Total chlorophyll was determined based on the equation by SCOR-UNESCO (1966):

$$\text{Chlorophyll } (\mu\text{g mL}^{-1}) = 11.64(A_{663} - A_{750}) \quad (5.1)$$

and total carotenoids were determined by the equation of Jaspars (1965):

$$\text{Carotenoids } (\mu\text{g mL}^{-1}) = 4.1 \times A_{450} - 0.0435 \times \text{Chlorophyll } a \quad (5.2)$$

both equations were truncated, since this genus is known to possess only chlorophyll *a* (Brown, 1987).

Individual carotenoids were assessed using a reversed-phase Beckman System Gold high performance liquid chromatography (HPLC; module 125 solvent) equipped with a diode array detector, model 168 Nouveau (Beckman Instruments, CA, USA), with a column Luna,

C8 (Phenomenex), according to Van Heukelem & Thomas (2001). All reagents were HPLC grade, except for tetrabutylammonium acetate salt solution (pH 6.5), which was prepared with distilled water and then filtered. Eluent solutions were: solvent A, 80:20 (v/v) methanol, 28 mM tetrabutylammonium acetate; solvent B, 100% methanol. For the elution, with a flow rate of 0.8 mL/min, a linear gradient was used as follows: starting with 100% solvent A, 100% of solvent B was reached in 25 min, which was maintained for 2 min, then 100% of solvent A was reached in 3 min.

5.2.3.4. Lipid analysis

Lipids were extracted in triplicate, according to Bligh & Dyer (1959) and quantified, according to Marsh & Weinstein (1966). The pellets obtained from 5 mL culture samples were centrifuged at 2650 *g* for 10 min and washed with sodium chloride solution (9 g L^{-1}). For extraction, a mixture of chloroform:methanol (1:2 v/v) was used, along with bead-beating for 5 min and sample heating in a thermoblock at 60 ºC for 3 min. Following extraction, the organic phase was collected and dried. Extracts were resuspended in a known volume of chloroform, and distributed in duplicate. The samples were heated in sulfuric acid at 200 ºC for 15 min, along with the prepared standard of tripalmitine (Sigma-Aldrich, USA). After the samples were cooled and distilled water duly added, the absorbance was read at 375 nm. Measurements are expressed in lipid percentage of DW.

5.2.3.5. Fatty acid analysis

Extraction and conversion of samples to fatty acid methyl esters (FAME) were carried out following a protocol by Folch et al. (1957) and Lepage & Roy (1984), with modifications as described by Pereira et al. (2012). Briefly, freeze-dried biomass samples were mixed in a reaction vessel with a methanol:acetyl chloride solution (20:1 v/v), and then homogenized with an IKA Ultra-Turrax T18 disperser (IKA-Werke GmbH & Co. KG, Staufen, Germany) set at 23000 rpm for 1.5 min. After adding *n*-hexane, the mixture was subjected to derivatization at 70ºC for 1 h. The lipidic phase was separated by vortexing the samples with distilled water and hexane, followed by centrifugation (this step was repeated three times). The residual water of the organic phase was removed via addition of anhydrous sodium sulfate. Extracts were filtered, dried under a nitrogen gas flow, and resuspended in gas chromatography (GC) grade hexane. Analysis was performed in a Bruker gas chromatograph, coupled to a mass spectrometry (MS) detector (Bruker SCION 456/GC, SCION TQ MS) equipped with a ZB-5MS capillary column (30 m × 0.25 mm internal diameter, 0.25 µm film thickness, Phenomenex) and using helium as carrier gas. The GC oven temperature profile was set to 60 ºC (1 min), 30 ºC min^{-1} to 120 ºC, 5 ºC min^{-1} to 250 ºC, and 20 ºC min^{-1} to 300 ºC (2 min). The commercial

standard, Supelco® 37 Component FAME Mix (Sigma-Aldrich, Sintra, Portugal), was used to prepare the required calibration curves. Results are expressed as percentage of total fatty acid content.

5.2.4. Data analysis

For the *in-situ* measurements made every 15 min, a non-parametric regression – locally estimated scatterplot smoothing (LOESS) – was applied to clarify the trend of the measurements. Pearson's correlation coefficient was used to check for linear correlations between fluorescence signals and biomass biochemical characteristics. Only coefficients above 0.8 or below −0.8, bearing a significance of $p < 0.01$, were considered. Outliers were removed based on the interquartile range (IQR) criterion.

5.3. Results and discussion

5.3.1. Growth

In this study, *N. oceanica* cultures were subjected to nitrate or replenishment (control) in 1-L flat plate PBR (Figure 5.1). Cultivation started with 0.37 g DW L^{-1}, and reached 3.12 ± 0.08 g DW L^{-1} after 92 h in the control culture. Whereas the one grown without nitrate reached a maximum of 1.01 ± 0.07 g DW L^{-1} after 40 h of cultivation, and remained stable during the following 20 h of cultivation (Figure 5.2).

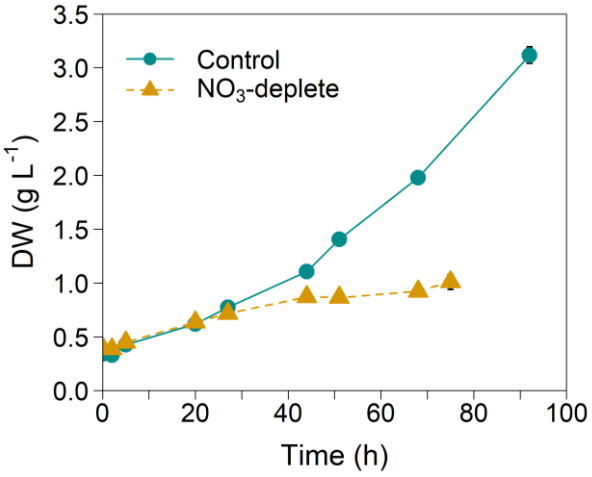

Figure 5.2. Variations of dry weight (DW; in g L^{-1}) over time (h) of the *Nannochloropsis oceanica* culture grown in nitrate replete (control; blue circles with solid line) and nitrate deplete (NO_3-deplete; yellow triangles with dashed line) conditions in 1-L flat plate photobioreactors (n = 1). Error bars represent standard deviation.

The control culture exhibited a mean specific growth rate (μ) of 0.578 d^{-1} and a mean productivity of 0.724 g L^{-1} d^{-1}, while the culture under NO_3-deplete conditions reached 0.302 d^{-1} and 0.197 g L^{-1} d^{-1}, respectively. The poor growth achieved by the latter, particularly during the first 40 h, was most likely supported by remaining intracellular N reserves, and by the presence of $NaHCO_3$ in the medium, together with CO_2 supplied via the pH control system (Nunez & Quigg, 2016; White et al., 2013). Analogous behavior was observed in *N. oceanica*, under similar conditions (NO_3-deplete) but with lower light (Liu et al., 2018).

5.3.2. Lipids

The changes in lipid content were followed throughout the experiment and are depicted in Figure 5.3.

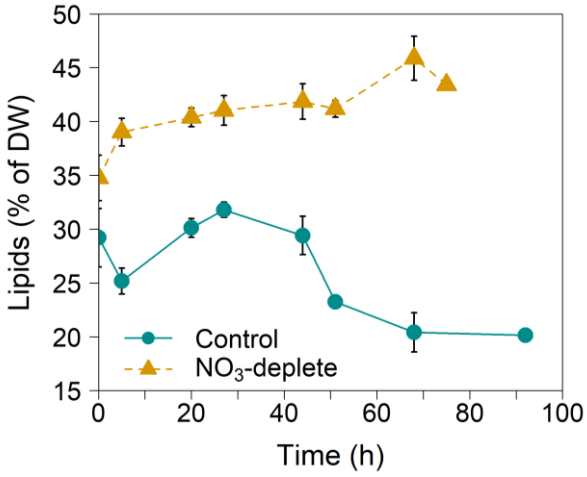

Figure 5.3. Variations of lipid content (% of DW) over time (h) of *Nannochloropsis oceanica* grown in nitrate replete (control; blue circles with solid line) and nitrate deplete (NO_3-deplete; yellow triangles with dashed line) conditions in 1-L flat plate photobioreactor (n = 1). Error bars represent standard deviation.

Lipid content decreased up to 20.1 ± 0.5 % of DW in the control, while it increased in the NO_3-deplete culture, reaching a maximum of 45.9 ± 2.1 % of DW, with a clear rise within 6 h of nitrogen starvation. The lipid accumulation under nitrate depletion was expected, since it serves as a sink for the excess reducing power when cells are under stress (Solovchenko, 2012). Lipid content variation is in agreement with previous results found in *Nannochloropsis* spp. (Guerra et al., 2021; San Pedro et al., 2016, 2013). However, the initial acclimation of the control culture for ca. 20 h was characterized by a reduction in storage lipids due to nitrate replenishment, followed by a lipid accumulation between 20 and 44 h from the beginning, most likely due to the strong light (Alboresi et al., 2016). After 2 d of cultivation, light availability decreased in the control culture due to the higher biomass concentration (Figure 5.2), which reduced lipid content. Previous reports have mentioned the reduction of lipid content during dark respiration in *Nannochloropsis*, which can also be applied to high-density cultures characterized by high self-shading (Carneiro et al., 2020; Fábregas et al., 2002).

5.3.3. Fatty acids

The fatty acid profile shown in Figure 5.4 reveals the effect of nitrate depletion upon the cultures of *N. oceanica*. Saturated fatty acids (SFA) ranged within 42-61%, and were composed of myristic (C14:0), palmitic (C16:0), and stearic (C18:0) acids; whereas monounsaturated fatty acids (MUFA) varied between 28-35%, and included palmitoleic (C16:1) and oleic (C18:1) acids; finally, polyunsaturated fatty acids (PUFA), composed of linoleic (C18:2*n*-6), arachidonic (C20:4*n*-6) and eicosapentaenoic (EPA; C20:5*n*-3) acids, varied between 6-28% of total fatty acids (TFA). The most abundant fatty acids in all cases were palmitic, followed by palmitoleic acid. These results are consistent with those found

elsewhere for this genus (Carneiro et al., 2020; Ma et al., 2014; San Pedro et al., 2013; Sukenik & Carmeli, 1989; Van Wagenen et al., 2012).

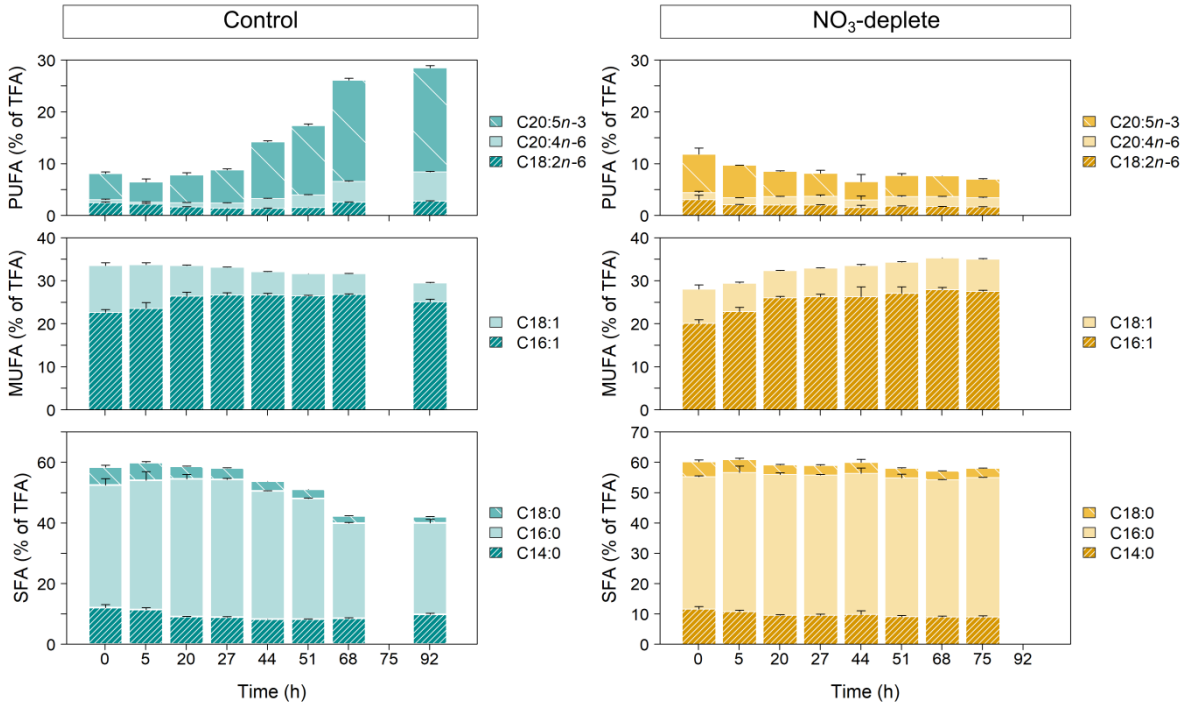

Figure 5.4. Variation of fatty acid profile, as percentage of total fatty acid (% of TFA) over time (h), of *Nannochloropsis oceanica* grown in nitrate replete (control; left plots in blue tones) and nitrate deplete (NO_3-deplete; right plots in yellow tones) conditions in 1-L flat plate photobioreactor (n = 1). The fatty acid order in the legends is the same as the plot regarding each polyunsaturated fatty acid (PUFA), monounsaturated fatty acid (MUFA), and saturated fatty acid (SFA). Error bars represent standard deviation.

In the control culture, an increase of PUFA was observed by 2 d of cultivation, mainly due to EPA but also arachidonic acid, largely at the expense of SFA, while MUFA remained stable. This high added-value PUFA, commonly found in *Nannochloropsis*, peaked (20.1±0.4% of TFA) by 4 d of cultivation. Since EPA serves as a structural component within the cells, its production is necessary to sustain growth – as was the case in the culture grown with nitrate (Sukenik, 1991). The increase of cell self-shading also contributed to the rise of fatty acid's unsaturation beyond 44 h, thus decreasing SFA (Fábregas et al., 2004). Palmitic and oleic TFA contents were reduced in the control culture, since synthesis of non-polar storage lipids was no longer necessary in the presence of nitrate (Guschina & Harwood, 2006; Solovchenko et al., 2014; Thompson, 1996).

On the other hand, when under nitrate depletion, MUFA increased slightly, now at the expense of PUFA. Under NO_3-deplete conditions, SFA and MUFA were the primary components of TFA, since they can generate more energy than carbohydrates upon oxidation, as previously reported under similar stress (Hoffmann et al., 2010; Rodolfi et al., 2009; Roessler, 1990). Catabolism of EPA decreased its content to a plateau of 3.9±0.4% of TFA,

while palmitoleic increased to 27.9±0.6% of TFA. Similar patterns where EPA decreased in microalgal cells at lower nitrate concentrations, were reported previously (Ferreira et al., 2009; Hoffmann et al., 2010).

5.3.4. Pigments

Chlorophyll content by the end of the experiment reached 2.33 ± 0.31 and 0.33 ± 0.04 % of DW for the cultures grown with and without nitrate, respectively (Annex II Supplementary Figure II.1A). At the same time, total carotenoid content (Annex II Supplementary Figure II.1B) reached 0.63% of DW for the control, and 0.21% of DW for NO_3-deplete cultures. The ratio between chlorophyll and carotenoids was approximately constant for the control culture (ratio of 3.7), but decreased in the culture under nitrate depletion (ratio of 1.6) mainly due to the decrease in chlorophyll. The initial decrease in chlorophyll in both cultures resulted from the photosynthetic apparatus acclimation process to high light, when cells were transferred to the PBR since the control culture was also negatively affected. Although cultures were pre-acclimated to 600 µmol photons m^{-2} s^{-1}, an approximate 10-fold dilution of the inoculum was applied, which strongly increased the available photons per cell. Both chlorophyll and carotenoid started to increase when the number of available photons per cell decreased after the control culture surpassed 1 g DW L^{-1} within less than 2 d. Previous studies have reported the negative impact of nitrate depletion and high light on chlorophyll and carotenoid contents (Alboresi et al., 2016; Dong et al., 2013; Pal et al., 2011; Steinbrenner and Linden, 2003).

The most abundant carotenoid found in both cultures was the light-harvesting xanthophyll violaxanthin. This carotenoid reached 0.38% of DW in the control and 0.09% of DW in NO_3-deplete, followed by the combination of vaucheriaxanthin in both ester and free form, reaching 0.16 and 0.07% of DW in the control and under NO_3-deplete conditions, respectively, by the end of the experiments. The xanthophyll cycle pigments also showed substantial differences between the two cultivation conditions (Figure 5.5).

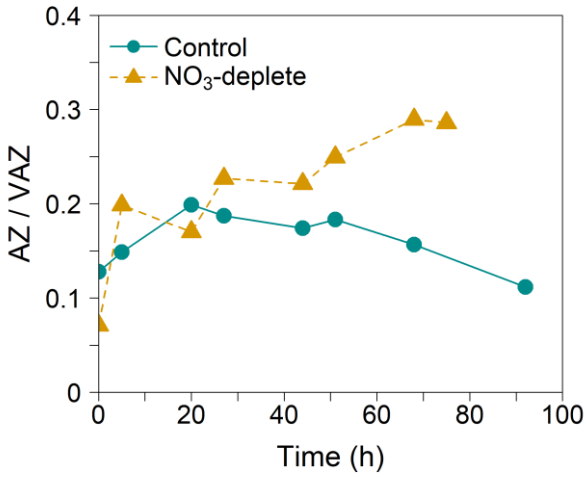

Figure 5.5. Variation of the xanthophyll cycle de-epoxidation state, expressed as the sum of antheraxanthin and zeaxanthin (AZ) on the total xanthophyll cycle pool pigments (VAZ) over time (h), of *Nannochloropsis oceanica* grown in nitrate replete (control; blue circles with solid line) and deplete (NO_3-deplete; yellow triangles with dashed line) conditions in 1-L flat plate photobioreactor (*n* = 1).

The ratio between the sum of antheraxanthin (A) and zeaxanthin (Z), and the total xanthophyll cycle pool, namely violaxanthin (V), antheraxanthin, and zeaxanthin, expresses the de-epoxidation state of the xanthophyll cycle pigments (A+Z/V+A+Z). This state increased continuously in the NO_3-deplete culture. Whereas it increased during the first 20 h of cultivation, and decreased thereafter in the control culture. The increase of the de-epoxidation state in the NO_3-deplete culture unfolded an increasing need to dissipate excess light energy by the cells (Masojídek et al., 2004), which originated from an increase of both zeaxanthin and antheraxanthin (Annex II Supplementary Figure II.2). This behavior was also observed in previous studies using *Nannochloropsis gaditana* (Lubián and Montero, 1998). Another report on *C. reinhardtii* under sulfur starvation also indicated an increase in zeaxanthin and the xanthophyll pool, to promote photoprotection of the PSII from photoinhibition (Faraloni et al., 2011). On the other hand, in the control culture, the decrease of de-epoxidation state should be an outcome of the reduced light irradiance to which the single cells were exposed to due to self-shading (Niyogi, 1999).

5.3.5. Fluorescence

Cultures were monitored using both *in-* and *ex-situ* chlorophyll *a* fluorescence. The time course of the *in-situ* measurements of the effective quantum yield of PSII ($\Delta F'/F_m'$) is shown in Figure 5.6A.

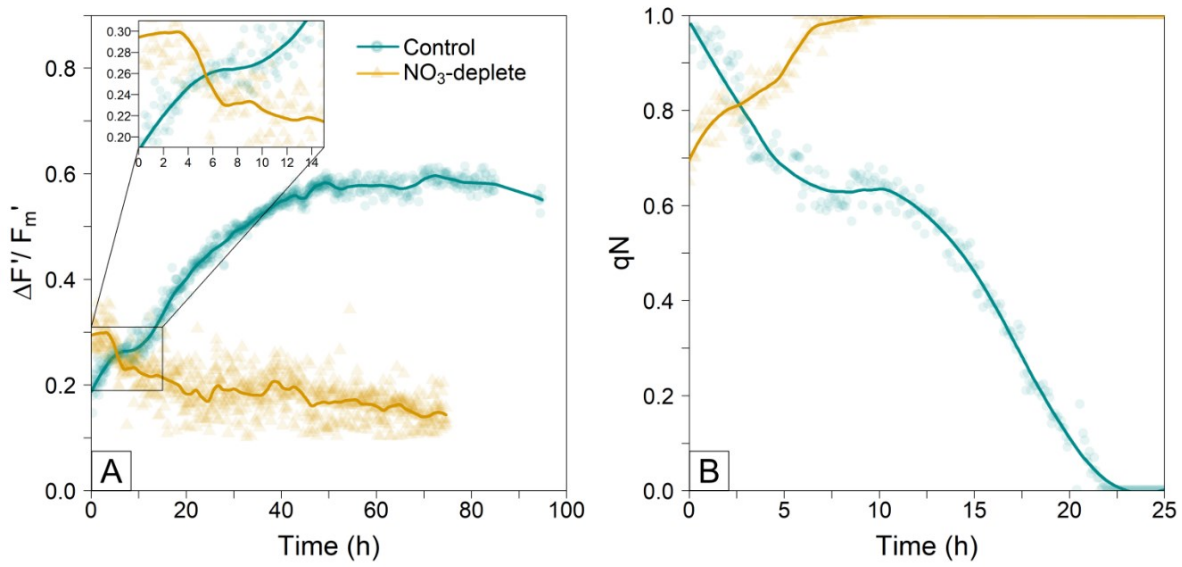

Figure 5.6. Effective quantum yield of PSII ($\Delta F'/F_m'$; **A**) and non-photochemical fluorescence quenching coefficient (qN; **B**) over time (h) showing the individual data points (semi-transparent points) and the corresponding locally weighted smoothing (LOESS; thick lines) measured with an *in-situ* pulse-amplitude-modulation (PAM) fluorometer of *Nannochloropsis oceanica*, grown in nitrate replete (control; blue dots) and nitrate deplete (NO_3-deplete; yellow triangles) conditions in 1-L flat plate photobioreactor (n = 1). Inset in 6A shows amplification of the plot over the first 15 h.

In-situ measurements reveal a clear drop in the PSII photochemistry efficiency in the NO_3-deplete culture after 5 h of exposure to nitrate deprivation (inset in Figure 5.6A). The decrease continued steadily throughout the following 27 h, after which stress became evident due to lack of growth, increase in lipid and decrease of chlorophyll contents, and fatty acid unsaturation (mainly PUFA). On the other hand, the control culture presented a logarithmic growth mirrored by an increased value of $\Delta F'/F_m'$ which stabilized close to 0.6, after ca. 40 h. This increase in effective quantum yield is readily explained by the increasing photo limitation caused by higher cell density in the control culture. Conversely, low growth and PSII photoinhibition were observed in the NO_3-deplete culture. A decrease of $\Delta F'/F_m'$ under nitrate deficiency has been previously reported in *N. oceanica* and began after intracellular nitrogen dropped below 5% of wet weight (Liu et al., 2018). A drop in the effective quantum yield of *C. reinhardtii* was also observed under sulfur starvation, due to an increased reduction state of the plastoquinone (PQ) pool (Faraloni and Torzillo, 2010). It has been reported that the degree of PQ pool reduction is one of the main triggering factors involved in the induction of a physiological response to stress conditions, which affect the PSII photosynthetic activity (Govindjee and Seufferheld, 2002).

In-situ measurements further included the qN coefficient (Figure 5.6B), which responded within the first 6 h. The control culture dropped swiftly near zero before 24 h had passed, while the qN of the NO_3-deplete culture rose to 1 (maximum value recorded by the instrument for qN) within 10 h. This result falls within the expected behavior since a rise in de-epoxidation of

the NO_3-deplete culture (Figure 5.5) was observed as well. The qN response seems to be slightly preceded by the decrease of xanthophylls de-epoxidation state, which is a mechanism to dissipate excess light as heat (Lubián and Montero, 1998). The relationship between carotenoid content, fluorescence quenching, and photoprotection has been previously established (Goodwin, 1980).

The results for the *ex-situ* measurements of the maximum quantum yield of PSII (F_v/F_m), shown in Figure 5.7A, reveal a similar trend to the *in-situ* measurements, reported for the $\Delta F'/F_m'$ in Figure 5.6A. The initial values of the F_v/F_m ratio were close to 0.6 and decreased during the following 10 h as a consequence of the strong dilution of the cultures. Thereafter, the F_v/F_m ratio recovered in the control culture, but continued to decline in the nutrient-deplete one, due to the inability of cells to repair photodamage under nitrogen stress (Marshall et al., 2000).

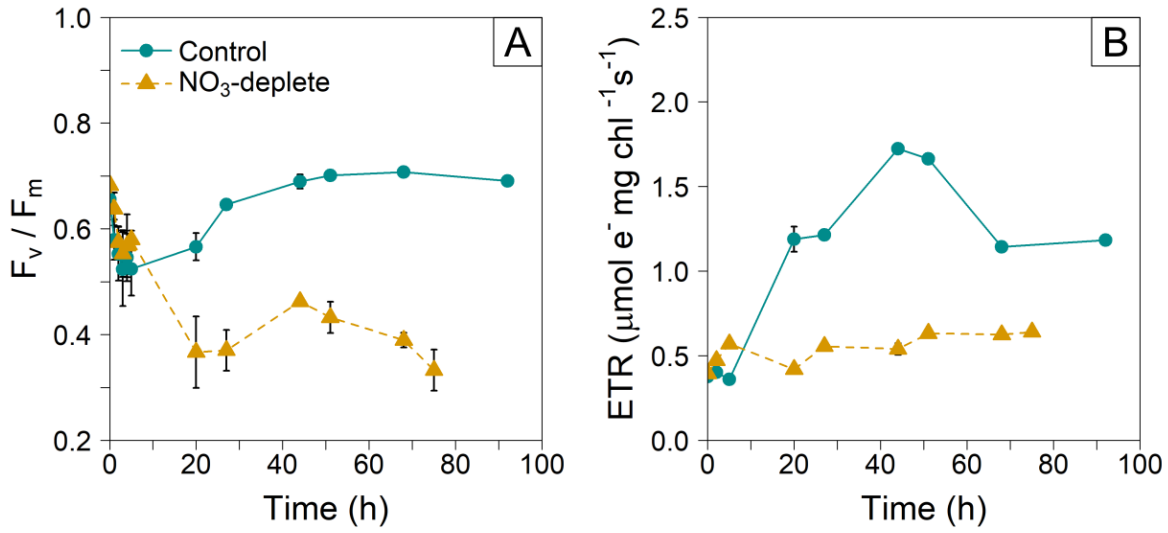

Figure 5.7. Variation of maximum quantum yield of PSII (F_v/F_m; **A**) measured *ex-situ*, and electron transport rate (ETR; **B**) from *in-situ* $\Delta F/F_m'$ measurements over time (h) with a pulse-amplitude-modulation (PAM) fluorometer, of *Nannochloropsis oceanica*, grown in nitrate replete (control; blue circles and solid line) and nitrate deplete (NO_3-deplete; yellow triangles and dashed line) conditions in 1-L flat plate photobioreactor (n = 1). Error bars represent standard deviation.

The maximum ETR achieved was 1.62 and 0.58 µmol e^- mg chl^{-1} s^{-1} for the control and NO_3-deplete cultures, respectively (Figure 5.7B). The initial acclimation process of the control culture revealed a high light absorption efficiency due to the growing ETR activity. However, the high cell density of the control culture also downregulated the activity of the ETR after 2 d, very likely due to acclimation of the cells to low light (Kromkamp et al., 2009). The culture grown without nitrate exhibited a much lower ETR, which was mimicked by oxygen evolution measurements (data not shown). With the ETR compromised, the increase of zeaxanthin and antheraxanthin pigments (Annex II Supplementary Figure II.2) points to the prevention of lipid peroxidation to avoid production of oxygen radicals (Sarry et al., 1994). However, the decrease

of the main target of lipid peroxidation, i.e., PUFAs (Figure 5.4), in NO_3-deplete cultures, suggests inability to cope with lipid peroxidation – thus leading to damage of the D1 protein (Chan et al., 2012). Low values of maximum relative ETR were also observed for *Chlorella* sp. in nitrate deficient media (White et al., 2011).

5.3.6. Transient curves

Specific variables from the transient curves were determined, normalized, and plotted for a better understanding of the PSII acclimation mechanism to nitrate stress in *N. oceanica* (Figure 5.8).

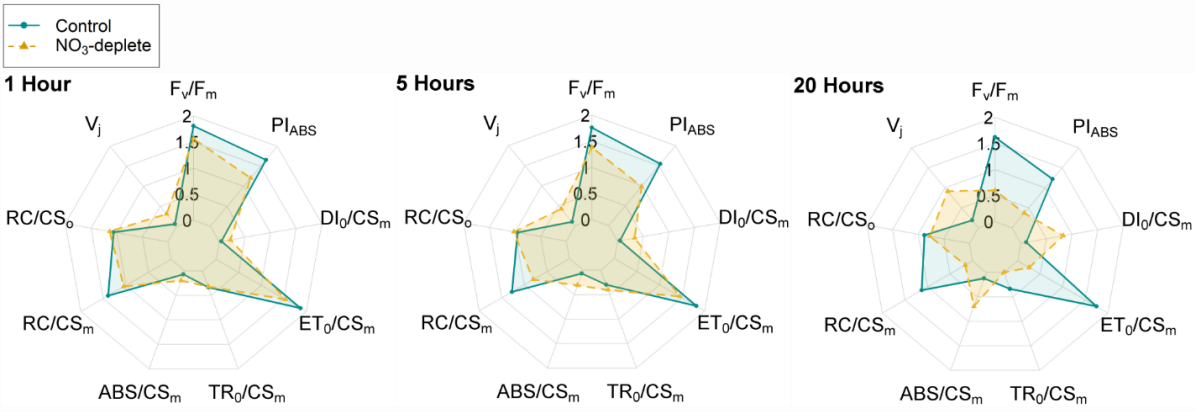

Figure 5.8. Normalized variables from transient curves (OJIP) after 1, 5 and 20 h of *Nannochloropsis oceanica*, grown in nitrate replete (control; blue area with dots and solid line) and nitrate deplete (NO_3-deplete; yellow area with triangles and dashed line) conditions in 1-L flat plate photobioreactor (n = 1).

The first inflection point of the transient curves (J) has been previously referred to as a "warning" for nitrate deprivation (Malapascua et al., 2014). This was also the case in this study and is perceptible when looking at the rise of V_j in NO_3-deplete cultures in Figure 5.8. The V_j variable represents the fraction of closed RC relative to the total RC that can be closed (Goltsev et al., 2016). The polyphasic transients O-J-I-P at 0, 3, 5, 20, and 44 h are provided in Annex II Supplementary Figure II.3, where a delayed rise and more pronounced J inflection are visible over time, suggesting metabolic incapacity of the culture under nitrate deprivation. This increase is due to the higher J inflection and a lower P as time elapses, translating into a lower efficiency in electron transport under nitrate depletion. The active RC per cross-section was also affected by nitrate depletion at O (RC/CS_o) and P (RC/CS_m), showing a decreased active RC density that was more pronounced for RC/CS_m. The energy absorbed (ABS/CS_m), as well as trapping (TR_o/CS_m) and dissipation (DI_o/CS_m) per excited cross-section, increased under nitrate depletion. Unlike these phenomenological fluxes, electron transport per excited cross-section (ET_o/CS_m) decreased. This could be explained by a hindered electron transport

beyond Q_A^-, shown by the J-I-P steps' slow rise. The performance index of PSII functional activity, normalized by the absorbed energy (PI_{ABS}), was similar to that of F_v/F_m. In a previous study using *C. vulgaris*, changes in the variables from the polyphasic transients O-J-I-P began after intracellular nitrate dropped below 3 ng NO_3 per cell, particularly a drop in maximum quantum yield (Plyusnina et al., 2020). The results reveal high electron absorption but with very low processing efficiency for electron transfer beyond Q_A^-. In addition, the V_j variable, together with ET_o/CS_m, seem to be the most sensitive to nitrate depletion in the first hours. OJIP variables are quite similar in the first 3 h, but start to diverge at 5 h, and markedly so after 20 h.

5.3.7. Relationship between photochemical and biochemical variables

According to the results reported in this study, the first triggering signal coupled to lipid accumulation was the drop in the $\Delta F'/F_m'$, recorded after 5 h of cultivation accompanied by an increase in xanthophylls de-epoxidation state, with differently affected values in the control and NO_3-deplete conditions. The increase of ETR after nitrate replenishment in the control was also noticeable, as well as the restoration of PUFA – although the latter presented a slower response. Pearson's correlation was sought among the quickest biochemical and fluorescence signals (Figure 5.9).

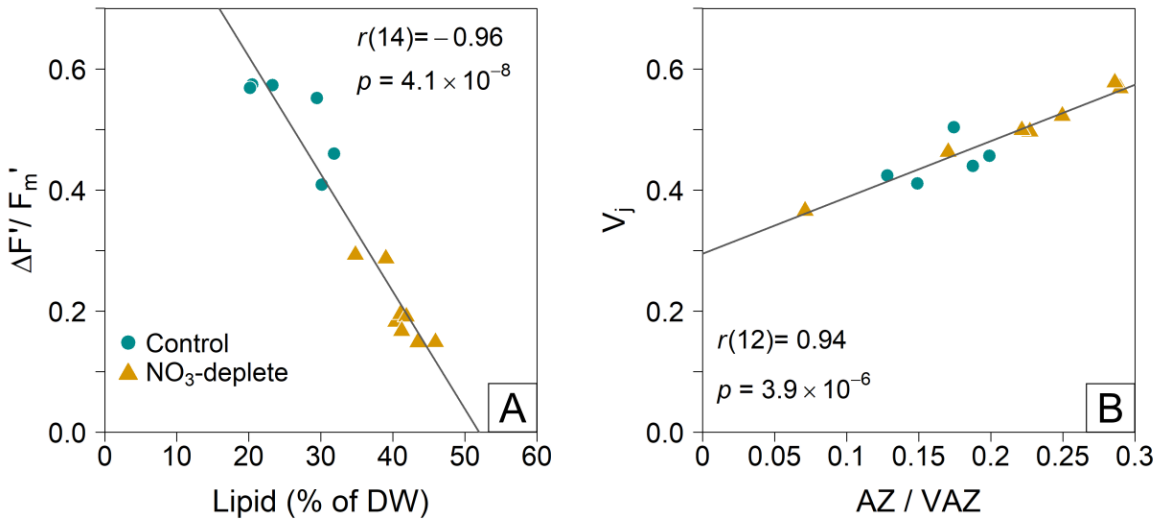

Figure 5.9. Correlations between *in-situ* effective quantum yield of PSII ($\Delta F/F_m'$) and lipid content (% of dry weight [DW]; **A**), and between V_j and de-epoxidation state (AZ/VAZ; **B**) of *Nannochloropsis oceanica*, grown in nitrate replete (control; blue circles) and nitrate deplete (NO_3-deplete; yellow triangles) conditions in 1-L flat plate photobioreactor. Significant (p <0.01) Pearson's correlations (r) are displayed in each respective plot (grey line).

A negative linear relationship was established between *in-situ* $\Delta F'/F_m'$ measurements and lipid content (Figure 5.9A; r (14) = −0.96, $p < 0.01$). In *N. oceanica*, nitrate depletion leads to lipid accumulation (Figure 5.3) while concomitantly affecting the photosynthetic apparatus (Figure 5.6), which is reflected in the fluorescence signal. Interestingly, changes in the lipid content of 5% of DW translated into changes of the *in-situ* signal $\Delta F'/F_m'$ in the order of 0.94 de- or increments. A correlation of *ex-situ* measurements of $\Delta F'/F_m'$ with intracellular nitrogen in *N. oceanica*, under 140 µmol photons m^{-2} s^{-1}, with light-dark periods has been previously reported (Liu et al., 2018).

A positive linear relationship was also found for the V_j variable from the OJIP measurements and the de-epoxidation state of the xanthophyll cycle (Figure 5.9B; r (12) = 0.94, $p < 0.05$). The increase in de-epoxidation state with V_j indicates a slowdown of electron transport (Ranglová et al., 2019), along with the activation of photoprotection mechanisms from the xanthophyll cycle. However, the small slope of the correlation produces a small change in Vj over large changes in de-epoxidation state. As a result, the most suitable relation would be between *in-situ* $\Delta F'/F_m'$ measurements and lipid content. Therefore, *in-situ* fluorescence monitoring could provide an immediate response regarding nitrate status, valid for nutrient replenishment or lipid induction needs.

5.4. Conclusions

Nitrate depletion triggered lipid accumulation with a high fatty acid saturation, thus promoting increased de-epoxidation state of xanthophyll cycle pigments, and concomitantly lowering chlorophyll content. This chain of events was preceded by a clear drop in effective quantum yield of fluorescence, within 5 h from the start of the experiments, and marked the metabolic shift to a nitrate-deplete state. This condition was further characterized by a very low processing efficiency of electron transfer observed in both ETR and the fast transient results. In conclusion, the use of *in-situ* chlorophyll *a* fluorescence in *Nannochloropsis* cultures under nitrogen stress supported detection of rapid changes in photosynthetic apparatus, and provided timely information on the start of lipid accumulation.

Chapter 6

Diel biochemical *and photosynthetic monitorization of Skeletonema costatum* and *Phaeodactylum tricornutum* grown in outdoor pilot-scale flat panel photobioreactors

This Chapter is based on the published article: Maia, I.B.*, Carneiro, M.*, Magina, T., Malcata, F.X., Otero, A., Navalho, J., Varela, J., Pereira, H., 2021. *Skeletonema costatum* and *Phaeodactylum tricornutum* grown in outdoor pilot-scale flat panel photobioreactors. Journal of Biotechnology 343, 110-119. DOI: 10.1016/j.jbiotec.2021.11.008.

Diatoms are currently considered valuable feedstocks for different biotechnological applications. To deepen the knowledge on the production of these microalgae, the diel pattern of batch growth, photosystem II performance, and accumulation of target metabolites of two commercially relevant diatoms, *Phaeodactylum tricornutum* and *Skeletonema costatum*, were followed outdoors in 100-L flat panel photobioreactors. *S. costatum* presented a higher light-to-biomass conversion resulting in higher growth than *P. tricornutum*. Both fluorescence data and principal component analysis pointed to temperature as a limiting factor for the growth of *P. tricornutum*. Higher protein and carbohydrate contents were found in *P. tricornutum*,

whereas *S. costatum* fatty acids were characterized by a higher unsaturation degree. Higher productivities were found at 1 p.m. for protein, lipid, and ash in the case of *S. costatum*. Overall, *S. costatum* showed great potential for outdoor cultivation, revealing a broader temperature tolerance and increased biomass productivity than *P. tricornutum*.

6.1. Introduction

Microalgae are photosynthetic organisms with increasing importance in several commercial sectors (Spolaore et al., 2006). Within this group, a growing interest in diatoms (*Bacillariophyceae*), characterized specifically by the presence of a silicified cell wall and chlorophyll *a* and *c* pigments, has been witnessed in recent years. Diatoms are mainly produced for the aquaculture sector, where they are used as live feed (Endar et al., 2013; Pudney et al., 2019). For instance, *Chaetoceros calcitrans*, *Thalassiosira pseudonana*, *Skeletonema costatum,* and *Phaeodactylum tricornutum* are in high demand for this sector (Lavens and Sorgeloos, 1996; Sørensen et al., 2016) due to their elevated content in polyunsaturated fatty acids (PUFA) and carotenoids, namely, fucoxanthin (Zulu et al., 2018). However, they are also emerging in other sectors: i) nutraceuticals, as a source of *n*-3 PUFA (Lebeau and Robert, 2003); ii) wastewater phytoremediation (Marella et al., 2020); iii) biomedical applications (Tramontano et al., 2020); and iv) and nanotechnology, due to their high silica content (Kröger and Poulsen, 2008).

Their expanding biotechnological potential urges provision of diatom biomass, which in turn calls for significant improvements in production thereof. Therefore, optimization of productivities of diatom species under industrial settings is of the utmost importance. Under outdoor conditions, where most commercial production of microalgae takes place, biomass productivities are affected by several biotic and abiotic factors. Light is one of these parameters, which is very difficult to control outdoors; whereas temperature is a costly factor to regulate. Because of the strong impact that light and temperature have on photosynthetic microorganisms (Carneiro et al., 2020; Cartaxana et al., 2013; Falkowski and Owens, 1978; Hitchcock, 1980; Khan et al., 1998; Montagnes and Franklin, 2001; Ras et al., 2013; Ting and Owens, 1994), it is crucial to find the best outdoor conditions in terms of these two abiotic factors that are suitable for the optimal growth of the selected species. However, it is hard to discriminate their effects outside of laboratory conditions where many factors come into play, as opposed to indoor laboratory cultures, which are subjected to a controlled environment. Therefore, fast screening methods are crucial to assess growth performance, when attempting to understand the impact of such factors upon microalgal physiology.

Originally developed for the evaluation of primary photosynthetic reactions and quenching mechanisms in higher plants (Schreiber et al., 1986), the analysis of chlorophyll *a* fluorescence is now a widespread method in the field of microalgal biotechnology (Masojídek et al., 2021; Torzillo et al., 1996; Vonshak et al., 1994). This non-invasive, highly sensitive, and fast analysis allows monitorization of the photosystem II (PSII) state in microalgae, and is crucial to pinpoint warning signals against stressful factors that might otherwise cause a lower performance, and even culture collapse (Masojídek et al., 2010). In microalgae production companies, monitorization of PSII represents a powerful tool to elucidate the best course of action throughout the whole biomass production pipeline, from culture inoculation to the optimal moment for biomass harvesting (Malapascua et al., 2014; Masojídek et al., 2021).

To the best of our knowledge, very few studies were conducted so far using *S. costatum* under outdoor conditions. Therefore, the objective of the present study was to cultivate *P. tricornutum* and *S. costatum* in outdoor pilot-scale flat panel photobioreactors (FP PBR), while monitoring growth, PSII performance and biochemical composition. The purpose of this monitorization was to allow the characterization and deeper understanding of the photosynthetic needs and the biochemical changes accompanying diatom growth, under real light and temperature conditions, besides elucidating the optimum harvesting timepoint based on target metabolites.

6.2. Methods

6.2.1. Strain selection and culture conditions

The two diatom strains, *Phaeodactylum tricornutum* and *Skeletonema costatum*, used in this study were provided by Necton S.A. (Olhão, Portugal), and the experiments were carried out at the company's facilities. The cultures were initially grown in 6-L balloons in the laboratory, at 20 ± 2 °C under a circadian light:dark regime (16h:8h light:dark) and mixed by bubbling a mixture of air and 1% CO_2 (v/v), filtered using 0.22 µm PTFE filters. The culture medium used was Nutribloom® Plus (NB+; Phytobloom by Necton, Belamandil, Portugal) at a final NO_3^- concentration of 4 mM, with addition of silicates (0.11 mM) in the case of *S. costatum*.

6.2.2. Outdoor trials in flat panel photobioreactors

The outdoor FP PBR used in this study consisted of a 0.3-mm thick plastic bag with 1.3 m length, 1 m height, and 0.08 m width, supported by a metal structure, providing a working volume of 100 L. Each FP PBR was equipped with a CO_2 injection pulse system that kept the pH around 8.5, and an individual aeration system filtered through a 0.22-µm PTFE filter. The systems were also equipped with water sprinklers to control the temperature of the culture, being activated when temperature surpassed 26 ºC. Environmental temperature and solar irradiance were provided by a WatchDog WD-2700 meteorological station, coupled to a LICOR LI-190R-BL-15 quantum sensor setup in the premises. Culture temperature and pH were measured using a pHep® HI98128 (HANNA instruments, Romania). The culture media used was identical to that described for laboratory growth.

Three FP PBRs were inoculated with the corresponding diatoms (*P. tricornutum* and *S. costatum*), at an initial dry weight (DW) of ca. 0.2 g L^{-1} and the cultures were allowed to grow in batch mode for 13 days. Nutrient consumption was monitored to prevent limitation, by measuring nitrates in the culture media according to the standard ultraviolet spectrophotometric method (Armstrong, 1963), and adding full medium to a final nitrate concentration of 4 mM when required. Sampling was performed five times during the experiment, and samples were collected throughout the day at 9 a.m., 1 and 5 p.m., and again at 9 a.m. on the following day. The experiments were conducted from February to April 2019 for *P. tricornutum* and from January to February 2020 for *S. costatum*.

6.2.3. Growth assessment

Microalgal growth was assessed by optical density (OD) and DW measurements. OD was measured at 750 nm using a UVmini-1240 spectrophotometer (Kyoto, Japan). DW was assessed, in triplicate, by filtering 10 mL of culture through pre-weighed 0.7-µm fiberglass filters (VWR), which were then washed with 10 mL of ammonium formate (35 g L^{-1}) and afterward oven-dried (60 ºC) until reaching constant weight (Zhu and Lee, 1997). Finally, a calibration curve between OD and DW was obtained.

Specific volumetric productivities (g L^{-1} d^{-1}) between measurements were determined according to equation (6.1):

$$\text{Specific Volumetric Productivity}\ (\text{g L}^{-1}\text{d}^{-1}) = \frac{X_1 - X_2}{(t_1 - t_2) \times V} \quad (6.1)$$

where X_1 and X_2 denote biomass (g) at time t_1 and t_2 (days), respectively, and V (L) denotes the culture volume.

6.2.3.1. Photosynthetic efficiency

The higher heating value (HHV) was calculated (Callejón-Ferre et al., 2011) using equation (6.2):

$$\mathrm{HHV}\ (\mathrm{J\ g^{-1}}) = (-3.393 + 0.507[\mathrm{C}] - 0.341[\mathrm{H}] + 0.067[\mathrm{N}]) \times 1000 \quad (6.2)$$

where C, H and N denote the carbon, hydrogen, and nitrogen contents as % of DW as per elemental analysis (see 6.2.5.1. Protein). Afterwards, the photosynthetic efficiency (PE) was determined using the following equation (6.3):

$$\mathrm{PE}(\%) = \frac{(\mathrm{X_f} - \mathrm{X_i}) \times \mathrm{HHV}}{H_e \times \mathrm{A}} \quad (6.3)$$

where "X_f" and "X_i" pertain to biomass (g) at final sampling and inoculation timepoints, respectively; "H_e" represents the radiant exposure (J m^{-2}) from inoculation until the final sampling timepoint; and "A" represents the ground area (m^2) occupied by the 100-L FP PBR (1.69 m2) within the complete FP PBR plant system used (which includes the space between reactors).

6.2.4. Fast fluorescence transients

Measurements of chlorophyll *a* fluorescence were carried out using a pulse amplitude modulation (PAM) fluorometer, AquaPen AP 110-C (Photon Systems Instruments, Czech Republic), together with the FluorPen 1.0 software. Established protocols provided by the manufacturer for fast chlorophyll fluorescence induction curves (OJIP) were used to measure samples *off-situ*. Samples were prepared in triplicate, diluted to ca. 0.25 g L^{-1}, and dark-adapted for 15 min, so that all reaction centers (RC) were fully open (oxidized plastoquinone; Q_A) (Malapascua et al., 2014).

OJIP curves were recorded by exposing samples to a weak measuring light (0.02 µmol photons m^{-2} s^{-1}; ML) followed by a saturating pulse (2850 µmol photons m^{-2} s^{-1}) to measure the polyphasic rise O-J-I-P. From the obtained data, two quantum efficiencies were used: the maximum quantum yield of primary photochemistry, $F_v/F_m = \varphi_{Po}$, commonly used as stress indicator (Masojídek et al., 2013; Parkhill et al., 2001; White et al., 2011), which also relates

to the efficiency of pheophytin (the primary electron acceptor of PSII) and Q_A (the primary plastoquinone electron acceptor of PSII) reduction with excitation energy from the primary electron donor of PSII, P680* (Stirbet et al., 2018); and a trapped exciton efficiency to move an electron further than Q_A^- into the electron transport chain, $1 – V_j = \psi_0$. The reader is referred to Strasser et al. (2000) for a more detailed description of such parameters.

6.2.5. Macronutrient analysis

The samples collected at 9 a.m. from the lag (day 1), logarithmic (log; day 7) and late logarithmic (late log; day 13) phases of growth were used for biochemical analysis. The samples were centrifuged at 10,000 *g* for 5 min (IEC CL40), lyophilized (LyoQuest Telstar, Terrassa, Spain) and stored at -20 ºC until further analysis.

6.2.5.1. Protein

Protein content was determined by elemental analysis of total nitrogen, using a Vario EL III (Elementar Analysensysteme GmbH, Germany), according to the manufacturer's procedure. Total nitrogen content was later multiplied by the conversion factors 4.87 and 4.63 for *P. tricornutum* and *S. costatum*, respectively, to obtain total protein content (Lourenço et al., 2004).

6.2.5.2. Lipid

Lipids were determined according to Bligh & Dyer's protocol (Bligh and Dyer, 1959), modified as described by Pereira et al. (2011). Briefly, freeze-dried biomass was homogenized using an IKA Ultra-Turrax disperser (25,000 rpm for 2 min; T18 digital ULTRA-TURRAX, IKA-Werke GmbH, Staufen, Germany), with a mixture of methanol, chloroform, and water (2:2:1). Phase separation was thereafter achieved by centrifugation (5,000 *g* for 10 min), and the organic phase (chloroform) was transferred into new glass tubes. Subsequently, a known volume of extract (0.7 mL) was transferred to previously weighed tubes and evaporated overnight in a dry bath (60 ºC). The total lipid content was then determined gravimetrically.

6.2.5.3. Ash

Ash content was obtained by burning 50 mg of freeze-dried biomass in a furnace (J.P. Selecta, Sel horn R9-L), for 8 h at 525 ºC (Barreira et al., 2017).

6.2.5.4. Carbohydrate

Carbohydrates were calculated by difference, by subtracting ash, protein, and lipid contents from 100%.

6.2.6. Fatty acid profile

The fatty acid profile was determined using the protocol by Folch et al. (1957) and Lepage and Roy (1984), and modified as described by Pereira et al. (2012). Briefly, approximately 20 mg of freeze-dried biomass were resuspended in 1.5 mL of derivatization solution (methanol:acetyl chloride 20:1 v/v), and an IKA Ultra-Turrax disperser (2 min at 25,000 rpm) was used to disrupt and homogenize the samples. Afterward, 1 mL of *n*-hexane was added, and derivatization was achieved in a water bath (70 ºC for 1 h). The samples were then transferred into centrifuge tubes, to which 1 mL of distilled water and 4 mL of *n*-hexane were added. The lipidic phase was obtained after vortexing the samples, and separation of phases occurred via centrifugation (2,000 *g* for 5 min). The hexane phase was transferred to new tubes, and the process was repeated twice. Anhydrous sodium sulphate was then used to remove residual water. The samples were filtered, the solvent evaporated under a nitrogen flow, and the pellet resuspended in a known volume (0.5 mL) of gas chromatography (GC) grade hexane.

Fatty acid methyl esters (FAME) were analyzed on a Bruker gas chromatographer, coupled to a mass spectrometry system (Bruker SCION 456-GC, SCION TQ MS) equipped with a ZB-5MS capillary column (30×0.25 mm of internal diameter with 0.25 µm film thickness; Phenomenex), with helium as carrier gas (1 mL min^{-1}). The temperature program was set to: 1 min at 60 ºC, 30 ºC min^{-1} to 120 ºC, 4 ºC min^{-1} to 250 ºC and 20 ºC min^{-1} to 300 ºC, hold for 4 min, with an injection temperature of 300 ºC in splitless mode. For FAME identification, a Supelco®37 component FAME Mix (Sigma-Aldrich, Sintra, Portugal) was used as a standard to prepare the different calibration curves. Results are expressed as percentage of total fatty acid (% TFA) content.

6.2.7. Statistical analysis

Data were calculated as mean of three independent repeats ± standard deviation (SD). A mixed effects model, using species for fixed factor and repetitions for random factor, was used to support the analysis of variance (ANOVA), with the significance level set at 0.05. A principal components analysis (PCA) was used to analyze the meteorological factors affecting

each species' volumetric productivity and biomass composition. Statistical treatment was performed with R software. Plots were designed with R software or SigmaPlot 11.0.

6.3. Results and discussion

6.3.1. Growth performance

The growth performance of *P. tricornutum* and *S. costatum* in 100-L FP PBR was assessed for 13 days in batch mode. The average daily maximum solar irradiance was higher during the *P. tricornutum* trials, with an average of 1578 ± 323 (maximum of 1938 μmol m^{-2} s^{-1}) compared to 1289 ± 124 μmol m^{-2} s^{-1} (maximum of 1416 μmol m^{-2} s^{-1}) during the *S. costatum* trials (Figure 6.1A). Minimum and maximum temperatures varied between 10.0 – 19.6 ºC (average of 14.8 ± 2.6 ºC), and between 8.6 – 20.3 ºC (average of 14.8 ± 2.7 ºC) during the *P. tricornutum* and *S. costatum* trials (Figure 6.1B), respectively. The average irradiance and temperatures, as well as their variability throughout the day, are two crucial factors that can dictate microalgal growth and severely impact biomass productivity (Carneiro et al., 2020; Fábregas et al., 2004; Grima et al., 1996; G Torzillo et al., 1991).

Regarding growth performance of the two species, cultures started with a biomass concentration of ca. 0.20 ± 0.01 g DW L^{-1} (lag phase) and reached their maximum concentrations on day 12 for both species, with 2.86 ± 0.02 and 1.90 ± 0.38 g DW L^{-1} for *S. costatum* and *P. tricornutum*, respectively (Figure 6.1C). A significantly ($p < 0.05$) higher growth rate was accordingly found for *S. costatum* when compared to that of *P. tricornutum*. Additionally, PE values for *P. tricornutum* at the end of the trial were 0.56 ± 0.11%, while they were significantly higher ($p < 0.05$) for *S. costatum* cultures, with 1.05 ± 0.09%.

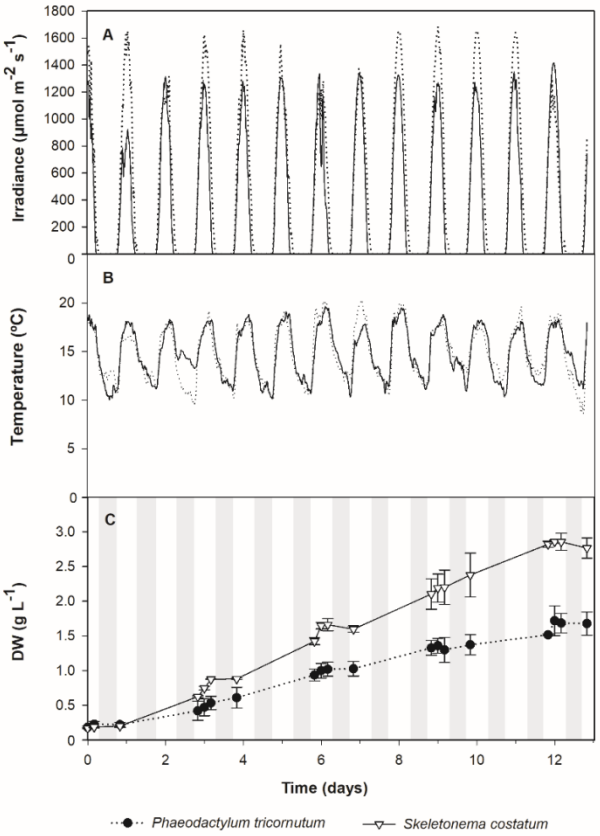

Figure 6.1. Average irradiance (µmol photons m^{-2} s^{-1}; **A**) and average temperature (ºC; **B**) measured during outdoor growth of *Phaeodactylum tricornutum* (dotted lines) and *Skeletonema costatum* (solid lines) (n = 3). Growth in biomass dry weight (DW; g L^{-1}; **C**) of *P. tricornutum* (● and dotted line) and *S. costatum* (▽ and solid line) in 100-L flat panel photobioreactors, in batch mode (n = 3). Error bars and background grey bars represent standard deviation and nighttime, respectively.

Among the two species under this study, *S. costatum* presented significantly (p < 0.05) higher average daylight (from 9 a.m. to 5 p.m.) volumetric productivities (0.55 ± 0.28 g L^{-1} d^{-1}) when compared with those of *P. tricornutum* (0.23 ± 0.38 g L^{-1} d^{-1}). Similar specific productivities were previously reported for a similar cultivation system, where *P. tricornutum* was grown in outdoors in a 40-L Green Wall Panel®-III PBRs in batch for 6 days, reaching biomass productivities of 0.55 and 0.39 g L^{-1} d^{-1} in the summer and spring, respectively (Rodolfi et al., 2017). On the other hand, *S. costatum* productivities hereby reported were relatively higher than those obtained for this species grown in 80-L PBR outdoors (Pérez et al., 2017), with productivities of ca. 0.03 g L^{-1} d^{-1} in 2 days of growth. However, there is a clear lack of studies under outdoor conditions encompassing *S. costatum* productivities, thus justifying further research on this topic.

The average temperature values – and particularly the low nighttime temperature – recorded during our experiment laid below the optimum temperatures reported for *P. tricornutum*, between ca. 20-21 ºC (Fawley, 1984; Ova Ozcan and Ovez, 2020; William and Morris, 1982), and 19-25 ºC for *S. costatum* (Hitchcock, 1980; Lefebvre et al., 2007; Tian et al., 2002). In fact, *S. costatum* seems to tolerate a wider range of temperatures than *P.*

tricornutum, with the former thriving at slightly lower temperatures (De Pauw et al., 1980), which could help explain the lower productivity observed for *P. tricornutum* in the current study. In fact, (Kudo et al., 2000), showed a maximum growth rate for *P. tricornutum* at a temperature of 20 ºC, defining it as optimal, with a decrease in growth rate for higher and lower temperatures. In addition, the initial irradiance was much higher for *P. tricornutum*, which could have led to photodamage during the first days, when the culture concentration was low, affecting its subsequent growth.

6.3.2. Fast transients

The maximum quantum yield of primary PSII photochemistry (F_v/F_m; also termed φ_{Po}) And the subsequent efficiency with which a PSII trapped electron moves beyond Q_A^- (ψ_o) were determined and are shown in Figure 6.2A and 6.2B, accordingly.

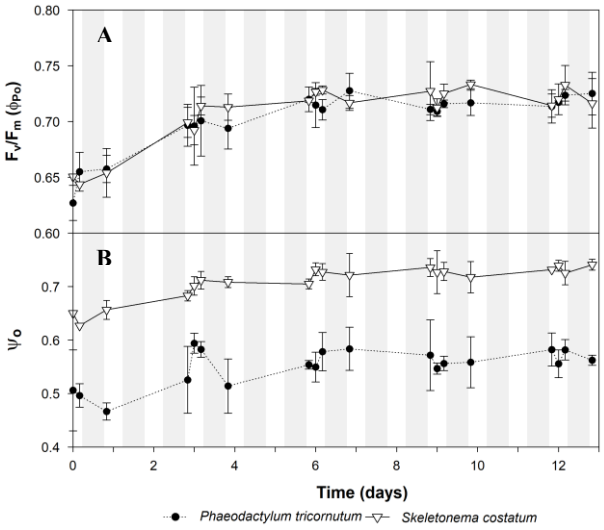

Figure 6.2. Average maximum quantum yield (F_v/F_m, also termed ϕ_{Po}) of primary photochemistry (**A**) and efficiency (ψ_o) with which a PSII trapped electron is transferred further than Q_A^- (**B**) in *Phaeodactylum tricornutum* (●, dotted lines) and *Skeletonema costatum* (▽, solid lines), cultivated in outdoor 100-L flat panel photobioreactors, in batch mode (*n* = 3). Error bars and background grey bars represent standard deviation and nighttime, respectively.

Both species exhibited similar maximum quantum yield of PSII (F_v/F_m) pattern that varied between 0.62 and 0.75. During the first two days, both species exhibited lower F_v/F_m values, probably caused by the transition to outdoor conditions where they were subjected to higher irradiances and lower temperature control together with lower cellular concentrations. Nonetheless, from day 3 onward, values stabilized at 0.72 ± 0.02 for both species. These values are in agreement with those previously reported for both species, with 0.6-0.74 for *P. tricornutum* (Acién Fernández et al., 2003; Lavaud et al., 2007; Lavaud and Lepetit, 2013;

Lepetit et al., 2017; Silva Benavides et al., 2013; Wagner et al., 2016) and 0.59-0.72 for *S. costatum* (Lavaud et al., 2007; Lavaud and Lepetit, 2013).

The efficiency of electron transport beyond Q_A^- was also lower in the beginning for both species, yet the values exhibited by *S. costatum* were, on average, significantly higher ($p < 0.05$). At the end of the trials, these values stabilized at 0.56 ± 0.04 for *P. tricornutum* and 0.72 ± 0.02 for *S. costatum*. There are few reports on ψ_o values for these species; however, values of 0.5 were reported for both S*keletonema marinoi-dohrnii* (Khanam et al., 2019) and *P. costatum* (Cabrita et al., 2018). The values for ψ_o of *P. tricornutum* are consistent with those found in the literature, but these were higher for *S. costatum*. Higher values of ψ_o – calculated as $1\text{-}V_j$ (where V_j is the relative variable fluorescence at 2 ms), have been previously reported to correlate with the temperature associated with higher growth rates (Ranglová et al., 2019). Indeed, *S. costatum* grew significantly faster than *P. tricornutum* (Figure 6.1). This indicates that the lower values of ψ_o of *P. tricornutum* might have favorably contributed to the observed slower growth. This shows the crucial photoprotection role of the electron cycle of PSII reaction centers in diatoms (Lavaud and Lepetit, 2013).

6.3.3. Biomass composition

Biomass composition in terms of protein, lipid, carbohydrate and ash contents presented some difference during the growth period of both species. During lag phase, *S. costatum* was the only species that showed a significantly different proximal composition, with an increase in ash content and lower lipid content ($p < 0.05$). The fact that *S. costatum* presented a higher ash content during the lag phase could be related to the presence of specialized silicate deposition vesicles, where silicates are absorbed and transported for later use, when available in the culture medium (Hildebrand, 2003). On the other hand, silicates are essential for *S. costatum* growth, a species characterized by heavily silicified cell walls (Brown and Jeffrey, 1995; Paasche, 1973), otherwise, poorly silicified cells develop, thus affecting the formation of complete cell chains (Taylor, 1985). The lower lipid content detected in *S. costatum* during lag phase is possibly related to the fact that photosynthetic energy was diverted to cell division and protein synthesis (Huerlimann et al., 2010).

In the log phase, *S. costatum* showed an increase in proteins and lipids ($p < 0.05$), while *P. tricornutum* showed an increase in proteins and a decrease in ashes ($p < 0.05$). Protein content has been reported as usually higher during the exponential growth phase, due to active growth of the cells and nitrogen availability in the culture medium (Piorreck and Pohl, 1984; Sui et al., 2020). With the advance of culture growth, lipid content can increase as a result of energy storage or even as a temporary energy storage to be used in the photosystem

(Klok et al., 2013). The decrease in ash content present in *P. tricornutum* during the log phase was possibly related to a corresponding increase in photosynthetic efficiency (Megía-Hervás et al., 2020). This ash content decrease in *P. tricornutum* has also already been mentioned by Fernández-Reiriz et al. (1989). However, both species did not present any significant changes in proximal composition during late logarithmic phases.

Comparison of biomass composition also revealed differences between the two diatoms (Table 6.1). Protein content varied between 26.5 and 31.6% of DW for *P. tricornutum* and was significantly higher than that found for *S. costatum*, ranging between 17.9 and 24.6% of DW. Protein contents of *P. tricornutum* were similar to those described in previous reports for this species, performed at lab- (Brown, 1991; Parsons et al., 1961) and pilot-scale (Rebolloso-Fuentes et al., 2001). Nevertheless, protein contents higher than 50% have been reported by Thomas et al. (1984) and Quelhas et al. (2019), the latter performed at industrial outdoor scale. As for *S. costatum*, the values obtained in the present study are similar to those reported by van Houcke et al. (2017), Lestari et al., (2014) and Brown (1991), of 23.3, 24.7 and 25% of DW, respectively. Higher protein content was also found by Monkonsit et al., (2011) and Parsons et al. (1961). However, it is important to note that these studies were performed under laboratory conditions.

Table 6.1. Proximal composition of proteins, lipids, carbohydrates, and ashes (% of DW) of *Phaeodactylum tricornutum* and *Skeletonema costatum* at 9 a.m. during the Lag, logarithmic (Log) and late logarithmic (Late log) growth phases (n = 3). Different letters indicate statistical differences ($p < 0.05$) between species.

	Phaeodactylum tricornutum			*Skeletonema costatum*		
	Lag	Log	Late log	Lag	Log	Late log
Proteins	26.5 ± 3.6^{a}	31.6 ± 3.5^{a}	27.9 ± 1.4^{a}	17.9 ± 4.1^{b}	24.6 ± 1.5^{b}	22.2 ± 3.7^{b}
Lipids	12.2 ± 3.6^{a}	14.6 ± 3.8^{a}	14.6 ± 4.7^{a}	7.8 ± 3.4^{b}	13.7 ± 2.2^{a}	14.1 ± 1.9^{a}
Carbohydrates	31.4 ± 5.1^{a}	31.2 ± 3.7^{a}	32.2 ± 4.3^{a}	23.9 ± 4.9^{b}	26.3 ± 3.0^{b}	29.6 ± 2.8^{a}
Ashes	28.9 ± 7.1^{b}	22.6 ± 6.1^{b}	25.2 ± 6.8^{b}	50.7 ± 3.2^{a}	35.4 ± 1.8^{a}	32.1 ± 2.4^{a}

Both species presented similar patterns of lipid accumulation, ranging from 12.2 to 14.6% of DW, except for *S. costatum* during the lag phase, which showed a significantly lower lipid content (7.8% of DW) than *P. tricornutum* at the same growth phase. These results are consistent with previously reported data (Brown, 1991; Rebolloso-Fuentes et al., 2001) for *P. tricornutum* and for *S. costatum* (Brown, 1991; van Houcke et al., 2017).

Carbohydrate content varied between 31.2 and 32.2% of DW in *P. tricornutum*, and 23.9 and 29.6% of DW for *S. costatum*. Carbohydrate content obtained in *P. tricornutum* cultures was higher than those previously reported (Brown, 1991; KaiXian and Borowitzka, 1993;

Parsons et al., 1961; Quelhas et al., 2019). Similar carbohydrate content (35% of DW) was found by Rebolloso-Fuentes et al. (2001) when growing *P. tricornutum* under higher light intensities in outdoor conditions. Similarly, *S. costatum* also showed higher carbohydrate content, as opposed to previous reports (20.8 to 21.5% of DW; Monkonsit et al., 2011; Parsons et al., 1961). In the present study, accumulation of carbohydrates was favored at the expense of lipids, possibly because the cultures were in nitrogen repletion conditions, since lipids are normally accumulated under nitrogen depletion (Palmucci et al., 2011).

Finally, ash content was significantly higher in *S. costatum*, varying between 32.1 and 50.7% of DW, with the maximum ash content observed during the lag phase. *P. tricornutum* presented lower ash content, between 22.6 and 28.97.1% of DW compared to *S. costatum*. Similar ash content for *S. costatum* (55.6% of DW) was previously described by Lestari et al. (2014). The lower ash content of *P. tricornutum*, when compared to *S. costatum*, could be explained by the absence of a silicified frustule in the fusiform morphotype – the major morphotype observed in this study (Borowitzka and Volcani, 1978; Lewin, 1958; Lewin et al., 1958). It is important to highlight that, despite the growth under outdoor conditions and the difference in culture volume, the biochemical composition obtained in the present study was similar to what has been previously reported, particularly for *S. costatum*, even though the latter were largely performed at lab-scale.

Biomass composition is very important, since it can alter the biomass market value. Nonetheless, biomass productivity provides an overview of the performance of the whole process, thus allowing the determination of its feasibility. In this sense, productivities for specific classes of biomolecules and ashes were analyzed in detail at three different times of the day, in an attempt at determining the timepoint associated with the highest productivity (Figure 6.3).

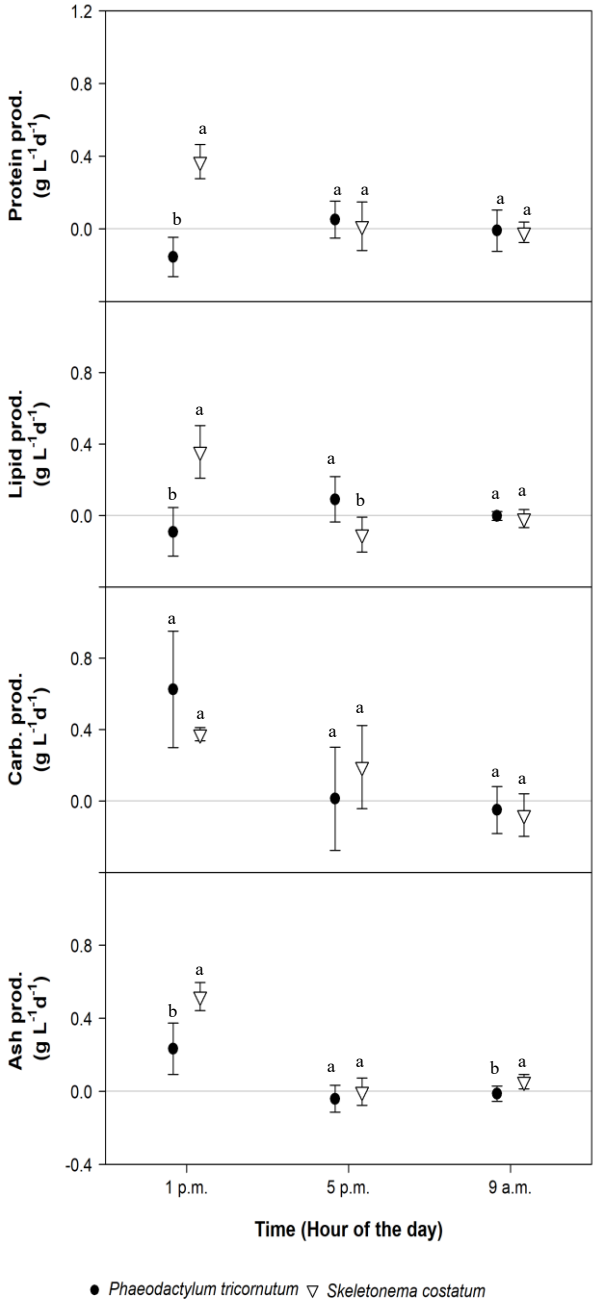

Figure 6.3. Productivity of the main classes of biomolecules and ashes in *Phaeodactylum tricornutum* (●) and *Skeletonema costatum* (▽), at different times of the day. Different letters indicate statistical differences ($p < 0.05$) between species for each timepoint. Error bars represent standard deviation.

When comparing both species, *P. tricornutum* exhibited higher protein and lipid productivities from 5 p.m. to 9 a.m., whereas *S. costatum* showed higher biomolecule productivities during the day (1 to 5 p.m.), even though *P. tricornutum* displayed higher protein contents (Table 6.1). Both carbohydrate and ash productivities were higher in the morning for both species compared to the other sampling timepoints, but only ash productivities unfolded significant differences between species (Figure 6.3).

The cultivation of *P. tricornutum* favored carbohydrate productivities during the day, over that of lipids and proteins. In addition, a decrease in overall productivities can be grasped from 5 p.m. to 9 a.m., caused by lower biomass growth, coupled with the need of carbohydrate consumption to support cell division. Energy reserves in the form of carbohydrates are usually catabolized in the dark (Handa, 1969; Vårum et al., 1986), where adenosine triphosphate (ATP) is used for cell division. Consequently, energy accumulated during the light period is used in the dark for continuous protein synthesis (Geider et al., 1989), thus allowing cell division. Chauton et al., (2013) showed a rapid increase in carbohydrate content in *P. tricornutum* cultures during the light period, which declined during the dark as a result of the consumption of ATP to support mitosis. Cell division also seems to occur during the dark period in *S. costatum* cultures (Anning et al., 2000; Owens et al., 1980). However, research on the productivity of biochemical compounds of *S. costatum* remains scarce.

Taken together, these results suggest that harvesting *S. costatum* biomass during the morning (9 a.m. to 1 p.m.) in an industrial setting might be advisable, as the productivity of all biomolecules were higher at this timepoint compared to the other times of the day. Conversely, for *P. tricornutum*, this was only true for carbohydrates and ashes, whereas the highest productivities for protein and lipids were attained in the afternoon (from 1 to 5 p.m.).

6.3.4. Fatty acids

The FAME profile of *P. tricornutum* was mainly composed of myristic (C14:0), palmitic (C16:0), palmitoleic (C16:1) and eicosapentaenoic (C20:5*n*-3; EPA) acids, while palmitolinolenic (C16:3) and docosahexaenoic (C22:6*n*-3; DHA) acids were detected at lower levels (Table 6.2). *S. costatum* had a similar profile, with myristic, palmitoleic, palmitolinolenic and EPA as major fatty acids, while DHA, palmitidonic (C16:4) and palmitic acids were represented less than 10% of total FAME (Table 6.2).

Table 6.2. Fatty acid profile of *Phaeodactylum tricornutum* and *Skeletonema costatum* (% of total FAME) during Lag, logarithmic (Log) and late logarithmic (Late log) phases of growth (n = 3). Fatty acids with concentrations below 5% were not included. Different letters indicate statistical differences ($p < 0.05$) between species for each growth phase. N.d. – not detected; SFA – saturated fatty acids; MUFA – monounsaturated fatty acids; PUFA – polyunsaturated fatty acids.

	Phaeodactylum tricornutum			*Skeletonema costatum*		
FAME	Lag	Log	Late log	Lag	Log	Late log
C14:0	11.3 ± 2.8	10.4 ± 2.2	10.1 ± 2.3	17.0 ± 1.9	17.6 ± 1.1	18.2 ± 0.6
C16:0	28.8 ± 8.3	19.0 ± 3.4	22.1 ± 6.2	7.7 ± 1.5	5.1 ± 0.4	4.0 ± 0.5
∑ SFA	**40.1 ± 10.8^{a}**	**29.5 ± 5.2^{a}**	**32.2 ± 5.1^{a}**	**24.7 ± 2.3^{b}**	**22.7 ± 1.0^{b}**	**22.2 ± 0.6^{b}**
C16:1	32.1 ± 3.2	29.5 ± 3.4	31.0 ± 1.3	24.9 ± 2.0	20.9 ± 1.6	19.6 ± 2.9
∑ MUFA	**34.5 ± 3.8^{a}**	**31.6 ± 3.3^{a}**	**33.7 ± 1.8^{a}**	**24.9 ± 2.0^{b}**	**20.9 ± 1.6^{b}**	**19.6 ± 2.9^{b}**
C16:3	3.6 ± 1.0	7.7 ± 2.2	6.0 ± 2.9	12.3 ± 2.5	14.4 ± 2.8	12.9 ± 0.3
C16:4	n.d.	n.d.	n.d.	5.9 ± 1.4	5.8 ± 1.0	3.6 ± 0.2
C20:5*n*-3	19.6 ± 12.3	28.9 ± 6.9	26.4 ± 4.8	22.4 ± 2.4	26.2 ± 3.5	29.0 ± 2.1
C22:6*n*-3	2.2 ± 1.8	2.4 ± 0.9	1.7 ± 0.2	4.8 ± 1.3	5.9 ± 1.6	8.2 ± 0.4
∑ PUFA	**25.4 ± 14.4^{b}**	**38.9 ± 8.4^{b}**	**34.1 ± 6.7^{b}**	**50.4 ± 3.0^{a}**	**56.4 ± 1.7^{a}**	**58.2 ± 2.8^{a}**

Saturated fatty acids (SFA) varied between 29.5 and 40.1% of total fatty acids (TFA) in *P. tricornutum,* and between 22.2 and 24.7% of TFA in *S. costatum*. Monounsaturated fatty acids (MUFA) varied between 31.6 and 34.5% of TFA in *P. tricornutum* and between 19.6% and 24.9% of TFA in *S. costatum*. The high amount of palmitic and palmitoleic acids resulted in a higher contribution (more than half of the total FAME profile) of SFA and MUFA of *P. tricornutum*. SFA and MUFA contents were significantly higher for *P. tricornutum* when compared with *S. costatum* for all growth phases.

PUFA ranged from 25.4% and 38.9% of TFA in *P. tricornutum*. On the other hand, *S. costatum* presented a significantly higher concentration of PUFA that ranged between 50.4% and 58.2% of TFA, thus accounting for more than half of total FAME content of this species. Palmitolinolenic, EPA and DHA accounted for the PUFA content in both species, while palmitidonic acid was only present in *S. costatum*. The presence of EPA and DHA on both species increases their value due to the high demand for these PUFA in the aquaculture sector (Patil et al., 2005). Similar fatty acid profiles of both species have been previously reported, where higher SFA and MUFA for *P. tricornutum* (Qiao et al., 2016; Quelhas et al., 2019; Yodsuwan et al., 2017) and higher PUFA content in *S. costatum* (Berge et al., 1995; Cardoso et al., 2020) were observed.

Storage lipids are mainly composed of SFA and MUFA and tend to accumulate when cultures are under unfavorable conditions with a consequent impact on growth and decline in PUFA, serving as a source of carbon and energy. PUFA are, in turn, considered to be structural lipids and thus extremely important in maintaining cell membrane fluidity when changes in abiotic factors occur, such as low temperatures (Carneiro et al., 2020; Chini Zittelli et al., 1999; Paliwal et al., 2017; Schüler et al., 2017; Sukenik, 1991). Since *S. costatum* presented a significantly higher growth performance (Figure 6.1), a higher PUFA content was expected since this group of fatty acids are linked to optimal growing conditions. As for *P. tricornutum*, the increased content in SFA and MUFA supports the conclusion obtained from the fluorescence analysis (Figure 6.3) that abiotic conditions, specifically temperature, were not optimal for this species.

6.3.5. Multivariate analysis (PCA)

A PCA was performed on the data of each species, and for both species combined, in order to assess the influence of the meteorological parameters measured, in terms of irradiance (total incident photons, average and maximum irradiance), ambient temperature (average, maximum and minimum temperatures), and pH on biomass volumetric productivity ($g\ L^{-1}\ d^{-1}$), as well as biomass composition in terms of proteins, lipids, carbohydrates and ashes (% of DW; Figure 6.4).

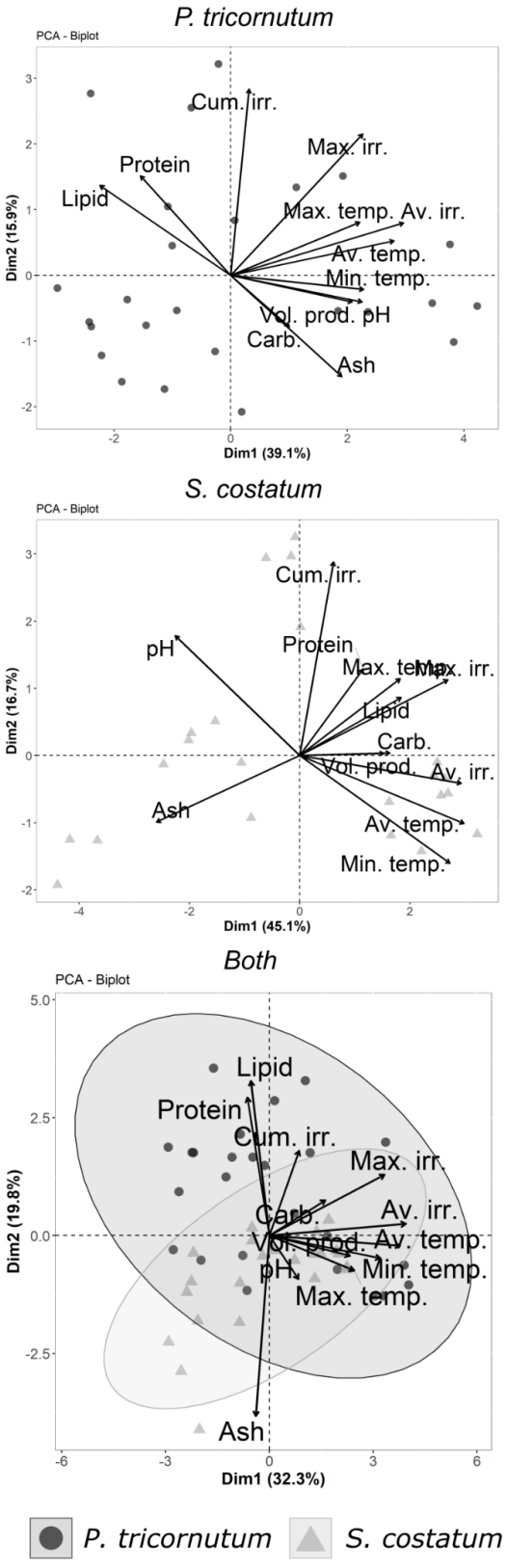

Figure 6.4. Principal component analysis (PCA) bi-plot, grouped for *Phaeodactylum tricornutum* (1st plot; *n* = 25), *Skeletonema costatum* (2nd plot; *n* = 23), and both diatoms (3rd plot; *n* = 48), grown in batch outdoors in 100-L flat panels in triplicate. The score plot is colored according to each species, for *P. tricornutum* (dark grey circles) and for *S. costatum* (light grey triangles). Variables shown: Vol. prod.: volumetric productivity; Cum. irr.: total incident photons; Av. irr: average irradiance; Max. irr.: maximum irradiance; Av. temp.: average temperature; Max. temp. and Min. temp.: maximum and minimum temperatures, respectively; pH; protein: biomass protein content; lipid: biomass lipid content; carb.: biomass carbohydrate content; ash: biomass ash content.

The models explain 39 and 16% of the data variability on the x- and y-axis, respectively, for *P. tricornutum*, 45 and 17% on the x- and y-axis, respectively, for *S. costatum*, and 32 and 20% on the x- and y-axis, respectively, for both species combined. Average and maximum irradiance, as well as minimum and average temperatures were the major contributors to the x-axis of *P. costatum*, *S. costatum* and both diatoms PCA. Protein and ash composition were the major contributors to the y-axis in PCA for *P. tricornutum* and both diatoms; total incident photons were associated to the y-axis in *P. tricornutum* and *S. costatum* analysis, while minimum temperature and pH were the main contributors to the y-axis in the case of *S. costatum* only.

It is interesting to explore the differences between PCAs of each species. Biomass volumetric productivity of *P. tricornutum* cultures was more related to average irradiance ($r(24) = 0.58$, $p < 0.05$) and minimum temperatures ($r(24) = 0.44$, $p < 0.05$), and productivity of *S. costatum* cultures was also correlated with average irradiance ($r(22) = 0.32$, $p < 0.05$), but was better correlated with average temperatures ($r(22) = 0.41$, $p = 0.054$) than minimum temperatures ($r(22) = 0.41$, $p > 0.10$). These results support those reported above, thus emphasizing that the low temperatures recorded during *P. tricornutum* cultivation affected the productivity of this diatom.

In the single PCA of *S. costatum*, lipid and carbohydrate content were positively related to average irradiance ($r(22) = 0.48$ for lipids and $r(22) = 0.43$ for carbohydrates, $p < 0.05$). In this study, carbohydrate content (% of DW) increased during the day until 5 p.m., while lipid content was maximum at 1 p.m. and both were lower in the following morning (9 a.m.; data not shown). Previous reports have observed carbohydrate accumulation (mainly *β*-1,3-glucan) during the light period in *S. costatum* (Handa, 1969; Vårum et al., 1986), and loss of carbohydrates and lipids during the dark period due to respiration (Handa, 1969).

In the combined PCA of both diatoms, average irradiance remained the principal parameter related to volumetric productivity ($r(48) = 0.55$, $p < 0.05$), overriding the effect of the minimum temperature observed in the single PCA of *P. tricornutum*. However, the high ash content of *S. costatum* was prominent in both single and combined PCAs, which together with protein and lipid contents (higher in *P. tricornutum*; Table 6.2), accounted for the three major parameters differentiating the two diatoms in the combined PCA.

6.4. Conclusion

The current study investigated the effect of outdoor conditions upon growth, electron cycle of PSII and biochemical composition of two diatom species. *S. costatum* exhibited a

higher growth performance, daylight volumetric productivity and photosynthetic efficiency when compared to *P. tricornutum*. Biochemical analysis of both diatoms revealed higher protein and carbohydrate contents in *P. tricornutum*, and higher ash content in *S. costatum*. However, *S. costatum* revealed higher protein, lipid, and ash productivities during the day (from 1 p.m. to 5 p.m.), most probably related to its faster growth, while *P. tricornutum* revealed higher protein and lipid productivities during the evening (5 p.m.). Regarding the fatty acid profile, higher concentrations of SFA and MUFA were found in *P. tricornutum*, while *S. costatum* revealed a higher PUFA content (above 50% of total FAME), thus improving the commercial value of its biomass. The electron transport rate of *P. tricornutum* was impaired – as indicated by fluorescence analysis – probably due to non-optimal temperatures during its cultivation, which resulted in lower growth, as compared to that of *S. costatum*. The PCA analysis supported those results, and indicated that minimum temperatures recorded during *P. tricornutum* cultivation were sub-optimal. In this study, the optimal harvesting timepoint for improved protein, lipid, and carbohydrate contents were set at the middle of the day (1 p.m.) for *S. costatum*, with optimal carbohydrate and ash content for *P. tricornutum* at the same timepoint. However, if protein or lipids are the targeted metabolites in *P. tricornutum*, harvesting should be performed in the afternoon. Overall, both diatoms presented relevant commercial profiles, although productivities of *P. tricornutum* still hold a margin for improvement. This study also revealed the benefits of monitoring fluorescence parameters in outdoor conditions and in industrial production scenarios, thus providing a valuable insight into the PSII status and adaptation of the culture.

Chapter 7

Effects of LED lighting on *Nannochloropsis oceanica* grown in outdoor raceway ponds

Growth in most microalgal mass cultivation systems is light-limited, particularly in raceway ponds (RWP) where the light path is higher. Artificial lighting can be a promising solution to diminish dark zones and enhance microalgal productivity. Therefore, our goal was to prevent cell shift from photosynthesis to a respiration-only stage by resorting to light emitting diode (LED) illumination. *Nannochloropsis oceanica* cultures were accordingly grown outdoors in a preliminary small-scale experiment, followed by pilot-scale trials. In the former, three 3.0-m^2 RWP were set up under three distinct conditions: 1) without LEDs (control); 2) LEDs turned on during the night; and 3) LEDs turned on for 24 hours. In the pilot-scale trial, one of two 28.9-m^2 pilot-scale RWPs was coupled to the best LED setup – determined in the small-scale preliminary experiment – using the same light intensity (normal mode) and half of the intensity (economy mode), with the second RWP serving as a control. In the preliminary experiment, the use of LEDs for 24 hours was deemed as not helpful during daytime, before the culture reached ≈ 0.5 g dry weight L^{-1} – when dark zones appeared during the day due to sunlight attenuation in the 0.1 m-deep cultures. Overall, use of LEDs increased biomass growth chiefly by increasing nighttime productivities – materialized in higher chlorophyll, protein, and carbohydrate productivities in LED-lit cultures. A higher impact of LED lighting was observed

under lower sunlight irradiances. A preliminary economic analysis indicates that use of LEDs in RWPs outdoors should be considered for high-value metabolites only.

7.1. Introduction

Currently, the expanding range of microalgae applications in various commercial sectors drives the growing demand for microalgal biomass and its derivatives. In turn, this pushes microalgae production facilities to improve their supply by increasing production as well as enhancing process efficiency. However, any putative strategy toward this end must be carefully assessed, otherwise production costs may go beyond the biomass market selling price. Industrial production systems for microalgal cultivation comprise closed or open systems, which differ significantly in productivity and costs. The former require substantial investment (Richardson et al., 2012), but productivities can reach 10 to 45 g m^{-2} day^{-1} (Acién et al., 2012; Guerra et al., 2021; Llamas et al., 2021). On the other hand, open production systems, such as raceway ponds (RWP), are considered to be one of the cheapest microalgae production systems (Davis et al., 2011) – even though at the expense of lower productivities, typically from 12 to 28 g m^{-2} day^{-1} (Davis et al., 2011; Llamas et al., 2021; Tredici, 2004). Further disadvantages include higher susceptibility to contamination by other microalgae, predators (e.g., rotifers and amoebae), and parasites (e.g., cryptofungi and chytrids), low CO_2 absorption, high O_2 build-up, and poor light distribution within the culture. Additionally, outdoor microalgae production systems are exposed to the elements (e.g., high variances in irradiance, temperature, humidity) with daily and seasonal fluctuations resulting in increased difficulties to control temperature, avoid photo-limitation and photoinhibition, among others. From all these factors, light has always been one of the major growths controlling factors in microalgae cultivation, particularly in RWP. This is due to the fact that RWP present one of the largest light paths – commonly found between 10 and 30 cm (Chisti, 2016; Grobbelaar and Soeder, 1985; Huesemann et al., 2017; Khawam et al., 2019; Sánchez Zurano et al., 2020; Vonshak et al., 2014) – compared to other commercial systems such as tubular photobioreactors with 2.5-14 cm (Pereira et al., 2018; Torzillo and Chini Zittelli, 2015), and flat panel photobioreactors (FP-PBR) with 4.5-9 cm (San Pedro et al., 2016; Tredici et al., 2016). Moreover, RWPs are limited to a one directional light exposure as opposed to the other mentioned cultivation systems. This makes light one of the most limiting factors in RWP-cultivation. Light penetration in algal cultures is also severely limited beyond 5 cm depth in algal concentrations above 0.3 g L^{-1}, meaning beyond this depth is virtual darkness where no photosynthetic processes occur (Khawam et al., 2019). One solution that was put forward was

the use of thin-layer systems with a column depth of ca. 0.5–5.0 cm, shading in these systems is quite low, but in the summer can also lead to lower photosynthetic efficiencies (Morillas-España et al., 2020). Therefore, the search for improvements in cultivation systems is still an ongoing process.

The utilization of artificial light has been extensively studied and can boost productivity, provide more stable and controllable growth conditions, and induce synthesis of specific metabolites (Demory et al., 2018; Nwoba et al., 2019; Pereira and Otero, 2019; Schulze et al., 2016, 2014). Although most industrial facilities producing autotrophic microalgae rely on natural lighting, artificial light has been routinely employed indoors in some facilities. Although LEDs have proven to be more efficient than other artificial light sources (Masojídek et al., 2021) they can still have a severe impact on production costs. Therefore, for mass cultures, the use of LEDs for artificial lighting must be coupled to the production of high-value products (e.g., omega-3 polyunsaturated fatty acids [PUFA] and astaxanthin) to balance the economic feasibility of the whole bioprocess.

Several studies have focused on microalgae cultivation in RWP indoors using artificial lighting (Grobbelaar and Soeder, 1985; Radmann et al., 2007), such as the previous study by Hueseman et al. (2017) that tested the ability of 800-L LED-lit indoor RWPs to simulate microalgae growth outdoors (Huesemann et al., 2017). However, to our knowledge, no studies have focused on the use of LEDs to increase productivity in RWPs outdoors – probably due to the clash between a low-cost cultivation system (RWP) and a high-cost upgrade (LEDs). Nonetheless, the integration of artificial lighting to improve biomass productivity merits to be explored, in attempts to ascertain the accompanying efficiency under outdoor conditions.

The current work consequently assessed the use of LEDs under outdoor conditions, using *Nannochloropsis oceanica* as model culture. This work focused on both the use of LED lighting during the night, when biomass losses usually occur, and for 24 hours, since sunlight penetration can be impaired by high biomass concentration, large depth of the water column or low irradiance. Therefore, a preliminary experiment in small-scale 3.0-m^2 RWPs was carried out to evaluate the use of LED lighting during the night and for 24 hours. Afterward, the best setup was tested at pilot-scale, using 28.9-m^2 RWPs under two different light configurations. To ascertain the increase in biomass cost due to LED lighting, a preliminary economic analysis was performed – which helped assess the economic feasibility of implementing LED systems in low cost RWPs.

7.2. Methods

Two trials were performed: the small-scale preliminary experiment took place at Necton S.A. facilities (Olhão, Portugal), between January 21st and May 8th, 2019; the subsequent pilot-scale trial was carried out at Allmicroalgae S.A. facilities (Pataias, Portugal), between March 17th and July 13th, 2020.

7.2.1. Microorganisms, media, and inocula

Commercial strains of the *Nannochloropsis* genus were used in each facility and trial – *Nannochloropsis oceanica* NAS0197 in Necton S.A. for the small-scale preliminary experiment, and *Nannochloropsis oceanica* CCAP 849/10 in Allmicroalgae S.A. for the pilot-scale trial. Both strains were pre-cultured in the laboratories in aerated (1% CO_2) round bottom 5-L flasks, and subsequently used to sequentially inoculate three FP-PBR of 100, 400, and 800 L outdoors – consisting of a plastic bag with 0.08 m width supported by a metal structure with flitered aeration and a CO_2 injection pulse system. The FP-PBR was, in turn, used to inoculate a pilot-scale tubular photobioreactor (PBR) with CO_2 injection on demand, with volumes of 3.2 and 2.5 m^3 for the small-scale preliminary experiment and pilot-scale trials, respectively. The resulting cultures served as inoculum in the experiments implemented afterward.

Cultures were grown in natural and artificial seawater (in the small-scale preliminary experiment and pilot-scale trials, respectively), adjusted to a salinity of 33 g L^{-1}. Seawater was supplemented with a concentrated culture medium based on Guillard's f/2 (Guillard and Ryther, 1962): NutriBloom® Plus medium medium (Phytobloom by Necton, Portugal; Olofsson et al., 2012) for the small-scale preliminary experiment, and Allmicroalgae's base medium (f/2 medium; Guillard and Ryther, 1962) for the pilot-scale trial. Nitrate concentration was monitored as per the NO_3 ultraviolet spectrophotometric standard method (Baird et al., 2017). Whenever nitrate levels reached 5 mM, complete medium was added up to a concentration of 8-9 mM NO_3 – to ensure sufficient nutrient availability.

7.2.2. Experimental setup

7.2.2.1. Small-scale preliminary experiment

Three identical 300-L RWPs, with a surface area of 3.0 m^2, were used to cultivate the microalgae outdoors at Necton's facilities (Olhão, Portugal). The RWPs consisted of two channels (0.39 m wide each) and a deflector baffle at each bend. The length of the channel straight zones measured 3.21 m; in one of the channels, the paddle wheel was placed 1.76 m

from the bend. The RWPs were equipped with dissolved O_2 and temperature probe (SUP-DM2800, Supmea, China), and pH probe (SUP-PH5013A, Supmea, China), all connected to a Supervisory Control and Data Acquisition (SCADA) control system. This system was also connected to a WatchDog WD-2700 meteorological station, coupled to a LICOR LI-190R-BL-15 quantum sensor installed at the facility and able to provide real-time weather data. The pH was pre-set at 8.1, with automatic addition of CO_2 when needed.

Since lighting RWP cultures from above would diminish sunlight penetration, and most RWPs are either opaque or buried in the ground, submersible LEDs were employed. Four LED strips (Figure 7.1A) of 3.2 m, and four of 1.75 m in length were evenly separated, strapped to two rigid inox structures of compatible length (which helped to remove the LEDs for more intensive cleaning of the RWP), and placed at the bottom of the RWP (Figure 7.1B). The 0.07 m-interspace between LEDs was defined to minimize "overlapping" irradiance between LED strips and maximize homogenous light distribution from the bottom of the RWP (Figure 7.1C). The LED strips covered 65% of the RWP's total area, and provided an estimated maximum power density of 72 W m^{-2}.

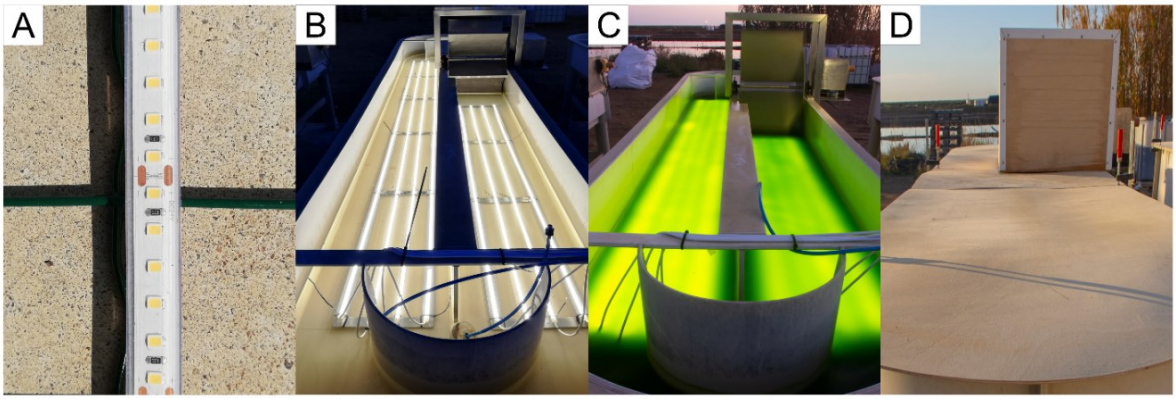

Figure 7.1. LED installation in the 3.0-m^2 RWPs for the small-scale preliminary experiment. Close-up of the LEDs used in this study (A); water-submerged LEDs at the bottom of the RWP during the night (B); RWP illuminated with LEDs in the evening and submerged in a *Nannochloropsis oceanica* culture (C); and birch plywood covers used to control the diel cycle (D).

Each 3.0-m^2 RWP was operated as one of three independent conditions: a RWP without LEDs (control), a RWP where the LEDs were turned on only during the dark periods (night LED), and a third RWP with LEDs turned on permanently for 24 hours (24h LED). The three different conditions were run simultaneously, starting from a culture concentration of ca. 0.12 g of biomass dry weight (DW) L^{-1} and a culture depth of 0.10 m. Cultures were grown batchwise for 9 days, and the experiment was repeated three times. The first, second, and third runs were performed from January 21st to 30th, from April 5th to 14th, and from April 30th to May 8th of 2019, respectively.

Biomass sampling was done twice a day, in the morning (08:30) and evening (17:00). Birch plywood covers were built, and used to cover the cultures (Figure 7.1D) to control the light:dark cycles (8.5L:15.5D). Cultures were covered after the evening sample was taken (sampling occurred in the light) but were left uncovered after the morning sample (sampling occurred in the dark).

7.2.2.2. Pilot-scale trial

A larger pilot-scale trial was performed at Allmicroalgae's facilities (Pataias, Portugal), using two outdoor 3754-L RWPs with a surface area of 28.9 m^2. The straight channels measured 13.2 meters in length, and the paddlewheel was located just after the bend (Cunha et al., 2020).

In these pilot-scale trials, one RWP corresponded to the control, while the second RWP received supplementary irradiance with LEDs. Culture growth in the LED-lit RWP comprised two stages. In the first one, LEDs were turned on only during the night (night LED), until the culture reached a predetermined concentration (ca. 0.5 g DW L^{-1} defined by the small-scale preliminary experiment). The second stage was initiated afterward, and the LEDs were left on for 24 h (24h LED) until the end of the experiment. Cultures from both control and LED-lit 28.9-m^2 RWPs were carried out simultaneously, starting from a culture concentration of ca. 0.30 g DW L^{-1} and a culture depth of 0.13 m (minimum water depth for adequate mixing in these RWPs). Sampling was done twice a day, in the morning (08:00) and evening (18:00).

This pilot-scale trial was composed of two independent sub-trials, comprising two different LED setups (LED quantity and light intensity): the normal and economy modes, that are described below.

7.2.2.2.1. Normal mode

In the normal mode, LED power density was adjusted to 72 W m^{-2} to mimic the one used in the small-scale preliminary experiment. Ten rows of LED strips of 12.0 m and ten of 11.0 m in length were strapped, 0.08 m apart, to two plasticized electro-welded meshes, and then placed at the bottom of the 28.9-m^2 RWP (Figure 7.2A and Figure 7.2B), thus covering 76% of the RWP area. Cultures were grown in batch mode for 10 days, until culture concentrations reached 1 g DW L^{-1}. The experiment was repeated another two times. The first, second, and third runs were performed from June 4th to 15th, from June 22nd to July 2nd, and from July 3rd to 13th of 2020, respectively.

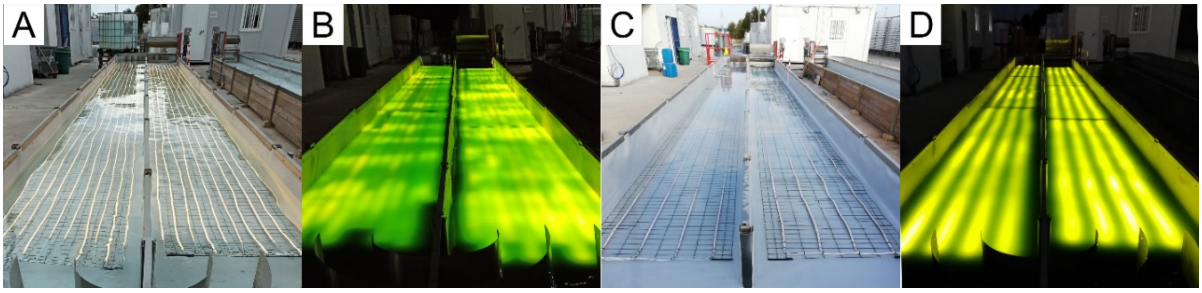

Figure 7.2. LED installation in the 28.9-m^2 RWP used in the pilot-scale trials. Panels A and B show the submerged LEDs used for the normal mode without (A) and with (B) *N. oceanica* culture in the afternoon and at night, respectively. Panels C and D show the LEDs setup for the economy mode, without (C) and with (D) culture in the morning and at night, respectively.

7.2.2.2.2. Economy mode

In the economy mode experiment, the number of LEDs was decreased to provide a power density of 29 W m^{-2}. Four LED strips of 12.0 m and four of 11.0 m were mounted 0.19 m apart to homogenize light distribution throughout the 28.9-m^2 RWP channels and covering 76% of the RWP total area (Figure 7.2C and Figure 7.2D). Cultures were grown in batch mode for 15 days, and the experiment was performed three times. The first, second, and third runs were performed from March 17th to April 1st, from April 2nd to 17th, and from April 17th to May 2nd, of 2020, respectively.

7.2.3. LED

Warm white (2,700 K) IP68 LED (2835, 24 V, 1280 Lm m^{-1}, 14.4 W m^{-1}, JustLIGHT, China) strips, with a luminous efficacy of 88.9 lm W^{-1}, were used in all trials (the corresponding emission spectrum is provided in Annex III Supplementary Figure III.1). The LEDs were operated in parallel, using a constant voltage power supply (24 V DC, 12.5 A, 300 W, IP66). The energy, expressed in mole of photons (*E*), was determined based on Planck's equation as per equation (7.1):

$$E\ (\mathrm{J\ \mu mol\ of\ photons^{-1}}) = \frac{h \times c \times N_A}{\lambda \times 10^6} \quad (7.1)$$

where *h* denotes Planck's constant (6.626 × 10^{-34} J s^{-1}), *c* denotes the speed of light (299 792 458 m s^{-1}), N_A denotes Avogadro's number (6.022×10^{23} mol^{-1}) and λ denotes the dominant wavelength of the LED used (6.07 × 10^{-11} m). The maximum intensity of radiant energy was then calculated by considering the total power provided and assuming an energy-to-power conversion efficiency of 50% (Morkoç, 2009) – see equation (7.2) for W m^{-2} and equation (7.3) for µmol m^{-2} s^{-1}:

$$P_{\text{opt max}}\ (\text{W m}^{-2}) = \frac{L \times \Phi_{e,\lambda} \times 0.5}{A_i} \quad (7.2)$$

$$\text{I}_{\text{max}}\ (\mu\text{mol m}^{-2}\ \text{s}^{-1}) = \frac{L \times \Phi_{e,\lambda} \times 0.5}{A_i \times E} \quad (7.3)$$

where L pertains to the total LED length used, $\Phi_{e,\lambda}$ to the LED's spectral flux (14.4 W m^{-1}), and A_i to the LED illuminated area of the RWPs.

7.2.4. Measurements

7.2.4.1. Growth

Growth was assessed using a calibration curve between biomass DW and optical density (OD). Measurements of DW were performed in duplicate, by filtering 10 mL of culture through pre-weighed 0.7 µm-glass microfiber filter membranes (698, VWR). The biomass on the filters was washed with 10 mL of ammonium formate (35 g L^{-1}), and oven-dried at 60 ºC until constant weight (Guerra et al., 2021; Zhu and Lee, 1997). The OD of the same samples was measured using a spectrophotometer (UVmini-1240, Kyoto, Japan in the small-scale preliminary experiment, and Genesys 10S UV-VIS, Thermo Fisher Scientific, in the pilot-scale trials), both at 540 nm.

Specific areal productivities (P_s), between measurements during the day and night periods, were determined according to equation (7.4) and (7.5), respectively:

$$\text{Daytime P}_\text{s}\ (\text{g m}^{-2}\text{d}^{-1}) = \frac{X_{\text{evening(n)}} - X_{\text{morning (n)}}}{\left(t_{\text{evening(n)}} - t_{\text{morning (n)}}\right) \times A} \quad (7.4)$$

$$\text{Nighttime P}_\text{s}\ (\text{g m}^{-2}\text{d}^{-1}) = \frac{X_{\text{morning (n+1)}} - X_{\text{evening (n)}}}{\left(t_{\text{morning (n+1)}} - t_{\text{evening (n)}}\right) \times A} \quad (7.5)$$

where $X_{\text{evening (n)}}$ and $X_{\text{morning (n)}}$ correspond to the biomass (g) of the culture on the same day "n" in the evening and morning, respectively, and $X_{\text{morning (n+1)}}$ to the biomass on the morning of the following day, whereas A (m^2) corresponds to the RWP's surface area occupied by the culture.

7.2.4.2. Fluorescence measurements

Off situ chlorophyll *a* fluorescence measurements were carried out in the small-scale preliminary experiment, using the pulse-amplitude-modulated fluorimeter AquaPen (AP 110-

C, Photon Systems Instruments, Czech Republic), coupled with FluorPen (version 1.0) software. Samples were pre-diluted to an OD_{540} of ca. 0.6 and incubated for 15 min in the dark to oxidize all plastoquinone (Q_A). Individual samples were used for the manufacturer protocol of rapid-light curves (RLC; protocol LC3). The light intensity to induce minimal chlorophyll fluorescence (measuring light; ML) was set to 0.014 µmol photon m^{-2} s^{-1}, whereas the saturating light to induce maximal chlorophyll fluorescence was set at 2400 µmol photon m^{-2} s^{-1}. Using the results from the default LC3 protocol, the relative electron transport rate (rETR) was determined based on Genty's relationship (Genty et al., 1989), as conveyed by equation (7.6):

$$\mathrm{rETR} = \frac{\Delta \mathrm{F}}{\mathrm{F'_m}} \times \mathrm{I_i} \tag{7.6}$$

where I_i is the incident photosynthetic photon flux density (µmol photon m^{-2} s^{-1}), thus leaving rETR to be expressed in µmol photon m^{-2} s^{-1}. RLC were fitted by the Eilers and Peeters' model (1988). The corresponding light-saturation parameter (E_k) was determined according to equation (7.7):

$$\mathrm{E_k} = \frac{\mathrm{rETR_{max}}}{\alpha} \tag{7.7}$$

where α represents the initial slope of the rETR curve, and $rETR_{max}$ the maximum value of rETR.

7.2.4.3. Pigments

Pigment extraction was performed on fresh biomass as described in Carneiro et al. (2020), using chlorophyll and carotenoid equations based on SCOR-UNESCO (1966) and Jaspars (1965), respectively (Carneiro et al., 2020; Jaspars, 1965; SCOR-UNESCO, 1966).

7.2.4.4. Gross biochemical composition

Culture samples were centrifuged and pooled to remove most of the water, and the remaining pellet was lyophilized (LyoQuest Telstar, Terrassa, Spain). The resulting dried biomass was stored at -20 ºC until use for subsequent analysis.

7.2.4.4.1. Lipid content

Lipid content was determined by gravimetry according to Bligh and Dyer (1959), with slight modifications in the disruption method, since an IKA Ultra-Turrax disperser (IKA-Werke GmbH, Staufen, Germany) was used (Pereira et al., 2011).

7.2.4.4.2. Protein content

Protein content was determined by elemental analysis of total nitrogen as per manufacturer's procedure, using a Vario EL III (Elementar Analysensysteme GmbH, Germany). Total nitrogen content was later multiplied by the conversion factor 4.95 to obtain total protein content (Lourenço et al., 2004).

7.2.4.4.3. Ash content

Approximately 50 mg of biomass were incinerated in a furnace (J.P. Selecta, Sel horn R9-L coupled with a program controller TC88, Bentrup) for 8 h at 525 ºC. Differences in weight between pre- and pos-incinerated biomass were calculated.

7.2.4.4.4. Carbohydrate content

Total carbohydrate content was determined by difference, by subtraction of lipid, protein, and ash results from 100%.

7.2.4.5. Fatty acid analysis

Extraction and conversion of samples to fatty acid methyl esters (FAME) were done following a protocol by Folch et al. (1957) and Lepage and Roy (1984), with modifications described by Pereira et al. (2012). Briefly, lyophilized biomass samples were resuspended in a methanol:acetyl chloride solution (20:1 v/v) and homogenized with an Ultra-Turrax disperser (1.5 min at 23000 rpm; T18 digital ULTRA-TURRAX, IKA-Werke GmbH & Co. KG, Staufen, Germany). Derivatization took place, after adding *n*-hexane, at 70 ºC for 1 h. The lipidic phase was separated by vortexing the samples with distilled water and hexane, followed by centrifugation (this step was repeated thrice). Residual water was removed with anhydrous sodium sulfate. Extracts were filtered, dried under a nitrogen gas flow, and resuspended in gas chromatography (GC) grade hexane. The analysis was performed in a Bruker gas chromatograph, coupled with a mass spectrometry (MS) detector (Bruker SCION 456/GC, SCION TQ MS) equipped with a ZB-5MS capillary column (30 m × 0.25 mm internal diameter, 0.25 µm film thickness, Phenomenex), using helium as the carrier gas. The GC oven temperature profile was set to 60 ºC (1 min), 30 ºC min^{-1} to 120 ºC, 5 ºC min^{-1} to 250 ºC, and

20 ºC min^{-1} to 300 ºC (2 min). Calibration curves were prepared with the commercial standard Supelco® 37 Component FAME Mix (Sigma-Aldrich, Sintra, Portugal). Results are expressed as percent of total fatty acid content (% of TFA).

7.2.5. Economic analysis

The economic analysis for the LEDs used in the pilot-scale trials includes only the higher capital investments (LED strips and power supplies; $CAPEX_{LED}$) and operational costs (electricity; $OPEX_{LED}$) – determined according to the local cost of electricity and an operation of 330 days per year. A conservative average usable life of 30,000 h for the LEDs and the power supply were considered for capital depreciation. Means of the resulting biomass in each mode were used as a proxy for the biomass produced – without including seasonal variations. The values presented of additional biomass produced are relative to the corresponding control (without LEDs). Hence, a detailed evaluation of CAPEX and OPEX expenses pertaining to the control was not included, since they do not significantly affect comparison between LED treatments – besides falling outside the scope of this work.

7.2.6. Statistical analysis

The three runs of each trial were aimed at determining the average with the respective standard deviations. Using these averages, an analysis of variance (ANOVA) followed by a post hoc (Tukey's test) were used to determine significant differences between conditions (control, LED night, and 24h LED), at a significance level of $\alpha = 0.05$. When data were of a non-parametric nature, a Kruskal-Wallis test was used. A paired *t*-test was used to compare evening and morning samples of the same condition. All statistical analyses and resulting plots were performed using R software.

7.3. Results and discussion

7.3.1. Small-scale preliminary experiment

7.3.1.1. Growth

The implementation of LEDs in RWPs outdoors was first evaluated in small scale 3.0-m^2 RWPs. Starting at a concentration of 0.12 ± 0.01 g DW L^{-1}, the cultures grew for 9 days in batch, and the growth of individual runs, and the average of three repetitions are shown in Figure 7.3 Meteorological data, including irradiance and temperature for each run of this experiment, are provided in Annex III Supplementary Figure III.2 and Supplementary Figure III.3, respectively.

By the end of the trial, the cultures reached, on average, 1.00 ± 0.18, 1.52 ± 0.49, and 1.8 ± 0.68 g DW L^{-1} for the control, night LED, and 24h LED cultures, respectively. The beneficial effect of using LEDs is perceptible just after 24 hours and increased over time. Beyond the 4^{th} day, the night LED and 24h LED cultures reached a ratio to the control of 1.38 ± 0.12 and 1.64 ± 0.13, respectively. Important differences in growth can be observed between the first run, performed in late January, and the third run, performed in early May, which caused higher standard deviations in the averaged values (Figure 7.3). This difference can be explained by the meteorological conditions, especially sunlight irradiance, which differed substantially between runs (see Annex III Supplementary Figure III.2). Nevertheless, a significant beneficial effect of LED illumination ($p < 0.05$) was found, using the average values of the three runs.

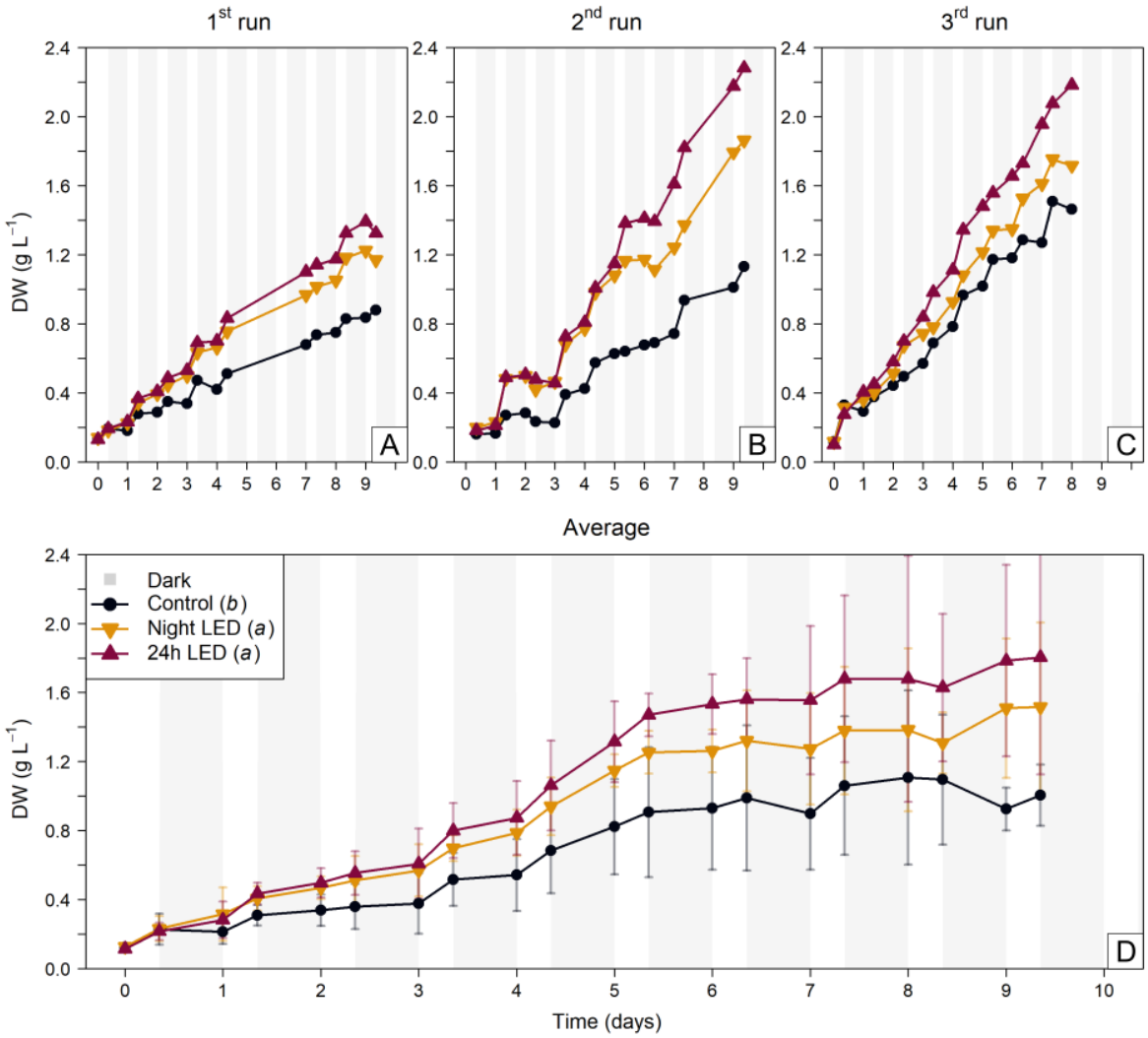

Figure 7.3. Growth, in terms of g of dry weight (DW) L^{-1}, over time (days) of *Nannochloropsis oceanica* grown in batch under three different conditions: without LEDs (control; dark grey circles), with LEDs turned on during the night (Night LED; yellow inverted triangles) and with LEDs turned on for 24 h (24h LED; red triangles) in three 3.0-m^2 raceway ponds (RWP) outdoors. The RWPs were manually covered between evening and morning samples, to control the dark periods and simulate nighttime (light grey vertical bars). Data from each run performed in January (A), April (B), and Late May (C), and the averaged values of the three (D) are shown. Conditions that do not share a letter (in brackets in the inset legend in the average plot) represent significant differences ($p < 0.05$). Error bars represent standard deviations.

A crucial point in these growth curves is when the night LED culture and the 24h LED culture started to diverge, with the 24h LED culture growing faster during daytime. This effect becomes visible in the averaged values in Figure 7.3D after day 3, when the night LED culture reached 0.57 g DW L^{-1}. From this point forward, sunlight could no longer penetrate down to the bottom of the 3.0-m^2 RWPs, as determined with a lux meter placed below an analogous replica of the RWP channel, with a transparent bottom filled with biomass at the same concentration as the RWP (data not shown). This can also be seen in *Supplementary Table III.1*, which shows the areal productivities for each growth phase: lag, logarithmic and late logarithmic, where LED-lit culture do not show any differences, and which only appear in the logarithmic phase. This light attenuation with column depth and biomass concentration proves

a major constraint when using RWPs for microalgae cultivation (Grobbelaar, 2013), and explains the observed improvement when LEDs were applied.

7.3.1.2. Areal productivity

To clarify the LED's impact on the culture growth during the day and nighttime that were masked by the differences between runs (see Figure 7.3), specific areal productivities of each run (boxplots) and their average (violin plot) are detailed in Figure 7.4.

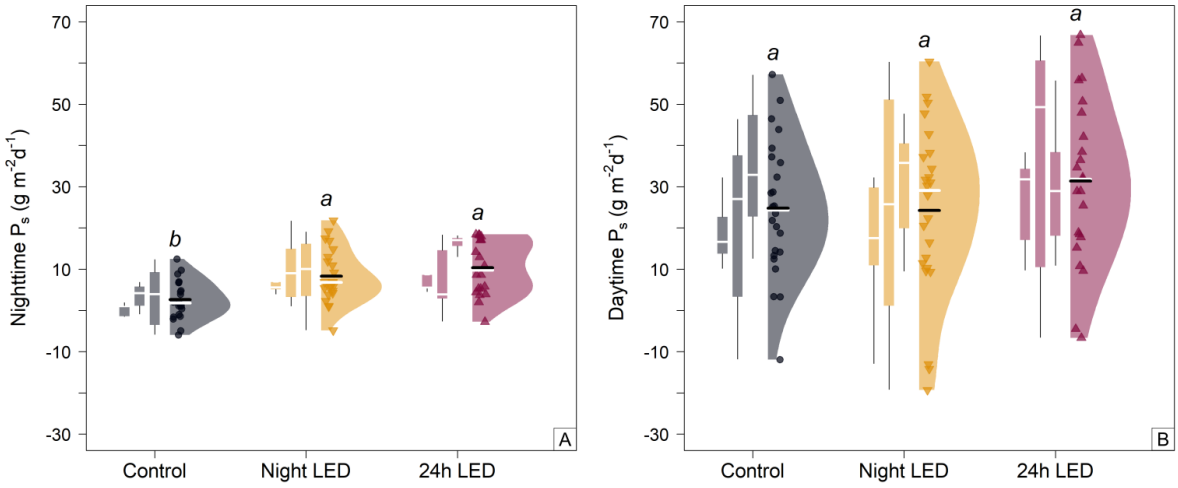

Figure 7.4. Comparison of specific areal productivities (g m^{-2} d^{-1}) during the night (Nighttime P_s; A) and day (Daytime P_s; B) periods of *Nannochloropsis oceanica* cultures grown in outdoor 3.0-m^2 raceways ponds without LEDs (Control; dark grey), with LEDs turned on during the night (Night LED; yellow) and with LEDs turned on for 24h (24h LED; red). The three boxplots represent the values for the first, second, and third runs, in this order. The violin plot combines the values of all three runs. The values that compose the violin plot are depicted as dots inside the violin region (Daytime P_s: n = 24; Nighttime P_s: n = 21). Horizontal white lines for both boxplots and violin plots represent the median, while the horizontal black line in the violin plot represents the average. Conditions that do not share a letter (on top of each violin plot) represent significant differences (p < 0.05).

The higher data dispersion in the average daytime productivities (violin plots of Fig. 4) was chiefly due to the higher weather variability conditions during the day particularly light and temperature, as during the night irradiance was steadily provided only by the LEDs. Hence, differences in night productivities among conditions became more apparent, with a significantly (p < 0.05) lower mean areal productivity for the control (2.3 ± 5.0 g m^{-2} d^{-1}) compared to those of the night LED (9.1 ± 7.2 g m^{-2} d^{-1}) and 24h LED (11.6 ± 8.5 g m^{-2} d^{-1}) cultures (Figure 7.4A). However, average daytime productivities (Figure 7.4B) did not vary significantly between conditions and exhibited a wider dispersion of values than their nighttime counterparts – reaching up to 29.4 ± 21.9 g m^{-2} d^{-1} in the 24h LED culture. Negative daytime productivities were significantly associated to a lower number of total photons received from the sun and LEDs combined (p < 0.05), as well as lower average temperatures (p < 0.10) (Annex III Supplementary Figure III.4). The values of areal productivities obtained lie within

the interval found for RWPs, i.e., 15-45 g m^{-2} d^{-1} (Acién et al., 2012; Brennan and Owende, 2010), with values of 20-25 g m^{-2} d^{-1} being more common in short operations (Tredici, 2004).

Global productivities were 9.5 ± 3.0, 12.8 ± 3.2 and 16.5 ± 4.9 g m^{-2} d^{-1} for the control, Night LED and 24h LED, respectively. The productivity of 24h LED-lit cultures were almost double the value of the control, and was also higher than previous studies using *N. gaditana* with 14 g m^{-2} d^{-1} and *N. salina* with 13.5 g m^{-2} d^{-1} using similar culture depths of 0.11 and 0.12 m and approximate volumes 800 and 300 L, respectively (Boussiba et al., 1987; Ledda et al., 2015). Previous studies using RWP with higher column depths of 0.25 m with similar areas of 1.2 and 3 m^2 reported areal productivities of 8.3 g m^{-2} d^{-1} for *Nannochloropsis oculata* and 3.3 for *N. salina* (Millán-Oropeza and Fernández-Linares, 2017). Compared to our study, LEDs brought about a significant improvement, particularly considering the lower column depth used in this trial (0.10 m).

7.3.1.3. Metabolite productivities and contents

Pigment analysis, in terms of chlorophyll and carotenoids, and gross biochemical composition, in terms of lipids, protein, and carbohydrates, were performed on the resulting biomass samples of the small-scale preliminary experiment. Variations in the productivities were compared between the three different conditions (control, night LED, and 24h LED) according to evening and morning samples of the late exponential growth phase using the averaged samples from the last two days of cultivation of each run (Figure 7.5).

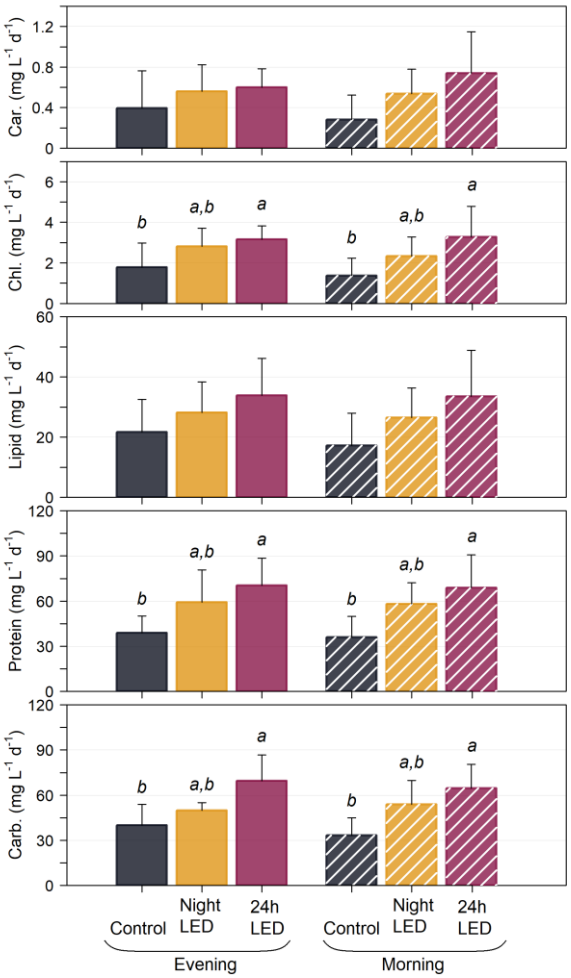

Figure 7.5. Volumetric productivities (mg L^{-1} d^{-1}) of pigments in terms of carotenoids (Car.; A) and chlorophyll (Chl; B) and macronutrients, namely lipids (C), protein (D) and carbohydrates (Carb.; E) of *Nannochloropsis oceanica* grown under three different conditions: without LEDs (Control; dark grey), with LEDs turned on during the night (Night LED; yellow) and with LEDs turned on for 24h (24h LED; red) in outdoor raceway ponds. Results are expressed as the average of the last two days (late exponential phase) of the three runs, grouped according to evening (solid bars) and morning (striped bars) samples. Different letters represent significant differences (p < 0.05) between conditions of the same time sampling group (evening or morning). Absence of letters means no statistical differences were detected between conditions. Error bars represent standard deviations.

Compared to the control culture (evening: 1.79 ± 1.19 mg L^{-1} d^{-1}; morning: 1.37 ± 0.86 mg L^{-1} d^{-1}), a significant increase (p < 0.05) in chlorophyll productivities of the cultures grown under the 24h LED condition (evening: 3.16 ± 0.66 mg L^{-1} d^{-1}; morning: 3.28 ± 1.50 mg L^{-1} d^{-1}) was detected. This is in agreement with previous reports of higher pigment content per cell of *Nannochloropsis gaditana* by the end of the light period (Fábregas et al., 2002) when biomass concentrations are also higher, thus contributing to the higher chlorophyll productivities. Even though chlorophyll content was lower in this study (1.84 ± 0.11% f DW) than previous studies using *N. oceanica* with 2.33% of DW (Carneiro et al., 2021) and 3.9% of DW (Wang and Jia, 2020), carotenoids (0.42 ± 0.02% of DW) were higher than those reported previously (Carneiro et al., 2021) (Supplementary Table S2). This could be due to

the differences between indoor and outdoor experiments where cells are exposed to much higher irradiances, leading to the activation of photoprotective pathways (Wang and Jia, 2020).

At the late exponential phase, the biomass of *N. oceanica* was mainly composed of protein and carbohydrates, with lower lipid contents (see Supplementary Table III.2). Control cultures exhibited lipid productivities of 21.8 ± 10.8 and 17.3 ± 10.7 mg L^{-1} d^{-1}, protein productivities of 39.0 ± 11.1 and 36.1 ± 13.8 mg L^{-1} d^{-1}, and carbohydrate productivities of 40.0 ± 13.9 and 33.3 ± 11.7 mg L^{-1} d^{-1}, in evening and morning samples, respectively. Overall, cultures grown under 24h LEDs presented significantly ($p < 0.05$) higher productivities in terms of protein (evening: 70.3 ± 18.1 mg L^{-1} d^{-1}; morning: 68.8 ± 22.0 mg L^{-1} d^{-1}) and carbohydrates (evening: 69.6 ± 17.2 mg L^{-1} d^{-1}; morning: 64.5 ± 16.0 mg L^{-1} d^{-1}) than those of the control. This can be partially justified by the differences found in DW, as both pigment and macronutrient productivities were lower in the control cultures. The biomass analysis revealed higher chlorophyll, protein, and carbohydrate productivities in the 24h hour LED-lit cultures, thus contributing to an increased valorization of LED-grown cultures. Biomass composition was similar to a previous study using *N. oceanica* grown outdoors in tubular PBR (Guerra et al., 2021) and the low lipid contents observed suggests that the cells were growing in the absence of nutrient stress (Carneiro et al., 2021; Molino et al., 2018). Higher differences were expected between productivities of morning and evening samples due to diel regulated metabolisms (Carneiro et al., 2020; Sukenik and Carmeli, 1990). Nonetheless, lipid productivities were higher using LED-lit cultures – mainly due to the higher biomass productivity of LED-lit cultures – than a previous study cultivating *N. oculata* in 200-L RWP resulting in 25 mg L^{-1} d^{-1} (Millán-Oropeza and Fernández-Linares, 2017). After pigments, lipids possess the highest market value compared to carbohydrates and lipids (Ruiz et al., 2016). Biomass composition, particularly in terms of high-value metabolites, can valorize the microalgal biomass and render the application of LEDs economically feasible.

Fatty acid profiles were also determined in *N. oceanica* cultures. Saturated fatty acids (SFA) corresponded to myristic (C14:0 < 5.8% of total fatty acids; TFA) and palmitic (C16:0) acids with contents ranging within 20.8-23.0 % of TFA; while monounsaturated fatty acids (MUFA), composed of palmitoleic (C16:1) and oleic (C18:1 < 2.5% of TFA) acids, varied within 31.1-34.3% of TFA. PUFA, consisting of linoleic (C18:2*n*-6 < 4.4% of TFA), arachidonic (C20:4*n*-3) and eicosapentaenoic (EPA; C20:5*n*-3) acids, varied between 43.6-47.5% of TFA. The most abundant fatty acids in all cases were palmitoleic acid and EPA. The variation of the main fatty acids (higher than 10% of TFA) in *N. oceanica*, grown under each condition, is shown in Table 7.1.

Table 7.1. Percentage of total fatty acid (% of TFA) of *Nannochloropsis oceanica* grown under three different conditions: without LEDs (control), with LEDs turned on during the night (Night LED), and with LEDs turned on for 24h (24h LED) in three outdoor raceway ponds. Results are expressed as mean ± standard deviation of the last two days (late logarithmic phase) of the three runs, grouped according to evening and morning samples. Different letters represent significant differences between conditions of the same time sampling group (evening or morning). Letters were omitted when no significant differences were detected.

	Evening			Morning		
	Control	Night LED	24h LED	Control	Night LED	24h LED
C16:0	18.6 ± 2.9	16.9 ± 2.9	16.9 ± 2.4	17.5 ± 2.8	15.9 ± 2.4	15.2 ± 1.0
C16:1	29.6 ± 1.0 (b)	32.5 ± 0.2 (a)	31.8 ± 1.2 (a)	29.0 ± 2.3 (b)	31.7 ± 0.8 (a)	33.0 ± 1.0 (a)
C20:4*n*-6	13.8 ± 2.0	10.1 ± 3.2	11.2 ± 3.9	11.9 ± 4.4	11.6 ± 3.4	8.7 ± 3.0
C20:5*n*-3	26.0 ± 0.7 (b)	28.7 ± 0.7 (a)	26.7 ± 0.2 (b)	30.0 ± 2.5	28.7 ± 1.8	31.4 ± 1.0
SFA	23.0 ± 3.3	22.4 ± 3.7	22.8 ± 3.0	21.4 ± 3.3	21.3 ± 2.8	20.8 ± 1.6
MUFA	32.1 ± 1.2 (b)	34.0 ± 0.1 (a)	33.2 ± 1.1 (a,b)	31.1 ± 2.2 (b)	33.2 ± 0.6 (a,b)	34.3 ± 1.2 (a)
PUFA	44.9 ± 3.3	43.6 ± 3.8	44.0 ± 2.5	47.5 ± 5.0	45.5 ± 2.6	44.9 ± 2.4

The reported fatty acids are consistent with those commonly found in the literature for this genus (Carneiro et al., 2020; Cunha et al., 2020; Fábregas et al., 2004; Guerra et al., 2021; Sukenik and Carmeli, 1989). Furthermore, natural fluctuations of SFA and PUFA, between evening and morning samples, are consistent with the results previously described for *N. oceanica* (Carneiro et al., 2020; Sukenik and Carmeli, 1989), with EPA being significantly ($p < 0.05$) higher in the morning.

Nonetheless, TFA composition was affected by LEDs, resulting in a significant ($p < 0.05$) increase in MUFA, particularly from palmitoleic acid, in both night LED and 24h LED cultures, in both evening and morning samples. Regardless, PUFA remained the major constituent of TFA, and were primarily composed by the structural EPA. Although lipid productivities were low compared to protein and carbohydrate (Figure 7.5), the high EPA content in TFA points to a high valorization of this fraction that can potentially increase the value of the final biomass.

7.3.1.4. Fluorescence

ETR can function as a proxy for the rate of electrons transported through the photosynthetic chain, providing additional insight into light-limited, saturated, or inhibited intervals for the cultures (Beer et al., 1998). Hence, RLCs and photosynthetic efficiency values (α; slopes in dashed lines) were classified according to the growth phase, for both evening and morning samples (Annex III Supplementary Figure III.5). All RLCs declined over time, except those of the control culture in the morning during the exponential phase. However,

photosynthetic efficiency values decreased with growth, with a more noticeable decrease of the control culture.

The intercept of α with $rETR_{max}$ supports the determination of the minimum saturating irradiance coefficient, E_k. Values above E_k are characterized by a low photosynthetic rate, which competes with energy dissipation (Malapascua et al., 2014). Specific values for E_k are displayed in Table 7.2.

Table 7.2. Average of light-saturation (E_k) coefficients determined from relative electron transport rate (rETR) versus PAR curves, shown in Annex III Supplementary Figure III.5 for *Nannochloropsis oceanica* cultures grown under three different conditions: without LEDs (Control), with LEDs turned on during the night (Night LED), and with LEDs turned on for 24h (24h LED) in three 3.0-m^2 raceway ponds outdoors. Results are expressed as mean ± standard deviation of grouped values according to growth phase: lag, logarithmic (log), and late logarithmic (late log) for evening and morning samples. Different letters depicted between brackets represent significant differences ($p < 0.05$) among conditions.

	Evening E_k (µmol m^{-2} s^{-1})			**Morning E_k** (µmol m^{-2} s^{-1})		
Growth phase	Control	Night LED	24h LED	Control	Night LED	24h LED
Lag	321 ± 30	323 ± 26	307 ± 27	258 ± 76	261 ± 49	279 ± 62
Log	348 ± 53	298 ± 46	297 ± 33	333 ± 52 (a)	260 ± 48 (b)	264 ± 47 (b)
Late log	360 ± 30 (a)	261 ± 38 (b)	271 ± 14 (b)	317 ± 61 (a)	244 ± 47 (a,b)	239 ± 41 (b)

Results pertaining to E_k were similar for the cultures grown with LEDs where values also decreased with the cultures' growth in both evening and morning samples. However, the results from the control increased with growth, showing significantly ($p < 0.05$) higher E_k than LED-lit cultures. Conversely, in morning samples, they peaked during the exponential phase. This suggests that, during dark periods (morning samples), the minimum light requirements were met by using LEDs supplying ca. 318 µmol m^{-2} s^{-1}, which was in fact above the E_k of LED-lit cultures. E_k values are in accordance with a previous study using *Nannochloropsis* cultivated in a FP-PBR (5 cm) and in a high rate algal pond (HRAP; 35 cm) where lower values were found for the more light limited system – HRAP – with light intensities between 264 and 162 µmol m^{-2} s^{-1} (Kromkamp et al., 2009) The slightly higher values found in our study could be explained by the lower column depth used (10 cm), which favored the light acclimation of the cells. However, it is interesting to note that the LEDs did not produce the same effect. While in the control E_k increased over time (in a culture undergoing higher self-shading due to higher cell concentrations), the LED-lit cultures presented the opposite effect, suggesting that LED-lit cultures were receiving excess light.

7.3.2. Pilot-scale trials

Considering the small-scale preliminary experiment results, the use of LEDs during daytime was deemed as not helpful until the culture reached ≈ 0.5 g DW L^{-1} (column depth of 0.10 m) when dark zones appeared during the day, due to sunlight attenuation in the culture column. Moreover, the LED light intensity tested (ca. 318 µmol m^{-2} s^{-1}) was saturating (E_k: 239-360 µmol m^{-2} s^{-1}). Based on these findings, the experimental setting was scaled up using 24h LEDs only after the culture surpassed ≈ 0.5 g DW L^{-1} and tested if a photon-limiting light intensity (below E_k) would still benefit growth while minimizing LED usage and operational costs.

7.3.2.1. Growth

In this trial, *N. oceanica* cultures started from concentrations of 0.29 ± 0.01 g DW L^{-1} and reached up to 1 g DW L^{-1}, with growth rates strongly affected by available irradiance. Averaged growth curves for both normal and economy modes are shown in Figure 7.6A and Figure 7.6B, respectively, together with the corresponding averaged specific areal productivities as depicted in Figure 7.6C and Figure 7.6D.

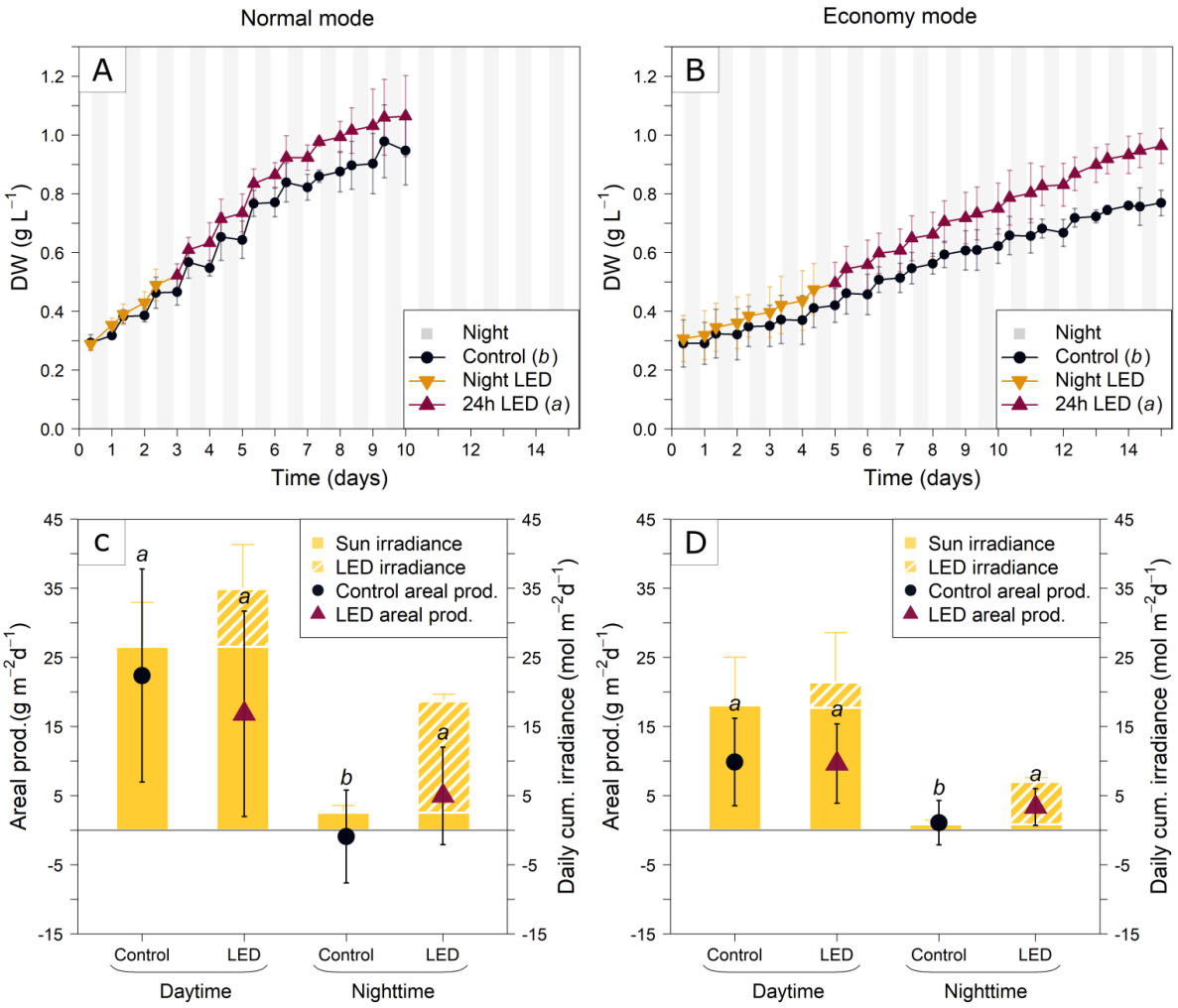

Figure 7.6. Averaged growth curves of three independent runs, using *Nannochloropsis oceanica* cultures, in g of dry weight (DW) L^{-1}, for each normal (**A**) and economy (**B**) modes of the pilot-scale trial where cultures were grown under two different conditions: without LEDs (control; dark blue circles), and with LEDs (Night LED; yellow inverted triangles and 24h LED; red triangles) in 28.9-m^2 outdoor raceway ponds. Light grey vertical bars represent the night periods. Conditions that do not share a letter (in brackets in the legend) represent significant differences ($p < 0.05$). In the two lower panels, the average daily specific areal productivities (Areal prod. in g m^{-2} d^{-1}; left Y-axis) is shown, for the control (dark blue circles) and LED-lit (red triangles) cultures during the day and nighttime under normal (**C**) and economy (**D**) modes. The bar plot represents the daily averaged photons received by the cultures from day 0 to the end of the experiments (Daily cum. irradiance in mol m^{-2} d^{-1}; right Y-axis) that originated from the sun (yellow solid bars) and the LEDs (yellow striped bars). Sun irradiance present during nighttime corresponds to the remaining irradiance between evening and morning samples (see Methods section 2.2.2. Pilot-scale trial). Conditions (control versus LED) that do not share a letter within each day and nighttime represent significant differences ($p < 0.05$). Error bars represent standard deviations.

In normal mode, the control reached an average biomass concentration of 0.95 ± 0.12 g DW L^{-1}, while the LED-lit cultures (72 W m^{-2}) attained 1.1 ± 0.14 g DW L^{-1}. The trial under this mode was cut short to 10 days since the cultures grew faster due to higher temperature and solar irradiance, which were indeed closer to the optimal values for this species (Annex III Supplementary Figure III.6 and Supplementary Figure III.7 for normal and economy modes, respectively). After 15 days in the economy mode, the control cultures reached 0.77 ± 0.04 g DW L^{-1} while the LED-lit culture (29 W m^{-2}) reached 0.96 ± 0.06 g DW L^{-1}. In both trials, cultures

lit with LEDs grew significantly faster ($p < 0.05$) than their respective controls, with a higher difference to the control in the economy mode trial.

The lower sun irradiance and temperature observed during economy mode runs made the additional LED lighting more effective. This effect can be seen in Figure 7.6C and Figure 7.6D, which show the average daily specific areal productivities of the cultures grown with LEDs during day- and nighttime, for each cultivation mode, together with the total daily photons received per day by the cultures from the sun and the LEDs.

Areal daily productivities for control cultures, under normal mode, reached 22.4 ± 15.4 and -0.91 ± 6.70 of g m^{-2} d^{-1} during day- and nighttime, respectively, while receiving 26.5 ± 6.4 mol of photons m^{-2} d^{-1}. For this trial, areal daily productivities of the LED-lit cultures were not significantly different (16.9 ± 14.9 g m^{-2} d^{-1}) than that of the control during daytime. However, they were able to prevent biomass loss during nighttime, with productivities of 4.97 ± 7.06 g m^{-2} d^{-1}, while receiving an additional 8.4 (after LEDs were left on for 24h) and 16.1 mol of photons m^{-2} d^{-1} from the LEDs during the day and nighttime, respectively. This is not surprising, in view of the positive relationship between growth and respiration arising from the cost of biomass synthesis (Geider et al., 1989), and further explains the lower daytime productivities in LED-lit cultures.

In the economy-mode experiment (Figure 7.6D), average areal daily productivities in the control cultures reached 9.88 ± 6.33 and 1.08 ± 3.22 of g m^{-2} d^{-1} in the day and nighttime, respectively, while receiving 18.1 ± 6.9 mol of photons m^{-2} d^{-1} from the sun. Control and LED-lit cultures displayed similar productivities during the daytime (9.64 ± 5.72 g m^{-2} d^{-1}). However, the latter showed higher values during nighttime (3.37 ± 2.66 g m^{-2} d^{-1}) compared to those of the control, while receiving 3.7 and 6.2 mol of additional photons m^{-2} d^{-1} from the LEDs during the day and nighttime, respectively, upon leaving these lights on for 24h. For both modes, significant differences ($p < 0.05$) were found between LED lighting conditions and controls during nighttime only. Areal productivities found in the pilot-scale trial are consistent with those previously reported in these RWP with a maximum of 18.1 g m^{-2} d^{-1} (considering a similar operation to the current trial) using *N. oceanica* (Cunha et al., 2020). Nonetheless, cultures in large commercial RWP rarely exceed 12-13 g m^{-2} d^{-1} (Tredici, 2004). Global productivities in the pilot trials were lower compared to the preliminary experiment with 4.24 ± 0.44 and 5.82 ± 0.38 g m^{-2} d^{-1} for the control and LED lit culture in economy mode, and 8.79 ± 1.87 and 10.44 ± 2.09 g m^{-2} d^{-1} in normal mode. Economy mode values are lower than those reported in RWP under similar conditions with 9.7 and 7.7 g m^{-2} d^{-1} using *Nannochloropsis* sp. and *N. oceanica* in 4.73 and 2.89 m^3 with 0.2 and 0.1 m of column depth (Cunha et al., 2020; de Vree et al., 2015). However, the LED-lit culture in normal mode was able to surpass both values.

It is interesting to note that the control culture from the normal mode experiment received almost the same daily photons (29.1 mol of photons m^{-2} d^{-1}) as the LED-lit culture in the

economy mode experiment (28.4 mol of photons m^{-2} d^{-1}). However, areal productivities between the two conditions varied considerably, owing to the increase in average temperatures and the faster growth during normal mode, which increased the extension of dark zones in RWPs. LED irradiance (72 W m^{-2}) was thus rendered less efficient due to higher light attenuation in the culture column. In this sense, the application of LEDs in microalgae cultivation seems to be more useful under lower sunlight irradiances, such as those prevailing in winter or in low irradiance locations. This agrees with the different specific areal productivities found in the small-scale preliminary experiment, for which higher differences from control values were found for microalgae being grown under lower sun irradiances during the first run.

7.3.2.2. LED operation costs

In industrial applications, increased biomass productivity can be meaningless if additional costs are not accounted for Table 7.3 presents the pilot-scale trial data considering the extra investment and biomass return, compared to the corresponding controls; and shows the depreciated initial additional investment in LED strips, and the necessary power supplies as well as the operational costs in terms of the additional electricity spent during an operational period of 330 days per year.

Table 7.3. Parameters of the LEDs used for the LED conditions in the pilot-scale trial, under normal and economy modes. An average usable life of 30.000 h for the LEDs and the power supply was used to determine the depreciation value for an yearly 330-day operation. Means of the resulting biomass in each mode were used as a proxy for the biomass produced without taking into account seasonal variations.

Parameters	**Pilot-scale trial**		Units
	Normal	Economy	
LED strips	794.37	317.75	€ $year^{-1}$
Power supply	410.65	186.66	€ $year^{-1}$
$CAPEX_{LED}$	1205.02	504.41	€ $year^{-1}$
Electricity	3152.33	1302.54	€ $year^{-1}$
$CAPEX_{LED}$ + $OPEX_{LED}$	4357.34	1806.94	€ $year^{-1}$
Extra biomass produced[1]	21.0	19.8	kg $year^{-1}$
Cost of extra biomass produced[1]	207.58	91.12	€ kg^{-1}

1 – Extra biomass produced compared to the respective control.

According to the pilot-scale trial results, yearly operation would result in 21 and 19.8 kg of additional biomass compared to that of the control, if the normal or economic modes were

chosen, respectively. Even though LED modes (normal and economy) do not differ substantially in terms of additional biomass produced, their production costs do. The resulting 21 kg of extra biomass using the normal mode led to an additional expense of 208 € kg^{-1}. In contrast, this value drops to less than half, 91 € kg^{-1}, for almost the same extra biomass (20 kg) from cultures grown under economy mode. Considering an average productivity of 2.7 kg m^{-2} $year^{-1}$ for the south of Spain (Ruiz et al., 2016), the extra biomass produced owing to the LED lighting (0.70 ± 0.02 kg m^{-2} $year^{-1}$) accounts for an increase by 25% of the yearly produced biomass.

For a 100-ha facility with productivities between 21 and 27 ton ha^{-1} $year^{-1}$, production costs have been previously reported to lie around 4.95 and 5.20 € kg^{-1} (Norsker et al., 2011; Ruiz et al., 2016), respectively. However, increasing the production scale can also lead to lower production costs (Acién et al., 2012; Llamas et al., 2021). In addition, a more concentrated culture reduces the culture volume to be processed, decreasing the biomass separation costs in the downstream process, since harvesting from RWPs can contribute with ca. 23% of the overall cultivation costs (Ruiz et al., 2016).

To compare overall photosynthetic efficiency (PE) conversion of luminous energy from the sun and LEDs to biomass were determined according to the biomass energy content of 22.2 MJ Kg^{-1} (Tredici et al., 2015). This resulted in values of 1.49 ± 0.34 and 1.08 ± 0.16% for the control of LED-lit cultures under normal cultivation and 1.09 ± 0.13 and 1.11 ± 0.17% for the control and LED-lit cultures under economy cultivation. PE increased greatly in the normal mode, when sun irradiance was stronger, thus characterizing this light-limited cultivation system. On the other hand, PE of LED-lit cultures remained constant for the cultivation of both modes enhancing the possible need of LED application only in light limited situations together with high-value applications of the biomass. As the LED efficiency in RWPs is dependent on weather conditions, particularly sunlight (since LEDs are more efficient at lower sun irradiances), as well as biomass density, continuous fine-tuning of the LED operation time can lead to more promising results in terms of value of the additional biomass produced. Even so, the feasibility of application should only be considered for high-value products, when sunlight is limiting at high latitude locations and/or under wintery weather conditions.

7.4. Conclusions

The application of LEDs in outdoor RWPs increased biomass growth mainly by increasing nighttime productivities. Consequently, a positive outcome was attained in terms of nutrient productivity, particularly protein and carbohydrates. The use of LEDs proved more

efficient under low irradiances in both small-scale and pilot-scale cultures. The E_k coefficient was helpful to determine a more economical LED setup within the light-limited region for the pilot-scale trials. The economy mode also proved more efficient, yielding almost the same extra biomass under normal mode, at less than half the cost. The incorporation of solar panels to generate electricity could, in the long run, appear as beneficial in terms of sustaining LED operation and diminishing OPEX (Morales et al., 2019). In any case, the incorporation of LEDs should be mainly considered for high-value products.

Chapter 8

Growth and bioactivity of two chlorophyte (*Chlorella* and *Scenedesmus*) strains co-cultured outdoors in two different thin-layer units using municipal wastewater as a nutrient source

This Chapter is based on the published article: Carneiro, M., Ranglová, K., Lakatos, G.E., Câmara Manoel, J.A., Grivalský, T., Kozhan, D.M., Toribio, A., Moreno, J., Otero, A., Varela, J., Malcata, F. X., Suárez Estrella, F., Acién-Fernández, F.G., Molnár, Z., Ördög, V., Masojídek, J., 2021. Growth and bioactivity of two chlorophyte (*Chlorella* and *Scenedesmus*) strains co-cultured outdoors in two different thin-layer units using municipal wastewater as a nutrient source.
Algal Research 56, 102299. DOI: 10.1016/j.algal.2021.102299.

The application of microalgae in wastewater treatment has recently been at the forefront of interest due to the increasing concern about environmental protection and economic sustainability. This work aimed at studying two chlorophyte species, *Chlorella vulgaris* and *Scenedesmus acutus*, co-cultured outdoors in centrate of municipal wastewater as nutrient source. Two different thin-layer units were used in these trials — thin-layer cascade (TLC) and thin-layer raceway pond (TL-RWP), suitable for this purpose due to their high biomass

productivity and better culture transparency when using muddy wastewater. The units were operated in batch, and subsequently in semi-continuous growth regime — and monitored in terms of photosynthetic performance, growth, nutrient removal rate, and bioactivity. The results showed that the co-cultures grew well in the centrate, where they achieved the maximum biomass densities of 1.3 and 2.1 g dry weight L^{-1} in TLC and TL-RWP, respectively, by the end of the batch regime and 1.9 and 2.0 g dry weight L^{-1} by the end of the semi-continuous regime. Although TL-RWP grown cultures showed faster growth, the TLC-one revealed better nutrient removal efficiencies batch wise than the culture grown in TL-RWP — removing up to 48% of total nitrogen and 43% of total phosphorus. Conversely, the latter was more efficient under the semi-continuous regime (54% and 42% consumption of total nitrogen and phosphorus, respectively). In the harvested biomass, an important antimicrobial activity (specifically antifungal) was detected. In this sense, the *in-vitro* growth of the oomycete *Pythium ultimum* was inhibited by up to 45% with regard to the control. However, no biostimulating activity was observed. The present findings confirm the possibility of using these two species for biomass production in municipal wastewater centrate using highly productive thin-layer systems. This technology can be a valuable contribution to circular economy since the produced biomass can be re-applied for agricultural purposes.

8.1. Introduction

The introduction of microalgae in wastewater treatment is currently under the spotlight due to its potential integration in circular economy applications under the EU Water Framework Directive goals through re-application of the phytoremediated microalgal biomass obtained in other activities.

The application of microalgae in wastewater treatment is intended at removing excess nutrients, heavy metals, and other organic contaminants while simultaneously benefiting from a reduction in biomass production costs (Luo et al., 2015; Oswald et al., 1957; Pittman et al., 2011; Wang et al., 2016). Selected microalgal species suitable for this purpose have a biological profile characterized by a high growth rate and tolerance to high nutrient concentrations (such as ammonium and carbon dioxide). *Chlorella* and *Scenedesmus* are well-established genera, utilized in wastewater treatments that are robust and possess the added benefit of producing metabolites with applications for low (biofertilizers) and high-value (biostimulants and biopesticides) products (Krichen et al., 2019; Krustok et al., 2015; Ronga et al., 2019). The added ability to synthesize compounds with market value is also necessary to render the whole process economically feasible. However, several other challenges also

need to be considered for successful production. Another relevant, yet complex variable in wastewater treatment pertains to the evolution of natural, or selected, populations as mono- or co-cultures. The use of microalgae in co-cultures, as opposed to monocultures in wastewater treatment has been reported to yield more stable cultures (i.e., less susceptible to crashes, as well as improve nutrient uptake (Gouveia et al., 2016; Qin et al., 2016). Previous studies have explored microalgal co-cultures of *Chlorella* and *Scenedesmus*, naturally assembled in high-rate algal ponds of wastewater treatment plants (Galès et al., 2019; Koreivienė et al., 2014; Krichen et al., 2019; Tao et al., 2017). An additional, growth-limiting factor that needs to be addressed in microalga-based wastewater treatments relates to light availability, which is greatly affected by the type of photobioreactor used and the cultivation regime applied (i.e., batch, semi-continuous). Open cultivation systems are characterized by low construction and maintenance costs compared to closed photobioreactors. Due to the presence of suspended solids and other particles in the wastewater that can interfere with light penetration, units with a short light path can provide a solution, especially in climates with less sunlight. To our knowledge, few studies have addressed the use of co-cultures grown in wastewater and in TL systems (Tejido-Nuñez et al., 2020) including bioactivity assessment. In this work, the behavior of co-cultures of two green microalgae, *Chlorella vulgaris* and *Scenedesmus acutus*, were studied when grown outdoors in two different TL outdoor units — a thin-layer cascade (TLC) and a thin-layer raceway pond (TL-RWP). Centrate from municipal wastewater, after secondary aerobic treatment, was employed as the sole nutrient source. Photosynthetic activity, growth, and nutrient removal efficiency were compared in both units, as well as biostimulant and antimicrobial activity of biomass extracts.

8.2. Methods

8.2.1. Strains and laboratory culture condition

Two green microalgal strains, *Chlorella vulgaris* MACC-1 (hereafter abbreviated to *C. vulgaris*) and *Scenedesmus acutus* MACC-677 (hereafter abbreviated to *S. acutus*) obtained from the Algal Culture Collection of the Széchényi István University, Mosonmagyaróvár, Hungary, were used in these trials. The strains were selected for their fast growth (Ördög et al., 2013), as well as biostimulating and biopesticide activities (V. Ördög, unpublished data). The cultures were initially grown as monocultures in BG-11 medium (Allen and Stanier, 1968;

Hughes et al., 1958) in 10-L Pyrex bottles in the laboratory at 28-30 ºC, under an irradiance of 200 µmol photons m^{-2} s^{-1}, and mixed by bubbling a mixture of air with 1% CO_2 (v/v).

8.2.2. Centrate preparation

The centrate used in the cultivation was collected directly from the municipal wastewater treatment plant (WWTP) in Třeboň (Czech Republic). To avoid cell aggregation, due to the automatic addition of flocculant in the process, the activated sludge was taken from WWTP just after secondary aerobic digestion (secondary-treated wastewater) and centrifuged at 3,000 *g* for 5 min (centrifuge Sigma 8KS) to separate liquid centrate from solid sludge (similar procedure as in the WWTP). The supernatant (centrate) of brownish color was collected and used (non-diluted) as nutrient medium (see the composition in Table 8.1). The total nitrogen (TN) to total phosphorus (TP) ratio in the centrate was ca. 1.5. However, comparing the centrate to the inorganic medium BG-11, commonly used for cultivation, the total content of nitrogen was similar (250 mg L^{-1} in BG-11); while phosphorus was more than 20 times higher (7 mg L^{-1} in BG-11).

Table 8.1. Minimum and maximum measured values (n = 3) of the wastewater centrate used in the cultivation trials concerning biochemical and chemical O_2 demand (BOD and COD respectively), total organic carbon (TOC), total nitrogen (TN), and total phosphorus (TP).

Measured variable	**Concentration (mg L^{-1})**
Biochemical O_2 demand (BOD)	180
Chemical O_2 demand (COD)	1000 – 1,100
Total organic carbon (TOC)	310 – 560
Total nitrogen (TN)	230 – 260
Total phosphorous (TP)	150 – 170

8.2.3. Cultivation trials in outdoor units

Two outdoor cultivation units – TLC and TL-RWP – were used to grow the selected microalgal strains. These two units differed in the circulation device used for moving the culture – paddle wheel versus centrifugal pump (Grivalský et al., 2019). Each of the 5 m^2 cultivation units was placed in a separate east-west oriented greenhouse placed side by side; they protected cultures from cross-contamination and unfavorable outdoor conditions. The units were described in detail elsewhere (Ranglová et al., 2021). Trials were carried out in July 2019

at Centre Algatech, Třeboň (N 48º59′, E 14º46′). The TL-RWP was operated continuously, with a volume of 100 L and a culture thickness of 18 mm; the flow speed was ca. 0.2 m s^{-1}. In both units, the automatic regulation of CO_2 supply kept pH between 7.8 and 8.2. The TLC was operated with a working volume of 70 L, using a culture depth of 10 mm; and the flow speed was ca. 0.5 m s^{-1}. The culture was circulated only during daytime, and stored in a retention tank during the nighttime, where it was mixed via air bubbling (light/dark regime of about 12/12 hours). The evaporation was compensated every morning by addition of tap water. Weather conditions (culture temperature and irradiance received) were recorded using a meteorological station (modular control system ADiS-AMiT) with a solar radiation sensor located by the units and submerged temperature sensors (Annex IV Supplementary Figure IV.1 and Supplementary Figure IV.2 for temperature and radiation, respectively).

Each unit was inoculated to the same biomass density, ca. 0.7 g of dry weight (DW) L^{-1}, using laboratory-grown cultures (TLC inoculated one day later than TL-RWP owing to technological complexity). The samples for various measurements were taken daily at 08:00 AM. The microalgae were grown in the batch regime for seven days to get a dense culture in the late logarithmic phase. Afterward, a semi-continuous growth regime was operated for another five days by harvesting 25% of each culture daily at 09:00 AM, and replacing it with fresh centrate – so as to mimic large-scale semi-continuous biomass production.

8.2.4. Photosynthesis measurements

Microalgal samples were taken from the outdoor cultures and analyzed *off-situ* after dilution to 0.2-0.3 g DW L^{-1} with tap water and dark-adapted for 10 min in the water bath, kept at the same temperature as in the outdoor units. Photosynthetic activity of the cultures was measured using a saturation pulse analysis of fluorescence quenching with a pulse-amplitude modulation fluorometer (PAM-2500, H. Walz, Germany) to construct RLCs. Data were recorded in triplicates. Analysis of RLCs was used to estimate changes in the actual photochemical yield through PSII, YII, in terms of dependence on light intensity. The relative electron transport rate (rETR) was calculated by multiplying the actual PSII photochemical yield by the corresponding PAR value (E_{PAR}) (Hofstraat et al., 1994; Ralph and Gademann, 2005; White et al., 2011). The RLCs were fitted by non-linear least-squares regression (Eilers and Peeters, 1988), using PamWin_3 software to estimate maximum ETR ($rETR_{max}$) and saturating irradiance. The experimental techniques used in this study are described in detail elsewhere (Babaei et al., 2020, 2017; Ranglová et al., 2019; Silva Benavides et al., 2017).

8.2.5. Analytical procedures

Measurement of biomass density was performed as described previously (Babaei et al., 2017; Ranglová et al., 2019). Biomass content (presented as g DW L^{-1}) was measured in triplicate by filtering 5 mL of culture samples on pre-weighed glass microfiber filters (GC-50). The cells were washed twice with deionized water, oven- dried at 105 ºC for 8 h, and finally transferred to a desiccator and weighed (precision of ±0.01 mg).

8.2.6. Nutrient analysis

Both centrate and samples from the co-cultures (25 mL) were centrifuged (12,000 *g*, 5 min) before syringe filtering (0.45 µm) and stored at -20 ºC until further analysis (performed by the laboratory Povodí Vltavy, České Budějovice). The parameters and nutrient content were determined according to specific protocols: biological oxygen demand (BOD) by suppression of nitrification, chemical oxygen demand (COD) using a commercial analytical kit (Merck), and total organic carbon (TOC) by thermal decomposition with Pt catalyst. Nitrite-nitrogen content (NO_2-N) was determined by automatic discrete photometry, ammonium-nitrogen content (NH_4-N) by acidimetry after distillation, and nitrate-nitrogen concentration (NO_3-N) was calculated as the sum to make up to TN content — which was, in turn, determined by thermal oxidation with electrochemical detection. Both TP and orthophosphate-phosphorus (PO_4-P) were assayed after mineralization using automatic discrete photometry. Nutrient removal was calculated as the difference between the supplied nutrient (TN and TP) content found in the wastewater and the one found in the respective cultures by the end of each culture regime (batch and semi-continuous). Results were expressed in g m^{-2} d^{-1} and as percentage of nutrients supplied in the wastewater.

8.2.7. Bioactivity tests

The resulting freeze-dried biomass harvested by the end of the semicontinuous regime was suspended in distilled water (10 mg DW L^{-1}), and sonicated (Branson sonicator 150, amplitude 40%, 3 min) before testing for two different agricultural applications: antimicrobial and biostimulating activities. The antimicrobial (biopesticide) activities of the samples were evaluated with an antagonism bioassay. Three different bioassays were used to detect plant biostimulating activities: the cress seed germination, the mung bean rooting and the wheat leaf chlorophyll retention. All bioassays were performed in triplicate.

8.2.7.1. Bioassays of germination index

Freeze-dried microalgal biomass (100 mg) was suspended in 10 mL of distilled water (10 g DW L^{-1}) for the germination index assay. The suspension was sonicated and then incubated with stirring and heating for 2 hours. The biostimulant activity was tested on 100 cress (*Lepidium sativum*) seeds using sonicated aqueous extracts of 0.5 and 2 g DW L^{-1} of microalgal biomass, as described elsewhere [27,28]. The percentage of seed germination, as well as radicle elongation were taken for the germination index (GI) calculation according to the following formula: GI (%) =(G_S × L_S) / (G_W ×L_W), where G_S denotes the percentage of germinated seeds in the presence of the microalgal extract, G_W the percentage of germinated seeds in the presence of distilled water, L_S the mean of radicle elongation (mm) in the presence of the microalgal extract, and L_W the mean of radicle elongation (mm) in the presence of distilled water.

8.2.7.2. Determination of auxin-like activity

The bioassay of auxin-like activity was performed according to Hess (1961). The algal suspensions at concentrations of 0.5, 1.0, 2.0, and 3.0 g DW L^{-1} were used for treatment of seedling cuttings of mung bean (*Vigna radiata* (*L.*) Wilczek) in the rooting tests. The number of roots (longer than 1 mm) was recorded after application of the biomass extract. A standard curve of indol-3-butyric acid (IBA) at concentrations of 0, 0.3, 0.5, 0.7, and 1 mg DW L^{-1}, was prepared for comparative purposes.

8.2.7.3. Determination of cytokinin-like activity

The bioassay of cytokinin-like activity was performed according to Kuhnle et al. (1977). Leaves from wheat (*Triticum aestivum L.*) seedlings (about 10 cm height) were collected and then cut 35 mm below their apical tip into 10 mm segments. The algal suspensions at concentrations of 0.5, 1.0, 2.0, and 3.0 g DW L^{-1} were applied to the detached leaf segments. After incubation for four days, the chlorophyll content of the leaf segments was measured. A standard curve of kinetin (KIN) at the concentrations of 0, 0.3, 0.5, 0.7, and 1 mg DW L^{-1}, was used for comparison.

8.2.7.4. Antagonism bioassays by dual culture

The aqueous extracts were tested against the growth of phytopathogenic fungi, bacteria, and oomycetes *in-vitro* using the dual culture technique according to published protocols (Sánchez San Fulgencio et al., 2018; Suárez-Estrella et al., 2014). The activity of the extracts was tested against two fungi – *Fusarium oxysporum* f. sp. *melonis* and *Rhizoctonia solani*

(further abbreviated as *F. oxysporum* and *R. solani*, respectively), two oomycetes – *Phytophthora capsici* and *Pythium ultimum* (further abbreviated as *P. capsici* and *P. ultimum*, respectively) and four bacteria strains – *Clavibacter michiganensis* subsp. *michiganensis*, *Xanthomonas campestris* pv. *vesicatoria*, *Pseudomonas syringae* pv. tomato, *Pectobacterium carotovorum* (further abbreviated as *C. michiganensis*, *X. campestris*, *P. syringae*, *P. carotovorum*, respectively). All strains were provided by the Spanish Type Culture Collection (STCC). The inhibition index was calculated according to the following formula in equation 8.1:

$$I = \frac{C - T}{C} \times 100 \quad (8.1)$$

where *I* is inhibition index in %, *C* is diameter of the zone of the pathogen patches in the absence of microalgal extract (mm), and *T* is diameter of the zone of the pathogen patches in the presence of microalgal extract (mm). In all cases, control bioassays were performed using distilled water.

8.2.8. Statistical analysis

One biological replicate was performed for each unit with several technical replicates performed under batch and semi-continuous growth until steady-state was achieved. A paired sample non-parametric test (Wilcoxon test) was used to check for significant differences between cultures grown in the different units (TLC and TL-RWP). Only results with $p < 0.05$ were considered statistically different. All tests and graphs were produced using R software.

8.3. Results and discussion

8.3.1. Growth

In the present study, two different species, *C. vulgaris* and *S. acutus* were grown as a co-culture in two different cultivation units – TLC and TL-RWP – in batch and subsequently in semi-continuous regime, using centrate from municipal wastewater as the only nutrient source. The culture grew faster in TL-RWP, reaching 2.1 ± 0.0 g DW L^{-1} (μ = 0.15 d^{-1}) after one week of the batch regime while it was only 1.3 ± 0.0 g DW L^{-1} (μ = 0.10 d^{-1}) in TLC. A more extended lag phase was observed in TLC's culture, probably due to the lower thickness of the culture layer (Figure 8.1). In any case, both TLC and TL-RWP cultures were

characterized by a steeply increasing biomass density under batch regime. According to our previous experience, when the biomass density reached about 1 g DW L^{-1}, both cultures in outdoor TL unit became photoadapted and started growing faster. However, the semi-continuous regime promoted a higher specific growth rate of the TLC culture (1.9 g DW L^{-1}; μ = 0.32 d^{-1}), which eventually reached a similar biomass density as that in TL-RWP (2.0 g DW L^{-1}; μ = 0.19 d^{-1}) with a lower specific growth rate. The thickness of culture layer in TL-RWP and high culture density at the end of the batch regime probably promoted photolimitation, allowing attainment of higher growth rates in the TLC culture under the semi-continuous regime.

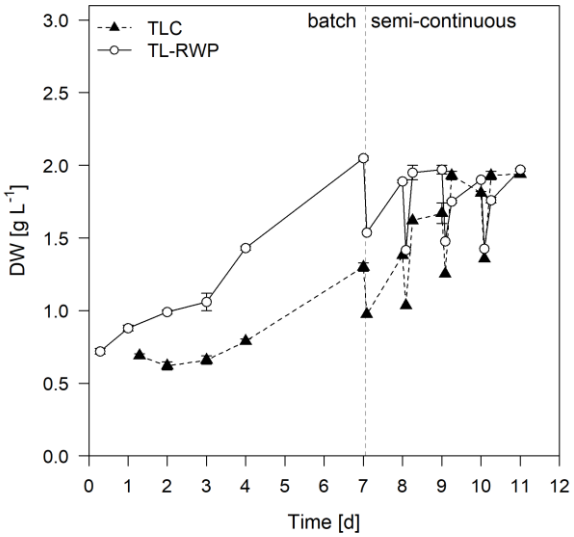

Figure 8.1. Growth in terms of g dry weight (DW) L^{-1} of co-cultures of *C. vulgaris* and *S. acutus* cultivated in a thin-layer cascade (TLC; black triangle with dashed line) and in a thin-layer raceway pond (TL-RWP; white circles with solid line) under batch and semi-continuous regime (25% dilution rate) using centrate as a nutrient source (*n* = 1). The culture in TLC was inoculated one day later than that in TL-RWP. Error bars represent analytical standard deviation, as DW was determined in triplicate.

After surpassing 0.8 g DW L^{-1}, the highest growth promoted in the TLC unit can also be attributed to a lower oxygen build-up, as this gas is released when the culture falls into the collection tank through a net that promotes degassing. In both units, pH was controlled and kept between 7.8 and 8.2, where even though the dominant form in the ammonium/ammonia (NH_4^+/NH_3) buffer system is NH_4^+ (ion dissociation constant, pKa, is about 9.25 at 25 ºC), at this set point values of pH, NH_4^+ conversion to NH_3 is already ongoing (Wang et al., 2019). As so, degassing can probably promote ammonia stripping and thus prevent algal growth inhibition (Álvarez and Otero, 2020). Nonetheless, all situations unfolded the possibility of using aerobic centrate as the sole nutrient source, which provided suitable growth conditions.

The biomass concentrations achieved in this study using TL systems surpassed the usual biomass density of 1 g DW L^{-1} achieved in high rate algal ponds or conventional RWP

– characterized by deep light paths (Cho et al., 2017; Ledda et al., 2015). The short optical path resulted in higher biomass density of the co-culture grown in both TL units, showing lower light absorption when the brownish centrate was used as nutrient source.

By the end of the trial, microscopic observation showed that the co-culture was dominated by *S. acutus* cells (Annex IV Supplementary Figure IV.3). It has already been reported (Krichen et al., 2019) that *Chlorella* is one of the first microalgae to colonize wastewater environments since it is a more stress-tolerant genus. Later on being overgrown by *S. acutus,* which is more sensitive to high concentrations of ammonium (Krichen et al., 2019). However, this balance can also be influenced by seasonality (Cho et al., 2015).

8.3.2. Photosynthetic performance

Changes in the photosynthetic activity can reflect adaptation mechanisms to higher irradiance as to minimize photo-stress. In this study, these changes were estimated as $rETR_{max}$ by chlorophyll fluorescence (Figure 8.2). Supplementary data estimated from the RLCs including the slope (α), the photosynthesis saturating irradiance (Ek = rETR/α) and non-photochemical quenching (NPQ) are shown in Supplementary Table IV.1**Error! Reference source not found.**. The $rETR_{max}$ values of the TLC culture increased at the beginning of the cultivation trial and remained relatively stable with only a slight decrease at the end of batch regime, reaching a maximum value of 349 ± 15 µmol e^- m^{-2} s^{-1} under the semi-continuous regime. On the other hand, $rETR_{max}$ in the TL-RWP cultures increased at the beginning of the cultivation trial and reached the maximum of 373 ± 3 µmol e^- m^{-2} s^{-1}; it started to decrease by the end of batch regime toward a minimum of 188 ± 0 µmol e^- m^{-2} s^{-1}. The recovery was seen in semi-continuous mode, although $rETR_{max}$ of in the TL-RWP culture remained lower than that of the TLC cultures.

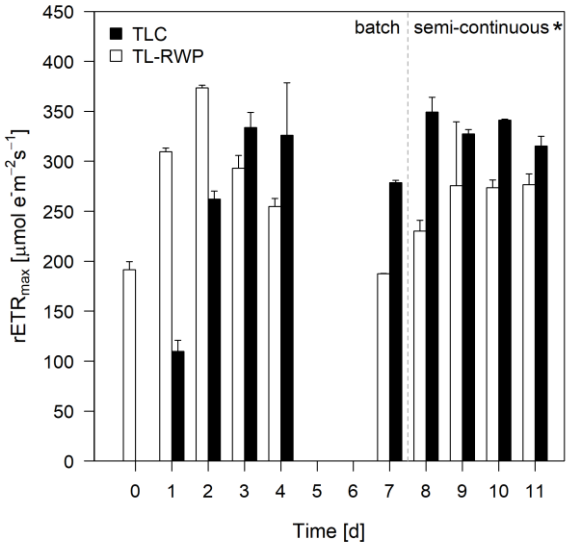

Figure 8.2. Maximum relative electron transport rate ($rETR_{max}$) of the co-culture of *C. vulgaris* and *S. acutus* cultivated in TLC (black bars) and TL-RWP (white bars) under batch and semi-continuous (25% dilution rate) regime using centrate as nutrient source (n = 1). Missing values represent non-sampling days. Error bars represent analytical standard deviation as the measurements were performed in triplicate. Growth regime marked with an asterisk (*) indicates statistically significant differences ($p < 0.05$) between TLC and TL-RWP units.

An initial photoacclimation was observable in the cultures grown in both units, although the lower initial values during the first days can also be attributed to ammonium inhibition (see Figure 8.3) that constrains electron transport in PSII (Li et al., 2019; Wang et al., 2019). Higher $rETR_{max}$ were found in TL-RWP during the first three days; overall, the TLC culture revealed significantly higher ($p < 0.05$) $rETR_{max}$ values. This was probably caused by higher averaged irradiance per cell in the thinner layer TLC culture (7-10 mm) compared to that in TL-RWP (15-25 mm). The slightly higher culture density (Figure 8.1), as well as culture depth, in the TL-RWP unit (compared to TLC) promoted a lower average cell irradiance, resulting in lower $rETR_{max}$ values by the end of batch regime. The lower $rETR_{max}$ values of both cultures at the last day of the batch regime can respond to nutrient deficiency in nitrogen-limited media (see Figure 8.3; White et al., 2011). This is supported by the later increase of $rETR_{max}$ in the semi-continuous regime when part of the culture was replaced by fresh centrate and N availability was again higher, and photolimitation was reduced.

8.3.3. Nutrient removal

The evolution of TN, TP and TOC removal efficiencies of *C. vulgaris* and *S. acutus* co-culture, when using centrate as nutrient source, was assessed during the experiment. Results are shown in Table 8.2.

Table 8.2. Nutrient removal efficiency in g m^{-2} d^{-1} (in %) of total nitrogen (TN), total phosphorus (TP) and total organic carbon (TOC) in the co-cultures of *C. vulgaris* and *S. acutus* grown in a thin-layer cascade (TLC) and a thin-layer raceway pond (TL-RWP) under batch and semi-continuous cultivation regime (25% dilution rate). The centrate of municipal wastewater was used as nutrient source (*n* = 1).

Unit	Cultivation mode	Removal efficiency in g m^{-2} d^{-1} (%)		
		TN	TP	TOC
TLC	Batch	0.35 (48%)	0.19 (43%)	-2.54 (-287%)
	Semi-continuous	0.89 (53%)	0.32 (29%)	1.15 (17%)
TL-RWP	Batch	0.22 (34%)	0.00 (0%)	-2.98 (-330%)
	Semi-continuous	1.13 (54%)	0.71 (42%)	2.76 (33%)

The removal efficiencies of TN and TP by the end of the batch regime were higher in the TLC grown culture reaching 48 and 43%, respectively, as opposed to the TL-RWP cultures that reached only 34 and 0%. Under the semi-continuous regime, the TN uptake was increased in both TLC (53%) and TL-RWP (54%), while the TP removal efficiency decreased in TLC (29%) and improved in the TL-RWP (42%) cultures. The inability of the co-culture in TL-RWP to uptake P in the batch regime is somehow surprising and points to another limiting element. As such, further experiments should be performed in order to establish the limiting factor toward increase in nutrient removal efficiency. Nonetheless, neither combination could reach the admissible values for wastewater discharge in sensitive areas of 10-15 mg L^{-1} of TN and 1-2 mg L^{-1} of TP (Directive 91/271/EEC, 1991). Still, the TN and TP removal efficiencies were improved by the use of a co-culture (*Chlorella* and *Scenedesmus*) when compared to a similar experiment performed with *Chlorella* monocultures (Ranglová et al., 2021). However, a longer residence time could improve performance (Galès et al., 2019).

The TOC concentrations increased in both cultures grown in batch mode, causing negative removal efficiencies (-287 and -330% in TLC and TL-RWP, respectively). This increase in TOC was probably caused by decomposition of natural organic matter present in the centrate (e.g., humic acid, amines, urea) as there is also evidence of a decrease of NH_4 during the lag phase at the beginning of the trial – Figure 8.3 (Hendricks, 2007) and by the presence of starch in gradually increasing number of microalgae cells during the batch regime. This resulted in negative TOC removal efficiency. The TOC left in the culture during the batch regime was higher than the one consumed by heterotrophic organisms, such as bacteria (Tao et al., 2017). The higher growth rate of the culture grown in TLC during the semi-continuous regime produced a higher density of the cells containing starch and thus, the TOC removal efficiency was lower (17%) as compared to that in TL-RWP (33%). As the centrate was added every day, the bacteria population proliferated quicker than microalgae, being able to uptake more TOC, which resulted in lower concentrations by the end of the semi-continuous regime.

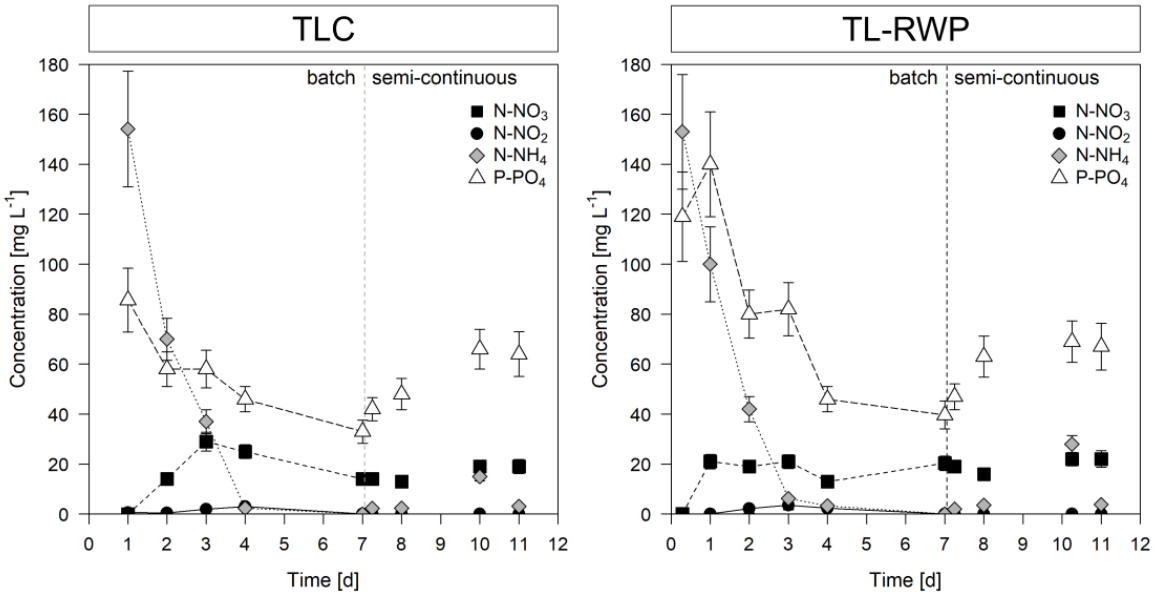

Figure 8.3. Concentration (mg L^{-1}) of nitrate-nitrogen ($N\text{-}NO_3$; black square), nitrite-nitrogen ($N\text{-}NO_2$; black circle), ammonium-nitrogen ($N\text{-}NH_4$; grey diamond), and phosphate-phosphorus ($P\text{-}PO_4$; white triangle) in the co-culture of *C. vulgaris* and *S. acutus* grown in a thin-layer cascade (TLC; left panel) and a thin-layer raceway pond (TL-RWP; right panel) under batch and semi-continuous (25% dilution rate) growth regimes using centrate as nutrient source (n = 1). Error bars represent analytical standard deviation as the measurement was performed in triplicate.

The specific nutrient uptake was more efficient in both cultivation units in the batch regime, whereas it was not fast enough in the semi-continuous one, resulting in accumulation of some nutrients in the cultivation medium, e.g., phosphate (Figure 8.3). Phosphate removal can be limited when $N\text{-}NH_4$ is exhausted (Galès et al., 2019). This is understandable as the TN/TP ratio (about 1.6) in the centrate (Table 8.1) was relatively low, considering the content of nitrogen and phosphorus in microalgal biomass is usually reported up to a maximum of 12% and 3% (ratio N/P of 4) of ash-free DW, respectively (Reynolds, 2006). The daily addition of tap water to compensate the evaporation contributed to the total nutrient with only 20 µg L^{-1} of NO_3^- and 28 µg L^{-1} of PO_4^{3-}; these are rather negligible amounts, and therefore, were not accounted for.

Nitrite-nitrogen was efficiently removed by the co-culture grown in both units, reaching values below 0.3 mg L^{-1}, which is the maximum admissible threshold in drinking water (World Health Organization, 2017). After three days of cultivation, ammonium-nitrogen concentration dropped significantly in both cultivation units achieving the value of 2.4 mg L^{-1} in TLC compared to 6.2 mg L^{-1} in TL-RWP. Being the preferred nitrogen source, ammonium-nitrogen concentrations dropped first under the batch regime, thus reflecting the opposite trend of nitrate-nitrogen. The decrease in ammonium concentration was accompanied by the increased nitrate concentration during the batch regime, probably due to bacterial nitrification.

Moreover, some ammonium may have been lost due to stripping to the atmosphere in gaseous form (Álvarez and Otero, 2020).

8.3.4. Biological activity

8.3.4.1. Determination of auxin- and cytokinin-like activity

No biostimulating activities were detected when two different concentrations of the microalgal extracts (0.5 and 2 g DW L^{-1}) were used for seed germination (data not shown). The mung bean rooting (data not shown) tests demonstrated no auxin-like activity. No chlorophyll retention was detected when the samples were tested for cytokinin-like activity (data not shown). Some inhibiting substances in the centrate could explain the absence of biostimulating activity in the freeze-dried biomass sample (Garcia et al., 1995). Another explanation for the absence of biostimulating activity could be due to the type of nutrient source used since previous studies were able to find such activities in *Chlorella* (Ranglová et al., 2021).

8.3.4.2. Antimicrobial activity

The biomass obtained from the co-cultures of microalgae grown in the centrate showed antagonistic activity against various phytopathogenic agents (Figure 8.4). Antifungal activities were the most noticeable in the co-cultures developed in both units. Similar inhibition of fungal activities of at least 43, 31, and 42% against *R. solani*, *F. oxysporum,* and *P. capsici*, respectively, were detected regardless of the cultivation unit. These results are similar to that obtained for monocultures of *Chlorella* MACC-1 (Ranglová et al., 2021) and *Scenedesmus* MACC-677 (manuscript submitted). The antifungal activity of 45% against *P. ultimum* was found only when the biomass was cultivated in TLC. This could indicate the predominant presence of *Chlorella* MACC-1 in the co-culture of TLC as no bioactivity of *Scenedesmus* MACC-677 against this pathogen was observed (unpublished). On the other hand, antibacterial activity against one microbial species, *C. michiganensis,* was detected only in the biomass harvested from TL-RWP.

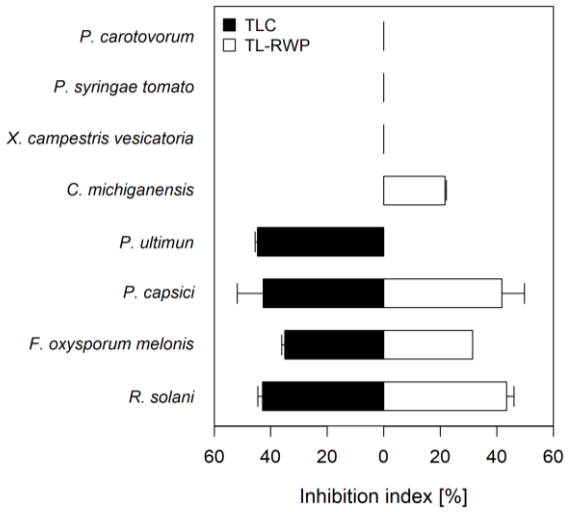

Figure 8.4. Antibacterial and antifungal activities of the resulting biomass of co-cultures of *C. vulgaris* and *S. acutus* grown in a thin-layer cascade (TLC; black bars) and in a thin-layer raceway pond (TL-RWP; white bars) in centrate. Results are expressed as inhibition index (%) against two fungi – *Rhizoctonia solani*, *Fusarium oxysporum* f. sp. *melonis*, two oomycetes – *Phytophthora capsici* and *Pythium ultimum* and four bacteria strains – *Clavibacter michiganensis* subsp. *michiganensis*, *Xanthomonas campestris* pv. *vesicatoria*, *Pseudomonas syringae* pv. *tomato* and *Pectobacterium carotovorum* (*n* = 3). Error bars represent standard deviation.

One reason for the loss of multi-antibacterial capacity, which has been previously reported in *Chlorella* cultures (Ranglová et al., 2021; Ronga et al., 2019) could be caused by the presence of a higher density of *S. acutus* cells found at the end of the trial. However, since culture conditions can influence antimicrobial agent production, it would be interesting to pursue a better understanding of the co-culturing influence on the biological activity of the microalgae, since keeping a monoculture in open systems can be a difficult task (Mudimu et al., 2014). Our results indicated that the resulting biomass had a high action capacity against several pathogens commonly found in crops, helping to fight several fungal and oomycete infections, thus preventing wilting, rotting, and ultimately host death (Kevan and Shipp, 2011; Lamour et al., 2012). Therefore, the agricultural application of microalgal biomass after wastewater treatment has added value, as it implies the potential use of a natural biopesticide that provides protection to crops, while concomitantly contributing to the implementation of a circular economy.

8.4. Conclusion

The use of municipal wastewater centrate as the sole nutrient source to grow a co-culture of two chlorophytes (*Chlorella* and *Scenedesmus*), in two different outdoor TL units, was overall feasible. After a short adaptation period, the cultures started to grow linearly and

were transferred to a semi-continuous regime. Although a longer residence time can probably provide better results, nutrient removal of macronutrients from the wastewater centrate was effective. Even though microalgae's co-culturing benefits depend on population succession dynamics, the resulting biomass revealed a potential application in agriculture as antimicrobial agents, specifically against common agriculture fungi and oomycetes. Both TL systems are suitable for biomass production as well-mixed cultures are exposed to ambient light resulting in high average cell irradiance. TL-RWP use provided very similar results to that of TLC, as they are operated at similar culture layer depth. However, the TLC culture provided overall higher productivity (and slightly better nutrient removal) under the semi-continuous regime compared to the culture grown in TL-RWP. In addition, the co-culture of *Chlorella* and *Scenedesmus* yielded better nutrient removals than *Chlorella* monocultures under similar experimental designs, reaffirming the usefulness of consortia in wastewater treatment. This study confirms that the centrate separated from municipal wastewater can be used as a nutrient medium for chlorophyte cultivation, while effectively stripping nutrients to reduce eutrophication. Moreover, a final product with agricultural application can be obtained, thus contributing to a circular economy.

Chapter 9

Conclusions and future work

9.1. Conclusions

The work presented in this thesis addressed the underlying difficulties of microalgae biomass production by resorting to a multiplicity of approaches. Previous experimental data on the improvement of microalgae cultivation was complemented by strategies to monitor and promote biomass or target metabolite productivities – duly tested with several commercially relevant species and photobioreactors. Together with cost-cutting designs, such approaches can bring closer the reality of microalgae production for medium and low-value products – as this thesis aimed to provide another piece of the underlying puzzle by improving stability and sustainability of microalgae production. In this sense, the work described from Chapters 3 to 8 can help to answer the proposed questions, defined in Chapter 1.3:

1) ***How do the tested growth conditions affect biomass productivity, and are they applicable at an industrial scale?***

Considering the desired final product (biomass or specific metabolites), the correct selection of a strain can define the success or failure of an operation. In Chapter 3, the semi-continuous cultivation with 10 and 30% renewal rates of five *Tetraselmis* strains reveals the significant growth and biochemical differences within the same genus, showing the extreme importance of strain selection, which is the first step in microalgae production. Semi-continuous cultivation is a common growth strategy used for microalgal production at industrial scale. The application of a 30% renewal of the culture volume in Chapter 3 resulted in

increased lipid content and productivity for the tested lipogenic and non-lipogenic *Tetraselmis* strains. Nonetheless, the rapid assessment of neutral lipids using flow cytometry revealed that this mode of cultivation lowered the fraction of neutral lipid content in the cells.

Temperature is a major contributor to the success of microalgae cultivation, but it is also one of the most complex and expensive parameters to control, both economically and sustainably. While open systems suffer from active evaporation, closed systems commonly depend on water sprinklers to cool down the cultures with operating temperatures that can surpass that of the surrounding air. In Chapter 4, *N. oceanica* cultures were grown at a temperature of 28 ºC or 18 ºC outdoors in 50-L tubular photobioreactor (PBR). Applying a suboptimal constant temperature (18 ºC) during the cultivation of *N. oceanica* led to a downregulation of the photosynthetic activity, inhibiting photosystem II (PSII) repair mechanisms, which could explain the lower biomass productivity under this condition. Conversely, the higher biomass productivities obtained at warmer temperatures (28 ºC) came at the cost of higher nighttime biomass losses. Even though results from Chapter 4 indicate a valorization of the biomass due to the higher PUFA contents found – particularly those of eicosapentaenoic acid (EPA) – when cells were grown at suboptimal temperatures, excessive cooling could still be counter-productive if biomass productivity is low. Therefore, the best strategy would be to select the most suitable season to grow the selected microalgae species/strains to minimize the need to cool or heat the culture. Another approach relies on selecting thermophilic strains that also tolerate a wide range of temperatures in an attempt to prevent irreversible damage to PSII and consequent lower productivities.

Nutrient manipulation can also be a powerful tool to induce accumulation of target metabolites, although it is usually associated with slower growth rates. In Chapter 5, the exhaustion of nitrate in the cultivation of *N. oceanica* led to limited growth and increased de-epoxidation of the xanthophyll cycle pigments, along with poor electron transfer efficiency. However, nitrate depletion promoted lipid accumulation, with a high content of saturated fatty acids. As a result of the deterred growth, nutrient limitation strategies are more commonly applied in a two-stage approach. This means the microalgae are firstly cultured under optimal conditions, preferably under continuous or semi-continuous operational mode, and when the log-phase biomass obtained is subjected to the selected nutrient limitation to induce the accumulation of a target metabolite.

Both cultivation mode and nutrient manipulation are feasible approaches applicable at industrial scale. However, temperature control presents a more challenging endeavor due to the low efficiency, sustainability, and high cost associated with the task. Therefore, the selection and characterization of the microalgae strain must be carefully accomplished to determine the most suitable environmental conditions for its growth.

2) *Is fluorometry a helpful tool to monitor and identify hindrances to cellular performance?*

In Chapter 5, the application of *in situ* chlorophyll *a* fluorescence measurements to monitor photochemical parameters resulting from changes in nitrate availability was successfully tested. The faster timescale of photon capture events (~10^{-6} s) than CO_2 fixation (~1 s) (Beardall and Raven, 2013) translated in readily detectable “congestions” in electron transport, which was further enhanced when nitrogen was exhausted, and CO_2 fixation was constrained, leading to lipid accumulation. The correlation between the effective quantum yield of PSII (*Δ*F’/Fm') and lipid content also revealed that small changes in lipid content produce a considerable variation of *Δ*F’/F_m’. The usefulness of such a fast and responsive variable is tremendous since it can provide rapid insight into the photosynthetic apparatus and thus support the prevention of culture problems or even prevent culture crashes.

Nonetheless, *ex-situ* fluorometers have also proven their worth. In Chapter 4, the maximum photochemical quantum yield of PSII (F_v/F_m) and Kautsky's curves (OJIP fluorescence induction kinetics) showed the downregulation of photosynthetic activity with a lower electron transfer efficiency at low temperatures. This was probably caused by a diminished reaction centre (RC) number as a self-defense mechanism to avoid low-temperature induced photoinhibition. The limited PSII repair mechanisms of *N. oceanica* at 18 ºC revealed a lower tolerance of this species to this temperature than at 28 ºC, for which repair occurred during the night.

In Chapter 6, the outdoor cultivation in 100-L flat panel photobioreactors (FP PBR) of two commercially relevant diatoms was biochemically and photochemically monitored. The monitorization of electron transport using both F_v/F_m and the probability that a photon trapped by the PSII RC moves an electron further than Q_A^- (ψ_o) in *S. costatum* and *P. tricornutum* allowed identification of temperature as a limiting factor for the growth of *P. tricornutum*. Indeed, the higher values of *S. costatum*’s ψ_o were linked to a higher growth rate when compared to *P. tricornutum,* at least in the conditions and strains tested.

Using rapid light curves (RLC) in Chapter 7, the monitorization of the minimum saturating irradiance coefficient (E_k) in raceway ponds (RWP) culture systems in which light emitting diodes (LED) were implemented, permitted to observe significantly higher E_k values in the control than in the LED-lit cultures. This information allowed to diminish LEDs' use to maximize the photosynthetic rate at a lower price since the minimum light requirements were already met by using LEDs supplying ca. 318 µmol m^{-2} s^{-1}.

In Chapter 8, maximum relative electron transport rate ($rETR_{max}$) was used to compare the photosynthetic efficiency of co-cultures of *C. vulgaris* and *S. acutus* grown under two different cultivation systems using wastewater as media. The results show a better

performance of the culture grown in the thin-layer cascade (TLC) characterized by overall higher biomass productivity, when compared to the culture grown in the thin-layer (TL) -RWP, probably due to the higher averaged irradiance per cell in the thinner layer of the TLC. In addition, the low values of $rETR_{max}$ also pointed to nutrient limitation at the end of the batch cultivation in both units.

Overall, chlorophyll *a* fluorescence *in* and *ex-situ* provided a valuable and fast "intel" of the photosynthetic status of the cells, thus elucidating or warning about several constraints in the photosynthetic process that can hamper growth and, as a consequence, productivity.

3) *Is artificial lighting a promising solution to enhance microalgal production in RWP cultivation systems?*

So far, the use of LEDs in microalgae cultivation has been employed at laboratory scale due to the LEDs higher efficiency compared to other artificial light sources. The use of LEDs is limited to industrial scale because of their high cost, but several companies have managed to use them indoors, providing a more controllable environment. However, the feasibility of such an application has only proved effective in producing high-value metabolites. Nonetheless, the study of the effect of LED implementation in cultivation systems outdoors to improve productivity is scarce. In Chapter 7, RWPs – one of the most light-limited cultivation systems, were used to test the effect of LEDs upon growth of *N. oceanica*. The results show that LEDs improved growth, particularly at night, when biomass losses can occur from respiration. Still, as referred to in Chapter 4, at high irradiances, the continuous growth during the night led to a lower growth during the following day. Thus, the final increased biomass productivities were not enough to compensate the use of LEDs other than for high-value products. However, since LED efficiency is higher with lower sunlight irradiances and is also dependent on the culture concentration, a less intensive operation, by using the LEDs below a pre-determined solar irradiance or coupling the LEDs with solar energy, may provide a more cost-effective solution in the near future.

4) *Can microalgae treat municipal wastewater centrate using TL cultivation systems and the resulting biomass be re-applicated in other activities?*

Conventional wastewater treatments require several improvements, since they demand vast amounts of energy to oxidize organic matter, release considerable amounts of greenhouse gases, and have a low removal efficiency of ammonia, nitrate, and phosphate. Therefore, more advanced technologies are needed. The water treatment cost of conventional wastewater treatment plants is around 0.2 € m^{-3}, with additional expenses for tertiary treatment

processes, including nitrogen and phosphorous removal (Acién et al., 2016). Using microalgae in wastewater treatment changes the existing paradigm, since wastewater is upgraded from effluent to resource. In this scenario, there is no further need to supply oxygen for the oxidation of the organic carbon, thus reducing emission of greenhouse gases and increasing release of oxygen to the atmosphere in addition to recovery of valuable nutrients for microalgae growth. Although the resulting biomass cannot be used for human consumption, possible applications include feed, bioenergy, and agriculture. In Chapter 8, a consortium of *C. vulgaris* and *S. acutus* was successfully grown in municipal wastewater centrate resorting to two different TL units. A major concern in wastewater treatment using microalgae is turbidity which can deter microalgae growth due to light limitation. Turbidity varies with different types of wastewater, but the use of TL systems has been put forward as a good solution to improve light availability allowing the treatment of wastewater with higher turbidity levels. Under batch growth mode, the TLC-grown cultures revealed better nutrient removal efficiencies; however, the TL-RWP culture was more efficient under a semi-continuous regime. Although no biostimulant activity was found in the final biomass, an important activity against common fungal pathogens found in agricultural crops was revealed. The valorization of biomass through biostimulant and biopesticide applications as opposed to the anaerobic digestion for biomethane production is more interesting due to the higher market value of these compounds compared to that of biofuels. Regardless, application of the resulting microalgal biomass in other sectors is essential for the process to be cost-sufficient.

9.1.1. Lessons to be learned

A major characteristic of this thesis is the performance of the described studies in different laboratories. This diversity allowed comparison of methodologies between laboratories along with recognition of the need to standardize several common protocols. The standardization would grant better data comparison when using similar experiments and conditions, which would permit more significant advances and collaborations in microalgae research.

Other relevant aspects are the scarce studies at industrial scale aimed at confirming the preliminary results of experiments performed at laboratory scale (and indoors). In the last decade, more and more authors corroborate their findings by performing experiments at pilot scale outdoors where weather conditions are uncontrollable. Growing microalgae outdoors results in different productivities and cultivation challenges that increase proportionally to the used scale. Connected to this task also comes the need for tailor-made processes for each

microalga. An inflexible cultivation strategy of one-fits-all will probably end up in an unsuccessful cultivation.

9.2. Future work

The growing biotechnological potential of microalgae and their derivatives drives the ongoing increase in the value of these microorganisms. As a result, process optimization linked to sustainable approaches is crucial to deliver the required biomass. This strategy should start with an extensive screening of different microalgae species, with a particular focus on extremophiles coupled with the application of adaptive laboratory evolution methodologies that favor the selection of robust strains with a commercially attractive composition. Further development should also focus on validation of such strategies at industrial scale. The usefulness of an *in-situ* fluorimeter probe should be validated with different microalgae and under different growth regimes. The results should be accompanied by the study of biotic and abiotic conditions observed during the cultivation to correct for natural fluctuations in the data. In addition, revamping of cultivation systems used in microalgae facilities is a never-ending process, since several limitations still exist. These include the ones associated with light integration, CO_2 absorption, O_2 build-up, temperature and contamination control, and microbiota equilibrium in the cultures that can interfere with microalgae productivity. Regardless of the strategy, future approaches should be accompanied by a life cycle assessment and integrate circular economy that includes the valorization of each biomass fraction and processing of wastes and effluents.

References

Acién, F.G., Fernández, J.M., Magán, J.J., Molina, E., 2012. Production cost of a real microalgae production plant and strategies to reduce it. Biotechnol. Adv. 30, 1344–1353. https://doi.org/10.1016/j.biotechadv.2012.02.005

Acién, F.G., Gómez-Serrano, C., Morales-Amaral, M.M., Fernández-Sevilla, J.M., Molina-Grima, E., 2016. Wastewater treatment using microalgae: how realistic a contribution might it be to significant urban wastewater treatment? Appl. Microbiol. Biotechnol. 100, 9013–9022. https://doi.org/10.1007/s00253-016-7835-7

Acién Fernández, F.., Hall, D.O., Cañizares Guerrero, E., Krishna Rao, K., Molina Grima, E., 2003. Outdoor production of *Phaeodactylum tricornutum* biomass in a helical reactor. J. Biotechnol. 103, 137–152. https://doi.org/10.1016/S0168-1656(03)00101-9

Acién Fernández, F.G., Gómez-Serrano, C., Fernández-Sevilla, J.M., 2018. Recovery of Nutrients From Wastewaters Using Microalgae. Front. Sustain. Food Syst. 2, 59. https://doi.org/10.3389/fsufs.2018.00059

Agusti, S., Duarte, C.M., Kalff, J., 1987. Algal cell size and the maximum density and biomass of phytoplankton. Limnol. Oceanogr. 32, 983–986. https://doi.org/10.4319/lo.1987.32.4.0983

Alboresi, A., Perin, G., Vitulo, N., Diretto, G., Block, M.A., Jouhet, J., Meneghesso, A., Valle, G., Giuliano, G., Maréchal, E., Morosinotto, T., 2016. Light remodels lipid biosynthesis in *Nannochloropsis gaditana* by modulating carbon partitioning between organelles. Plant Physiol. 171, 2468–2482. https://doi.org/10.1104/pp.16.00599

Allen, M.M., Stanier, R.Y., 1968. Growth and Division of Some Unicellular Blue-green Algae. J. Gen. Microbiol. 51, 199–202. https://doi.org/10.1099/00221287-51-2-199

Álvarez, X., Otero, A., 2020. Nutrient removal from the centrate of anaerobic digestion of high ammonium industrial wastewater by a semi-continuous culture of *Arthrospira* sp. and *Nostoc* sp. PCC 7413. J. Appl. Phycol. https://doi.org/10.1007/s10811-020-02175-4

Anning, T., Macintyre, H.L., Pratt, S.M., Sammes, P.J., Gibb, S., Geider, R.J., 2000. Photoacclimation in the marine diatom *Skeletonema costatum*. Limnol. Ocean. 45, 1807–1817. https://doi.org/10.4319/lo.2000.45.8.1807

Antal, T., Konyukhov, I., Volgusheva, A., Plyusnina, T., Khruschev, S., Kukarskikh, G., Goryachev, S., Rubin, A., 2019. Chlorophyll fluorescence induction and relaxation system for the continuous monitoring of photosynthetic capacity in photobioreactors. Physiol. Plant. 165, 476–486. https://doi.org/10.1111/ppl.12693

Antonkine, M.L., Golbeck, J.H., 2004. Photosystem I: FX, FA, and FB Iron–Sulfur Clusters, in: Encyclopedia of Biological Chemistry. Elsevier, pp. 348–356. https://doi.org/10.1016/b0-12-443710-9/00489-0

Arashiro, L.T., Montero, N., Ferrer, I., Acién, F.G., Gómez, C., Garfí, M., 2018. Life cycle assessment of high rate algal ponds for wastewater treatment and resource recovery. Sci. Total Environ. 622–623, 1118–1130. https://doi.org/10.1016/j.scitotenv.2017.12.051

Araújo, R., Vázquez Calderón, F., Sánchez López, J., Azevedo, I.C., Bruhn, A., Fluch, S., Garcia Tasende, M., Ghaderiardakani, F., Ilmjärv, T., Laurans, M., Mac Monagail, M., Mangini, S., Peteiro, C., Rebours, C., Stefansson, T., Ullmann, J., 2021. Current status of the algae production industry in Europe: An emerging sector of the blue bioeconomy. Front. Mar. Sci. 7. https://doi.org/10.3389/fmars.2020.626389

Armstrong, F.A.J., 1963. Determination of nitrate in water by ultraviolet spectrophotometry. Anal. Chem. 35 (9), 10–12. https://doi.org/10.1021/ac60202a036 pp. 10–12

Asada, K., 1999. The water-water cycle in chloroplasts: Scavenging of active oxygens and dissipation of excess photons. Annu. Rev. Plant Physiol. Plant Mol. Biol. 50, 601–639. https://doi.org/10.1146/annurev.arplant.50.1.601

Babaei, A., Ranglová, K., Malapascua, J.R., Torzillo, G., Shayegan, J., Silva Benavides, A.M., Masojídek, J., 2020. Photobiochemical changes in *Chlorella* g120 culture during trophic conversion (metabolic pathway shift) from heterotrophic to phototrophic growth regime. J. Appl. Phycol. https://doi.org/10.1007/s10811-020-02137-w

Babaei, A., Ranglová, K., Malapascua, J.R.R., Masojídek, J., Ranglova, K., Malapascua, J.R.R., Masojídek, J., 2017. The synergistic effect of Selenium (selenite, $-SeO_3^{2-}$) dose and irradiance intensity in *Chlorella* cultures. AMB Express 7, 56. https://doi.org/10.1186/s13568-017-0348-7

Baird, R.B., Eaton, A.D., Rice, E.W. (Eds.), 2017. Standard methods for the examination of water and wastewater, 23rd ed. American Public Health Association, American Water Works Association, Water Environment Federation.

Baker, N.R., 2008. Chlorophyll fluorescence: A probe of photosynthesis *in vivo*. Annu. Rev. Plant Biol. 59, 89–113. https://doi.org/10.1146/annurev.arplant.59.032607.092759

Barreira, L., Resek, E., Rodrigues, M.J., Rocha, M.I., Pereira, H., Bandarra, N., da Silva, M.M., Varela, J., Custódio, L., 2017. Halophytes: Gourmet food with nutritional health benefits? J. Food Compos. Anal. 59, 35–42. https://doi.org/10.1016/j.jfca.2017.02.003

Beardall, J., Berman, T., Heraud, P., Omo Kadiri, M., Light, B.R., Patterson, G., Roberts, S.,

Sulzberger, B., Sahan, E., Uehlinger, U., Wood, B., 2001a. A comparison of methods for detection of phosphate limitation in microalgae. Aquat. Sci. 63, 107–121. https://doi.org/10.1007/PL00001342

Beardall, J., Raven, J.A., 2013. Limits to phototrophic growth in dense culture: CO_2 supply and light, in: Borowitzka, M.A., Moheimani, N.R. (Eds.), Algae for Biofuels and Energy. Springer Netherlands, Dordrecht, pp. 91–97. https://doi.org/10.1007/978-94-007-5479-9_5

Beardall, J., Young, E., Roberts, S., 2001b. Approaches for determining phytoplankton nutrient limitation. Aquat. Sci. 63, 44–69. https://doi.org/10.1007/PL00001344

Beer, S., Vilenkin, B., Weil, A., Veste, M., Susel, L., Eshel, A., 1998. Measuring photosynthetic rates in seagrasses by pulse amplitude modulated (PAM) fluorometry. Mar. Ecol. Prog. Ser. 174, 293–300. https://doi.org/10.3354/meps174293

Benvenuti, G., Bosma, R., Cuaresma, M., Janssen, M., Barbosa, M.J., Wijffels, R.H., 2015. Selecting microalgae with high lipid productivity and photosynthetic activity under nitrogen starvation. J. Appl. Phycol. 27, 1425–1431. https://doi.org/10.1007/s10811-014-0470-8

Berge, J.-P., Gouygou, J.-P., Dubacq, J.-P., Durand, P., 1995. Reassessment of lipid composition of the diatom, *Skeletonema costatum*. Phytochemistry 39, 1017–1021. https://doi.org/10.1016/0031-9422(94)00156-N

Berges, J.A., Charlebois, D.O., Mauzerall, D.C., Falkowski, P.G., 1996. Differential effects of nitrogen limitation on photosynthetic efficiency of photosystems I and II in microalgae. Plant Physiol. 110, 689–696. https://doi.org/10.1104/pp.110.2.689

Bligh, E.G.G., Dyer, W.J.J., 1959. A rapid method of total lipid extraction and purification. Can. J. Biochem. Physiol. 37, 911–917. https://doi.org/10.1139/o59-099

Bondioli, P., Della Bella, L., Rivolta, G., Chini Zittelli, G., Bassi, N., Rodolfi, L., Casini, D., Prussi, M., Chiaramonti, D., Tredici, M.R., 2012. Oil production by the marine microalgae *Nannochloropsis* sp. F&M-M24 and *Tetraselmis suecica* F&M-M33. Bioresour. Technol. 114, 567–572. https://doi.org/10.1016/j.biortech.2012.02.123

Borowitzka, M.A., 2013. High-value products from microalgae—their development and commercialisation. J. Appl. Phycol. 25, 743–756. https://doi.org/10.1007/s10811-013-9983-9

Borowitzka, M.A., Volcani, B.E., 1978. The polymorphic diatom *Phaeodactylum tricornutum*: Ultrastructure of its morphotypes. J. Phycol. 14, 10–21. https://doi.org/10.1111/j.1529-8817.1978.tb00625.x

Boussiba, S., Vonshak, A., Cohen, Z., Avissar, Y., Richmond, A., 1987. Lipid and biomass production by the halotolerant microalga *Nannochloropsis salina*. Biomass 12, 37–47. https://doi.org/10.1016/0144-4565(87)90006-0

Brennan, L., Owende, P., 2010. Biofuels from microalgae—A review of technologies for production, processing, and extractions of biofuels and co-products. Renew. Sustain. Energy Rev. 14, 557–577. https://doi.org/http://dx.doi.org/10.1016/j.rser.2009.10.009

Brown, J.S., 1987. Functional organization of chlorophyll *a* and carotenoids in the alga, *Nannochloropsis salina*. Plant Physiol. 83, 434–437.

Brown, M.R., 1991. The amino-acid and sugar composition of 16 species of microalgae used in mariculture. J. Exp. Mar. Bio. Ecol. 145, 79–99. https://doi.org/https://doi.org/10.1016/0022-0981(91)90007-J

Brown, M.R., Garland, C.D., Jeffrey, W.S., Jameson, I., Leroi, J.M., 1993. The gross and amino acid compositions of batch and semi-continuous cultures of *Isochrysis*, *Pavlova* and *Nannochloropsis*. J. Appl. Phycol. 5, 285–296. https://doi.org/10.1007/BF02186231

Brown, M.R., Jeffrey, S.W., 1995. The amino acid and gross composition of marine diatoms potentially useful for mariculture. J. Appl. Phycol. 7, 521–527. https://doi.org/10.1007/BF00003938

Butler, W.L., 1978. Energy distribution in the photochemical apparatus of photosynthesis. Annu. Rev. Plant Physiol. 29, 345–378. https://doi.org/10.1146/annurev.pp.29.060178.002021

Butler, W.L., Kitajima, M., 1975. Fluorescence quenching in Photosystem II of chloroplasts. Biochim. Biophys. Acta - Bioenerg. 376, 116–125. https://doi.org/10.1016/0005-2728(75)90210-8

Cabrita, M.T., Duarte, B., Gameiro, C., Godinho, R.M., Caçador, I., 2018. Photochemical features and trace element substituted chlorophylls as early detection biomarkers of metal exposure in the model diatom *Phaeodactylum tricornutum*. Ecol. Indic. 95, 1038–1052. https://doi.org/10.1016/j.ecolind.2017.07.057

Callejón-Ferre, A.J., Velázquez-Martí, B., López-Martínez, J.A., Manzano-Agugliaro, F., 2011. Greenhouse crop residues: Energy potential and models for the prediction of their higher heating value. Renew. Sustain. Energy Rev. 15, 948–955. https://doi.org/https://doi.org/10.1016/j.rser.2010.11.012

Cao, X., Xi, Y., Liu, J., Chu, Y., Wu, P., Yang, M., Chi, Z., Xue, S., 2019. New insights into the CO_2-steady and pH-steady cultivations of two microalgae based on continuous online parameter monitoring. Algal Res. 38, 101370. https://doi.org/10.1016/j.algal.2018.11.021

Capelli, B., Bagchi, D., Cysewski, G.R., 2013. Synthetic astaxanthin is significantly inferior to algal-based astaxanthin as an antioxidant and may not be suitable as a human nutraceutical supplement. Nutrafoods 12, 145–152. https://doi.org/https://doi.org/10.1007/s13749-013-0051-5

Cardona, T., Sedoud, A., Cox, N., Rutherford, A.W., 2012. Charge separation in Photosystem II: A comparative and evolutionary overview. Biochim. Biophys. Acta - Bioenerg.

https://doi.org/10.1016/j.bbabio.2011.07.012

Cardoso, C., Pereira, H., Franca, J., Matos, J., Monteiro, I., Pousão-Ferreira, P., Gomes, A., Barreira, L., Varela, J., Neng, N., Nogueira, J.M., Afonso, C., Bandarra, N.M., 2020. Lipid composition and some bioactivities of 3 newly isolated microalgae (*Tetraselmis* sp. IMP3, *Tetraselmis* sp. CTP4, and *Skeletonema* sp.). Aquac. Int. 28, 711–727. https://doi.org/10.1007/s10499-019-00489-w

Carneiro, M., Chini Zittelli, G., Cicchi, B., Touloupakis, E., Faraloni, C., Maia, I.B., Pereira, H., Santos, T., Malcata, F.X., Otero, A., Varela, J., Torzillo, G., 2021. In situ monitoring of chlorophyll *a* fluorescence in *Nannochloropsis oceanica* cultures to assess photochemical changes and the onset of lipid accumulation during nitrogen deprivation. Biotechnol. Bioeng. 118, 4375–4388. https://doi.org/10.1002/bit.27906

Carneiro, M., Cicchi, B., Maia, I.B., Pereira, H., Zittelli, G.C., Varela, J., Malcata, F.X., Torzillo, G., 2020. Effect of temperature on growth, photosynthesis and biochemical composition of *Nannochloropsis oceanica*, grown outdoors in tubular photobioreactors. Algal Res. 49, 101923. https://doi.org/10.1016/j.algal.2020.101923

Cartaxana, P., Domingues, N., Cruz, S., Jesus, B., Laviale, M., Serôdio, J., Marques da Silva, J., 2013. Photoinhibition in benthic diatom assemblages under light stress. Aquat. Microb. Ecol. 70, 87–92. https://doi.org/10.3354/ame01648

Carvalho, A.P., Monteiro, C.M., Malcata, F.X., 2009. Simultaneous effect of irradiance and temperature on biochemical composition of the microalga *Pavlova lutheri*. J. Appl. Phycol. 21, 543–552. https://doi.org/10.1007/s10811-009-9415-z

Červený, J., Šetlík, I., Trtílek, M., Nedbal, L., 2009. Photobioreactor for cultivation and real-time, *in-situ* measurement of O_2 and CO_2 exchange rates, growth dynamics, and of chlorophyll fluorescence emission of photoautotrophic microorganisms. Eng. Life Sci. 9, 247–253. https://doi.org/10.1002/elsc.200800123

Cessna, S., Demmig-Adams, B., Adams III, W.W., 2010. Exploring photosynthesis and plant stress using inexpensive chlorophyll fluorometers. J. Nat. Resour. Life Sci. Educ. 39, 22–30. https://doi.org/https://doi.org/10.4195/jnrlse.2009.0024u

Chan, T., Shimizu, Y., Pospíšil, P., Nijo, N., Fujiwara, A., Taninaka, Y., Ishikawa, T., Hori, H., Nanba, D., Imai, A., Morita, N., Yoshioka-Nishimura, M., Izumi, Y., Yamamoto, Yoko, Kobayashi, H., Mizusawa, N., Wada, H., Yamamoto, Yasusi, 2012. Quality control of photosystem II: Lipid peroxidation accelerates photoinhibition under excessive illumination. PLoS One 7, e52100. https://doi.org/10.1371/journal.pone.0052100

Chauton, M.S., Winge, P., Brembu, T., Vadstein, O., Bones, A.M., 2013. Gene regulation of carbon fixation, storage, and utilization in the diatom *Phaeodactylum tricornutum* acclimated to light/dark cycles. Plant Physiol. 161, 1034–1048. https://doi.org/10.1104/pp.112.206177

Chen, M., Li, J., Dai, X., Sun, Y., Chen, F., 2011. Effect of phosphorus and temperature on chlorophyll *a* contents and cell sizes of *Scenedesmus obliquus* and *Microcystis aeruginosa*. Limnology 12, 187–192. https://doi.org/10.1007/s10201-010-0336-y

Chini Zittelli, G., Lavista, F., Bastianini, A., Rodolfi, L., Vincenzini, M., Tredici, M.R., 1999. Production of eicosapentaenoic acid by *Nannochloropsis* sp. cultures in outdoor tubular photobioreactors. J. Biotechnol. 70, 299–312. https://doi.org/10.1016/S0168-1656(99)00082-6

Chini Zittelli, G., Pastorelli, R., Tredici, M.R., 2000. A Modular Flat Panel Photobioreactor (MFPP) for indoor mass cultivation of *Nannochloropsis* sp. under artificial illumination. J. Appl. Phycol. 12, 521–526. https://doi.org/10.1023/A:1008165606234

Chini Zittelli, G., Rodolfi, L., Biondi, N., Tredici, M.R., 2006. Productivity and photosynthetic efficiency of outdoor cultures of *Tetraselmis suecica* in annular columns. Aquaculture 261, 932–943. https://doi.org/10.1016/j.aquaculture.2006.08.011

Chisti, Y., 2016. Large-Scale Production of Algal Biomass: Raceway Ponds, in: Algae Biotechnology. Green Energy and Technology. pp. 21–40. https://doi.org/10.1007/978-3-319-12334-9_2

Cho, D.-H., Choi, J.-W., Kang, Z., Kim, B.-H., Oh, H.-M., Kim, H., Ramanan, R., 2017. Microalgal diversity fosters stable biomass productivity in open ponds treating wastewater. Sci. Rep. 7, 1979. https://doi.org/10.1038/s41598-017-02139-8

Cho, D.-H., Ramanan, R., Heo, J., Kang, Z., Kim, B.-H., Ahn, C.-Y., Oh, H.-M., Kim, H.-S., 2015. Organic carbon, influent microbial diversity and temperature strongly influence algal diversity and biomass in raceway ponds treating raw municipal wastewater. Bioresour. Technol. 191, 481–487. https://doi.org/10.1016/j.biortech.2015.02.013

Converti, A., Casazza, A.A., Ortiz, E.Y., Perego, P., Del Borghi, M., 2009. Effect of temperature and nitrogen concentration on the growth and lipid content of *Nannochloropsis oculata* and *Chlorella vulgaris* for biodiesel production. Chem. Eng. Process. Process Intensif. 48, 1146–1151. https://doi.org/10.1016/j.cep.2009.03.006

Crowe, B., Attalah, S., Agrawal, S., Waller, P., Ryan, R., Van Wagenen, J., Chavis, A., Kyndt, J., Kacira, M., Ogden, K.L., Huesemann, M., 2012. A comparison of *Nannochloropsis salina* growth performance in two outdoor pond designs: Conventional raceways versus the ARID pond with superior temperature management. Int. J. Chem. Eng. 2012, 1–9. https://doi.org/10.1155/2012/920608

Cunha, P., Pereira, H., Costa, M., Pereira, J., Silva, J.T., Fernandes, N., Varela, J., Silva, J., Simões, M., 2020. *Nannochloropsis oceanica* cultivation in pilot-scale raceway ponds—From design to cultivation. Appl. Sci. 10, 1725. https://doi.org/10.3390/app10051725

Custódio, L., Soares, F., Pereira, H., Barreira, L., Vizetto-Duarte, C., Rodrigues, M.J., Rauter, A.P., Alberício, F., Varela, J., 2014. Fatty acid composition and biological activities of

Isochrysis galbana T-ISO, *Tetraselmis* sp. and *Scenedesmus* sp.: possible application in the pharmaceutical and functional food industries. J. Appl. Phycol. 26, 151–161. https://doi.org/10.1007/s10811-013-0098-0

D'Orazio, N., Gemello, E., Gammone, M., de Girolamo, M., Ficoneri, C., Riccioni, G., 2012. Fucoxantin: A treasure from the sea. Mar. Drugs 10, 604–616. https://doi.org/10.3390/md10030604

Dahmen-Ben Moussa, I., Chtourou, H., Karray, F., Sayadi, S., Dhouib, A., 2017. Nitrogen or phosphorus repletion strategies for enhancing lipid or carotenoid production from *Tetraselmis marina*. Bioresour. Technol. 238, 325–332. https://doi.org/https://doi.org/10.1016/j.biortech.2017.04.008

Dammak, M., Hadrich, B., Miladi, R., Barkallah, M., Hentati, F., Hachicha, R., Laroche, C., Michaud, P., Fendri, I., Abdelkafi, S., 2017. Effects of nutritional conditions on growth and biochemical composition of *Tetraselmis* sp. Lipids Health Dis. 16, 41. https://doi.org/10.1186/s12944-016-0378-1

Davis, R., Aden, A., Pienkos, P.T., 2011. Techno-economic analysis of autotrophic microalgae for fuel production. Appl. Energy 88, 3524–3531. https://doi.org/10.1016/j.apenergy.2011.04.018

Davison, I.R., 1991. Environmental effects on algal photosynthesis: temperature. J. Phycol. 27, 2–8. https://doi.org/10.1111/j.0022-3646.1991.00002.x

De Pauw, N., Verlet, H., De Leenheer Jr., L., 1980. Heated and unheated outdoor cultures of marine algae with animal manure, in: Shelef, G., Soeder, C.J. (Eds.), Production and Use of Microalgae Biomass. Elsevier/North-Holland Biomedical Press, pp. 315–341.

de Vree, J.H., Bosma, R., Janssen, M., Barbosa, M.J., Wijffels, R.H., 2015. Comparison of four outdoor pilot-scale photobioreactors. Biotechnol. Biofuels 8, 215. https://doi.org/10.1186/s13068-015-0400-2

de Wijn, R., van Gorkom, H.J., 2001. Kinetics of electron transfer from Q_A to Q_B in photosystem II. Biochemistry 40, 11912–11922. https://doi.org/10.1021/bi010852r

Demmig-Adams, B., Garab, G., Adams III, W., Govindjee (Eds.), 2014. Non-photochemical quenching and energy dissipation in plants, algae and cyanobacteria, Advances in Photosynthesis and Respiration. Springer Netherlands, Dordrecht. https://doi.org/10.1007/978-94-017-9032-1

Demory, D., Combe, C., Hartmann, P., Talec, A., Pruvost, E., Hamouda, R., Souillé, F., Lamare, P.O., Bristeau, M.O., Sainte-Marie, J., Rabouille, S., Mairet, F., Sciandra, A., Bernard, O., 2018. How do microalgae perceive light in a high-rate pond? Towards more realistic Lagrangian experiments. R. Soc. Open Sci. 5. https://doi.org/10.1098/rsos.180523

Deore, P., Beardall, J., Noronha, S., 2020. Non-photochemical quenching, a non-invasive

probe for monitoring microalgal grazing: influence of grazing-mediated total ammonia-nitrogen. Appl. Phycol. 1, 32–43. https://doi.org/10.1080/26388081.2020.1715255

Directive 91/271/EEC, C., 1991. Council Directive of 21 May 1991 concerning urban waste water treatment, Official Journal of the European Communities. Council of the European Union.

Dong, H.-P., Williams, E., Wang, D. -z., Xie, Z.-X., Hsia, R. -c., Jenck, A., Halden, R., Li, J., Chen, F., Place, A.R., 2013. Responses of *Nannochloropsis oceanica* IMET1 to long-term nitrogen starvation and recovery. Plant Physiol. 162, 1110–1126. https://doi.org/10.1104/pp.113.214320

Duysens, L., Sweers, H., 1963. Mechanism of two photochemical reactions in algae as studied by means of fluorescence, in: Japanese Society of Plant Physiologists (Ed.), Studies on Microalgae and Photosynthetic Bacteria. University of Tokyo Press, Tokyo, pp. 353–372.

EC, 2020. A new Circular Economy Action Plan for a cleaner and more competitive Europe [WWW Document]. Commision Commun. COM/2020/98. URL https://eur-lex.europa.eu/resource.html?uri=cellar:9903b325-6388-11ea-b735-01aa75ed71a1.0017.02/DOC_1&format=PDF (accessed 5.4.21).

EC, 2019. The European Green Deal [WWW Document]. Commision Commun. COM/2019/640. URL https://ec.europa.eu/info/sites/default/files/european-green-deal-communication_en.pdf (accessed 5.4.21).

EC, 2018. A sustainable Bioeconomy for Europe: Strengthening the connection between economy, society and the environment [WWW Document]. Commision Commun. COM/2018/673. URL https://eur-lex.europa.eu/legal-content/EN/TXT/PDF/?uri=CELEX:52018DC0673&from=en (accessed 5.4.21).

Edmundson, S.J., Huesemann, M.H., 2015. The dark side of algae cultivation: Characterizing night biomass loss in three photosynthetic algae, *Chlorella sorokiniana*, *Nannochloropsis salina* and *Picochlorum* sp. Algal Res. 12, 470–476. https://doi.org/10.1016/j.algal.2015.10.012

Eilers, P.H.C., Peeters, J.C.H., 1988. A model for the relationship between light intensity and the rate of photosynthesis in phytoplankton. Ecol. Modell. 42, 199–215. https://doi.org/10.1016/0304-3800(88)90057-9

Endar, V., Sarjito, ., Hutabarat, J., Prayitno, B., 2013. Effect of using guillard and walne technical culture media on growth and fatty acid profiles of microalgae *Skeletonema* sp. in mass culture. J. Coast. Dev. 16, 50–56.

Fábregas, J., Abalde, J., Herrero, C., Cabezas, B., Veiga, M., 1984. Growth of the marine microalga *Tetraselmis suecica* in batch cultures with different salinities and nutrient concentrations. Aquaculture 42, 207–215. https://doi.org/10.1016/0044-8486(84)90101-7

Fábregas, J., Garcia, D., Morales, E., Dominguez, A., Otero, A., 1998. Renewal rate of semicontinous cultures of the microalga *Porphyridium cruentum* modifies phycoerythrin, exopolisaccharide and fatty acid production. J. Ferment. Bioeng. 86, 477–481. https://doi.org/http://dx.doi.org/10.1016/S0922-338X(98)80155-4

Fábregas, J., Maseda, A., Domínguez, A., Ferreira, M., Otero, A., 2002. Changes in the cell composition of the marine microalga, *Nannochloropsis gaditana*, during a light:dark cycle. Biotechnol Lett 24. https://doi.org/10.1023/A:1020661719272

Fábregas, J., Maseda, A., Domínguez, A., Otero, A., 2004. The cell composition of *Nannochloropsis* sp. changes under different irradiances in semicontinuous culture. World J. Microbiol. Biotechnol. 20, 31–35. https://doi.org/10.1023/B:WIBI.0000013288.67536.ed

Fábregas, J., Patino, M., Morales, E.D., Cordero, B., Otero, A., 1996. Optimal renewal rate and nutrient concentration for the production of the marine microalga *Phaeodactylum tricornutum* in semicontinuous cultures. Appl. Environ. Microbiol. 62, 266–268. https://doi.org/10.1128/AEM.62.1.266-268.1996

Fábregas, J., Patiño, M., Vecino, E., Cházaro, F., Otero, A., 1995. Productivity and biochemical composition of cyclostat cultures of the marine microalga *Tetraselmis suecica*. Appl. Microbiol. Biotechnol. 43, 617–621. https://doi.org/10.1007/BF00164763

Fakhry, E.M., El Maghraby, D.M., 2015. Lipid accumulation in response to nitrogen limitation and variation of temperature in *Nannochloropsis salina*. Bot. Stud. 56, 1–8. https://doi.org/10.1186/s40529-015-0085-7

Falkowski, P.G., Owens, T.G., 1980. Light—Shade Adaptation. Plant Physiol. 66, 592–595. https://doi.org/10.1104/pp.66.4.592

Falkowski, P.G., Owens, T.G., 1978. Effects of light intensity on photosynthesis and dark respiration in six species of marine phytoplankton. Mar. Biol. 45, 289–295. https://doi.org/10.1007/BF00391815

Falkowski, P.G., Raven, J.A., 2013. An Introduction to Photosynthesis in Aquatic Systems, in: Aquatic Photosynthesis. Princeton University Press, pp. 1–43. https://doi.org/10.1515/9781400849727.1

Faraloni, C., Ena, A., Pintucci, C., Torzillo, G., 2011. Enhanced hydrogen production by means of sulfur-deprived *Chlamydomonas reinhardtii* cultures grown in pretreated olive mill wastewater. Int. J. Hydrogen Energy 36, 5920–5931. https://doi.org/10.1016/j.ijhydene.2011.02.007

Faraloni, C., Torzillo, G., 2010. Phenotypic characterization and hydrogen production in *Chlamydomonas reinhardtii* Q_B-binding D1-protein mutants under sulfur starvation: changes in chl fluorescence and pigment composition. J. Phycol. 46, 788–799. https://doi.org/10.1111/j.1529-8817.2010.00857.x

Fawley, M.W., 1984. Effects of light intensity and temperature interactions on growth characteristics of *Phaeodactylum tricornutum* (Bacillariophyceae). J. Phycol. 20, 67–72. https://doi.org/10.1111/j.0022-3646.1984.00067.x

Fernández-Reiriz, M.J., Perez-Camacho, A., Ferreiro, M.J., Blanco, J., Planas, M., Campos, M.J., Labarta, U., 1989. Biomass production and variation in the biochemical profile (total protein, carbohydrates, RNA, lipids and fatty acids) of seven species of marine microalgae. Aquaculture 83, 17–37. https://doi.org/10.1016/0044-8486(89)90057-4

Ferreira, M., Coutinho, P., Seixas, P., Fábregas, J., Otero, A., 2009. Enriching Rotifers with "Premium" Microalgae. *Nannochloropsis gaditana*. Mar. Biotechnol. 11, 585–595. https://doi.org/10.1007/s10126-008-9174-x

Figueroa, F.L., Jerez, C.G., Korbee, N., 2013. Use of *in vivo* chlorophyll fluorescence to estimate photosynthetic activity and biomass productivity in microalgae grown in different culture systems. Lat. Am. J. Aquat. Res. 41, 801–819. https://doi.org/103856/vol41-issue5-fulltext-1

Folch, J., Lee, M., Sloane Stanley, G.H., 1957. A simple method for the isolation and purification of total lipides from animal tissues. J Biol Chem 226.

Fon-Sing, S., Borowitzka, M.A., 2016. Isolation and screening of euryhaline *Tetraselmis* spp. suitable for large-scale outdoor culture in hypersaline media for biofuels. J. Appl. Phycol. 28, 1–14. https://doi.org/10.1007/s10811-015-0560-2

Galès, A., Bonnafous, A., Carré, C., Jauzein, V., Lanouguère, E., Le Floc'h, E., Pinoit, J., Poullain, C., Roques, C., Sialve, B., Simier, M., Steyer, J.-P., Fouilland, E., 2019. Importance of ecological interactions during wastewater treatment using High Rate Algal Ponds under different temperate climates. Algal Res. 40, 101508. https://doi.org/10.1016/j.algal.2019.101508

Gangl, D., Zedler, J.A.Z., Rajakumar, P.D., Martinez, E.M.R., Riseley, A., Włodarczyk, A., Purton, S., Sakuragi, Y., Howe, C.J., Jensen, P.E., Robinson, C., 2015. Biotechnological exploitation of microalgae. J. Exp. Bot. 66, 6975–6990. https://doi.org/10.1093/jxb/erv426

Garcia, C., Ceccanti, B., Masciandaro, G., Hernandez, T., 1995. Fractionation and characterization of humic substance fractions with different molecular weights, obtained from animal wastes. Soil Sci. Plant Nutr. 41, 649–658. https://doi.org/10.1080/00380768.1995.10417015

Garrido-Cardenas, J.A., Manzano-Agugliaro, F., Acién-Fernández, F.G., Molina-Grima, E., 2018. Microalgae research worldwide. Algal Res. 35, 50–60. https://doi.org/10.1016/j.algal.2018.08.005

Geider, R., Macintyre, Graziano, L., McKay, R.M., 1998. Responses of the photosynthetic apparatus of *Dunaliella tertiolecta* (Chlorophyceae) to nitrogen and phosphorus limitation.

Eur. J. Phycol. 33, 315–332. https://doi.org/10.1080/09670269810001736813

Geider, R., Osborne, B. a., Geider, J., Osborne, R., 1989. Respiration and microalgal growth: a review of the quantitative relationship between dark respiration and growth. New Phytol 112, 327–341. https://doi.org/10.1111/j.1469-8137.1989.tb00321.x

Geider, R., Roche, J., Greene, R.M., Olaizola, M., 1993. Response of the photosynthetic apparatus of *Phaeodactylum tricornutum* (Bacillariophyceae) to nitrate, phosphate or iron starvation. J. Phycol. 29, 755–766. https://doi.org/10.1111/j.0022-3646.1993.00755.x

Genty, B., Briantais, J.M., Baker, N.R., 1989. The relationship between the quantum yield of photosynthetic electron transport and quenching of chlorophyll fluorescence. Biochim. Biophys. Acta - Gen. Subj. 990, 87–92. https://doi.org/10.1016/S0304-4165(89)80016-9

Gerotto, C., Norici, A., Giordano, M., 2020. Toward enhanced fixation of CO_2 in aquatic biomass: Focus on microalgae. Front. Energy Res. 8. https://doi.org/10.3389/fenrg.2020.00213

Giannelli, L., Scoma, A., Torzillo, G., 2009. Interplay between light intensity, chlorophyll concentration and culture mixing on the hydrogen production in sulfur-deprived *Chlamydomonas reinhardtii* cultures grown in laboratory photobioreactors. Biotechnol. Bioeng. 104, 76–90. https://doi.org/10.1002/bit.22384

Gill, S.S., Willette, S., Dungan, B., Jarvis, M.J., Schaub, T., VanLeeuwen, M.D., St. Hilaire, R., Holguin, O.F., 2018. Suboptimal temperature acclimation affects Kennedy pathway gene expression, lipidome and metabolite profile of *Nannochloropsis salina* during PUFA enriched TAG synthesis. Mar. Drugs. https://doi.org/10.3390/md16110425

Goltsev, V.N., Kalaji, H.M., Paunov, M., Bąba, W., Horaczek, T., Mojski, J., Kociel, H., Allakhverdiev, S.I., 2016. Variable chlorophyll fluorescence and its use for assessing physiological condition of plant photosynthetic apparatus. Russ. J. Plant Physiol. 63, 869–893. https://doi.org/10.1134/S1021443716050058

Goodwin, T., 1980. The biochemistry of the Carotenoids. Vol. I: Plants, 2nd ed. Springer Netherlands. https://doi.org/10.1007/978-94-009-5860-9

Gorbunov, M.Y., Falkowski, P.G., 2021. Using chlorophyll fluorescence kinetics to determine photosynthesis in aquatic ecosystems. Limnol. Oceanogr. 66, 1–13. https://doi.org/10.1002/lno.11581

Gouveia, L., Graça, S., Sousa, C., Ambrosano, L., Ribeiro, B., Botrel, E.P., Neto, P.C., Ferreira, A.F., Silva, C.M., 2016. Microalgae biomass production using wastewater: Treatment and costs Scale-up considerations. Algal Res. 16, 167–176. https://doi.org/10.1016/j.algal.2016.03.010

Govindjee, 2004. Chlorophyll *a* fluorescence: A bit of basics and History, in: Papageorgiou, G.C., Govindjee, G. (Eds.), Chlorophyll a Fluorescence. Springer Netherlands, Dordrecht, pp. 1–41. https://doi.org/10.1007/978-1-4020-3218-9_1

Govindjee, Seufferheld, M.J., 2002. Non-photochemical quenching of chlorophyll *a* fluorescence: early history and characterization of two xanthophyll-cycle mutants of *Chlamydomonas reinhardtii*. Funct. Plant Biol. 29, 1141. https://doi.org/10.1071/FP02061

Greene, R.M., Geider, R.J., Kolber, Z., Falkowski, P.G., 1992. Iron-induced changes in light harvesting and photochemical energy conversion processes in eukaryotic marine algae. Plant Physiol. 100, 565–575. https://doi.org/10.1104/pp.100.2.565

Grima, E.M., Prez, J. a S., Camacho, F.G., Sevilla, J.M.F., Fernandez, F.G.A., 1996. Productivity analysis of outdoor chemostat culture in tubular air-lift photobioreactors. J. Appl. Phycol. 8, 369–380. https://doi.org/10.1007/BF02178580

Grivalský, T., Ranglová, K., da Câmara Manoel, J.A., Lakatos, G.E., Lhotský, R., Masojídek, J., 2019. Development of thin-layer cascades for microalgae cultivation: milestones (review). Folia Microbiol. (Praha). 64, 603–614. https://doi.org/10.1007/s12223-019-00739-7

Grobbelaar, J.U., 2013. Mass production of microalgae at optimal photosynthetic rates, in: Dubinsky, Z. (Ed.), Photosynthesis. IntechOpen, pp. 357–371. https://doi.org/10.5772/55193

Grobbelaar, J.U., Nedbal, L., Tichý, V., 1996. Influence of high frequency light/dark fluctuations on photosynthetic characteristics of microalgae photoacclimated to different light intensities and implications for mass algal cultivation. J. Appl. Phycol. 8, 335–343. https://doi.org/10.1007/BF02178576

Grobbelaar, J.U., Soeder, C.J., 1985. Respiration losses in planktonic green algae cultivated in raceway ponds. J. Plankton Res. 7, 497–506.

Guerra, I., Pereira, H., Costa, M., Silva, J.T., Santos, T., Varela, J., Mateus, M., Silva, J., 2021. Operation regimes: A comparison based on *Nannochloropsis oceanica* biomass and lipid productivity. Energies 14, 1542. https://doi.org/10.3390/en14061542

Guidi, L., Tattini, M., Landi, M., 2017. How does chloroplast protect chlorophyll against excessive light?, in: Jacob-Lopes, E., Zepka, L.Q., Queiroz, M.I. (Eds.), Chlorophyll. InTech. https://doi.org/10.5772/67887

Guillard, R.R.L., Ryther, J.H., 1962. Studies of marine planktonic diatoms: I. *Cyclotella nana* Hustedt, and *Detonula confervacea* (Cleve) Gran. Can. J. Microbiol. 8, 229–239. https://doi.org/10.1139/m62-029

Guiry, M.D., Guiry, G.M., 2021. AlgaeBase [WWW Document]. World-wide Electron. Publ. Natl. Univ. Ireland, Galw. URL https://www.algaebase.org/ (accessed 5.5.21).

Gunawan, N.R., Tessman, M., Schreiman, A.C., Simkovsky, R., Samoylov, A.A., Neelakantan, N.K., Bemis, T.A., Burkart, M.D., Pomeroy, R.S., Mayfield, S.P., 2020. Rapid biodegradation of renewable polyurethane foams with identification of associated microorganisms and decomposition products. Bioresour. Technol. Reports 11, 100513.

https://doi.org/10.1016/j.biteb.2020.100513

Gururani, M.A., Venkatesh, J., Ganesan, M., Strasser, R.J., Han, Y., Kim, J.-I., Lee, H.-Y., Song, P.-S., 2015. *In vivo* assessment of cold tolerance through chlorophyll-*a* fluorescence in transgenic Zoysiagrass expressing mutant phytochrome A. PLoS One 10, e0127200. https://doi.org/10.1371/journal.pone.0127200

Guschina, I.A., Harwood, J.L., 2006. Lipids and lipid metabolism in eukaryotic algae. Prog. Lipid Res. 45, 160–186. https://doi.org/10.1016/j.plipres.2006.01.001

Guzmán, H.M., de la Jara Valido, A., Duarte, L.C., Presmanes, K.F., Valido, A., La, J., Duarte, L.C., Presmanes, K.F., 2010. Estimate by means of flow cytometry of variation in composition of fatty acids from *Tetraselmis suecica* in response to culture conditions. Aquac. Int. 18, 189–199. https://doi.org/10.1007/s10499-008-9235-1

Haefner, B., 2003. Drugs from the deep: Marine natural products as drug candidates. Drug Discov. Today 8, 536–544. https://doi.org/10.1016/S1359-6446(03)02713-2

Hallmann, A., 2016. Algae Biotechnology – Green Cell-Factories on the Rise. Curr. Biotechnol. 4, 389–415. https://doi.org/10.2174/2211550105666151107001338

Handa, N., 1969. Carbohydrate metabolism in the marine diatom *Skeletonema costatum*. Mar. Biol. 4, 208–214. https://doi.org/10.1007/BF00393894

He, Q., Yang, H., Hu, C., 2016. Culture modes and financial evaluation of two oleaginous microalgae for biodiesel production in desert area with open raceway pond. Bioresour. Technol. 218, 571–579. https://doi.org/10.1016/j.biortech.2016.06.137

Hendricks, D.W., 2007. Water treatment unit processes: Physical and chemical. CRC Press.

Herbert, D., Phipps, P.J., Strange, R.E., 1971. Chemical analysis of microbial cells. Methods Microbiol. 58, 209–344.

Hess, C.E., 1961. Mung bean bioassay for the detection of root promoting substances. Plant Physiol. 36.

Hildebrand, M., 2003. Biological processing of nanostructured silica in diatoms. Prog. Org. Coatings 47, 256–266. https://doi.org/10.1016/S0300-9440(03)00142-5

Hill, R., Bendall, F., 1960. Function of the two cytochrome components in chloroplasts: A working hypothesis. Nature 186, 136–137. https://doi.org/10.1038/186136a0

Hitchcock, G.L.L., 1980. Influence of temperature on the growth rate of *Skeletonema costatum* in response to variations in daily light intensity. Mar. Biol. 57, 261–269. https://doi.org/10.1007/BF00387569

Hoffmann, M., Marxen, K., Schulz, R., Vanselow, K.H., 2010. TFA and EPA productivities of *Nannochloropsis salina* influenced by temperature and nitrate stimuli in turbidostatic controlled experiments. Mar. Drugs. https://doi.org/10.3390/md8092526

Hofstraat, J.W., Peeters, J.C.H., Snel, J.F.H., Geel, C., 1994. Simple determination of photosynthetic efficiency and photoinhibition of *Dunaliella tertiolecta* by saturating pulse

fluorescence measurements. Mar. Ecol. Prog. Ser. 103, 187–196.

Hu, Q., Sommerfeld, M., Jarvis, E., Ghirardi, M., Posewitz, M., Seibert, M., Darzins, A., 2008. Microalgal triacylglycerols as feedstocks for biofuel production: perspectives and advances. Plant J. 54, 621–639. https://doi.org/10.1111/j.1365-313X.2008.03492.x

Hu, Qiang, 2013. Environmental effects on cell composition, in: Richmond, A., Hu, Q. (Eds.), Handbook of Microalgal Culture: Applied Phycology and Biotechnology. John Wiley & Sons, Ltd, Oxford, UK, pp. 114–122. https://doi.org/10.1002/9781118567166.ch7

Huerlimann, R., de Nys, R., Heimann, K., 2010. Growth, lipid content, productivity, and fatty acid composition of tropical microalgae for scale-up production. Biotechnol. Bioeng. 107, 245–257. https://doi.org/10.1002/bit.22809

Huesemann, M., Dale, T., Chavis, A., Crowe, B., Twary, S., Barry, A., Valentine, D., Yoshida, R., Wigmosta, M., Cullinan, V., 2017. Simulation of outdoor pond cultures using indoor LED-lighted and temperature-controlled raceway ponds and Phenometrics photobioreactors. Algal Res. 21, 178–190. https://doi.org/10.1016/j.algal.2016.11.016

Hughes, E.O., Gorham, P.R., Zehnder, A., 1958. Toxicity of a unialgal culture of *Microcystis aeruginosa*. Can. J. Microbiol. 4, 225–236. https://doi.org/10.1139/m58-024

Hulatt, C.J., Wijffels, R.H., Bolla, S., Kiron, V., 2017. Production of fatty acids and protein by *Nannochloropsis* in flat-plate photobioreactors. PLoS One 12, 1–17. https://doi.org/10.1371/journal.pone.0170440

Jaspars, E.M.J., 1965. Pigmentation of tobacco crown-gall tissues cultured *in vitro* in dependence of the composition of the medium. Physiol. Plant. 18, 933–940. https://doi.org/10.1111/j.1399-3054.1965.tb06990.x

Jensen, P.E., Leister, D., 2014. Cyanobacteria as an experimental platform for modifying bacterial and plant photosynthesis. Front. Bioeng. Biotechnol. 2. https://doi.org/10.3389/fbioe.2014.00007

Jerez, C.G., Malapascua, J.R., Sergejevová, M., Masojídek, J., Figueroa, F.L., 2016. *Chlorella fusca* (Chlorophyta) grown in thin-layer cascades: Estimation of biomass productivity by *in-vivo* chlorophyll *a* fluorescence monitoring. Algal Res. 17, 21–30. https://doi.org/10.1016/j.algal.2016.04.010

KaiXian, Q., Borowitzka, M.A., 1993. Light and nitrogen deficiency effects on the growth and composition of *Phaeodactylum tricornutum*. Appl. Biochem. Biotechnol. 38, 93–103. https://doi.org/10.1007/BF02916415

Kalaji, H.M., Jajoo, A., Oukarroum, A., Brestic, M., Zivcak, M., Samborska, I.A., Cetner, M.D., Łukasik, I., Goltsev, V., Ladle, R.J., 2016. Chlorophyll *a* fluorescence as a tool to monitor physiological status of plants under abiotic stress conditions. Acta Physiol. Plant. 38, 102. https://doi.org/10.1007/s11738-016-2113-y

Kalaji, H.M., Oukarroum, A., Alexandrov, V., Kouzmanova, M., Brestic, M., Zivcak, M.,

Samborska, I.A., Cetner, M.D., Allakhverdiev, S.I., Goltsev, V., 2014. Identification of nutrient deficiency in maize and tomato plants by *in vivo* chlorophyll *a* fluorescence measurements. Plant Physiol. Biochem. 81, 16–25. https://doi.org/10.1016/j.plaphy.2014.03.029

Karemore, A., Ramalingam, D., Yadav, G., Subramanian, G., Sen, R., 2015. Photobioreactors for Improved Algal Biomass Production: Analysis and Design Considerations BT - Algal Biorefinery: An Integrated Approach, in: Das, D. (Ed.), . Springer International Publishing, Cham, pp. 103–124. https://doi.org/10.1007/978-3-319-22813-6_5

Kautsky, H., Hirsch, A., 1931. Neue Versuche zur Kohlensäureassimilation. Naturwissenschaften 19, 964. https://doi.org/10.1007/BF01516164

Kevan, P., Shipp, L., 2011. Biological control and biotechnological amelioration in managed ecosystems, in: Moo-Young, M.B.T.-C.B. (Second E. (Ed.), Comprehensive Biotechnology. Elsevier, Burlington, pp. 757–761. https://doi.org/10.1016/B978-0-08-088504-9.00473-6

Khan, S., Haque, M.M., Onoue, Y., 1998. Physiological observations on a diatom *Skeletonema costatum* (Greville) Cleve. Bangladesh J Fish Res 2, 109–118.

Khanam, M.R.M., Shimasaki, Y., Tsuyama, M., Goto, H., Qiu, X., Mukai, K., Oshima, Y., 2019. Presumption of toxic mechanism of tributyltin on photosystem in marine diatoms by comparison to diuron as a reference agent through chlorophyll *a* fluorescence transient analysis. Japanese J. Environ. Toxicol. 22, 13–29. https://doi.org/https://doi.org/10.11403/jset.22.13

Khawam, G., Waller, P., Gao, S., Edmundson, S., Huesemann, M., Attalah, S., Ogden, K.L., 2019. Simulation of shading and algal growth in experimental raceways. Algal Res. 41, 101575. https://doi.org/10.1016/j.algal.2019.101575

Kliphuis, A.M.J., Janssen, M., van den End, E.J., Martens, D.E., Wijffels, R.H., 2011. Light respiration in *Chlorella sorokiniana*. J. Appl. Phycol. 23, 935–947. https://doi.org/10.1007/s10811-010-9614-7

Klok, A.J., Martens, D.E., Wijffels, R.H., Lamers, P.P., 2013. Simultaneous growth and neutral lipid accumulation in microalgae. Bioresour. Technol. 134, 233–243. https://doi.org/https://doi.org/10.1016/j.biortech.2013.02.006

Kolber, Z., Zehr, J., Falkowski, P., 1988. Effects of growth irradiance and nitrogen limitation on photosynthetic energy conversion in photosystem II. Plant Physiol. 88, 923–929. https://doi.org/10.1104/pp.88.3.923

Koreivienė, J., Valčiukas, R., Karosienė, J., Baltrėnas, P., 2014. Testing of *Chlorella*/*Scenedesmus* microalgae consortia for remediation of wastewater, CO_2 mitigation and algae biomass feasibility for lipid production. J. Environ. Eng. Landsc. Manag. 22, 105–114. https://doi.org/10.3846/16486897.2013.911182

Koyande, A.K., Chew, K.W., Rambabu, K., Tao, Y., Chu, D.-T., Show, P.-L., 2019. Microalgae: A potential alternative to health supplementation for humans. Food Sci. Hum. Wellness 8, 16–24. https://doi.org/10.1016/j.fshw.2019.03.001

Krichen, E., Rapaport, A., Le Floc'h, E., Fouilland, E., 2019. Demonstration of facilitation between microalgae to face environmental stress. Sci. Rep. 9, 16076. https://doi.org/10.1038/s41598-019-52450-9

Kröger, N., Poulsen, N., 2008. Diatoms—From cell wall biogenesis to nanotechnology. Annu. Rev. Genet. 42, 83–107. https://doi.org/10.1146/annurev.genet.41.110306.130109

Kromkamp, J., Limbeek, M., 1993. Effect of short-term variation in irradiance on light harvesting and photosynthesis of the marine diatom *Skeletonema costatum*: a laboratory study simulating vertical mixing. J. Gen. Microbiol. 139, 2277–2284. https://doi.org/10.1099/00221287-139-9-2277

Kromkamp, J.C., Beardall, J., Sukenik, A., Kopecky, J., Masojídek, J., van Bergeijk, S., Gabai, S., Shaham, E., Yamshon, A., 2009. Short-term variations in photosynthetic parameters of *Nannochloropsis* cultures grown in two types of outdoor mass cultivation systems. Aquat. Microb. Ecol. 56, 309–322. https://doi.org/10.3354/ame01318

Kromkamp, J.C., Forster, R.M., 2003. The use of variable fluorescence measurements in aquatic ecosystems: Differences between multiple and single turnover measuring protocols and suggested terminology. Eur. J. Phycol. 38, 103–112. https://doi.org/10.1080/0967026031000094094

Krustok, I., Truu, J., Odlare, M., Truu, M., Ligi, T., Tiirik, K., Nehrenheim, E., 2015. Effect of lake water on algal biomass and microbial community structure in municipal wastewater-based lab-scale photobioreactors. Appl. Microbiol. Biotechnol. 99, 6537–6549. https://doi.org/10.1007/s00253-015-6580-7

Kudo, I., Miyamoto, M., Noiri, Y., Maita, Y., 2000. Combined effects of temperature and iron on the growth and physiology of the marine diatom *Phaeodactylum tricornutum* (Bacillariophyceae). J. Phycol. 36, 1096–1102. https://doi.org/10.1046/j.1529-8817.2000.99042.x

Kuhnle, J.A., Fuller, G., Corse, J., Mackey, B.E., 1977. Antisenescent activity of natural cytokinins. Physiol. Plant. 41, 14–21. https://doi.org/10.1111/j.1399-3054.1977.tb01514.x

Lakatos, G.E., Ranglová, K., Câmara Manoel, J., Grivalský, T., Masojídek, J., 2021. Photosynthetic monitoring techniques indicate maximum glycogen accumulation in nitrogen-limited *Synechocystis* sp. PCC 6803 culture. Algal Res. 55, 102271. https://doi.org/10.1016/j.algal.2021.102271

Lamour, K.H., Stam, R., Jupe, J., Huitema, E., 2012. The oomycete broad-host-range pathogen *Phytophthora capsici*. Mol. Plant Pathol. 13, 329–337.

https://doi.org/10.1111/j.1364-3703.2011.00754.x

Lavaud, J., Lepetit, B., 2013. An explanation for the inter-species variability of the photoprotective non-photochemical chlorophyll fluorescence quenching in diatoms. Biochim. Biophys. Acta - Bioenerg. 1827, 294–302. https://doi.org/10.1016/j.bbabio.2012.11.012

Lavaud, J., Strzepek, R.F., Kroth, P.G., 2007. Photoprotection capacity differs among diatoms: Possible consequences on the spatial distribution of diatoms related to fluctuations in the underwater light climate. Limnol. Oceanogr. 52, 1188–1194. https://doi.org/10.4319/lo.2007.52.3.1188

Lavens, P., Sorgeloos, P., 1996. Manual on the production and use of live food for aquaculture (Eds.), FAO Fisheries Technical Paper 361. Food and Agriculture Organization of the United Nations. https://doi.org/10.1017/CBO9781107415324.004

Lebeau, T., Robert, J.M., 2003. Diatom cultivation and biotechnologically relevant products. Part II: Current and putative products. Appl. Microbiol. Biotechnol. 60, 624–632. https://doi.org/10.1007/s00253-002-1177-3

Ledda, C., Romero Villegas, G.I., Adani, F., Acién Fernández, F.G., Molina Grima, E., 2015. Utilization of centrate from wastewater treatment for the outdoor production of *Nannochloropsis gaditana* biomass at pilot-scale. Algal Res. 12, 17–25. https://doi.org/https://doi.org/10.1016/j.algal.2015.08.002

Leegood, R.C., 2004. Photosynthesis, in: Lennarz, W.J., Lane, M.D. (Eds.), Encyclopedia of Biological Chemistry. Elsevier, pp. 330–335.

Lefebvre, S., Mouget, J.-L., Loret, P., Rosa, P., Tremblin, G., 2007. Comparison between fluorimetry and oximetry techniques to measure photosynthesis in the diatom *Skeletonema costatum* cultivated under simulated seasonal conditions. J. Photochem. Photobiol. B Biol. 86, 131–139. https://doi.org/10.1016/j.jphotobiol.2006.08.012

Lepage, G., Roy, C.C., 1984. Improved recovery of fatty acid through direct transesterification without prior extraction or purification. J. Lipid Res. 25, 1391–1396. https://doi.org/10.1016/S0022-2275(20)34457-6

Lepetit, B., Gélin, G., Lepetit, M., Sturm, S., Vugrinec, S., Rogato, A., Kroth, P.G., Falciatore, A., Lavaud, J., 2017. The diatom *Phaeodactylum tricornutum* adjusts nonphotochemical fluorescence quenching capacity in response to dynamic light via fine-tuned Lhcx and xanthophyll cycle pigment synthesis. New Phytol. 214, 205–218. https://doi.org/10.1111/nph.14337

Lestari, D.P., Ekawati, A.W., Maftuch, M., 2014. Dried *Skeletonema costatum* in feed formulation for the growth of vaname shrimp (*Litopenaeus vannamei*). J. Exp. Life Sci. 4, 45–49. https://doi.org/10.21776/ub.jels.2014.004.02.04

Lewin, J.C., 1958. The taxonomic position of *Phaeodactylum tricornutum*. J. Gen. Microbiol.

18, 427–432. https://doi.org/10.1099/00221287-18-2-427

Lewin, J.C., Lewin, R.A., Philpott, D.E., 1958. Observations on *Phaeodactylum tricornutum*. J. Gen. Microbiol. 18, 418–426. https://doi.org/10.1099/00221287-18-2-418

Lewin, R.A., Cheng, L., 1989. Some lipogenic, eukariotic, picopleuston algae from the Caribbean region. Phycologia 28, 96–108.

Li, T., Wang, W., Yuan, C., Zhang, Y., Xu, J., Zheng, H., Xiang, W., Li, A., 2020. Linking lipid accumulation and photosynthetic efficiency in *Nannochloropsis* sp. under nutrient limitation and replenishment. J. Appl. Phycol. 32, 1619–1630. https://doi.org/10.1007/s10811-020-02056-w

Li, X., Li, W., Zhai, J., Wei, H., Wang, Q., 2019. Effect of ammonium nitrogen on microalgal growth, biochemical composition and photosynthetic performance in mixotrophic cultivation. Bioresour. Technol. 273, 368–376. https://doi.org/10.1016/j.biortech.2018.11.042

Liang, J., Wen, F., Liu, J., 2019. Transcriptomic and lipidomic analysis of an EPA-containing *Nannochloropsis* sp. PJ12 in response to nitrogen deprivation. Sci. Rep. 9, 4540. https://doi.org/10.1038/s41598-019-41169-2

Lichtenthaler, H.K., Miehé, J.A., 1997. Fluorescence imaging as a diagnostic tool for plant stress. Trends Plant Sci. 2, 316–320. https://doi.org/10.1016/S1360-1385(97)89954-2

Lim, D.K.Y.Y., Garg, S., Timmins, M., Zhang, E.S.B.B., Thomas-hall, S.R., Schuhmann, H., Li, Y., Schenk, P.M., 2012. Isolation and evaluation of oil-producing microalgae from subtropical coastal and brackish waters. PLoS One 7. https://doi.org/10.1371/journal.pone.0040751

Liu, J., Yao, C., Meng, Y., Cao, X., Wu, P., Xue, S., 2018. The ΔF/Fm′-guided supply of nitrogen in culture medium facilitates sustainable production of TAG in *Nannochloropsis oceanica* IMET1. Biotechnol. Biofuels 11, 168. https://doi.org/10.1186/s13068-018-1168-y

Llamas, B., Suárez-Rodríguez, M.C., González-López, C. V., Mora, P., Acién, F.G., 2021. Techno-economic analysis of microalgae related processes for CO_2 bio-fixation. Algal Res. 57, 102339. https://doi.org/10.1016/j.algal.2021.102339

Logan, B.A., 2014. Context, quantification, and measurement guide for non-photochemical quenching of chlorophyll fluorescence, in: Demmig-Adams, B., Garab, G., Adams III, W., Govindjee (Eds.), Non-Photochemical Quenching and Energy Dissipation in Plants, Algae and Cyanobacteria. Springer Science+Business Media Dordrecht, pp. 187–202. https://doi.org/10.1007/978-94-017-9032-1_7

Lourenço, S.O., Barbarino, E., Lavín, P.L., Marquez, U.M.L., Aidar, E., 2004. Distribution of intracellular nitrogen in marine microalgae: Calculation of new nitrogen-to-protein conversion factors. Eur. J. Phycol. 39, 17–32.

https://doi.org/https://doi.org/10.1080/0967026032000157156

Lowry, O.H., Rosebrough, N.J., Farr, A.L., Randall, R.J., 1951. Protein measurement with the folin phenol reagent. J. Biol. Chem. 193, 265–275.

Lubián, L.M., Montero, O., 1998. Excess light-induced violaxanthin cycle activity in *Nannochloropsis gaditana* (Eustigmatophyceae): effects of exposure time and temperature. Phycologia 37, 16–23. https://doi.org/10.2216/i0031-8884-37-1-16.1

Luo, L., Lai, X., Chen, B., Lin, L., Fang, L., Tam, N.F.Y., Luan, T., 2015. Chlorophyll catalyse the photo-transformation of carcinogenic benzo[*a*]pyrene in water. Sci. Rep. 5, 12776. https://doi.org/10.1038/srep12776

Ma, X.-N., Liu, B., Yang, B., Guo, B.-B., Liu, J., Chen, F., 2018. Physiochemical and gene expression analyses reveal differential responses of the marine oleaginous alga *Nannochloropsis salina* under different lipid-induction conditions. J. Appl. Phycol. 30, 909–919. https://doi.org/10.1007/s10811-017-1318-9

Ma, X.-N.N., Chen, T.-P.P., Yang, B., Liu, J., Chen, F., 2016. Lipid production from *Nannochloropsis*. Mar. Drugs 14, 61. https://doi.org/10.3390/md14040061

Ma, Y., Wang, Z., Yu, C., Yin, Y., Zhou, G., 2014. Evaluation of the potential of 9 *Nannochloropsis* strains for biodiesel production. Bioresour. Technol. 167, 503–509. https://doi.org/10.1016/j.biortech.2014.06.047

Malapascua, J.R.F., Jerez, C.G., Sergejevová, M., Figueroa, F.L., Masojídek, J., 2014. Photosynthesis monitoring to optimize growth of microalgal mass cultures: Application of chlorophyll fluorescence techniques. Aquat. Biol. 22, 123–140. https://doi.org/10.3354/ab00597

Malerba, M.E., Palacios, M.M., Palacios Delgado, Y.M., Beardall, J., Marshall, D.J., 2018. Cell size, photosynthesis and the package effect: an artificial selection approach. New Phytol. 219, 449–461. https://doi.org/10.1111/nph.15163

Marella, T.K., López-Pacheco, I.Y., Parra-Saldívar, R., Dixit, S., Tiwari, A., 2020. Wealth from waste: Diatoms as tools for phycoremediation of wastewater and for obtaining value from the biomass. Sci. Total Environ. 724, 137960. https://doi.org/10.1016/j.scitotenv.2020.137960

Marsh, J.B., Weinstein, D.B., 1966. Simple charring method for determination of lipids. J. Lipid Res. 7, 574–576.

Marshall, H.L., Geider, R.J., Flynn, K.J., 2000. A mechanistic model of photoinhibition. New Phytol. 145, 347–359. https://doi.org/10.1046/j.1469-8137.2000.00575.x

Martínez-Macías, R., Meza-Escalante, E., Serrano-Palacios, D., Gortáres-Moroyoqui, P., Ruíz-Ruíz, P.E., Ulloa-Mercado, G., 2018. Effect of fed-batch and semicontinuous regimen on *Nannochloropsis oculata* grown in different culture media to high-value products. J. Chem. Technol. Biotechnol. 93, 585–590. https://doi.org/10.1002/jctb.5405

Masojidek, J., 2001. Photosystem II electron transport rates and oxygen production in natural waterblooms of freshwater cyanobacteria during a diel cycle. J. Plankton Res. 23, 57–66. https://doi.org/10.1093/plankt/23.1.57

Masojídek, J., Kopecká, J., Koblížek, M., Torzillo, G., 2004. The xanthophyll cycle in green algae (Chlorophyta): Its role in the photosynthetic apparatus. Plant Biol. 6, 342–349. https://doi.org/10.1055/s-2004-820884

Masojídek, J., Kopecký, J., Giannelli, L., Torzillo, G., 2011. Productivity correlated to photobiochemical performance of *Chlorella* mass cultures grown outdoors in thin-layer cascades. J. Ind. Microbiol. Biotechnol. 38, 307–317. https://doi.org/10.1007/s10295-010-0774-x

Masojídek, J., Ranglová, K., Lakatos, G.E., Silva Benavides, A.M., Torzillo, G., 2021. Variables governing photosynthesis and growth in microalgae mass cultures. Processes 9, 820. https://doi.org/10.3390/pr9050820

Masojídek, J., Sergejevová, M., Rottnerová, K., Jirka, V., Korečko, J., Kopecký, J., Zaťková, I., Torzillo, G., Štys, D., 2009. A two-stage solar photobioreactor for cultivation of microalgae based on solar concentrators. J. Appl. Phycol. 21, 55–63. https://doi.org/10.1007/s10811-008-9324-6

Masojídek, J., Torzillo, G., Koblížek, M., 2013. Photosynthesis in microalgae, in: Richmond, A., Hu, Q. (Eds.), Handbook of Microalgal Culture: Applied Phycology and Biotechnology. Wiley-Blackwell, pp. 21–36. https://doi.org/10.1002/9781118567166.ch2

Masojídek, J., Torzillo, G., Koblížek, M., Kopecký, J., Bernardini, P., Sacchi, A., Komenda, J., 1999. Photoadaptation of two members of the Chlorophyta (*Scenedesmus* and *Chlorella*) in laboratory and outdoor cultures: changes in chlorophyll fluorescence quenching and the xanthophyll cycle. Planta 209, 126–135. https://doi.org/10.1007/s004250050614

Masojídek, J., Vonshak, A., Torzillo, G., 2010. Chlorophyll fluorescence applications in microalgal mass cultures, in: Suggett, D.J., Prášil, O., Borowitzka, M.A. (Eds.), Chlorophyll *a* Fluorescence in Aquatic Sciences: Methods and Applications. Springer Netherlands, Dordrecht, pp. 276–292. https://doi.org/10.1007/978-90-481-9268-7

Maxwell, K., Johnson, G.N., 2000. Chlorophyll fluorescence - a practical guide. J. Exp. Bot. 51, 659–668. https://doi.org/10.1093/jxb/51.345.659

Megía-Hervás, I., Sánchez-Bayo, A., Bautista, L.F., Morales, V., Witt-Sousa, F.G., Segura-Fornieles, M., Vicente, G., 2020. Scale-Up Cultivation of Phaeodactylum tricornutum to Produce Biocrude by Hydrothermal Liquefaction. Processes 8, 1072. https://doi.org/10.3390/pr8091072

Michels, M.H.A., Camacho-Rodríguez, J., Vermuë, M.H., Wijffels, R.H., 2014. Effect of cooling in the night on the productivity and biochemical composition of *Tetraselmis suecica*. Algal Res. 6, Part B, 145–151. https://doi.org/http://dx.doi.org/10.1016/j.algal.2014.11.002

Michels, M.H.A.A., Slegers, P.M., Vermuë, M.H., Wijffels, R.H., 2014. Effect of biomass concentration on the productivity of *Tetraselmis suecica* in a pilot-scale tubular photobioreactor using natural sunlight. Algal Res. 4, 12–18. https://doi.org/10.1016/j.algal.2013.11.011

Millán-Oropeza, A., Fernández-Linares, L., 2017. Biomass and lipid production from *Nannochloropsis oculata* growth in raceway ponds operated in sequential batch mode under greenhouse conditions. Environ. Sci. Pollut. Res. 24, 25618–25626. https://doi.org/10.1007/s11356-016-7013-6

Miyagishima, S., Era, A., Hasunuma, T., Matsuda, M., Hirooka, S., Sumiya, N., Kondo, A., Fujiwara, T., 2019. Day/night separation of oxygenic energy metabolism and nuclear DNA replication in the unicellular red alga *Cyanidioschyzon merolae*. MBio 10, e00833-19. https://doi.org/10.1128/mBio.00833-19

Molina Grima, E., Sánchez Pérez, J.A., García Camacho, F., Fernández Sevilla, J.M., Acién Fernández, F.G., Urda Cardona, J., 1995. Biomass and eicosapentaenoic acid productivities from an outdoor batch culture of *Phaeodactylum tricornutum* UTEX 640 in an airlift tubular photobioreactor. Appl. Microbiol. Biotechnol. 42, 658–663. https://doi.org/10.1007/BF00171940

Molino, A., Iovine, A., Casella, P., Mehariya, S., Chianese, S., Cerbone, A., Rimauro, J., Musmarra, D., 2018. Microalgae Characterization for Consolidated and New Application in Human Food, Animal Feed and Nutraceuticals. Int. J. Environ. Res. Public Heal. . https://doi.org/10.3390/ijerph15112436

Monkonsit, S., Powtongsook, S., Pavasant, P., 2011. Comparison between airlift photobioreactor and bubble column for *Skeletonema costatum* cultivation. Eng. J. 15, 53–64. https://doi.org/10.4186/ej.2011.15.4.53

Montagnes, D.J.S., Franklin, M., 2001. Effect of temperature on diatom volume, growth rate, and carbon and nitrogen content: Reconsidering some paradigms. Limnol. Oceanogr. 46, 2008–2018. https://doi.org/10.4319/lo.2001.46.8.2008

Montero, M.F., Aristizábal, M., García Reina, G., 2011. Isolation of high-lipid content strains of the marine microalga *Tetraselmis suecica* for biodiesel production by flow cytometry and single-cell sorting. J. Appl. Phycol. 23, 1053–1057. https://doi.org/10.1007/s10811-010-9623-6

Morales, M., Hélias, A., Bernard, O., 2019. Optimal integration of microalgae production with photovoltaic panels: environmental impacts and energy balance. Biotechnol. Biofuels 12, 239. https://doi.org/10.1186/s13068-019-1579-4

Morillas-España, A., Lafarga, T., Gómez-Serrano, C., Acién-Fernández, F.G., González-López, C.V., 2020. Year-long production of *Scenedesmus almeriensis* in pilot-scale raceway and thin-layer cascade photobioreactors. Algal Res. 51, 102069.

https://doi.org/10.1016/j.algal.2020.102069

Morkoç, H., 2009. Light-emitting diodes and lighting, in: Handbook of Nitride Semiconductors and Devices. Vol. 3: GaN-Based Optical and Electronic Devices. WILEY-VCH Verlag GmbH & Co. KGaA, Weinheim, p. 902.

Mudimu, O., Rybalka, N., Bauersachs, T., Born, J., Friedl, T., Schulz, R., 2014. Biotechnological screening of microalgal and cyanobacterial strains for biogas production and antibacterial and antifungal effects. Metabolites 4, 373–393. https://doi.org/10.3390/metabo4020373

Muller, P., Li, X.P., Niyogi, K.K., 2001. Non-photochemical quenching. A response to excess light energy. Plant Physiol 125, 1558–1566. https://doi.org/10.1104/pp.125.4.1558

Murata, N., Takahashi, S., Nishiyama, Y., Allakhverdiev, S.I., 2007. Photoinhibition of photosystem II under environmental stress. Biochim. Biophys. Acta - Bioenerg. 1767, 414–421. https://doi.org/10.1016/j.bbabio.2006.11.019

Nedbal, L., Trtílek, M., Červený, J., Komárek, O., Pakrasi, H.B., 2008. A photobioreactor system for precision cultivation of photoautotrophic microorganisms and for high-content analysis of suspension dynamics. Biotechnol. Bioeng. 100, 902–910. https://doi.org/10.1002/bit.21833

Nikolaou, A., Hartmann, P., Sciandra, A., Chachuat, B., Bernard, O., 2016. Dynamic coupling of photoacclimation and photoinhibition in a model of microalgae growth. J. Theor. Biol. 390, 61–72. https://doi.org/10.1016/j.jtbi.2015.11.004

Niyogi, K.K., 1999. Photoprotection revisited: Genetic and molecular approaches. Annu Rev Plant Physiol Plant Mol Biol 50, 333–359. https://doi.org/10.1146/annurev.arplant.50.1.333

Norsker, N.-H., Barbosa, M.J., Vermuë, M.H., Wijffels, R.H., 2011. Microalgal production — A close look at the economics. Biotechnol. Adv. 29, 24–27. https://doi.org/10.1016/j.biotechadv.2010.08.005

Nugent, J.H.A., Purton, S., Evans, M.C.W., 2003. Oxygenic photosynthesis in algae and cyanobacteria: electron transfer in photosystems I and II, in: Larkum, A.W.D., Douglas, S.E., Raven, J.A. (Eds.), Photosynthesis in Algae. Advances in Photosynthesis and Respiration. Springer, Dordrecht, pp. 133–156. https://doi.org/10.1007/978-94-007-1038-2_7

Nunez, M., Quigg, A., 2016. Changes in growth and composition of the marine microalgae *Phaeodactylum tricornutum* and *Nannochloropsis salina* in response to changing sodium bicarbonate concentrations. J. Appl. Phycol. 28, 2123–2138. https://doi.org/10.1007/s10811-015-0746-7

Nwoba, E.G., Parlevliet, D.A., Laird, D.W., Alameh, K., Moheimani, N.R., 2019. Light management technologies for increasing algal photobioreactor efficiency. Algal Res. 39,

101433. https://doi.org/10.1016/j.algal.2019.101433

Ogbonna, J.C., Tanaka, H., 1996. Night biomass loss and changes in biochemical composition of cells during light/dark cyclic culture of *Chlorella pyrenoidosa*. J. Ferment. Bioeng. 82, 558–564. https://doi.org/http://dx.doi.org/10.1016/S0922-338X(97)81252-4

Olofsson, M., Lamela, T., Nilsson, E., Bergé, J.P., del Pino, V., Uronen, P., Legrand, C., 2012. Seasonal variation of lipids and fatty acids of the microalgae *Nannochloropsis oculata* grown in outdoor large-scale photobioreactors. Energies 5, 1577–1592. https://doi.org/10.3390/en5051577

Ördög, V., Stirk, W.A., Bálint, P., Lovász, C., Pulz, O., van Staden, J., 2013. Lipid productivity and fatty acid composition in *Chlorella* and *Scenedesmus* strains grown in nitrogen-stressed conditions. J. Appl. Phycol. 25, 233–243. https://doi.org/10.1007/s10811-012-9857-6

Ördög, V., Stirk, W.A., Bálint, P., van Staden, J., Lovász, C., 2012. Changes in lipid, protein and pigment concentrations in nitrogen-stressed *Chlorella minutissima* cultures. J. Appl. Phycol. 24, 907–914. https://doi.org/10.1007/s10811-011-9711-2

Oswald, W.J., Gotaas, H.B., Golueke, C.G., Kellen, W.R., Gloyna, E.F., Hermann, E.R., 1957. Algae in waste treatment. Sewage Ind. Waste. 29, 437–457.

Otero, A., Fábregas, J., 1997. Changes in the nutrient composition of *Tetraselmis suecica* cultured semicontinuously with different nutrient concentrations and renewal rates. Aquaculture 159, 111–123. https://doi.org/10.1016/S0044-8486(97)00214-7

Otero, A., García, D., Fábregas, J., 1997. Factors controlling eicosapentaenoic acid production in semicontinuous cultures of marine microalgae. J Appl Phycol 9, 465–469. https://doi.org/10.1023/A:1007930804367

Ova Ozcan, D., Ovez, B., 2020. Evaluation of the interaction of temperature and light intensity on the growth of *Phaeodactylum tricornutum*: Kinetic modeling and optimization. Biochem. Eng. J. 154, 107456. https://doi.org/10.1016/j.bej.2019.107456

Owens, T.G., Falkowski, P.G., Whitledge, T.E., 1980. Diel periodicity in cellular chlorophyll content in marine diatoms. Mar. Biol. 59, 71–77. https://doi.org/10.1007/BF00405456

Paasche, E., 1973. Silicon and the ecology of marine plankton diatoms. II. Silicate-uptake kinetics in five diatom species. Mar. Biol. 19, 262–269. https://doi.org/10.1007/BF02097147

Pal, D., Khozin-Goldberg, I., Cohen, Z., Boussiba, S., 2011. The effect of light, salinity, and nitrogen availability on lipid production by *Nannochloropsis* sp. Appl. Microbiol. Biotechnol. 90, 1429–1441. https://doi.org/10.1007/s00253-011-3170-1

Paliwal, C., Mitra, M., Bhayani, K., Bharadwaj, S.V.V., Ghosh, T., Dubey, S., Mishra, S., 2017. Abiotic stresses as tools for metabolites in microalgae. Bioresour. Technol. 244, 1216–1226. https://doi.org/10.1016/j.biortech.2017.05.058

Palmucci, M., Ratti, S., Giordano, M., 2011. Ecological and evolutionary implications of carbon allocation in marine phytoplankton as a function of nitrogen availability: a Fourier transform infrared spectroscopy approach. J. Phycol. 47, 313–323. https://doi.org/10.1111/j.1529-8817.2011.00963.x

Papageorgiou, G.C., Govindjee, 2014. The non-photochemical quenching of the electronically excited state of chlorophyll *a* in plants: definitions, timelines, viewpoints, open questions, in: Demmig-Adams, B. (Ed.), Non-Photochemical Quenching and Energy Dissipation in Plants, 1 Algae and Cyanobacteria. Springer Science+Business Media Dordrecht, pp. 1–44. https://doi.org/10.1007/978-94-017-9032-1_1

Papageorgiou, G.C., Tsimilli-Michael, M., Stamatakis, K., 2007. The fast and slow kinetics of chlorophyll *a* fluorescence induction in plants, algae and cyanobacteria: a viewpoint. Photosynth. Res. 94, 275–290. https://doi.org/10.1007/s11120-007-9193-x

Parkhill, J.-P., Maillet, G., Cullen, J.J., 2001. Fluorescence-based maximal quantum yield for PSII as a diagnostic of nutrient stress. J. Phycol. 37, 517–529. https://doi.org/10.1046/j.1529-8817.2001.037004517.x

Parsons, T.R., Stephens, K., Strickland, J.D.H., 1961. On the chemical composition of eleven species of marine phytoplankters. J. Fish. Res. Board Canada 18, 1001–1016. https://doi.org/10.1139/f61-063

Patil, V., Reitan, K., Mortensen, L., Källqvist, T., Olsen, Y., Vogt, G., Gislerød, H., 2005. Microalgae as a source of polyunsaturated fatty acids for aquaculture. Curr. Top. plant Biol. 6, 57–65.

Pereira, H., Barreira, L., Figueiredo, F., Custódio, L., Vizetto-Duarte, C., Polo, C., Resek, E., Engelen, A., Varela, J., 2012. Polyunsaturated fatty acids of marine macroalgae: Potential for nutritional and pharmaceutical applications. Mar. Drugs 10, 1920–1935. https://doi.org/10.3390/md10091920

Pereira, H., Barreira, L., Mozes, A., Florindo, C., Polo, C., Duarte, C. V, Custódio, L., Varela, J., 2011. Microplate-based high throughput screening procedure for the isolation of lipid-rich marine microalgae. Biotechnol. Biofuels 4, 61. https://doi.org/10.1186/1754-6834-4-61

Pereira, H., Gangadhar, K.N., Schulze, P.S.C., Santos, T., De Sousa, C.B., Schueler, L.M., Custódio, L., Malcata, F.X., Gouveia, L., Varela, J., Barreira, L., 2016. Isolation of a euryhaline microalgal strain, *Tetraselmis* sp. CTP4, as a robust feedstock for biodiesel production. Sci. Rep. 6, 1–11. https://doi.org/10.1038/srep35663

Pereira, H., Páramo, J., Silva, J., Marques, A., Barros, A., Maurício, D., Santos, T., Schulze, P., Barros, R., Gouveia, L., Barreira, L., Varela, J., 2018. Scale-up and large-scale production of *Tetraselmis* sp. CTP4 (Chlorophyta) for CO2 mitigation: From an agar plate to 100-m3 industrial photobioreactors. Sci. Rep. 8. https://doi.org/10.1038/s41598-018-

23340-3

Pereira, S., Otero, A., 2019. Effect of light quality on carotenogenic and non-carotenogenic species of the genus *Dunaliella* under nitrogen deficiency. Algal Res. 44, 101725. https://doi.org/10.1016/j.algal.2019.101725

Pérez, L., Salgueiro, J.L., González, J., Parralejo, A.I., Maceiras, R., Cancela, Á., 2017. Scaled up from indoor to outdoor cultures of *Chaetoceros gracilis* and *Skeletonema costatum* microalgae for biomass and oil production. Biochem. Eng. J. 127, 180–187. https://doi.org/10.1016/j.bej.2017.08.016

Pierangelini, M., Stojkovic, S., Orr, P.T., Beardall, J., 2015. Photo-acclimation to low light—Changes from growth to antenna size in the cyanobacterium *Cylindrospermopsis raciborskii*. Harmful Algae 46, 11–17. https://doi.org/10.1016/j.hal.2015.04.004

Piorreck, M., Pohl, P., 1984. Formation of biomass, total protein, chlorophylls, lipids and fatty acids in green and blue-green algae during one growth phase. Phytochemistry 23, 217–223. https://doi.org/10.1016/S0031-9422(00)80305-2

Pittman, J.K., Dean, A.P., Osundeko, O., 2011. The potential of sustainable algal biofuel production using wastewater resources. Bioresour. Technol. 102, 17–25. https://doi.org/10.1016/j.biortech.2010.06.035

Plyusnina, T.Y., Khruschev, S.S., Degtereva, N.S., Konyukhov, I.V., Solovchenko, A.E., Kouzmanova, M., Goltsev, V.N., Riznichenko, G.Y., Rubin, A.B., 2020. Special issue in honour of Prof. Reto J. Strasser - Gradual changes in the photosynthetic apparatus triggered by nitrogen depletion during microalgae cultivation in photobioreactor. Photosynthetica 58, 443–451. https://doi.org/10.32615/ps.2020.002

Plyusnina, T.Y., Khruschev, S.S., Frolov, A.E., Degtereva, N.S., Konyukhov, I. V., Pogosyan, S.I., Riznichenko, G.Y., Rubin, A.B., 2019. Monitoring of the photosynthetic activity of the microalgae *Chlorella* under nitrogen depletion conditions. Biophysics (Oxf). 64, 358–366. https://doi.org/10.1134/S0006350919030175

Pniewski, F., Piasecka-Jędrzejak, I., 2020. Photoacclimation to constant and changing light conditions in a benthic diatom. Front. Mar. Sci. 7. https://doi.org/10.3389/fmars.2020.00381

Porra, R.J., Thompson, W.A., P.E., K., 1989. Determination of accurate extinction coefficients and simultaneous equations for assayin chlorophylls *a* and *b* extracted with four different solvents. Biochim. Biophys. Acta.

Prášil, O., Kolber, Z., Berry, J.A., Falkowski, P.G., 1996. Cyclic electron flow around Photosystem II *in vivo*. Photosynth. Res. 48, 395–410. https://doi.org/10.1007/BF00029472

Pudney, A., Gandini, C., Economou, C.K., Smith, R., Goddard, P., Napier, J.A., Spicer, A., Sayanova, O., 2019. Multifunctionalizing the marine diatom *Phaeodactylum tricornutum*

for sustainable co-production of omega-3 long chain polyunsaturated fatty acids and recombinant phytase. Sci. Rep. 9, 11444. https://doi.org/10.1038/s41598-019-47875-1

Qiao, H., Cong, C., Sun, C., Li, B., Wang, J., Zhang, L., 2016. Effect of culture conditions on growth, fatty acid composition and DHA/EPA ratio of *Phaeodactylum tricornutum*. Aquaculture 452, 311–317. https://doi.org/10.1016/j.aquaculture.2015.11.011

Qiao, Y., Rong, J., Chen, H., He, C., Wang, Q., 2015. Non-invasive rapid harvest time determination of oil-producing microalgae cultivations for biodiesel production by using chlorophyll fluorescence. Front. Energy Res. 3, 1–10. https://doi.org/10.3389/fenrg.2015.00044

Qin, L., Wang, Z., Sun, Y., Shu, Q., Feng, P., Zhu, L., Xu, J., Yuan, Z., 2016. Microalgae consortia cultivation in dairy wastewater to improve the potential of nutrient removal and biodiesel feedstock production. Environ. Sci. Pollut. Res. 23, 8379–8387. https://doi.org/10.1007/s11356-015-6004-3

Quelhas, P.M., Trovão, M., Silva, J.T., Machado, A., Santos, T., Pereira, H., Varela, J., Simões, M., Silva, J.L., 2019. Industrial production of *Phaeodactylum tricornutum* for CO_2 mitigation: biomass productivity and photosynthetic efficiency using photobioreactors of different volumes. J. Appl. Phycol. 31, 2187–2196. https://doi.org/10.1007/s10811-019-1750-0

Radmann, E.M., Reinehr, C.O., Costa, J.A.V., 2007. Optimization of the repeated batch cultivation of microalga *Spirulina platensis* in open raceway ponds. Aquaculture 265, 118–126. https://doi.org/10.1016/j.aquaculture.2007.02.001

Raja, R., Hemaiswarya, S., Kumar, N.A., Sridhar, S., Rengasamy, R., 2008. A perspective on the biotechnological potential of microalgae. Crit. Rev. Microbiol. 34, 77–88. https://doi.org/10.1080/10408410802086783

Ralph, P.J., Gademann, R., 2005. Rapid light curves: A powerful tool to assess photosynthetic activity. Aquat. Bot. 82, 222–237. https://doi.org/https://doi.org/10.1016/j.aquabot.2005.02.006

Ranglová, K., Lakatos, G.E., Manoel, J.A.C., Grivalský, T., Estrella, F.S., Fernández, F.G.A., Molnár, Z., Ördög, V., Masojídek, J., 2021. Growth, biostimulant and biopesticide activity of the MACC-1 *Chlorella* strain cultivated outdoors in inorganic medium and wastewater. Algal Res. 53, 102136. https://doi.org/https://doi.org/10.1016/j.algal.2020.102136

Ranglová, K., Lakatos, G.E., Manoel, J.A.C., Grivalský, T., Masojídek, J., 2019. Rapid screening test to estimate temperature optima for microalgae growth using photosynthesis activity measurements. Folia Microbiol. (Praha). https://doi.org/10.1007/s12223-019-00738-8

Ras, M., Steyer, J.-P., Bernard, O., 2013. Temperature effect on microalgae: a crucial factor for outdoor production. Rev. Environ. Sci. Bio/Technology 12, 153–164.

https://doi.org/10.1007/s11157-013-9310-6

Raven, J.A., Beardall, J., Quigg, A., 2020. Light-driven oxygen consumption in the water-water cycles and photorespiration, and light stimulated mitochondrial respiration, in: Larkum, A.W.D. (Ed.), Photosynthesis in Algae: Biochemical and Physiological Mechanisms. Springer Nature Switzerland, pp. 161–178. https://doi.org/10.1007/978-3-030-33397-3_8

Rebolloso-Fuentes, M.M., Navarro-Pérez, A., Ramos-Miras, J.J., Guil-Guerrero, J.L., 2001. Biomass nutrient profiles of the microalga *Phaeodactylum tricornutum*. J. Food Biochem. 25, 57–76. https://doi.org/10.1111/j.1745-4514.2001.tb00724.x

Reynolds, C.S. (Ed.), 2006. Nutrient uptake and assimilation in phytoplankton, in: The Ecology of Phytoplankton, Ecology, Biodiversity and Conservation. Cambridge University Press, Cambridge, pp. 145–177. https://doi.org/DOI: 10.1017/CBO9780511542145.005

Richardson, J.W., Johnson, M.D., Outlaw, J.L., 2012. Economic comparison of open pond raceways to photo bio-reactors for profitable production of algae for transportation fuels in the Southwest. Algal Res 1.

Ritchie, R.J., Larkum, A.W.D., 2012. Modelling photosynthesis in shallow algal production ponds. Photosynthetica 50, 481–500. https://doi.org/10.1007/s11099-012-0076-9

Rochaix, J.-D., 2020. The dynamics of the photosynthetic apparatus in algae, in: Larkum, A.W.D. (Ed.), Photosynthesis in Algae: Biochemical and Physiological Mechanisms. Springer Nature Switzerland, pp. 57–82. https://doi.org/10.1007/978-3-030-33397-3_4

Rodolfi, L., Biondi, N., Guccione, A., Bassi, N., D'Ottavio, M., Arganaraz, G., Tredici, M.R., 2017. Oil and eicosapentaenoic acid production by the diatom *Phaeodactylum tricornutum* cultivated outdoors in Green Wall Panel (GWP®) reactors. Biotechnol. Bioeng. 114, 2204–2210. https://doi.org/10.1002/bit.26353

Rodolfi, L., Chini Zittelli, G., Bassi, N., Padovani, G., Biondi, N., Bonini, G., Tredici, M.R., 2009. Microalgae for oil: Strain selection, induction of lipid synthesis and outdoor mass cultivation in a low-cost photobioreactor. Biotechnol. Bioeng. 102, 100–112. https://doi.org/10.1002/bit.22033

Roessler, P.G., 1990. Environmental control of glycerolipid metabolism in microalgae: commercial implications and future research directions. J. Phycol. 26, 393–399. https://doi.org/10.1111/j.0022-3646.1990.00393.x

Ronga, D., Biazzi, E., Parati, K., Carminati, D., Carminati, E., Tava, A., 2019. Microalgal biostimulants and biofertilisers in crop productions. Agronomy. https://doi.org/10.3390/agronomy9040192

Ruiz, J., Olivieri, G., De Vree, J., Bosma, R., Willems, P., Reith, J.H., Eppink, M.H.M.M., Kleinegris, D.M.M.M., Wijffels, R.H., Barbosa, M.J., 2016. Towards industrial products from microalgae. Energy Environ. Sci. 9, 3036–3043. https://doi.org/10.1039/C6EE01493C

San Pedro, A., González-López, C.V., Acién, F.G., Molina-Grima, E., 2016. Outdoor pilot production of *Nannochloropsis gaditana*: Influence of culture parameters and lipid production rates in flat-panel photobioreactors. Algal Res. 18, 156–165. https://doi.org/10.1016/j.algal.2016.06.011

San Pedro, A., González-López, C.V. V., Acién, F.G.G., Molina-Grima, E., 2013. Marine microalgae selection and culture conditions optimization for biodiesel production. Bioresour. Technol. 134, 353–361. https://doi.org/10.1016/j.biortech.2013.02.032

San Pedro, A., González-López, C. V, Acién, F.G., Molina-Grima, E., 2014. Outdoor pilot-scale production of *Nannochloropsis gaditana*: Influence of culture parameters and lipid production rates in tubular photobioreactors. Bioresour. Technol. 169, 667–676. https://doi.org/https://doi.org/10.1016/j.biortech.2014.07.052

Sánchez San Fulgencio, N., Suárez-Estrella, F., López, M.J., Jurado, M.M., López-González, J.A., Moreno, J., 2018. Biotic aspects involved in the control of damping-off producing agents: The role of the thermotolerant microbiota isolated from composting of plant waste. Biol. Control 124, 82–91. https://doi.org/10.1016/j.biocontrol.2018.04.015

Sánchez Zurano, A., Garrido Cárdenas, J.A., Gómez Serrano, C., Morales Amaral, M., Acién-Fernández, F.G., Fernández Sevilla, J.M., Molina Grima, E., 2020. Year-long assessment of a pilot-scale thin-layer reactor for microalgae wastewater treatment. Variation in the microalgae-bacteria consortium and the impact of environmental conditions. Algal Res. 50, 101983. https://doi.org/10.1016/j.algal.2020.101983

Sandnes, J.M., Källqvist, T., Wenner, D., Gislerød, H.R., 2005. Combined influence of light and temperature on growth rates of *Nannochloropsis oceanica*: Linking cellular responses to large-scale biomass production. J. Appl. Phycol. 17, 515–525. https://doi.org/10.1007/s10811-005-9002-x

Sansone, C., Galasso, C., Orefice, I., Nuzzo, G., Luongo, E., Cutignano, A., Romano, G., Brunet, C., Fontana, A., Esposito, F., Ianora, A., 2017. The green microalga *Tetraselmis suecica* reduces oxidative stress and induces repairing mechanisms in human cells. Sci. Rep. 7, 41215.

Sarry, J.-E., Montillet, J.-L., Sauvaire, Y., Havaux, M., 1994. The protective function of the xanthophyll cycle in photosynthesis. FEBS Lett. 353, 147–150. https://doi.org/10.1016/0014-5793(94)01028-5

Satpati, G.G., Pal, R., 2015. Rapid detection of neutral lipid in green microalgae by flow cytometry in combination with Nile red staining—an improved technique. Ann. Microbiol. 65, 937–949. https://doi.org/10.1007/s13213-014-0937-5

Schiphorst, C., Bassi, R., 2020. Chlorophyll-xanthophyll antenna complexes: In between light harvesting and energy dissipation, in: Larkum, A.W.D. (Ed.), Photosynthesis in Algae: Biochemical and Physiological Mechanisms. Springer Nature Switzerland, pp. 27–55.

https://doi.org/10.1007/978-3-030-33397-3_3

Schreiber, U., Schliwa, U., Bilger, W., 1986. Continuous recording of photochemical and non-photochemical chlorophyll fluorescence quenching with a new type of modulation fluorometer. Photosynth. Res. 10, 51–62. https://doi.org/10.1007/BF00024185

Schüler, L.M., Schulze, P.S.C., Pereira, H., Barreira, L., León, R., Varela, J., 2017. Trends and strategies to enhance triacylglycerols and high-value compounds in microalgae. Algal Res. 25, 263–273. https://doi.org/10.1016/j.algal.2017.05.025

Schulze, P.S.C., Barreira, L.A., Pereira, H.G.C., Perales, J.A., Varela, J.C.S., 2014. Light emitting diodes (LEDs) applied to microalgal production. Trends Biotechnol. 32, 422–430. https://doi.org/10.1016/j.tibtech.2014.06.001

Schulze, P.S.C., Pereira, H.G.C., Santos, T.F.C., Schueler, L., Guerra, R., Barreira, L.A., Perales, J.A., Varela, J.C.S., 2016. Effect of light quality supplied by light emitting diodes (LEDs) on growth and biochemical profiles of *Nannochloropsis oculata* and *Tetraselmis chuii*. Algal Res. 16, 387–398. https://doi.org/10.1016/j.algal.2016.03.034

SCOR-UNESCO, 1966. Determination of photosynthetic pigments in seawater, in: Monographs on Oceanographic Methodology 1. Paris: UNESCO.

Sekar, S., Chandramohan, M., 2008. Phycobiliproteins as a commodity: Trends in applied research, patents and commercialization. J. Appl. Phycol. 20, 113–136. https://doi.org/10.1007/s10811-007-9188-1

Serôdio, J., Schmidt, W., Frankenbach, S., 2017. A chlorophyll fluorescence-based method for the integrated characterization of the photophysiological response to light stress. J. Exp. Bot. erw492. https://doi.org/10.1093/jxb/erw492

Serôdio, J., Vieira, S., Cruz, S., Coelho, H., 2006. Rapid light-response curves of chlorophyll fluorescence in microalgae: relationship to steady-state light curves and non-photochemical quenching in benthic diatom-dominated assemblages. Photosynth. Res. 90, 29–43. https://doi.org/10.1007/s11120-006-9105-5

Sharma, K., Li, Y., Schenk, P.M., 2014. UV-C-mediated lipid induction and settling, a step change towards economical microalgal biodiesel production. Green Chem. 16, 3539–3548. https://doi.org/10.1039/c4gc00552j

Shepelev, Y.Y., 1975. Biological life-support sytems, in: Calvin, M. (Ed.), Foundations of Space Biology and Medicine: Space Medicine and Biotechnology. Scientific and Technical Information Office, National Aeronautics and Space Administration, pp. 274–310.

Silva Benavides, A.M., Ranglová, K., Malapascua, J.R., Masojídek, J., Torzillo, G., 2017. Diurnal changes of photosynthesis and growth of *Arthrospira platensis* cultured in a thin-layer cascade and an open pond. Algal Res. 28, 48–56. https://doi.org/10.1016/j.algal.2017.10.007

Silva Benavides, A.M., Torzillo, G., Kopecký, J., Masojídek, J., 2013. Productivity and biochemical composition of *Phaeodactylum tricornutum* (Bacillariophyceae) cultures grown outdoors in tubular photobioreactors and open ponds. Biomass and Bioenergy 54, 115–122. https://doi.org/10.1016/j.biombioe.2013.03.016

Simionato, D., Block, M.A., La Rocca, N., Jouhet, J., Maréchal, E., Finazzi, G., Morosinotto, T., 2013. The response of *Nannochloropsis gaditana* to nitrogen starvation includes de novo biosynthesis of triacylglycerols, a decrease of chloroplast galactolipids, and reorganization of the photosynthetic apparatus. Eukaryot. Cell 12, 665–676. https://doi.org/10.1128/EC.00363-12

Six, C., Finkel, Z. V., Rodriguez, F., Marie, D., Partensky, F., Campbell, D.A., 2008. Contrasting photoacclimation costs in ecotypes of the marine eukaryotic picoplankter *Ostreococcus*. Limnol. Oceanogr. 53, 255–265. https://doi.org/10.4319/lo.2008.53.1.0255

Slocombe, S.P., Zhang, Q., Ross, M., Anderson, A., Thomas, N.J., Lapresa, Á., Rad-Menéndez, C., Campbell, C.N., Black, K.D., Stanley, M.S., Day, J.G., 2015. Unlocking nature's treasure-chest: Screening for oleaginous algae. Sci. Rep. 5, 1–17. https://doi.org/10.1038/srep09844

Solovchenko, A., Lukyanov, A., Solovchenko, O., Didi-Cohen, S., Boussiba, S., Khozin-Goldberg, I., 2014a. Interactive effects of salinity, high light, and nitrogen starvation on fatty acid and carotenoid profiles in *Nannochloropsis oceanica* CCALA 804. Eur. J. Lipid Sci. Technol. 116, 635–644. https://doi.org/10.1002/ejlt.201300456

Solovchenko, A., Pogosyan, S., Chivkunova, O., Selyakh, I., Semenova, L., Voronova, E., Scherbakov, P., Konyukhov, I., Chekanov, K., Kirpichnikov, M., Lobakova, E., 2014b. Phycoremediation of alcohol distillery wastewater with a novel *Chlorella sorokiniana* strain cultivated in a photobioreactor monitored on-line via chlorophyll fluorescence. Algal Res. 6, 234–241. https://doi.org/10.1016/j.algal.2014.01.002

Solovchenko, A.E., 2012. Physiological role of neutral lipid accumulation in eukaryotic microalgae under stresses. Russ. J. Plant Physiol. 59, 167–176. https://doi.org/10.1134/S1021443712020161

Sørensen, M., Berge, G.M., Reitan, K.I., Ruyter, B., 2016. Microalga *Phaeodactylum tricornutum* in feed for Atlantic salmon (*Salmo salar*) —Effect on nutrient digestibility, growth and utilization of feed. Aquaculture 460, 116–123. https://doi.org/10.1016/j.aquaculture.2016.04.010

Sosik, H.M., Mitchell, B.G., 1991. Absorption, fluorescence, and quantum yield for growth in nitrogen-limited *Dunaliella tertiolecta*. Limnol. Oceanogr. 36, 910–921. https://doi.org/10.4319/lo.1991.36.5.0910

Spoehr, H. a, Milner, H.W., 1949. The chemical composition of *Chlorella*; Effect of

environmental conditions. Plant Physiol. 24, 120–149. https://doi.org/10.1104/pp.24.1.120

Spolaore, P., Joannis-Cassan, C., Duran, E., Isambert, A., 2006. Commercial applications of microalgae. J. Biosci. Bioeng. 101, 87–96. https://doi.org/http://dx.doi.org/10.1263/jbb.101.87

Srivastava, A., Strasser, R.J., Govindjee, 1999. Greening of peas: parallel measurements of 77 K emission spectra, OJIP chlorophyll a fluorescence transient, period four oscillation of the initial fluorescence level, delayed light emission, and P700*. Photosynthetica 37, 365–392. https://doi.org/10.1023/A:1007199408689

Steinbrenner, J., Linden, H., 2003. Light induction of carotenoid biosynthesis genes in the green alga *Haematococcus pluvialis*: regulation by photosynthetic redox control. Plant Mol Biol 52, 343–356. https://doi.org/10.1023/A:1023948929665

Stirbet, A., Govindjee, 2011. On the relation between the Kautsky effect (chlorophyll *a* fluorescence induction) and Photosystem II: Basics and applications of the OJIP fluorescence transient. J. Photochem. Photobiol. B Biol. 104, 236–257. https://doi.org/10.1016/j.jphotobiol.2010.12.010

Stirbet, A., Lazar, D., Kromdijk, J., Govindjee, G., 2018. Chlorophyll *a* fluorescence induction: Can just a one-second measurement be used to quantify abiotic stress responses? Photosynthetica 56, 86–104. https://doi.org/10.1007/s11099-018-0770-3

Strasser, B.J., Strasser, R.J., 1995. Measuring fast fluorescence transients to address environmental questions: The JIP test, in: Mathis, P. (Ed.), Photosynthesis: From Light to Biosphere. Vol 5. Kluwer Academic Publishers, Dordrecht, pp. 977–980.

Strasser, R.J., Srivastava, A., Tsimilli-Michael, M., 2000. The fluorescence transient as a tool to characterize and screen photosynthetic samples, in: Yunus, M., Pathre, U., Mohanty, P. (Eds.), Probing Photosynthesis: Mechanism, Regulation & Adaptation. Taylor and Francis, London, pp. 445–483.

Strasser, R.J., Srivastava, A., Tsimilli-Michael, M., Strasser, R. J. Srivastava, A., Tsimilli-Michael, M., 1999. Screening the vitality and photosynthetic activity of plants by fluorescence transient, in: Behl, R.K., Punia, M.S., Lather, B.P.S. (Eds.), Crop Improvement for Food Security. SSARM, Hisar, India, pp. 72–115.

Strasser, R.J., Tsimilli-Michael, M., Srivastava, A., 2004. Analysis of the chlorophyll *a* fluorescence transient, in: Papageorgiou, G.C., Govindjee (Eds.), Chlorophyll a Fluorescence: A Signature of Photosynthesis. Springer Netherlands, Dordrecht, pp. 321–362. https://doi.org/10.1007/978-1-4020-3218-9_12

Suárez-Estrella, F., Ros, M., Vargas-García, M.C., López, M.J., Moreno, J., 2014. Control of *Xanthomonas campestris* pv *vesicatoria* using agroindustrial waste-based compost. J. Plant Pathol. 96, 243–248. https://doi.org/10.4454/JPP.V96I2.028

Suggett, D.J., Le Floc'H, E., Harris, G.N., Leonardos, N., Geider, R.J., 2007. Different strategies of photoacclimation by two strains of *Emiliania huxleyi* (Haptophyta). J. Phycol. 43, 1209–1222. https://doi.org/10.1111/j.1529-8817.2007.00406.x

Sui, Y., Jiang, Y., Moretti, M., Vlaeminck, S.E., 2020. Harvesting time and biomass composition affect the economics of microalgae production. J. Clean. Prod. 259, 120782. https://doi.org/10.1016/j.jclepro.2020.120782

Sukenik, A., 1991. Ecophysiological considerations in the optimization of eicosapentaenoic acid production by *Nannochloropsis* sp. (Eustigmatophyceae). Bioresour Technol 35, 263–269.

Sukenik, A., Beardall, J., Kromkamp, J.C., Kopecký, J., Masojídek, J., Van Bergeijk, S., Gabai, S., Shaham, E., Yamshon, A., 2009. Photosynthetic performance of outdoor *Nannochloropsis* mass cultures under a wide range of environmental conditions. Aquat. Microb. Ecol. 56, 297–308. https://doi.org/10.3354/ame01309

Sukenik, A., Carmeli, Y., 1990. Lipid synthesis and fatty acid composition in *Nannochloropsis* sp. (Eustigmatophyceae) grown in a light-dark cycle. J. Phycol. 26, 463–469. https://doi.org/10.1111/j.0022-3646.1990.00463.x

Sukenik, A., Carmeli, Y., 1989. Regulation of fatty acid composition by irradiance level in the eustigmatophyte *Nannochloropsis* sp. J. phycol. 25.

Sukenik, A., Zmora, O., Carmeli, Y., Nannochloropsis, I.I., 1993. Biochemical quality of marine unicellular algae with special emphasis on lipid composition. II. *Nannochloropsis* sp. Aquaculture 117, 313–326. https://doi.org/https://doi.org/10.1016/0044-8486(93)90328-V

Suleria, H., Osborne, S., Masci, P., Gobe, G., 2015. Marine-based nutraceuticals: an innovative trend in the food and supplement industries. Mar. Drugs 13, 6336–6351. https://doi.org/10.3390/md13106336

Tamaki, S., Mochida, K., Suzuki, K., 2021. Diverse biosynthetic pathways and protective functions against environmental stress of antioxidants in microalgae. Plants 10, 1250. https://doi.org/10.3390/plants10061250

Tamburic, B., Guruprasad, S., Radford, D.T., Szabó, M., Lilley, R.M.C., Larkum, A.W.D., Franklin, J.B., Kramer, D.M., Blackburn, S.I., Raven, J.A., Schliep, M., Ralph, P.J., 2014. The effect of diel temperature and light cycles on the growth of *Nannochloropsis oculata* in a photobioreactor matrix. PLoS One 9. https://doi.org/10.1371/journal.pone.0086047

Tao, R., Kinnunen, V., Praveenkumar, R., Lakaniemi, A.-M., Rintala, J.A., 2017. Comparison of *Scenedesmus acuminatus* and *Chlorella vulgaris* cultivation in liquid digestates from anaerobic digestion of pulp and paper industry and municipal wastewater treatment sludge. J. Appl. Phycol. 29, 2845–2856. https://doi.org/10.1007/s10811-017-1175-6

Taylor, N.J., 1985. Silica incorporation in the diatom *Cosinodiscus granii* as affected by light

intensity. Br. Phycol. J. 20, 365–374. https://doi.org/10.1080/00071618500650371

Tejido-Nuñez, Y., Aymerich, E., Sancho, L., Refardt, D., 2020. Co-cultivation of microalgae in aquaculture water: Interactions, growth and nutrient removal efficiency at laboratory- and pilot-scale. Algal Res. 49, 101940. https://doi.org/10.1016/j.algal.2020.101940

Thomas, W.H., Seibert, D.L.R., Alden, M., Neori, A., Eldridge, P., 1984. Yields, photosynthetic efficiencies and proximate composition of dense marine microalgal cultures. I. Introduction and Phaeodactylum tricornutum experiments. Biomass 5, 181–209. https://doi.org/http://dx.doi.org/10.1016/0144-4565(84)90022-2

Thompson, G.A., 1996. Lipids and membrane function in green algae. Biochim. Biophys. Acta - Lipids Lipid Metab. 1302, 17–45. https://doi.org/10.1016/0005-2760(96)00045-8

Tian, Y., Mingjiang, Z., Peiyuan, Q., 2002. Combined effects of temperature, irradiance and salinity on growth of diatom *Skeletonema costatum*. Chin. J. Ocean. Limnol. 20, 237–243. https://doi.org/https://doi.org/10.1007/BF02848852

Ting, C.S., Owens, T.G., 1994. The effects of excess irradiance on photosynthesis in the marine diatom *Phaeodactylum tricornutum*. Plant Physiol. 106, 763–770. https://doi.org/10.1104/pp.106.2.763

Torzillo, G., Accolla, P., Pinzani, E., Masojídek, J., 1996. *In situ* monitoring of chlorophyll fluorescence to assess the synergistic effect of low temperature and high irradiance stresses in *Spirulina* cultures grown outdoors in photobioreactors. J. Appl. Phycol. 8, 283–291. https://doi.org/10.1007/BF02178571

Torzillo, G., Bernardini, P., Masojídek, J., 1998. On-line monitoring of chlorophyll fluorescence to assess the extent of photoinhibition of photosynthesis induced by high oxygen concentration and low temperature and its effect on the productivity of outdoor cultures of *Spirulina platensis* (cyanoba. J. Phycol. 34, 504–510. https://doi.org/10.1046/j.1529-8817.1998.340504.x

Torzillo, G., Carlozzi, P., Pushparaj, B., Montaini, E., Materassi, R., 1993. A two-plane tubular photobioreactor for outdoor culture of *Spirulina*. Biotechnol. Bioeng. 42, 891–898. https://doi.org/10.1002/bit.260420714

Torzillo, G., Chini Zittelli, G., 2015. Tubular Photobioreactors, in: Algal Biorefineries. Springer International Publishing, Cham, pp. 187–212. https://doi.org/10.1007/978-3-319-20200-6_5

Torzillo, G., Faraloni, C., Silva, A.M., Kopecký, J., Pilný, J., Masojídek, J., 2012. Photoacclimation of *Phaeodactylum tricornutum* (Bacillariophyceae) cultures grown outdoors in photobioreactors and open ponds. Eur. J. Phycol. 47, 169–181. https://doi.org/10.1080/09670262.2012.683202

Torzillo, G, Sacchi, A., Materassi, R., 1991. Temperature as an important factor affecting productivity and night biomass loss in *Spirulina platensis* grown outdoors in tubular

photobioreactors. Bioresour. Technol. 38, 95–100. https://doi.org/10.1016/0960-8524(91)90137-9

Torzillo, G., Sacchi, A., Materassi, R., Richmond, A., 1991. Effect of temperature on yield and night biomass loss in *Spirulina platensis* grown outdoors in tubular photobioreactors. J. Appl. Phycol. 3, 103–109. https://doi.org/10.1007/BF00003691

Touloupakis, E., Cicchi, B., Torzillo, G., 2015. A bioenergetic assessment of photosynthetic growth of *Synechocystis* sp. PCC 6803 in continuous cultures. Biotechnol. Biofuels 8, 1–11. https://doi.org/10.1186/s13068-015-0319-7

Tramontano, C., Chianese, G., Terracciano, M., de Stefano, L., Rea, I., 2020. Nanostructured biosilica of diatoms: From water world to biomedical applications. Appl. Sci. 10, 6811. https://doi.org/10.3390/app10196811

Tran, N.-A.T., Padula, M.P., Evenhuis, C.R., Commault, A.S., Ralph, P.J., Tamburic, B., 2016. Proteomic and biophysical analyses reveal a metabolic shift in nitrogen deprived *Nannochloropsis oculata*. Algal Res. 19, 1–11. https://doi.org/10.1016/j.algal.2016.07.009

Tredici, M.R., 2004. Mass production of microalgae: Photobioreactors, in: Handbook of Microalgal Culture. Blackwell Publishing Ltd, Oxford, UK, pp. 178–214. https://doi.org/10.1002/9780470995280.ch9

Tredici, M.R., Bassi, N., Prussi, M., Biondi, N., Rodolfi, L., Zittelli, G.C., Sampietro, G., 2015. Energy balance of algal biomass production in a 1-ha "' Green Wall Panel "' plant : How to produce algal biomass in a closed reactor achieving a high Net Energy Ratio q. Appl. Energy 154, 1103–1111. https://doi.org/10.1016/j.apenergy.2015.01.086

Tredici, M.R., Rodolfi, L., Biondi, N., Bassi, N., Sampietro, G., 2016. Techno-economic analysis of microalgal biomass production in a 1-ha Green Wall Panel (GWP®) plant. Algal Res. 19, 253–263. https://doi.org/10.1016/j.algal.2016.09.005

Tsai, H.P., Chuang, L. Te, Chen, C.N.N., 2016. Production of long chain omega-3 fatty acids and carotenoids in tropical areas by a new heat-tolerant microalga *Tetraselmis* sp. DS3. Food Chem. 192, 682–690. https://doi.org/10.1016/j.foodchem.2015.07.071

Tulli, F., Chini Zittelli, G., Giorgi, G., Poli, B.M., Tibaldi, E., Tredici, M.R., 2012. Effect of the inclusion of dried *Tetraselmis suecica* on growth, feed utilization, and fillet composition of European sea bass juveniles fed organic diets. J. Aquat. Food Prod. Technol. 21, 188–197. https://doi.org/10.1080/10498850.2012.664803

Van Heukelem, L., Thomas, C.S., 2001. Computer-assisted high-performance liquid chromatography method development with applications to the isolation and analysis of phytoplankton pigments. J. Chromatogr. A 910, 31–49. https://doi.org/10.1016/S0378-4347(00)00603-4

van Houcke, J., Medina, I., Maehre, H.K., Cornet, J., Cardinal, M., Linssen, J., Luten, J., 2017.

The effect of algae diets (*Skeletonema costatum* and *Rhodomonas baltica*) on the biochemical composition and sensory characteristics of Pacific cupped oysters (*Crassostrea gigas*) during land-based refinement. Food Res. Int. 100, 151–160. https://doi.org/10.1016/j.foodres.2017.06.041

Van Wagenen, J., Miller, T.W., Hobbs, S., Hook, P., Crowe, B., Huesemann, M., 2012. Effects of light and temperature on fatty acid production in *Nannochloropsis salina*. Energies 5, 731–740. https://doi.org/10.3390/en5030731

Vårum, K.M., Østgaard, K., Grimsrud, K., 1986. Diurnal rhythms in carbohydrate metabolism of the marine diatom *Skeletonema costatum* (Grev.) Cleve. J. Exp. Mar. Bio. Ecol. 102, 249–256. https://doi.org/10.1016/0022-0981(86)90180-2

Vecchi, V., Barera, S., Bassi, R., Dall'Osto, L., 2020. Potential and challenges of improving photosynthesis in algae. Plants 9, 67. https://doi.org/10.3390/plants9010067

Vonshak, A., Laorawat, S., Bunnag, B., Tanticharoen, M., 2014. The effect of light availability on the photosynthetic activity and productivity of outdoor cultures of Arthrospira platensis (Spirulina). J. Appl. Phycol. 26, 1309–1315. https://doi.org/10.1007/s10811-013-0133-1

Vonshak, A., Torzillo, G., Tomaseli, L., 1994. Use of chlorophyll fluorescence to estimate the effect of photoinhibition in outdoor cultures of *Spirulina platensis*. J. Appl. Phycol. 6, 31–34. https://doi.org/10.1007/BF02185901

Wagner, H., Jakob, T., Lavaud, J., Wilhelm, C., 2016. Photosystem II cycle activity and alternative electron transport in the diatom *Phaeodactylum tricornutum* under dynamic light conditions and nitrogen limitation. Photosynth. Res. 128, 151–161. https://doi.org/10.1007/s11120-015-0209-7

Walker, D., 1992. Energy, Plants and Man. Oxygraphics.

Wang, B., Jia, J., 2020. Photoprotection mechanisms of *Nannochloropsis oceanica* in response to light stress. Algal Res. 46, 101784. https://doi.org/10.1016/j.algal.2019.101784

Wang, J., Zhou, W., Chen, H., Zhan, J., He, C., Wang, Q., 2019. Ammonium nitrogen tolerant *Chlorella* strain screening and its damaging effects on photosynthesis. Front. Microbiol. 9, 3250. https://doi.org/10.3389/fmicb.2018.03250

Wang, Y., Ho, S.-H.H., Cheng, C.-L.L., Guo, W.-Q.Q., Nagarajan, D., Ren, N.-Q.Q., Lee, D.-J.J., Chang, J.-S.S., 2016. Perspectives on the feasibility of using microalgae for industrial wastewater treatment. Bioresour. Technol. 222, 485–497. https://doi.org/10.1016/j.biortech.2016.09.106

Wei, L., Huang, X., Huang, Z., 2015. Temperature effects on lipid properties of microalgae *Tetraselmis subcordiformis* and *Nannochloropsis oculata* as biofuel resources. Chinese J. Oceanol. Limnol. 33, 99–106. https://doi.org/10.1007/s00343-015-3346-0

White, D.A., Pagarette, A., Rooks, P., Ali, S.T., 2013. The effect of sodium bicarbonate

supplementation on growth and biochemical composition of marine microalgae cultures. J. Appl. Phycol. 25, 153–165. https://doi.org/10.1007/s10811-012-9849-6

White, S., Anandraj, A., Bux, F., 2011. PAM fluorometry as a tool to assess microalgal nutrient stress and monitor cellular neutral lipids. Bioresour. Technol. 102, 1675–1682. https://doi.org/https://doi.org/10.1016/j.biortech.2010.09.097

Whitmarsh, J., Govindjee, 2003. Photosynthesis, in: Digital Encyclopedia of Applied Physics. Wiley-VCH Verlag GmbH & Co. KGaA, Weinheim, Germany. https://doi.org/10.1002/3527600434.eap327

Whitmarsh, J., Govindjee, 1995. Photosynthesis. Encycl. Appl. Phys. 13, 513–532.

Wijffels, R.H., Barbosa, M.J., 2010. An outlook on microalgal biofuels. Science (80-.). 329, 796–799. https://doi.org/10.1126/science.1189003

William, K.W.L., Morris, I., 1982. Temperature adaptation in *Phaeodactylum tricornutum* Bohlin: Photosynthetic rate compensation and capacity. J. Exp. Mar. Bio. Ecol. 58, 135–150. https://doi.org/10.1016/0022-0981(82)90125-3

World Health Organization, 2017. Guidelines for drinking-water quality: fourth edition incorporating first addendum, 4th ed + 1. ed. World Health Organization, Geneva PP - Geneva.

Xu, D., Gao, Z., Li, F., Fan, X., Zhang, X., Ye, N., Mou, S., Liang, C., Li, D., 2013. Detection and quantitation of lipid in the microalga *Tetraselmis subcordiformis* (Wille) Butcher with BODIPY 505/515 staining. Bioresour. Technol. 127, 386–390. https://doi.org/10.1016/j.biortech.2012.09.068

Yang, L., Li, H., Liu, T., Zhong, Y., Ji, C., Lu, Q., Fan, L., Li, J., Leng, L., Li, K., Zhou, W., 2019. Microalgae biotechnology as an attempt for bioregenerative life support systems: problems and prospects. J. Chem. Technol. Biotechnol. 94, 3039–3048. https://doi.org/10.1002/jctb.6159

Yao, C., Ai, J., Cao, X., Xue, S., Zhang, W., 2012. Enhancing starch production of a marine green microalga *Tetraselmis subcordiformis* through nutrient limitation. Bioresour. Technol. 118, 438–444. https://doi.org/10.1016/j.biortech.2012.05.030

Yodsuwan, N., Sawayama, S., Sirisansaneeyakul, S., 2017. Effect of nitrogen concentration on growth, lipid production and fatty acid profiles of the marine diatom *Phaeodactylum tricornutum*. Agric. Nat. Resour. 51, 190–197. https://doi.org/10.1016/j.anres.2017.02.004

Zallen, D., 1993. The “light” organism for the job: Green algae and photosynthesis research. J. Hist. Biol. 26, 269–279.

Zhang, Y., Wu, H., Yuan, C., Li, T., Li, A., 2019. Growth, biochemical composition, and photosynthetic performance of *Scenedesmus acuminatus* during nitrogen starvation and resupply. J. Appl. Phycol. 31, 2797–2809. https://doi.org/10.1007/s10811-019-01783-z

Zhao, L.-S.S., Li, K., Wang, Q.-M.M., Song, X.-Y.Y., Su, H.-N.N., Xie, B.-B. Bin, Zhang, X.-Y.Y., Huang, F., Chen, X.-L.L., Zhou, B.-C.C., Zhang, Y.-Z.Z., 2017. Nitrogen starvation impacts the photosynthetic performance of *Porphyridium cruentum* as revealed by chlorophyll *a* fluorescence. Sci. Rep. 7, 1–11. https://doi.org/10.1038/s41598-017-08428-6

Zhu, C.J., Lee, Y.K., 1997. Determination of biomass dry weight of marine microalgae. J. Appl. Phycol. 9, 189–194. https://doi.org/10.1023/A:1007914806640

Zulu, N.N., Zienkiewicz, K., Vollheyde, K., Feussner, I., 2018. Current trends to comprehend lipid metabolism in diatoms. Prog. Lipid Res. 70, 1–16. https://doi.org/10.1016/j.plipres.2018.03.001

Supplementary Material

Annex I

Supplementary Table I.1. Temperature influence on daily volumetric productivity and nighttime biomass loss (± SD) in *Nannochloropsis oceanica*, grown outdoors in a semi-continuous mode, under different temperature regimes in two independent trials. Daily volumetric productivity (g L^{-1} d^{-1}) was determined by subtracting the final dry biomass concentration of the evening (g L^{-1}) with the dry biomass concentration in the morning of the same day (after dilution; g L^{-1}) and dividing by the determined period (in this case, one day). Daily volumetric nighttime biomass loss (g L^{-1} d^{-1}) was determined similarly, but by subtracting the final dry biomass concentration of the evening (g L^{-1}) with the dry biomass concentrations of the following morning (before dilution; g L^{-1}) and dividing by the same period. Nighttime biomass loss (%) was determined by subtracting the final dry biomass concentration of the evening (g L^{-1}) with the dry biomass concentrations of the following morning (before dilution; g L^{-1}) and dividing by the same value of final dry biomass concentration in the evening (g L^{-1}).

Trial 1						
Time (days)	**Daily volumetric productivity (g L^{-1} d^{-1})**		**Daily volumetric nighttime biomass loss (g L^{-1} d^{-1})**		**Nighttime biomass loss (%)**	
	28:18 ºC (L:D)	28:28 ºC (L:D)	28:18 ºC (L:D)	28:28 ºC (L:D)	28:18 ºC (L:D)	28:28 ºC (L:D)
0	0.496 ± 0.111	0.596 ± 0.061	0.260 ± 0.125	0.173 ± 0.105	27.7 ± 13.7	16.1 ± 9.79
1	0.436 ± 0.071	0.484 ± 0.028	0.170 ± 0.091	0.050 ± 0.076	21.0 ± 11.3	5.21 ± 7.93
2	0.615 ± 0.014	0.539 ± 0.028	0.240 ± 0.045	0.250 ± 0.051	22.9 ± 4.27	23.6 ± 4.85
3	0.706 ± 0.071	0.570 ± 0.042	0.260 ± 0.072	0.130 ± 0.042	23.0 ± 6.54	13.1 ± 4.32
4	0.657 ± 0.057	0.532 ± 0.014	0.400 ± 0.102	0.320 ± 0.045	37.0 ± 9.64	31.7 ± 4.45
5	0.784 ± 0.042	0.654 ± 0.099	0.540 ± 0.045	0.410 ± 0.099	47.8 ± 4.35	39.8 ± 10.3
6	0.553 ± 0.028	0.569 ± 0.028	0.320 ± 0.040	0.290 ± 0.032	38.1 ± 4.93	32.2 ± 3.66
7	0.540 ± 0.028	0.367 ± 0.000	0.350 ± 0.032	0.115 ± 0.007	39.8 ± 3.81	15.5 ± 0.956
Daily average	*0.598 ± 0.107*	*0.539 ± 0.080*	*0.318 ± 0.107*	*0.217 ± 0.113*	***32.2 ± 9.20***	***22.2 ± 10.9***
Trial 2						
Time (days)	**Daily volumetric productivity (g L^{-1} d^{-1})**		**Daily volumetric nighttime biomass loss (g L^{-1} d^{-1})**		**Nighttime biomass loss (%)**	
	28:18 ºC (L:D)	18:18 ºC (L:D)	28:18 ºC (L:D)	18:18 ºC (L:D)	28:18 ºC (L:D)	18:18 ºC (L:D)
1	0.426 ± 0.042	0.255 ± 0.057	0.130 ± 0.121	0.080 ± 0.080	14.3 ± 13.3	10.3 ± 10.3

2	0.459 ± 0.042	0.415 ± 0.000	0.130 ± 0.051	0.030 ± 0.014	14.0 ± 5.52	3.41 ± 1.61
3	0.527 ± 0.085	0.373 ± 0.014	0.180 ± 0.089	0.050 ± 0.032	18.0 ± 9.07	5.49 ± 3.48
4	0.449 ± 0.085	0.238 ± 0.042	0.210 ± 0.086	0.060 ± 0.045	23.3 ± 9.81	7.79 ± 5.82
5	0.468 ± 0.042	0.330 ± 0.014	0.190 ± 0.051	0.100 ± 0.045	21.3 ± 5.82	12.0 ± 5.39
6	0.507 ± 0.028	0.336 ± 0.028	0.140 ± 0.028	0.020 ± 0.117	14.9 ± 3.04	2.50 ± 14.6
7	0.452 ± 0.028	0.254 ± 0.071	0.120 ± 0.040	0.070 ± 0.076	13.0 ± 4.37	8.86 ± 9.67
Daily average	*0.470 ± 0.033*	*0.314 ± 0.062*	*0.157 ± 0.033*	*0.059 ± 0.026*	***17.0 ± 3.71***	***7.19 ± 3.28***

Supplementary Table I.2. Averaged daily areal productivities (gross and net) and nighttime biomass loss (± SD) of *Nannochloropsis oceanica* cultures grown under different temperature regimes in tubular photobioreactors (PBR) outdoors in two independent trials. Gross areal productivity (g m^{-2} d^{-1}) was determined by dividing the daily average biomass produced (g d^{-1}) with the PBR's area (m^2). Growth yield (g MJ^{-1}) was obtained by dividing the gross areal productivity with the daily irradiance. Net areal productivity (g m^{-2} d^{-1}) was determined by subtracting the gross areal productivity with the night biomass loss (g m^{-2} d^{-1}). The nighttime biomass loss was calculated by dividing the daily average biomass loss (g d^{-1}) with the PBR's area (m^2); in brackets is reported the percentage of biomass loss regarding the biomass synthesized during the light period.

Trial	Condition	Mean daily irradiance (MJ m^{-2} day^{-1})	Gross areal productivity (g m^{-2} d^{-1})	Growth yield (g MJ^{-1})	Net areal productivity (g m^{-2} d^{-1})	Nighttime biomass loss (g m^{-2} d^{-1})
1	28:18 ºC (L:D)	20.3 ± 3.21	30.8 ± 5.53	1.52 ± 0.36	14.5 ± 7.81	16.4 ± 5.52 (53.1%)
	28:28 ºC (L:D)		27.8 ± 4.11	1.37 ± 0.30	16.6 ± 7.13	11.2 ± 5.82 (40.3%)
2	28:18 ºC (L:D)	16.4 ± 4.03	24.2 ± 1.68	1.48 ± 0.38	16.1 ± 2.39	8.10 ± 1.69 (33.5%)
	18:18 ºC (L:D)		16.2 ± 3.21	0.99 ± 0.31	13.2 ± 3.48	3.02 ± 1.33 (18.6%)

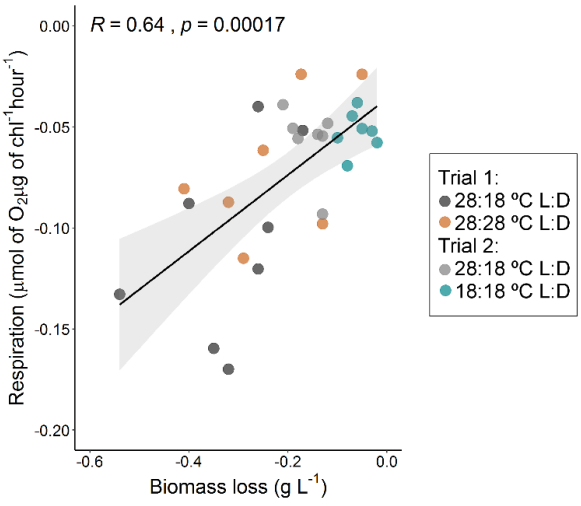

Supplementary Figure I.1. Correlation between biomass loss (g L^{-1}) and respiration values (µmol of O_2 µg of chlorophyll^{-1} hour^{-1}), combining data points from both trials and conditions using *Nannochloropsis oceanica*, grown outdoors in tubular photobioreactors under different temperatures. Data points from the 28:18 ºC (L:D; controls) kept cultures are depicted in dark (Trial 1) and light (Trial 2) grey; cells kept at 28:28 ºC (L:D; Trial 1) and 18:18 ºC (L:D; Trial 2) are depicted in orange and blue, respectively. The shaded grey area represents the confidence interval (95%) of Pearson's correlation. The correlation coefficient (r = 0.64) and the significance level (p < 0.05) are shown in the upper left corner of the plot (n = 29).

Annex II

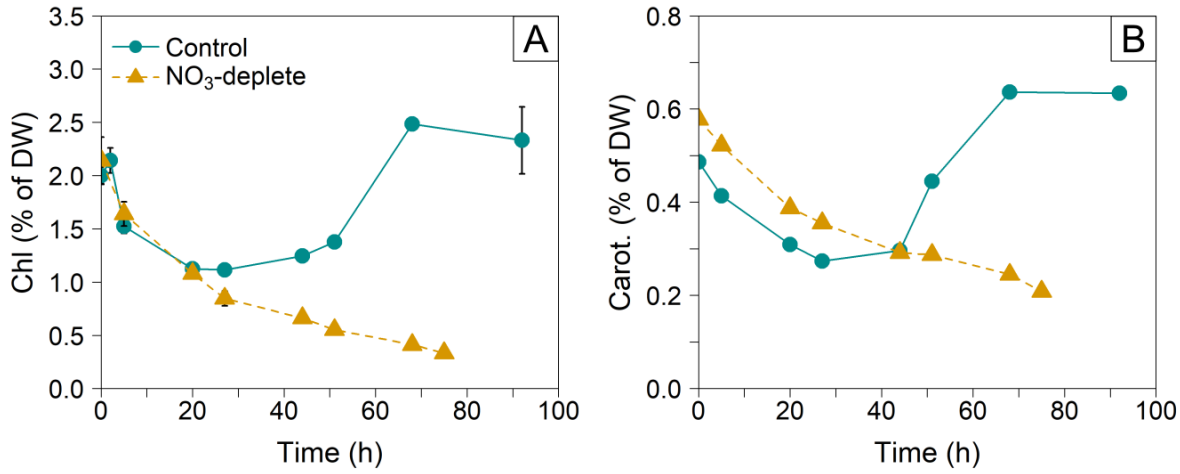

Supplementary Figure II.1. Variation of chlorophyll (% of dry weight [DW]; **A**) and carotenoid (% of DW; **B**) over time (h) of *Nannochloropsis oceanica* grown in nitrate replete (control; blue circles with solid line) and deplete (NO_3-deplete; yellow triangles with dashed line) conditions in 1-L flat plate photobioreactor (*n* = 1). Error bars represent standard deviation.

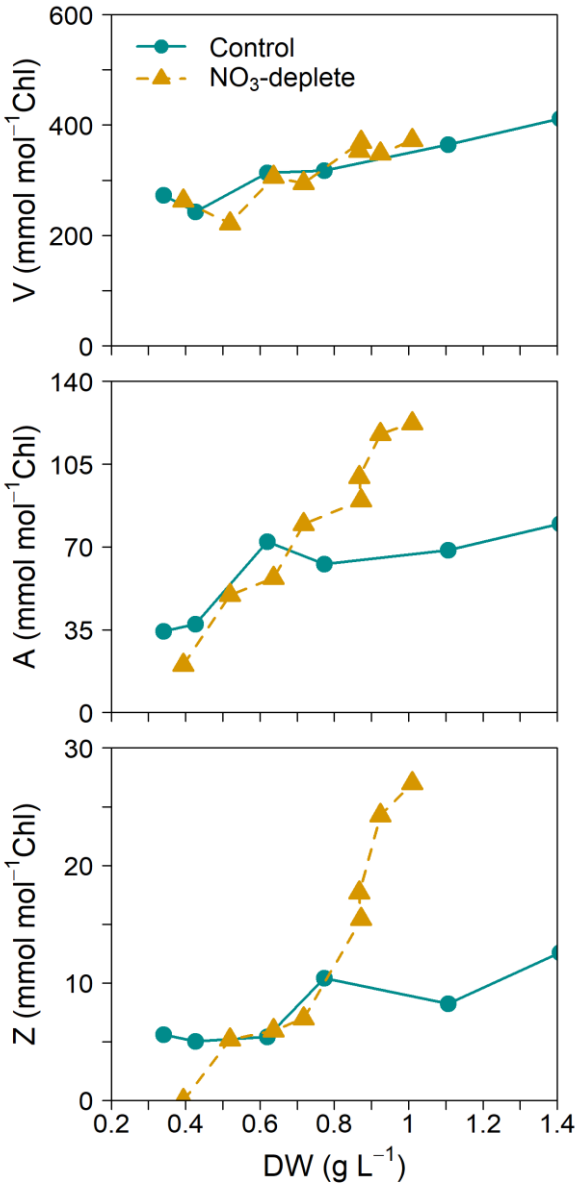

Supplementary Figure II.2. Xanthophyll components variation, violaxanthin (V), antheraxanthin (A) and zeaxanthin (Z), on a chlorophyll basis in response to the *Nannochloropsis oceanica* culture growth (in g DW L^{-1}) in nitrate replete (control; blue circles with solid line) and deplete (NO_3-deplete; yellow triangles with dashed line) conditions in a 1-L flat plate photobioreactor (n = 1).

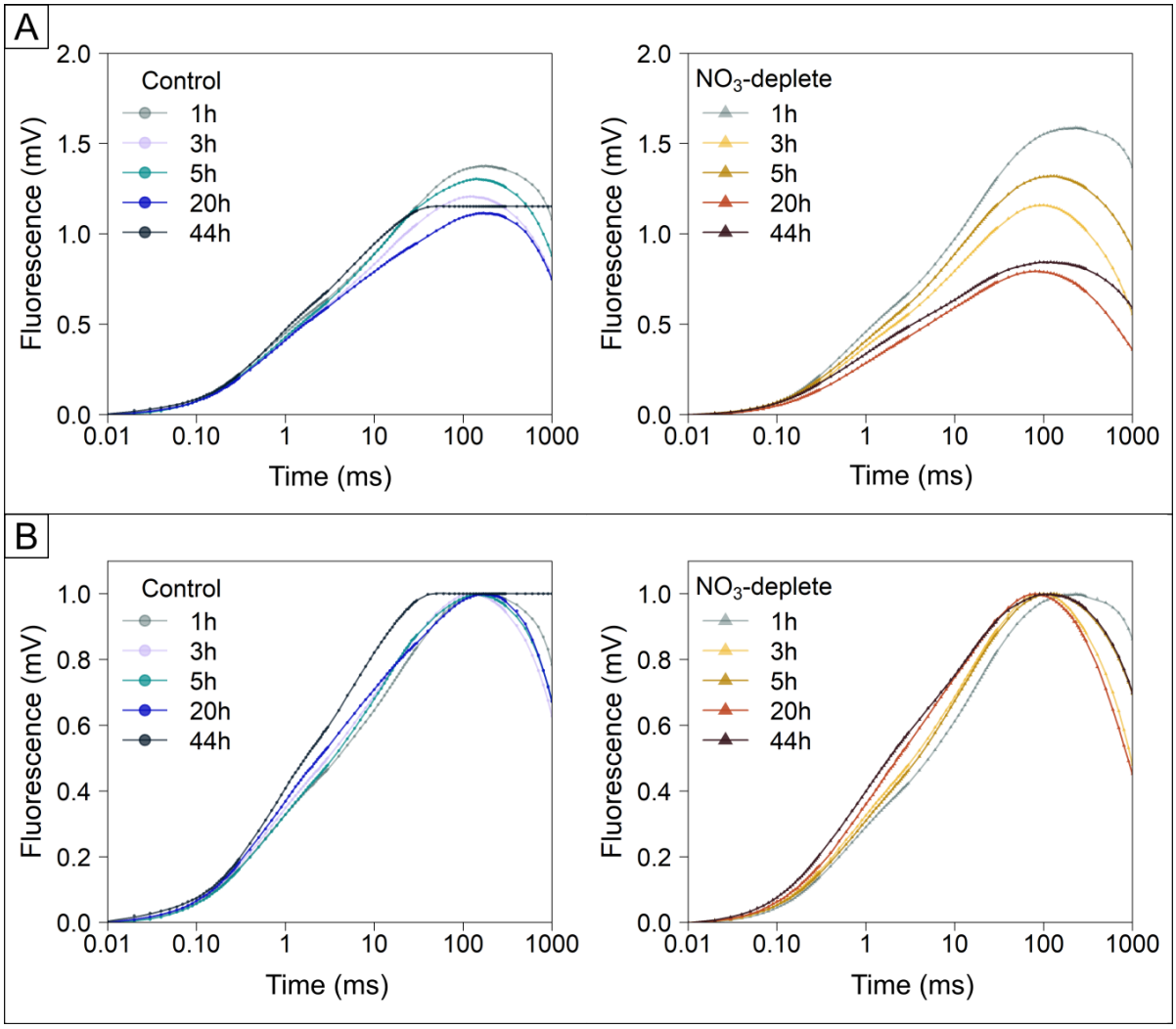

Supplementary Figure II.3. Transient curves (OJIP) after 0, 3, 5, 20 and 44h of *Nannochloropsis oceanica* grown in nitrate replete (control; left plots) and nitrate deplete (NO_3-deplete; right plots) conditions in 1-L flat plate photobioreactor (n = 1). In panel A curves were normalized to F_o. In Panel B curves were double normalized to both F_o and F_m.

Annex III

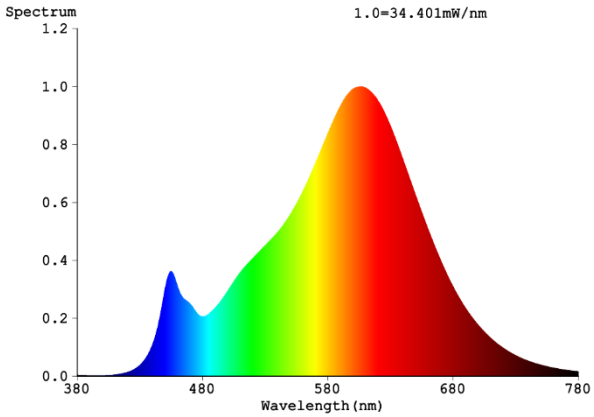

Supplementary Figure III.1. Emission spectra of the used LEDs.

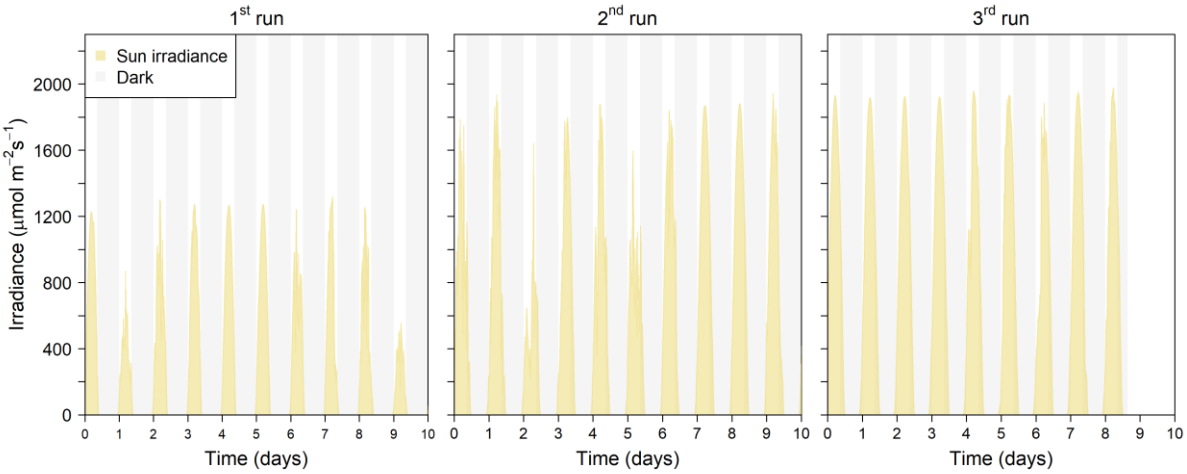

Supplementary Figure III.2. Irradiance from sunlight (in yellow) and LEDs (in orange) throughout the days of each of the three runs of the small-scale preliminary trial. Grey bars represent the dark periods when the cultures were covered, simulating nighttime.

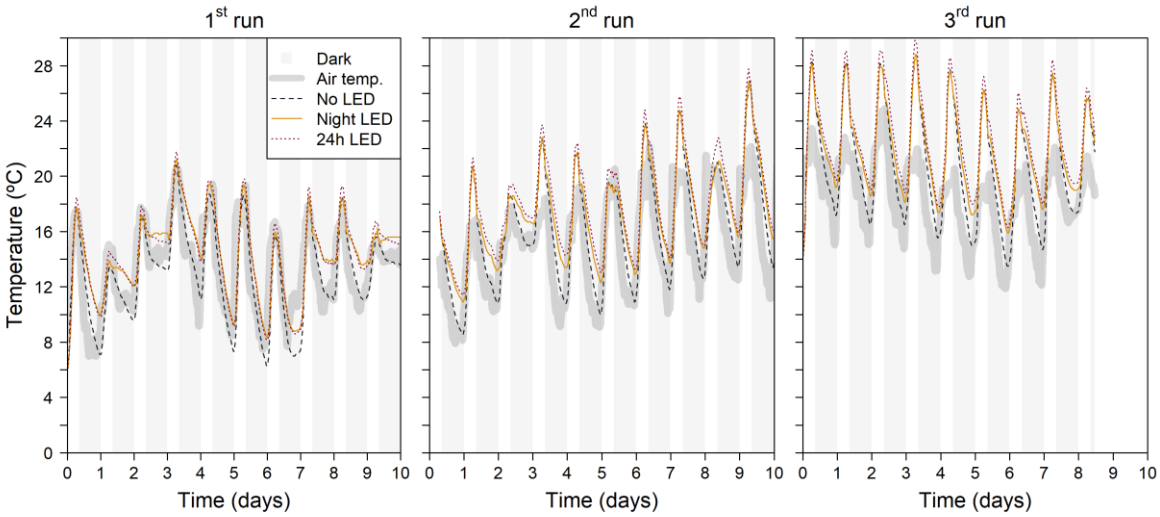

Supplementary Figure III.3. Temperature measured in the cultures of each condition: Control (blue dashed line), Night LED (yellow line), and 24h LED (red dotted line) throughout the days of each of the three runs that composed the small-scale preliminary trial. Air temperature is depicted in a thick grey line. Grey bars represent the dark periods when the cultures were covered, simulating nighttime.

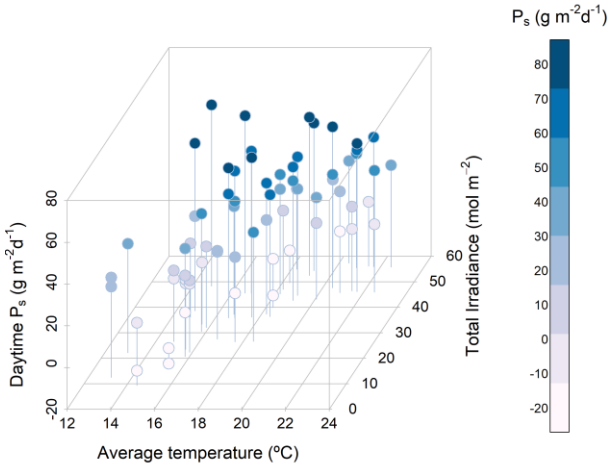

Supplementary Figure III.4. Daytime specific areal productivities (Daytime Ps; g m^{-2} d^{-1}) of *Nannochloropsis* sp. cultures grown under all conditions in outdoor 3.0-m^2 raceways ponds as a function of average temperature (ºC) and total irradiance (sunlight and LED).

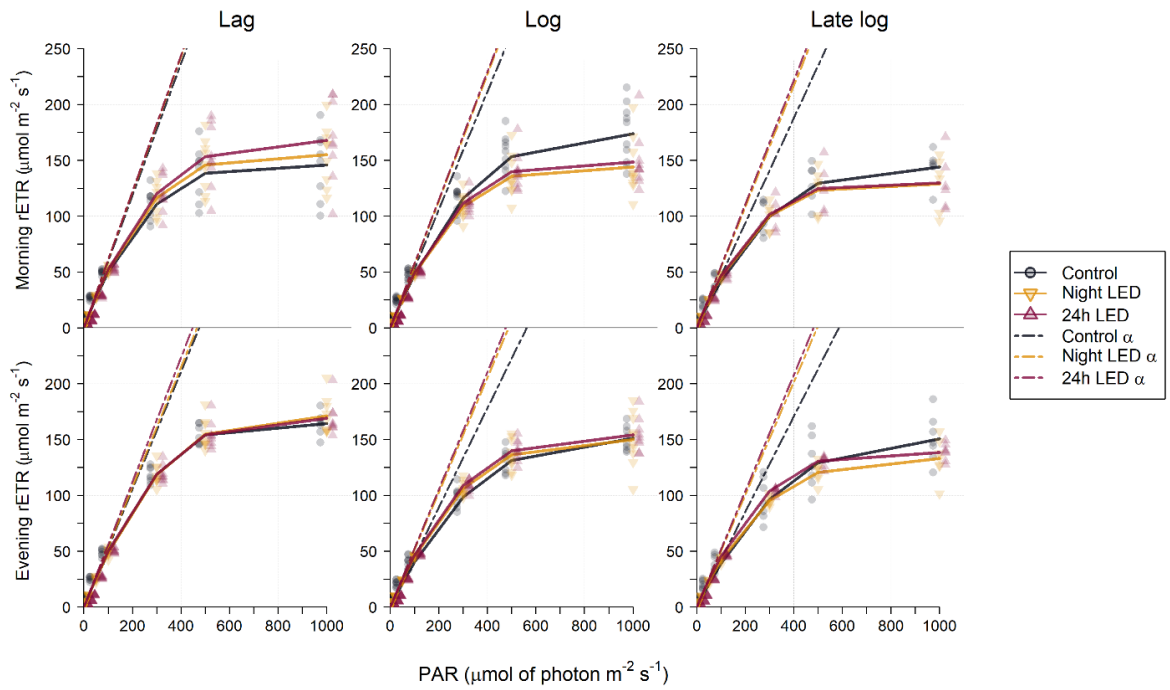

Supplementary Figure III.5. Relative electron transport rate (rETR) of *Nannochloropsis* sp. grown in three different conditions: without LEDs (Control; dark grey), with LEDs turned on during the night (Night LED; yellow), and with LEDs turned on for 24h (24h LED; red) in three outdoor raceways. The individual data points that make up the rapid light curves (RLC) are plotted in lighter colors and were grouped according to growth phase: lag, log, and late log for dark and light samples. Dashed lines represent the associated slopes, α of each RLC.

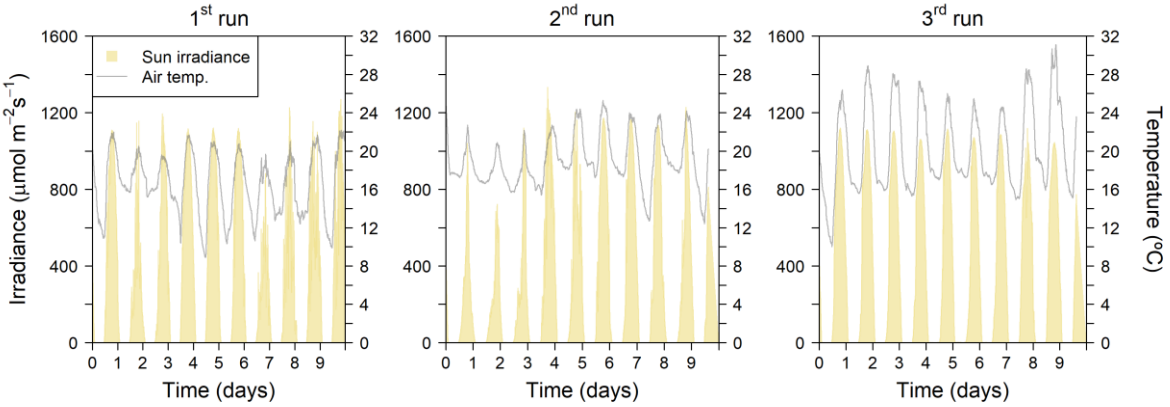

Supplementary Figure III.6. Sun irradiance (yellow peaks; left Y-axis) and air temperature (grey line; right Y-axis) measured throughout the days of each of the three runs that composed the normal mode of the pilot-scale trial. Irradiance from LEDs is not included.

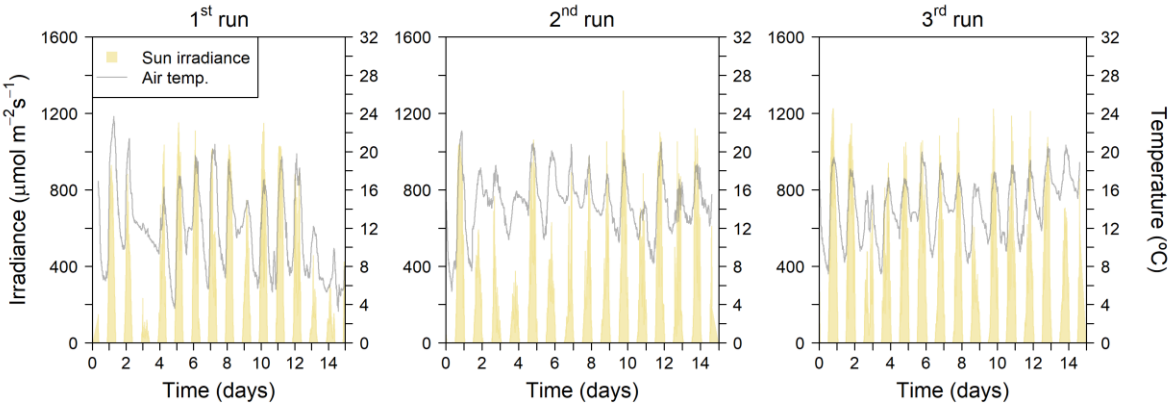

Supplementary Figure III.7. Sun irradiance (yellow peaks; left Y-axis) and air temperature (grey line; right Y-axis) measured throughout the days of the three runs that composed the economy mode of the pilot-scale trial. Irradiance from LEDs is not included.

Supplementary Table III.1. Average ± standard deviation of areal productivities for *Nannochloropsis oceanica* cultures grown under three different conditions: without LEDs (Control), with LEDs turned on during the night (Night LED), and with LEDs turned on for 24h (24h LED) in three 3.0-m^2 raceway ponds outdoors. Results are expressed as mean ± standard deviation of grouped values according to growth phase: lag, logarithmic (log), and late logarithmic (late log).

Condition	Productivities (g m^{-2} d^{-1})		
	Lag	Log	Late log
Control	6.9 ± 5.5	12.5 ± 5.0	9.4 ± 2.7
Night LED	12.2 ± 4.9	15.7 ± 5.2	14.7 ± 3.4
24h LED	13.7 ± 6.4	20.8 ± 7.7	18.8 ± 5.6

Supplementary Table III.2. Average ± standard deviation of biomass composition (% of dry weight; % DW) of pigments in terms of carotenoids (Car.) and chlorophyll (Chl.) and macronutrients, namely lipids, protein and carbohydrates (Carb.) of Nannochloropsis oceanica grown under three different conditions: without LEDs (Control), with LEDs turned on during the night (Night LED) and with LEDs turned on for 24h (24h LED) in outdoor raceway ponds. Results are expressed as the average of the last two days (late exponential phase) of the three runs, grouped according to evening and morning samples.

Sampling	Condition	Car. (%DW)	Chl. (%DW)	Lipid (%DW)	Protein (%DW)	Carb. (%DW)
Evening	Control	0.42 ± 0.18	1.78 ± 0.58	17.4 ± 2.1	32.6 ± 2.6	36.5 ± 2.1
Evening	Night LED	0.44 ± 0.12	2.02 ± 0.39	17.6 ± 2.0	36.4 ± 3.8	32.3 ± 5.0
Evening	24h LED	0.39 ± 0.12	1.86 ± 0.38	17.1 ± 2.0	35.4 ± 1.1	35.0 ± 1.7
Morning	Control	0.40 ± 0.09	1.75 ± 0.43	16.8 ± 2.9	35.6 ± 1.8	33.2 ± 3.8
Morning	Night LED	0.41 ± 0.08	1.75 ± 0.27	16.1 ± 1.7	36.7 ± 2.4	33.8 ± 1.7
Morning	24h LED	0.45 ± 0.12	1.90 ± 0.40	17.0 ± 2.5	35.5 ± 1.9	34.1 ± 4.1

Annex IV

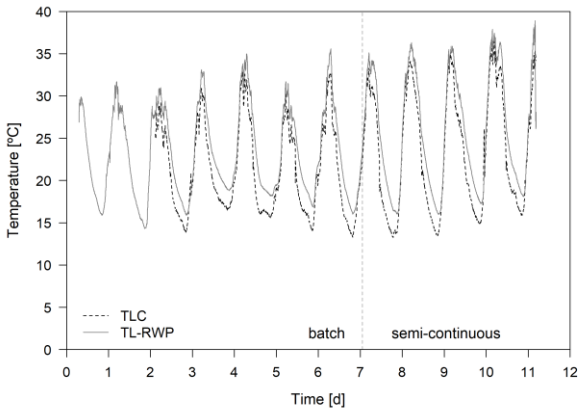

Supplementary Figure IV.1. Temperature changes (ºC) in the cultures during the trial grown in batch and semi-continuous regime in both thin-layer cascade (TLC; dashed blue line) and in the thin-layer raceway pond (TL-RWP; solid yellow line).

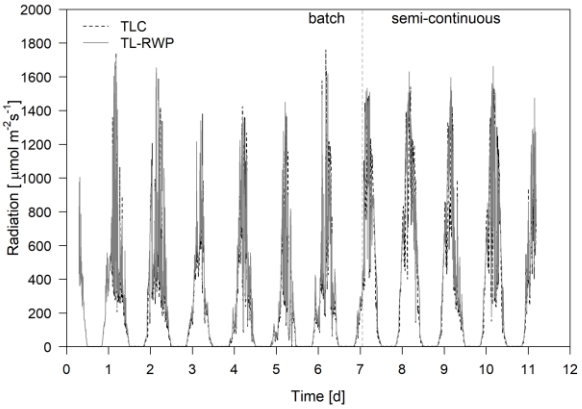

Supplementary Figure IV.2. Changes in the irradiance intensity reaching the cultivation units placed in greenhouses during the trial where thin-layer cascade (TLC; dashed blue line) and the thin-layer raceway pond (TL-RWP; solid yellow line) units were used to grow the co-culture in centrate in batch and semi-continuous regime.

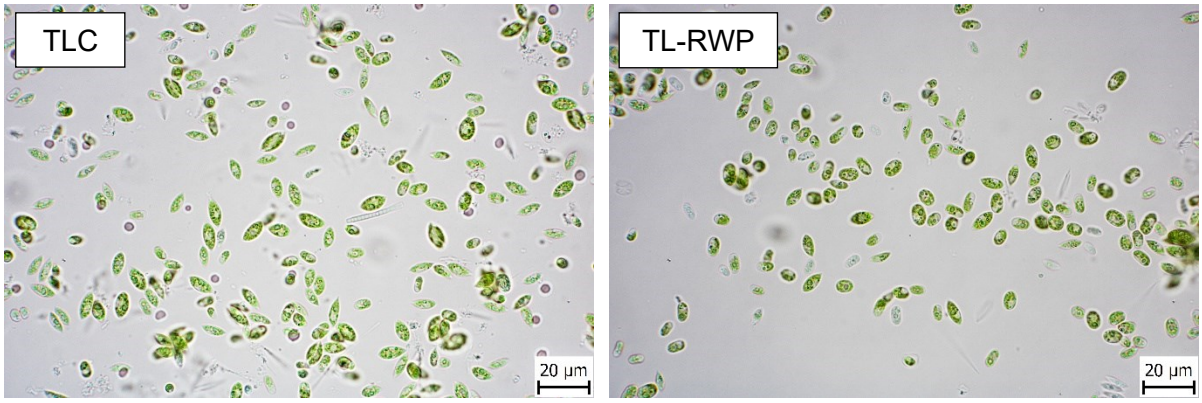

Supplementary Figure IV.3. Microscopic picture of the co-culture of *Chlorella* sp. and *Scenedesmus* sp. grown in the thin-layer cascade (TLC) and the thin-layer raceway pond (TL-RWP) in centrate on the last day of the semi-continuous growth regime.

Supplementary Table IV.1. Changes of variables estimated from saturation pulse analysis of fluorescence quenching: the slope (α) and non-photochemical quenching (NPQ) of the co-cultures of *C. vulgaris* and *S. acutus* grown in a thin-layer raceway pond (TL-RWP) and a thin-layer cascade (TLC) during the cultivation in batch and semi-continuous regime (25% dilution rate). Results are expressed as means ± standard deviation as measurements were carried out in triplicate.

Time [day]	**TL-RWP**		**TLC**	
	α	NPQ	*α*	NPQ
0	0.61 ± 0.037	0.06 ± 0.004	x	x
1	0.70 ± 0.030	0.05 ± 0.018	0.55 ± 0.038	0.06 ± 0.004
2	0.72 ± 0.003	0.08 ± 0.016	0.66 ± 0.018	0.11 ± 0.040
3	0.74 ± 0.034	0.05 ± 0.004	0.61 ± 0.017	0.13 ± 0.005
4	0.78 ± 0.024	0.09 ± 0.010	0.82 ± 0.015	0.11 ± 0.040
7	0.70 ± 0.058	0.40 ± 0.130	0.78 ± 0.056	0.17 ± 0.007
8	0.71 ± 0.041	0.37 ± 0.055	0.73 ± 0.036	0.22 ± 0.001
9	0.75 ± 0.088	0.39 ± 0.086	0.74 ± 0.024	0.24 ± 0.001
10	0.73 ± 0.016	0.45 ± 0.138	0.71 ± 0.030	0.23 ± 0.027
11	0.76 ± 0.004	0.21 ± 0.022	0.80 ± 0.008	0.13 ± 0.015